Development of HIF-mimicking materials for chronic wound healing

Carolina Ramos Rivera

A dissertation submitted in partial fulfilment

of the requirements for the degree of

Doctor of Philosophy

of

University College London

Division of Surgery and Interventional Science

University College London

2020

Declaration

I, Carolina Ramos Rivera confirm that the work presented in this thesis is my own. Where information has been derived from other sources, I confirm that this has been indicated in the thesis.

Signature:

Date:

I. Acknowledgements

I would like to express my sincere gratitude and appreciation to several people; without their generous support I would not have been able to complete this research.

First and foremost, I want to give thanks to my primary supervisor, Dr. Gavin Jell for being amazing these past years and I would like to thank you for your patience, immeasurable knowledge, kindness and support. Thank you also to Prof Julian Jones for sharing your time and expertise so willingly. Finally, to Mr. Kaveh Shakib, thank you for your advice and guidance throughout my research. To Prof Marilena Loizidou, as head of the department, thank you for creating such a supportive research environment and also for your caring and kind words. A special thanks to Dr. Amir Gander and Dr. Nathan Griffiths for your support and understanding. And to all the lab technicians and Ms. Julie Cheek for all you have done for me.

Now to all the past and present members of my research group: Amy, Wai, Azadeh, Joel, Medina, Louise, Deniz, Weijia, Lizzie, Jia and Elena B. I am deeply thankful for the constant exchange of knowledge and ideas and for all the fun and support in the lab. I also want to acknowledge the contributions of the MSc students I had the opportunity to supervise, Denisse and Akshay.

To Katerina, Elena P, Elena Z, Alex, Tania, Patricia, Fabiola, Naheem, Pilar, Salfarina and Agata, I can never thank you enough for your friendship and all the lab help throughout these years, thank you for keeping me motivated. Thanks to all my lab friends and colleagues for always giving me a good laugh and being so supportive, especially in the stages of my thesis writing.

A special mention to David, Sofia, Santiago, Mara, Yanaina, Ana, Manuel, Fabiola, Citlali, Lucía, Caro, Teresita, Juan, Ciro, Florian, Patricio, Melissa, Oriana and Meli who have been my friends and family in London. I want to thank the UCL Mexican community for giving me a sense of home. Thanks to all my friends that have been supporting me throughout this period. .

I would also like to thank CONACyT for funding my research and making this all possible.

Finally, I want to dedicate this thesis to my parents, my sisters and my godfather. These last few years would have been impossible without all of you. Thank you for all your love and support throughout my life.

II. Abstract

Non-healing (chronic) wounds are a major health problem; they are painful, cause considerable morbidity and costs the NHS between £4.5 and £5.1 billion annually. New approaches to wound healing that target tissue regeneration, rather than infection management, are urgently needed. The cellular response to oxygen via the Hypoxia Inducible Factor (HIF) pathway is vital for healthy wound repair and activates a number of processes important for wound regeneration including; the recruitment of inflammatory cells, metabolic adaptation, cell survival and a plethora of pro-angiogenic factors. Considering that patients with increased chance of developing chronic wounds (e.g. diabetic and elderly patients) have an impaired response to hypoxia, wound dressings that artificially targets the HIF pathway may offer some promise in restoring chronic wound healing. Here we investigate if HIF mimetics (DMOG, DFO and cobalt) and HIF mimicking bioactive glasses as a possible strategy for chronic wound repair.

To test the effect of these HIF mimetics an in vitro hyperglycaemic model, that mimics the impaired HIF response observed in diabetic patients, was developed. HaCaT preconditioned with high glucose levels for 28 days, resulted in an impaired response to hypoxia (reduced VEGF expression and reduced HIF stabilisation, $p<0.5$). By comparing a range of glucose levels and pre-conditioning periods, this study provides a comprehensive guide to in vitro modelling of wound healing responses, not currently present in the literature. In the hyperglycaemic model, HIF mimetics (DFO and cobalt), restored HIF-1α stabilisation and VEGF expression to a similar (DFO) or greater level (cobalt) to that observed in the normal glucose response to hypoxia ($p<0.0001$). DMOG also increased VEGF expression, but in mechanism that appeared to be independent to HIF-1α stabilisation.

Considering that topical oxygen therapy of chronic wounds is a current treatment modality with some evidence of success, despite the inevitable oxidative stress caused, it was investigated if HIF mimetics would enhance cell survival and activate the regenerative approaches associated with HIF stabilisation (regardless of the local oxygen pressure). HaCaTs were subjected to 100% O_2 which caused cell death within 48 hours. Interestingly, HIF stabilisation levels were higher under hyperoxygen conditions in the hyperglycaemic conditions, when compared to normal levels of glucose ($p=0.003$). This is in line with the increased cell survival observed in hyperglycaemic cells at a prolonged exposure to 85% O_2 ($p>0.001$).

Silica-based bioactive glasses containing cobalt (and other ions that may enhance wound healing, Mg & Zn) were prepared via the melt-derived route. Controlled Co release from the glasses was observed in the physiological range of HIF stabilisation. Zinc ions promoted cell proliferation under hypoxic conditions but not normoxic conditions ($p<0.01$). The dissolution products from the Cobalt-containing glasses stimulated VEGF secretion linearly to the percentage of cobalt molarity in the glass compositions. Cobalt and zinc-releasing glasses demonstrated the potential use in advanced wound dressings for chronic wounds.

III. Impact Statement

This thesis investigates the development of new chronic wounds treatments by targeting the cellular pathway involved in responding to changes in oxygen pressure, the Hypoxia Inducible Factor (HIF) pathway. The thesis will have a number of impacts:

1. Patient impact

Chronic wounds disproportionately affect the diabetic and elderly population, having an important impact in the patient's quality of life. Chronic wounds are painful, unsightly, cause morbidity and are leading cause of limb amputation. Despite a number of tissue engineering and artificial skin substitutes emerging as potential treatments, they are expensive and there is limited evidence of success in treating full dermal wounds in diabetic and elderly patients. Wound dressings that provide signals that enhance the patient's own wound healing capabilities (by targeting an underlying mechanism that is impaired in these patients – namely the HIF pathway) would offer a number of advantages in terms of cost, application in remote communities and (possibly) efficacy. Using a model of the diabetic environment (hyperglycaemia) this thesis has demonstrated that HIF mimetics can help restore the normal wound response.

2. Societal impact

Chronic wound management costs the NHS between £4.5 and £5.1 billion annually. Improvements in chronic wound healing rate would have substantial economic impact in terms of the cost to health services. This thesis suggested a new approach to wound dressings (via the controlled release of HIF mimetics) that would reduce chronic wound healing time through increased anti-microbial activity, promotion of angiogenic factors and increased cell survival.

3. Commercial and translational impacts

The thesis advanced the translation of new diabetic wound healing treatments by the development an in vitro model that resembles the diabetic phenotype in normal and low oxygen levels (as wounds) in two important cell lines in wound healing. This enables a reliable in vitro 2-D model of chronic wounds (diabetic and elderly) for drug-development research. The commercial creation of new wound healing dressings with the use of cobalt containing bioactive glasses (as demonstrated in this thesis) or with the controlled release of other HIF mimetics would have a considerable economic impact, the global advanced wound dressing market is estimated at £8-20 billion by 2024. Here we describe a simple, off-the-shelf cost-effective approach to wound dressings that avoids the expense and regulatory hurdles of using cells or material (ECM) derived from animals.

4. **Scientific impacts**

There are a number scientific impacts that will further our knowledge of how cells behave in high glucose and hypoxic conditions, and in how different HIF mimetics behave differently. The capacity of the HIF mimetics is commonly evaluated under normal oxygen conditions in terms of HIF-1α stabilisation and VEGF expression. However, this is the first report of the response of three HIF mimetics (each with a different mechanism of HIF induction) under low oxygen and hyperglycaemic conditions. HIF mimetics were able to increase HIF-1α accumulation in the hyperglycaemic model and increased VEGF expression. HIF stabilisation under 100% O_2 was also found to be glucose dependent. These findings help develop our understanding of HIF and high glucose, gaining knowledge that will enable new insight and new treatments for chronic wounds.

IV. Table of Contents

V. List of Figures

VI. List of Tables

VII. Abbreviations

%MS percentage molar substitution

ABTS 2, 2'-azino-bis(3-ethylbenzothiazoline-6-sulfonic acid

ADP adenosine diphosphate

AGE advanced glycation end-product

AKB-4924 hypoxia-inducible factor-1 alpha stabilizer

ALDA glycolytic enzymes aldolase A

AMPK 5' adenosine monophosphate-activated protein kinase

ANGPT2 angiopoietin-2

ARNT aryl hydrocarbon receptor nuclear translocator

ARPE-19 human retinal pigment epithelial cell line

ATP adenosine triphosphate

Bcl-2 B-cell lymphoma 2

bFGF basic fibroblast growth factor

BG bioactive glass

bHLH basic helix-loop-helix

BO bridging oxygen

BSA bovine serum albumin

CA9 carbonic anhydrase 9

CBP/p300 CREB-binding protein, transcriptional co-activating proteins

CCS copper chaperone for superoxide dismutase

CFE colony forming efficiency

CHIP carboxyl terminus of the hsc70-interacting protein

Co-BG cobalt bioactive glass

CoA coenzyme a

COX cyclooxygenase

D-Glc deoxyglucose

DAG diacylglycerol

DAPI 4′,6-diamidino-2-phenylindole

DCF dichlorofluorescein diacetate

DFO desferrioxamine

DHB ethyl-3–4-dihydroxybenzoic acid

DMEM Dulbecco’s modified Eagle’s medium

DMOG dimethyloxalylglycine

DMSO dimethyl sulfoxide

EC endothelial cell

ECM extracellular matrix

EDTA ethylenediaminetetraacetic acid

EGF epidermal growth factor

EGFR epidermal growth factor receptor

ELISA enzyme-linked immunosorbent assay

EPCs Endothelial Progenitor Cells

EPO Erythropoietin

FACS Fluorescence-activated cell sorting

FADH2 Flavin adenine dinucleotide

FBS Foetal bovine serum

FDA Food and Drug Administration

FGF fibroblast growth factor

FTIR Fourier-transform infrared spectroscopy

G-CSF granulocyte-colony stimulating factor

GHS growth hormone secretagogue, ghrelin

Glc glucose

GLO1 glyoxalase 1

GLUT1 glucose transporter 1

GSH/GSSG reduced glutathione / oxidized glutathione

H2DCFDA 2',7'-dichlorodihydrofluorescein diacetate

HA hydroxyapatite

HaCaT human skin keratinocyte cell line

HCT/P human cells, tissues, and cellular and tissue-based products

HDF human dermal fibroblast

HEK-DAT dopamine transporter transfected human embryonic kidney cells

HeLa immortal cervical adenocarcinoma cells

Hep3B human hepatocellular carcinoma cells

HIF hypoxia-inducible factor

Hnpc human neural progenitor cell

HPS hypoxia preconditioned serum

HRE hypoxia-responsive element

ICIE-1 bioactive glass

ICP Inductively Coupled Plasma

ICP-AES Inductively coupled plasma atomic emission spectroscopy

ICP-OES Inductively coupled plasma optical emission spectrometry

IGF Insulin-like growth factor

IL Interleukin

IP-10 human interferon-inducible protein 10

iPSCs induced pluripotent stem cells

JG1 anti-grp75/mot antibody

Kv voltage-gated potassium channels

LDH lactate dehydrogenase

LDHA lactate dehydrogenase a

LG low glucose

MCP-1 monocyte chemoattractant protein 1

MGO methylgloxal

miR-210 microRNA-210

MMP matrix metallopeptidases

MPX multiplex assay

mRNAs messenger RNA

mTOR mammalian target of rapamycin

mtROS mitochondrial ROS

MTs methallothionenins

MTT 3-(4,5-dimethylthiazol-2-yl)-2,5-diphenyltetrazolium bromide

NAC N-acetylcysteine

NAD nicotinamide adenine dinucleotide

NADH reduced nicotinamide adenine dinucleotide

NADPH nicotinamide adenine dinucleotide phosphate

NC network connectivity

NF necrosis factor

NF-kB nuclear factor kappa-light-chain-enhancer of activated b cells

NK1.1+ pan-natural killer cell marker

NOG noggin

nonBO non bridging oxygen

NPC Neuroprogenitor cell

ODDD oxygen-dependent degradation domain

PAD peripheral arterial disease

PAS Per-ARNT-Sim domain

PBS phosphate buffered saline

PDGF platelet-derived growth factor

PES polyethersulfone

PFKL 6-phosphofructokinase

PGK1 phosphoglycerate kinase 1

PHD prolyl hydroxylase

PKC protein kinase C

PKM pyruvate kinase muscle

PMA premarket approval

PRP-gel platelet-rich plasma gel

PsaA surface adhesin A

pVHL von Hippel-Lindau

R2 coefficient of determination

RAGE receptor for advanced glycation end-products

ROS reactive oxygen species

SD standard deviation

SDF-1 stromal derived factor 1

SE substantially equivalent

SINBAD Site, Ischemia, Neuropathy, Bacterial Infection, and Depth system

siRNA small interfering RNA

SOD2 superoxide dismutase 2

TAD transactivation domain

TAD-C translational activation domain - carboxyl terminal

TAD-N translational activation domain -nitro terminal

TCA tricarboxylic acid

TGF-β transforming growth factor beta

TIMPs tissue inhibitors of metalloproteinases

TNF-α tumour necrosis factor alpha

VEGF vascular endothelial growth factor

XRD X-ray powder diffraction

Chapter 1. General Introduction

1.1 **The clinical need for improved chronic wound healing**

A chronic wound, as defined by The Wound Healing Society, "is a wound that fails to heal in a timely and orderly rate, without restoring functionality or anatomical integrity".[1] The timeliness is subjective, determined by the origin and complexity of the wounding, however the orderliness relates to the sequential process of wound healing. Chronic wounds can occur following trauma, from surgical procedures or can be caused by pressure ulcers, diabetic ulcers and burns.[2]

Chronic wounds are painful, cause considerable morbidity and have large treatment costs. In the US, the estimated treatment cost of chronic wounds is estimated to be $25 billion, whilst in the UK it is estimated that 2-3% of the health budget is spent on the treatment of chronic wounds, with a prevalence if 3.7 per 1000 patients.[3–7] Furthermore, it has been estimated that 85% of the lower limb amputations are related to chronic wounds.[8] It was reported, by the Public Health England, that between 2015-2018 there were 147,067 hospital spells for diabetic foot ulcers, where 33% of the patients were admitted more than once for ulcer treatment and that 8.7% of this population had an amputation.[9] Guest et al. (2016) estimated that 5% of the diabetic population within the UK have a foot ulcer.[10] Ulceration not only reduces the quality of life of the patient, but is also associated with increased mortality due to amputation and depression.[11,12] With the increasing ageing population and the alarming increase in diabetes, it is expected that chronic wounds will affect one person in 10 by 2040. The development of new treatments and technologies for chronic wound healing are urgently needed[13] and in order to increase the translation of these new technologies, better in vitro models of diabetic wounds are needed.

1.1.1 **Wounds Classification**

Chronic wounds are classified through different systems to diagnose, predict the clinical outcome and selection of optimal treatment. Initially, the Wagner system classified the wounds depending on their depth, the presence of gangrene, loss of perfusion and introduced the ischemic index as a predictor factor of healing. A cut-off point in the ischemic index between diabetics and non-diabetic patients was also set -0.45 and 0.35 a.u. accordingly-, where the difference populations is associated to the comorbidities in diabetes such as vascular disease and basement membrane

thickening,[14] affecting the re-oxygenation of the wounded tissue. The University of Texas (UT) system classifies them into 4 stages with 3 grades each incorporating the presence of infection and/or ischemia.[15] The Site, Ischemia, Neuropathy, Bacterial Infection, and Depth system (SINBAD) classifies wounds based on a score of 6 points taking into account the wounded site and the presence of neuropathy as prediction variables.[16] As the stage and grade of severity increase along of the duration of the wound, so does the risk of prevalence of microbial flora and biofilm development.[17] The NICE[a] guidelines recommend the UT and SINBAD classifications, as they are considered clinically descriptive, simple and applicable to the UK practice and already widely used.[18]

1.2 **Current approaches for chronic wound healing**

The first line of response to a wound is offloading (if a pressure ulcer), debridement and the use of wound dressings. The main factors to be addressed in managing chronic wounds are: 1) the identification of the physical cause of the wound, and when possible the correction, 2) pressure control, 3) control of infection 4) restoration of pulsatile blood flow and 4) metabolic control.[18,19] A number of different treatment approaches exist to encourage wound healing depending on the site, type and size of wound[18] defined as adjunctive treatments (see Table 1-2).

The majority of wounds are currently treated by debridement, considered to be a gold standard step in wound bed preparation.[18,20–22] Debridement consists on the removal of nonviable tissue and debris at the wound bed and margins, and can be through surgery, wet-to-dry dressings, bio-surgery, enzyme preparations and hydrogels.[20] After debridement the use of a wound dressing is generally required. In the same manner, it has been reported that advanced wound dressings efficiency improves after debridement.[18,20,23–26]

1.2.1 **Wound dressings**

The purpose of wound dressings is to protect the wound from infection, absorb and control the exudate and retain moisture whilst allowing gas exchange. Ideally, wound dressings should be non-adhesive, prevent infection and biofilm formation and enhance healing without forming a scar; at the same time, they should be cost-efficient and manageable for the patient.[27,28] There are a wide range of potential dressings currently

[a]The National Institute for Health and Care Excellence (NICE) provides national guidance and advice to improve health and social care.

available (Table 1-1, Figure 1-1). Although NICE has adopted wound classifying systems and established recommendations on wound care, there is no specific recommendation of the choice of dressing. NICE considered that the evidence supporting different wound dressings (Table 1-1) is limited or inconclusive, although they state that factors such as availability, wound severity, infection control and patient decisions must be taken into consideration when selecting the wound dressing.[18] However, NICE acknowledges that the low-cost dressings currently used may not be the most appropriate dressing for the patients, and thus can result in worsen of the wound, patient dissatisfaction, and be a waste of resource.[18,23,29,30]

Table 1-1 Characteristics of advanced wound dressings.[18,21,23,31–34]

Dressing Type	Characteristics	Companies/Suppliers
Gauze (traditional, non-advanced)	Absorbent and low cost, requires constant replacement and do not protect from exogenous bacteria	Generic, Smith & Nephew, Kendall, Mölnlycke
Foams	Absorb wound exudate, maintain moisture, can include film coatings as barriers, can occasion malodorous smell	Smith & Nephew, 3M, Braun, ConvaTec, Mölnlycke,
Transparent films	Can act as bacterial barriers, permeable to water and oxygen, retain moisture and promote epithelialisation, may strip skin.	Kendall, Johnson & Johnson, Smith and Nephew, 3M
Hydrocolloid	Promotes auto-debridement, absorbent, may promote over granulation, long lasting, can occasion bad smell and strip skin.	Smith and Nephew, ConvaTec, Coloplast, Hollister, Systagenix
Capillary-Action	Highly absorbent, two low-adherent contact layers with hydrophilic fibres core, prevent maceration.	Advancis, Protex, McKesson.
Alginates	Highly absorbent, forming gel when in contact with wound, maintain moisture, may produce fibrous debris	Smith & Nephew, 3M, ConvaTec, Covidien, Bertek, Maersk, Unomedical
Antimicrobial dressings	Deliver antimicrobial agents (iodine, silver, honey), effective against pathogens, high cost.	Smith & Nephew, 3M, ConvaTec, Coloplast, Johnson and Johnson, Medline, Healthpoint

The prescription costs for the NHS in one year to July 2018 in advanced wound and antimicrobial dressing materials in primary care in England were almost £92 million.

Advanced wound dressings actively improve the environment of the wound through a physical (e.g. moisture control) o chemical means[23] (see Table 1-2). The use of antimicrobial dressings is advised by NICE when clinical signs or symptoms of infection are present. It must also be considered that while antimicrobial dressings help manage infection and thereby prevent worsening of the wound, they do not directly promote tissue regeneration, and may even by cytotoxic to wound healing cells as well. This issue may be important in patients that have reduced regenerative capacity e.g. diabetic or elderly patients.

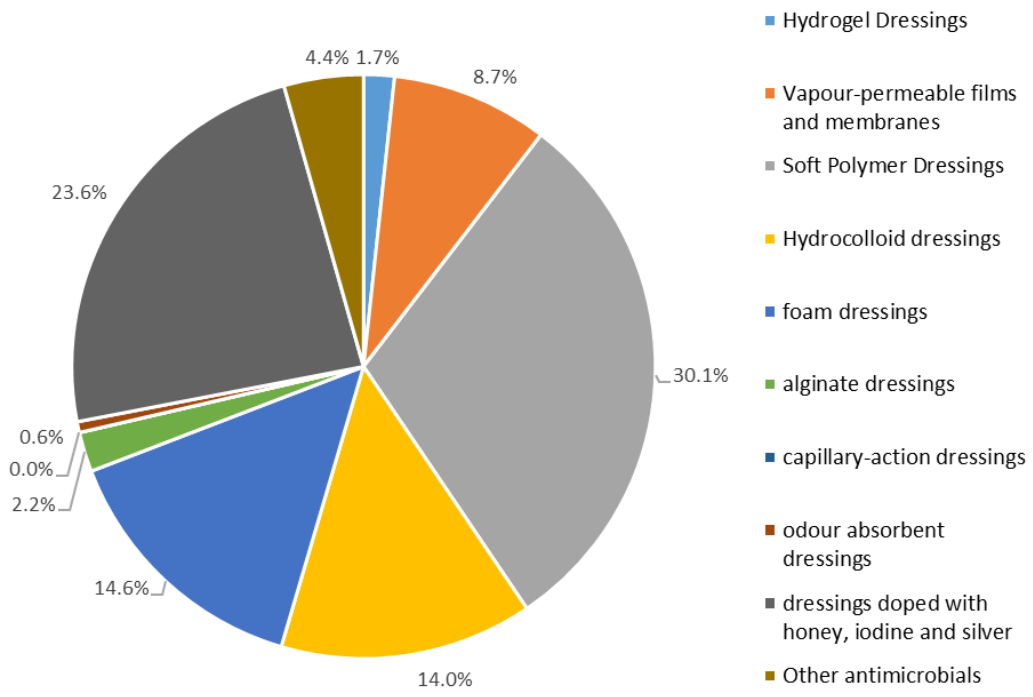

Figure 1-1 Advanced wound dressing in England. The percentage of advanced wound dressings used in primary care settings in England from August 2017 to July 2018. *Original figure data obtained from NICE* [35]

1.3 Adjunctive treatments for chronic wound healing

The delay in the wound closure and tissue remodelling in diabetic patients, require not only the regulation of the wound environment, but also the promotion of the healing process, thus advanced wound therapies are complementary treatments to aid wound regeneration in these patients. These treatments include the use of angiogenic growth factors, (such as βFGF, the only FDA approved pro-angiogenic treatment for diabetic foot ulcers), bioengineered skin grafts containing acellular ECM components of skin (e.g. Integra) and cellular components (e.g. Apligraf®), physical stimuli (e.g.

mechanical stimulation) or oxygen therapies (Table 1-2). NICE have published recommendations against the treatment of diabetic wounds through hormonal growth factors, autologous PRP-gel, electrical stimulation and dalteparin (low molecular weight heparin), unless as part of a clinical study as they considered not to prove a significant effect in wound healing and/or are not cost effective.[18(b)] They also report that negative pressure therapy treatment has been found to improve significantly the wound outcome and should be preceded by surgical debridement.[18,36]

Table 1-2 Adjunctive treatments for chronic wound healing (* FDA approved)

Type	Subtype
Topical treatments	Dalteparin® (heparin mechanism) [18,37,38] *
	bFGF (basic Fibroblast Growth Factor) [39–41]
	EGF (commercialised as REGEN-D) [42–44] *
	PDGF (Becaplermin- Regranex Gel) [25,45,46] *
	TGF-β (transforming growth factor beta)[47–50]
	G-CSF (Neupogen® & Leucomax®)[51–53] *
	VEGF (topical) [54] VEGF (Gene encoding growth factor) [55,56]
	Insulin[57–60]
	Platelet-Rich Plasma (PRP) [26,61,62]
Grafts[23,35] **(bioengineered alternative tissues)**	Apligraf® / Graftskin® [63–66] *
	Dermagraf® [64,67,68] *
	Urgostart®[27,69–71]
	Grafix®[72,73]
	Integra Dermal Regeneration Template®[74,75] *
External physical stimuli	Phototherapy[76,77]
	Negative pressure therapy[78–81]
	Acoustic energy[81–84]
	Electrical stimulation[85–87]
Oxygen therapies	Aqueous oxygen[88–90]
	Hyperbaric oxygen[18,91]
	Topical oxygen [92–95]
	Continuous diffusion of oxygen[92,96]

Several skin substitutes and graft systems exist, as reviewed and classified by Davidson-Kotler et al. (2018), who separated these according to their base material, if cellular content is present and the permanence of the graft. However, not all of them have FDA approval or according to the U.S. Department of Health and Human

(b) NICE report (2015): Recommendation 55

Services, have enough supporting evidence of their efficiency.[4,32,97–99] Nevertheless, NICE recommends the consideration of skin substitutes when the healing has not progressed, while the use of regenerative wound matrices is not recommended unless part of a clinical study.[18(c)] Dermagraft® is a nenonatal dermal fibroblast in a polyglactin bio-absorbable mesh, that allow the native cells to migrate into the scaffold. The use of cells within skin substitute is likely to act via its secretome (production of growth factors, cytokine and chemokines).[67,100] Urgostart® is an interactive dressing that inhibits protease activity, specifically matrix metalloproteinases, whilst controlling the wound humidity.[64,67,68] Apligraf® -previously called Graftskin®- is a collagen and cultured allogeneic fibroblast and keratinocytes.[63–66] Of the skin substitutes listed in Table 1-2, only Apligraf®, Dermagraft® and Integra Dermal Regeneration Template® have obtained the premarket approval (PMA) by the FDA (2019).[4] There are twenty six products that have a 510(k) premarketing submission,[d] as they are based on synthetic and animal sources, and 45 products derived from human cadaver skin and placental membranes are have a HCT/P submission[e], both regulated through the FDA.[4]

The use of phototherapy, which involves applying ultraviolet and near infra-red light into the wounded site, causing a reported increase in cell metabolic activity and proliferation (which could be associated to ROS production).[76,77,101] Phototherapy is not considered by NICE to have a significant difference when compared to standard care and has not sufficient evidence supporting its use,[18] however, it is considered by the FDA to have a positive effect.[76]

High oxygen therapies are growing in use as adjunctive therapies. They increase the oxygen pressure in the wounds, obeying Henry's law, which states that the amount of dissolved gas in a liquid is directly proportional to its partial pressure.[93,102] The oxygenation of a healthy tissue can vary between 25-100 mm Hg, and when wounded the oxygen partial pressure drops to between 5-20 mm Hg.[85,103] However, in a chronic wound the ischemic tissue can reach 0-5 mm Hg. Topical oxygen therapy consists on the application of a high concentration of oxygen at an atmospheric pressure, while continuous diffusion of oxygen consists of applying a highly oxygen concentration flow, increasing the tissue oxygen pressure between 100- 250 mm Hg. Hyperbaric oxygen treatment, is where patients are placed in chambers where the ambient oxygen

(c) NICE report (2015): Recommendation 54

(d) "A submitter of a premarket notification submission (510(k)) must demonstrate to the Food and Drug Administration (FDA) that the "new device" is "substantially equivalent" (SE) to a legally marketed predicate device." [536]

(e) An FDA regulation for human cells or tissue intended for implantation, transplantation, infusion, or transfer into a human recipient.[537]

pressure is higher than atmospheric, which is reported to increase tissue oxygen levels.[104] The oxygen increase in the treated tissue results in an increased in ROS production, and associated increases in angiogenic (e.g. VEGF) and stem cell recruiting factors (e.g. SDF-1).[93,102,105]

1.4 **Pathogenesis of diabetic and elderly chronic wounds**

1.4.1 **Why are diabetic wounds less likely to heal?**

Diabetes Mellitus is characterised by hyperglycaemia, having a multifactorial effect in the development of chronic wound healing. Hyperglycaemia inhibits the response to hypoxia, via an impairment of the Hypoxia Inducible Factor (HIF) pathway. High glucose is also responsible of altering the polyol, hexosamine, and diacylglycerol pathways and Advanced Glycation End products (AGE) accumulation as reviewed by Huang et al. (2014).[106] Diabetic patients have an increased expression inflammatory markers resulting from hyperglycaemia which induces expression of interleukin-1β (IL-1β).[107,108] The sustained pro-inflammatory environment can translate into endothelial and smooth muscle cell dysfunction including dysregulation of vasoconstriction, blood flow and cell migration. Diabetic patients also display differences in nitric oxide expression and platelet function.[109,110] Skin changes have also been reported in diabetic patients, with an increase of epidermal thickness, inferior mechanical properties (e.g. increased rigidity and brittleness of tissues),[111] a reduced production of collagen type I, and dysregulation of metalloproteinases, as reviewed by Quondamatteo et al. (2014.[112] These molecular and physiological changes have been reported to lead to a reduced response to injury, impaired re-vascularisation and re-oxygenation after an ischemic event such as a wound.[109,110] Peripheral artery disease (PAD), is also common in diabetic patients and can not only cause wounds, but also prevent healing.[113]

Biofilms (persistent microbial colonies) are often present in chronic, open wounds (~60%),[114] and are often resistant to antibiotics due to the protective self-produced ECM. Several authors suggest that this biofilm is the principle treatment target and cause for chronic wound development.[2,114,115]

1.5 The role of oxygen and oxygen sensing pathways in wound healing

1.5.1 Oxygen supply importance and as signalling factor

Hypoxia is a physiological stimulus that regulates mammalian oxygen homeostasis having an effect on a myriad of cellular processes including, metabolism, differentiation, proliferation, migration and ECM production. Tissue responds to the decrease of oxygen pressure via Hypoxia Inducible Factor (HIF) pathway, governed by the HIF-1α transcription factor. In hypoxia HIF-1α avoids degradation, allowing it's migration to the nucleus, binding to HIF-1β and the expression of ~300 Hypoxic Responsive Element genes, including genes involved with wound healing such as, vascular regulation, glucose uptake, glycolysis, angiogenesis, lymphangiogenesis chemokine production (Figure 1-2). The knockout of HIF-1α molecule has demonstrated its importance in the regulation of vascularisation,[116] chondrogenesis,[117] adipogenesis,[118] osteogenesis,[119] haematopoiesis,[120] innate immunity[108,121] and wound healing.[122]

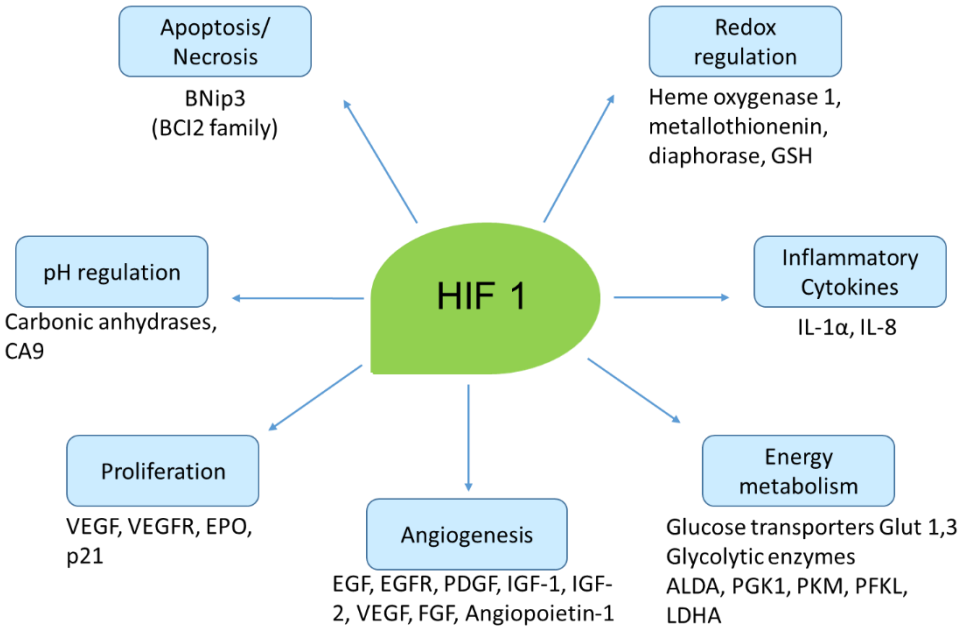

Figure 1-2 Involvement of HIF 1 in cell-regulatory systems. HIF is a master regulator of oxygen homeostasis and driving factor in development, metabolism, inflammation and wound repair.

The response to hypoxia is cell-type specific and the HIF pathway is activated when oxygen metabolic demand outstrips supply. HIF-1 is a heterodimer that increases the transcription of several genes when it binds into the DNA in 5'-RCTGTG-3'. It is constituted by two proteins, HIF-1α and HIF-1β, (Figure 1-3) the latter also known as ARNT (Aryl hydrocarbon Receptor Nuclear Translocator). Both proteins have an amine

terminal, a bHLH domain (basic-Helix-Loop-Helix) and 2 PAS domains (Period clock-Aryl hydrocarbon receptor nuclear translocator-Single minded). The domain bHLH regulates the dimerization of HIF-1, controlling it's binding to ADN.[123–126]

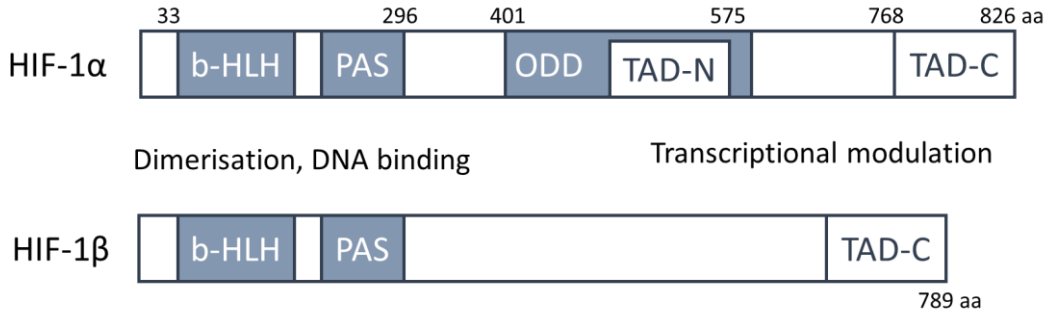

Figure 1-3 Diagram of protein structure of HIF-1(α/β). bHLH: basic Helix-Loop-Helix; PAS: Period ARNT; ODD (Oxygen-dependent degradation domain; TAD-C Translational Activation Domain - Carboxy terminal; TAD-N Translational Activation Domain -Nitro Terminal. *Image adapted from* [127].

The stabilisation of HIF-1α in hypoxia is achieved via the inhibition of oxygen sensitive enzymes, namely factor inducible hypoxia (FIH) and prolyl hydroxylases-2 (PHD-2) (**Figure 1-4**). Both PHD and FIH depend upon oxygen and oxoglutarate dehydrogenase complex (2-OG) as substrates, in addition to iron and ascorbate as co-factors. Under normoxic conditions, HIF-1α is hydroxylated in the ODDD (Oxygen-dependent degradation domain) in prolines 549-572 by PHD; allowing interaction with the amino acids 549-572 from von Hippel-Lindau (pVHL) β domain. The pVHL is a component of the E3 ubiquitin ligase complex responsible to ubiquitinise HIF-1α, previous to be degraded by the proteosomal. However, if HIF-1α is not degraded, the transcriptional activity can be blocked through asparagine hydroxylation preventing the binding to the transcriptional CBP/p300.[124,125,127] Under normoxia, the half-life of HIF-1α is 5 minutes,[128] conversely under hypoxia 1% the half-life can be extended to 30 minutes.

Under normoxic pathological conditions, HIF-1α can be stabilised and its degradation prevented, creating a pseudo-hypoxia stage. However, in normoxic conditions and under the presence of HIF mimetic factors, HIF-1α can be stabilised as the ubiquitination decreases. Following HIF-1α accumulation, through hypoxia or artificially, HIF-1α translocates into the nucleus, binding to HIF-1β and forming the HIF-1 complex. The HIF-1 complex then activates the hypoxia response element (HRE) which results in the upregulation of the genes involved in tissue survival and regeneration.[124,129]

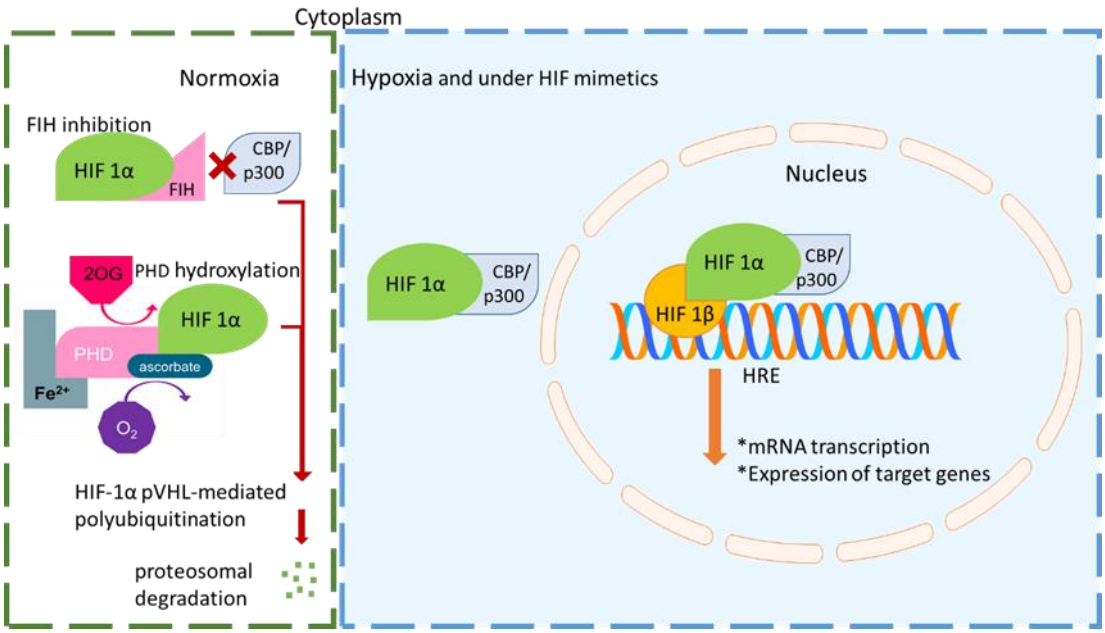

Figure 1-4 HIF-1α stabilisation. HIF-1α is stabilised under hypoxic conditions, translocating into the nucleus where it binds to HIF-1β and activates HRE genes. Under normoxic conditions, it is rapidly degraded by the FIH and PHDs, polyubiquitinated by the von Hippel-Lindau protein followed by proteosomal degradation. *Original figure adapted from* [130,131]

The metabolic switch to glycolytic respiration, which is related to the cell proliferation, is regulated through the HIF 1 pathway. This metabolic switch, named the Pasteur Effect, is when the cells transition from the oxidative phosphorylation pathway the glycolysis in order to generate sufficient ATP under restricted oxygen conditions. The HIF pathway stimulates the expression of glycolytic enzymes, increasing the catabolism of glucose and lactic acid production.[132] Under pathological conditions in which HIF is unregulated, such as tumours, the Warburg effect takes place. The cells adapt to hypoxia and depend permanently on glycolysis in order to survive, even when subjected to normoxic levels.[132,133]

1.5.2 **HIF in wound healing**

The oxygenation of the dermis ranges between 1.5 and 5% O_2, whilst the oxygenation in the epidermis can be as low as 0.2% O_2.[134] Following injury and damage to the microvasculature the dermis oxygen pressure can reduce close to anoxia[135–138] and this, together with increased metabolic demand causes activation of the HIF pathway. HIF-1α stabilisation is responsible of activating a number of wound healing regenerative processes (Figure 1-4) including: 1) the inflammatory response (inflammatory cell recruitment and monocytes differentiation), antimicrobial activity (phagocytic activity is increased following HIF stabilisation),[139,140] 2) vascularization (HIF stabilisation

increases the production of number of pro-angiogenic factors)[116,141] and 3) remodelling (e.g. collagen synthesis by fibroblasts).[142]

The HIF pathway is linked to every stage of wound healing (as detailed in Figure 1-5). After injury, haemostasis occurs. Platelets degranulate and release histamine, and a number of factors known to be important in angiogenesis (e.g. EGF, PDGF, TGF-β and VEGF-A).[143] In response to the oxygen drop, surrounding keratinocytes release IL-1 and Macrophage Chemo-attractant protein (MCP-1) to attract monocytes, macrophages, T-cells and mast cells.[144] Hypoxia also induces keratinocytes migration from around the wound edge towards the lesion, proliferating in order to restore the barrier function[145]. The monocytes differentiate into macrophages between day 2 and 3 after injury, releasing further inflammatory and angiogenic factors IL-1 and IL-6, TNF-α, FGF, TGF-β and PDGF.[143,146] Hypoxia has been demonstrated to enhance monocyte differentiation into macrophages.[147] Macrophages also release reactive oxygen species (ROS) due to an oxygen consuming respiratory burst, and this is involved in bacteria killing and prevention of infection, as well as redox signalling modulating the healing process.[148,149] In response to hypoxia and by the chemotactic gradient produced by resident cells, fibroblasts migrate into the wound at day 2. There is a strong cross-talk between keratinocytes and fibroblasts,[150] orchestrating the wound healing process across different types of skin and immune cells, which has also been shown to HIF dependant.[45,150,151]

In the proliferation stage, new tissue is formed under hypoxic conditions, including the formation of new blood vessels, driven by the angiogenic factors VEGF, PDGF and SDF-1.[152,153] Granulation tissue is constructed due to the deposition of collagen by fibroblasts and the new capillary network.[154] The new vascularisation allows the gradual restoration of the oxygenation, however the remodelling phase is still driven under hypoxic levels. In the remodelling phase, keratinocytes differentiate led by contact inhibition, into a basal phenotype of stratified squamous keratinizing epidermal cells. TGF-β1, which is secreted by keratinocytes and macrophages in early stages of wound healing, signals fibroblast to differentiate into a myofibroblast phenotype, which will synthesise new collagen.[144,155] The remodelling phase is aided by the metalloproteinases (MMP) and regulatory TIMPs produced by the keratinocytes and fibroblasts, breaking down of old collagen forming a scar.[144,156,157] The new microvasculature matures in this process. Even though when the wound has closed and no visual signals of injury are perceived, the remodelling phase can be extended to months.

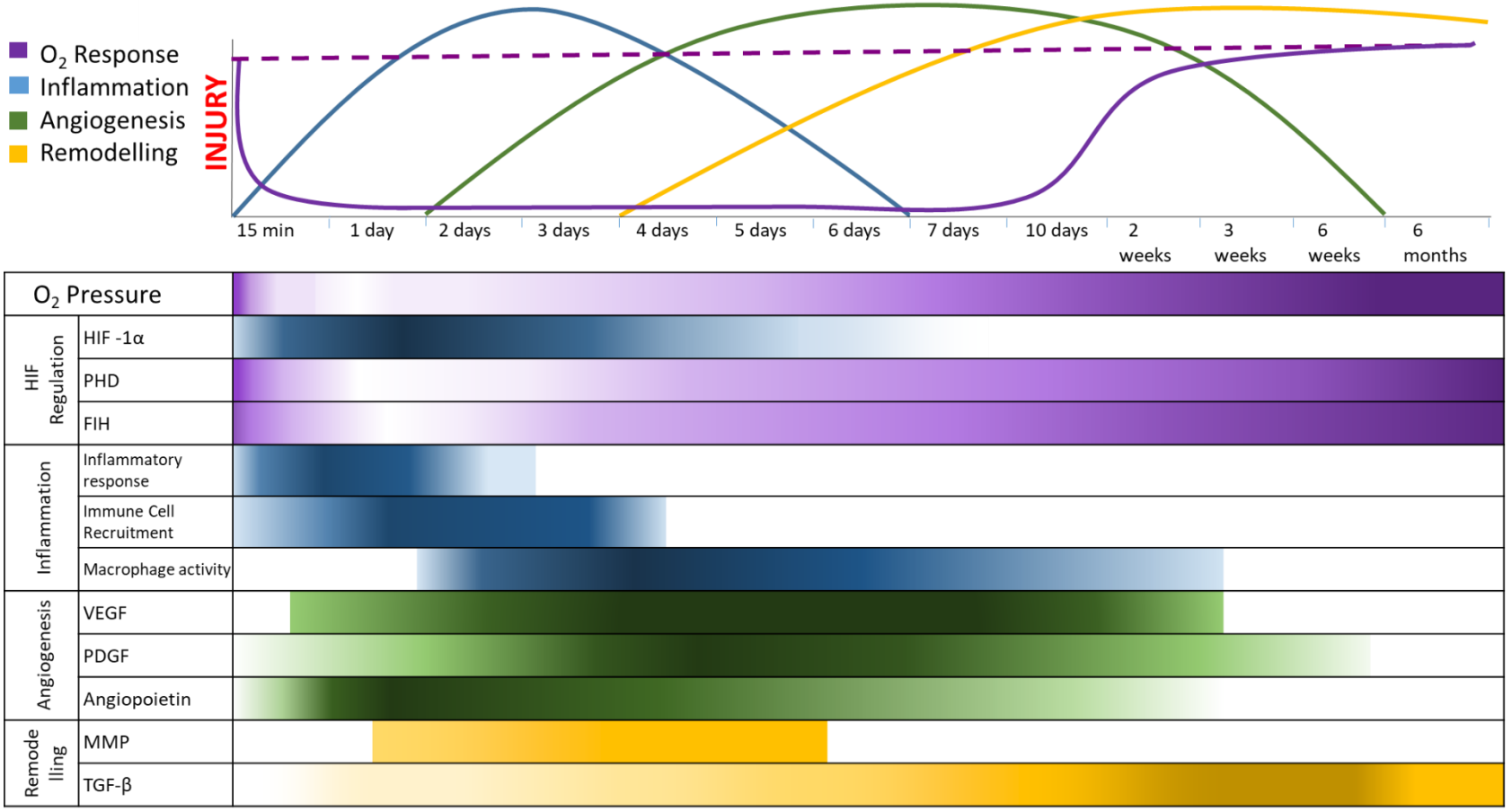

Figure 1-5 Involvement of HIF-1α in the wound healing process. The PHD and FIH functional dependence on oxygen allows the rapid stabilisation of HIF-1α following a drop in O_2 pressure caused by microvasculature damage from injury. HIF-cell response is cell-type de dependant and in all stages of wound healing: 1) inflammation: HIF stabilisation increases interleukin, chemokine and cytokine production by resident cells causing inflammatory cell recruitment, monocyte differentiation into macrophages and increased macrophages phagocytic activity; 2) Angiogenic response, HIF stabilisation induces resident cells to produce angiogenic factors, and induce endothelial and fibroblast migration and proliferation; 3) wound remodelling, increasing TGF-β expression, collagen synthesis, fibroblast infiltration and MMP production, permitting wound closure and collagen degradation.

1.5.3 **Chronic wound healing**

Chronic wounds are characterised by a prolonged period of inflammation, lack of restoration of the oxygen supply and the dysregulation of the growth factors and cytokines coordinating the healing process. Chronic inflammatory results in elevated IL-1β and TNF-α secretion, and higher interstitial collagenases, gelatinases and stromelysins expression,[107,158–160] thus a reduction in the granulation tissue and collagen content is observed.[161] The sustained expression of MCP-1 and Interferon Inducible Protein-10 (IP-10) in chronic wounds prolongs the inflammatory response by continuously recruiting lymphocytes and other inflammatory cells. Chronic wounds are also characterised by increased IL-8 expression, which under normal conditions induces the expression of MMPs and stimulates tissue remodelling, but when increased in a chronic fashion, decreases keratinocyte proliferation and decreases collagen lattice contraction.[160,162]

Under impaired healing, there is a substantial degradation of exogenous EGF. EGF is secreted by platelets, fibroblasts and macrophages and involved in cell migration, proliferation and re-epithelialisation. In non-healing wound edges, the EGF Receptor is found predominantly within the cytoplasm, instead of the membrane.[42,160,163] TGF-β (a major component of tissue repair), is present throughout all the wound phases and strongly linked to VEGF regulation. In chronic wounds TGF-β levels are decreased, possibly through the presence of increased amounts of proteolytic enzymes.[160] The expression of PDGF is also fundamental in wound healing for blood vessel maturation and it is expressed by platelets, macrophages, vascular endothelial cells, fibroblasts and keratinocytes. In chronic wound healing it is decreased by proteolytic degradation and increased MMP activity.[157,160] In combination with hypoxia induces VEGF expression and is indispensable for vessel maturation.

Angiogenesis is a vital component of wound healing, as is initiated by the release of angiogenic growth factors released by resident cells in response to hypoxia and by recruited immune cells in response to the inflammatory milieu present.[164] Angiogenesis starts in the inflammation period and extends to the remodelling phase with blood vessel maturation. The restoration of the vasculature is essential to provide oxygen to the wounded site and supply the metabolic demand. Angiogenesis is a hypoxia-driven process involving several types of cells and expressed cytokines, as reviewed by Pugh and Ratcliffe (2003). However in diabetic and elderly patients, the response to hypoxia is reduced, impairing the angiogenic process.[165–167]

1.6 **HIF Response: Diabetes and chronic wounds**

Diabetic patients and hyperglycaemia have been shown to inhibit the cellular response to a drop in oxygen pathway,[109] through the continued destruction of HIF-1α, leading to hypoxia unresponsive cells, hindering the antimicrobial response and hindering the formation of a viable vasculature.[123,168] Under hyperglycaemic conditions keratinocytes have been demonstrated to have reduced migration and decreased proliferation rates, delaying wound closure.[169] Hyperglycaemia also alters the epidermal cell expression of the tight junction protein (ZO-1), with reduced expression of Keratin 5 and 14.[170] In a diabetic wound mouse model, it was observed that a decreased level of PDGF was due to the reduced expression by monocytes and macrophages.[171] In hyperglycaemia there has also been reported a reduction in the expression of heat shock protein 68 (HSP) and HSP70 compared to non-hyperglycaemic controls.[172]

The endothelial progenitor cells (EPCs) are key effectors of the neovascularization and re-epithelialization and are mobilized in response to trauma to the injured site. Diabetic patients have a 40% EPCs number reduction[173] and it has been reported that EPCs isolated from diabetic patients have an impaired response to hypoxia and inflammatory factors when compared to healthy EPCs[54]

Diabetes is a metabolic disorder considered as an inflammatory disease, which is characterised by increased oedema and inflammatory cytokine levels. The prolonged exposure to hypoxia will result in an irreversible state of cell cycle arrest.[174] The inflammation granulomata in chronic wounds further induces an increased local metabolism and oxygen demand. The inability of a damaged tissue to restore its normal oxygen conditions through vascularisation often leads to inflammatory lesions, prolonging the metabolic shift and oxygen demand ratio the tissue is subject to.[175]

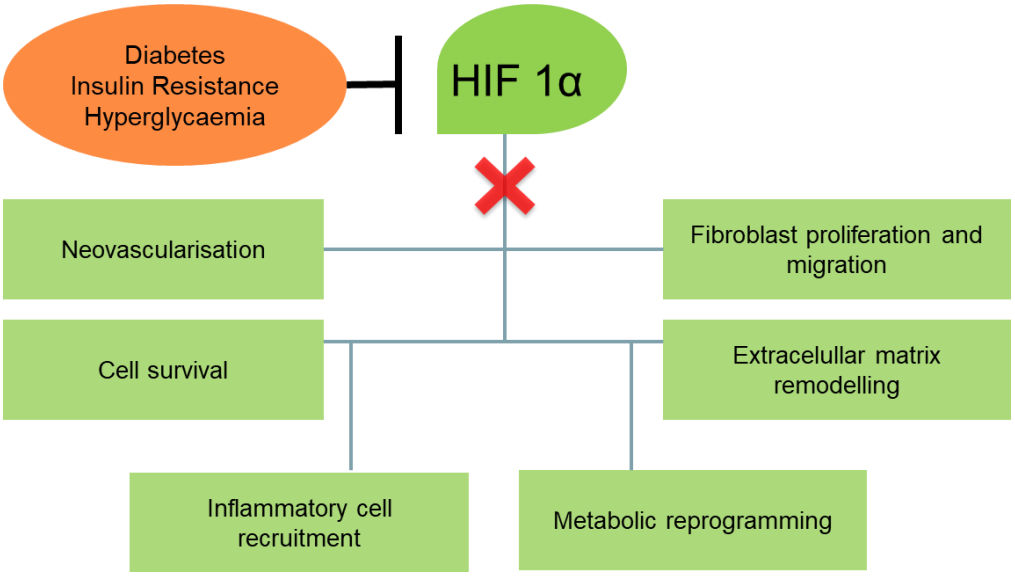

Figure 1-6 Diabetes and the HIF response. Hyperglycaemia inhibits the response to hypoxia inducing prolonged inflammation, angiogenesis and ECM remodelling and thereby disabling the normal wound healing response.

Diabetic tissues have a higher VEGF expression under normoxic conditions than non-diabetic tissues. This phenomenon may result from an increased oxygen consumption of the mitochondria from hyperglycaemic-induced increase of glycolysis, tricarboxylic acid cycle and oxidative phosphorylation.[176] The gradient of VEGF expression in healthy wounds follow the hypoxic gradient, however even when VEGF is expressed in a chronic wound environment, the high glucose blunts VEGF response to hypoxia.[177,178]

1.6.1 **Altered Glycolysis under hyperglycaemia**

Glucose is metabolized by glycolysis and the tricarboxylic acid (TCA) cycle, which yields ATP, NADH, and FADH2. Electrons from NADH and FADH2 are then transferred to molecular oxygen, and the energy released from these oxidation/reduction reactions is used to drive the synthesis of ATP from ADP during oxidative phosphorylation, also known as the electron transport chain cycle. Therefore, in the metabolism of glucose, oxygen is consumed. However, hyperglycaemia may increase oxygen consumption in mitochondria, resulting in cellular hypoxia. The changes in metabolic activity and their relative intermediates can modulate the HIF pathway.[179] As increased glycolysis, TCA cycle, and oxidative phosphorylation were the source of hyperglycaemia-induced mtROS generation. While ROS enhance the stabilisation of HIF-1α by succinate accumulation, fumarate hydratase accrual has also shown to modulate HIF.[180,181]

Hypoxia can stimulate several survival mechanisms (Figure 1-7Figure 1-7), which are intricately related through their expressed cytokines. However under pathological conditions such as hyperglycaemia, the secretions and interactions are altered. Increased glycosylation transcription factors, induced by mitochondrial superoxide overproduction enhancing hexosamine synthesis, increases the expression of cytokines such as TGF-α and TGF-β1.[106,182] Under high glucose concentrations, aldose reductase reduces the glucose to sorbitol through the polyol pathway, consuming nicotinamide adenine dinucleotide phosphate (NADPH) in the process. NADPH is a cofactor for reduced glutathione (GSH), an intracellular antioxidant. As NADPH results to be insufficient for both processes, increasing vulnerability to intracellular oxidative stress.[106,183,184] Hyperglycaemia increases the synthesis of diaglycerol (DAG), a co-factor for the Protein Kinase C (PKC) pathway, activating the nuclear factor kappa-light-chain-enhancer (NF-kB) of activated B cells, TGF-β and activate NAD(P)H-dependent oxidase leading to an increase in ROS production.[106,185] The protein modification by reducing sugars, leads to the formation of Advanced Glycation End-products (AGE), which can upregulate VEGF and alter the HIF and PKC pathways.[106,186]

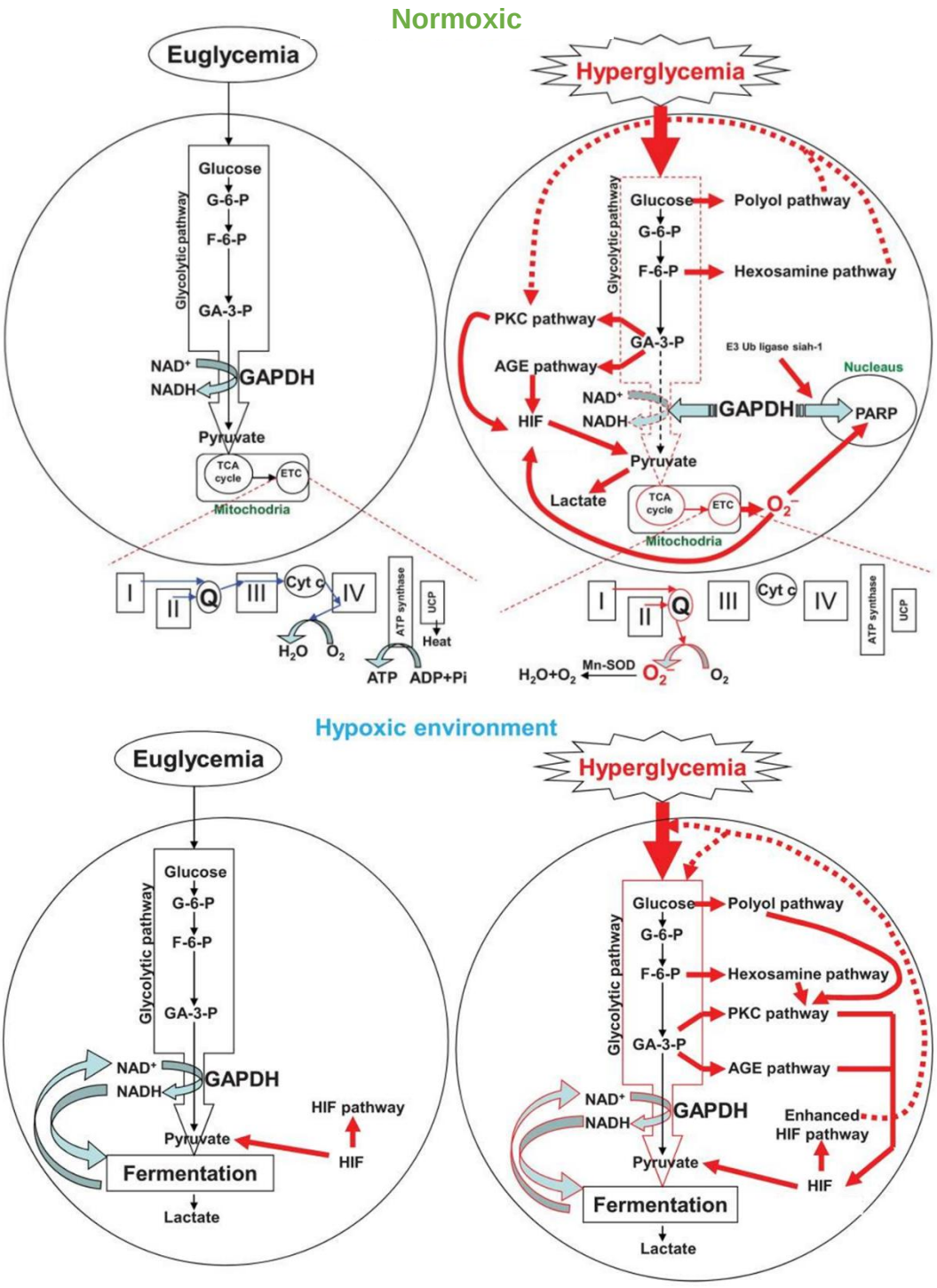

Figure 1-7 Hyperglycaemia and cell metabolism. Hyperglycaemia influences cell metabolism under normoxia and hypoxia conditions, to support the glycolytic pathway under increased influx of glucose, cells rely on four glycolysis-related pathways 1)intracellular production of AGE (advanced glycation end product) precursors, (2) increased flux through the polyol pathway, (3) protein kinase C (PKC) activation, and (4) increased hexosamine pathway activity. These altered mechanisms induce an increase mitochondria-derived reactive oxygen species (ROS) pathway and may induce VEGF expression at normal oxygen conditions. Reprinted with permission from Elsevier.[106]

1.6.2 **Ageing and HIF Response**

It is known that elderly patients have a reduced cellular response to hypoxia, having a negative effect on the wound healing process. Elderly patients have been shown, similarly to hyperglycaemic conditions, to have a reduction in the expression of antioxidants, increased oxidative stress and AGE protein modifications.[187] Age has also been shown to decrease the angiogenic response to hypoxia, and have a lower HIF-1α transcription activity response.[152,167,188] Aged skin (>80 years old) has been found to express higher levels of metalloproteinases (MMP-1) reflecting in a loss of type I collagen fibrils, elastin and skin elastic properties.[189,190] Other studies have reported that the HIF-1α protein has a reduced binding activity to DNA in response to hypoxia in aged muscle cells, even if HIF-1α-mRNA expression was shown to be similar to young.[191] A possible mechanism that contributes to this impairment is the increase of PhD3 mRNA expression with age (Figure 1-8), as reported by Rohrbach et al. (2005).[192]

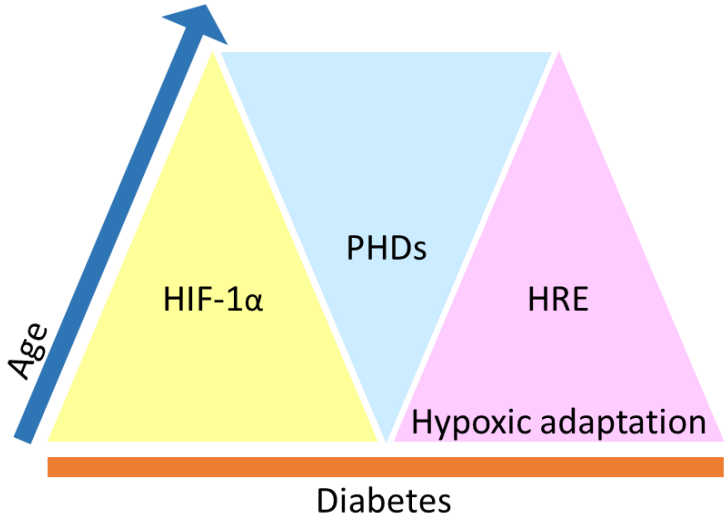

Figure 1-8 Age & diabetic dependent impairment of HIF-1a stabilisation. As age increases, the production of HIF-1α decreases and so does the expression of Hypoxia Response Element genes, however the production of prolyl hydroxylases increase. In chronic diabetes, all of these changes occur.

1.6.3 **Advanced Glycation End products (AGE) in diabetic and ageing population**

The AGE precursors trigger different pathological outcomes through (1) directly inducing intracellular glycation of proteins, (2) inhibiting the protein degradation, (3) modifying the nearby cells by diffusing out of cell, and (4) modifying plasma proteins that induce inflammatory cytokines, growth factors, and oxidative stress, as reviewed by Huang et al. (2014).[106] Although the formation of AGE occurs as a result of normal

metabolism, the number of extracellular matrix crosslinking increases with age, which is similar to that observed in diabetic patients.[193] In diabetic patients and elderly, the increase of the AGE is also related to an increased oxidative stress and hyperlipidaemia.[111,194]

Methylglyoxal (MGO), an AGE precursor is elevated under diabetic conditions as it is a by-product of glycolysis. It is considered to impede dimerization with HIF-1β, through heat-shock interaction with the cognate protein 70, leading to proteosomal degradation, or covalent interaction with p300.[195,196] Methylglyoxal-derived AGE measured in skin biopsies of diabetic patients were strongly associated to neuropathy progression. Moreover, the skin collagen AGEs were associated as prediction markers for diabetic retinopathy and nephropathy.[197]

1.7 **Delivery of HIF modulating factors for wound healing**

As discussed previously, elderly and diabetic patients have an impaired wound healing response, which may be related to an impaired ability to sense (on a cellular) a drop in oxygen pressure. Artificial (chemical or biological) activation of the HIF pathway may restore normal wound healing responses,[109,198] included neovascularisation, metabolic adaptation, antioxidant production and antimicrobial activity. A common approach in wound healing and emerging wound dressing is the release of growth factors important in wound healing (which considering the importance of restoring vascularisation, often involve the release of angiogenic factors –see Table 1-2). Targeting the upstream HIF pathway has a number of advantages over these strategies, including overcoming the short half-life of growth factors, activating multiple angiogenic factors in a sequential manner and activating a range of other genes also important in wound healing (Figure 1-5). Indeed, it has been demonstrated that constitutive expression of HIF-1α delivered by an adenovirus produced stabilised functional blood vasculature,[199] rather than the pro-inflammatory vasculature by VEGF alone. Others have shown that transdermal delivery of the HIF mimetic deferoxamine (DFO), an iron-chelating agent, prevented pressure ulcer formation in diabetic mice, upregulated VEGF secretion and improved wound healing.[200]

The prolonged stabilisation of HIF-1α is, however, associated with chronic inflammation,[177,201] increased ECM turnover and even tumorigenesis.[202] A number of HIF mimetics have been demonstrated to be cytotoxic to cells at high concentrations, to have adverse systemic effects (e.g. oxygen carrying capacity)[203] or unable to

stabilise HIF at low concentrations. The controlled spatial, temporal and concentration dependant delivery of HIF mimetics is therefore essential for the successful use of HIF mimetics as a wound dressing.

1.7.1 **HIF mimetic factors- Inducing artificially the HIF pathway**

The earliest of use of a HIF mimetic ($CoCl_2$) to stimulate VEGF production was demonstrated ~25 years ago by Ijichi (1995). In the same year Semenza published his seminal work of the role of HIF-1a which enabled the use of a number of drugs and small molecules that inhibit the degradation of the HIF-1α molecule.[204] The PHD-2 enzyme requires the presence of the co-substrates 2-oxoglutarate, with a binding site for iron, the presence of oxygen and ascorbic acid as a reducing agent to be able to hydroxylate the proline residues of the HIF-1α molecule (**Figure 1-3**, **Figure 1-4**). The inhibition of HIF-1α hydroxylation is possible through different mechanisms, a) the substitution of iron ions (Fe^{2+}), b) induced iron deficiency through iron chelators, c) analogues of the 2-Oxoglutarate molecules. The mechanism of inactivation of the PHDs will be further described in Chapter 4.

Despite the known importance of HIF in angiogenesis and cell survival, most research on HIF related topics was focussed on HIF destruction for cancer therapy. The earliest use of artificial stabilisation of the HIF pathway for increased wound healing was by Trentin (2006). The controlled release cobalt from bioactive glasses for promoting angiogenesis in bone tissue engineering was in 2010.[205] There have been, however, only two publications that have looked at scaffolds that release HIF stabilising factors for wound healing, namely Chen et. al in 2016 who used desferrioxamine (DFO) release from nanofibrous scaffolds[206] and Martin et al. (2013) who used siRNA release from polyurethane scaffolds.[207] There is a lack of knowledge, however, on the comparison of efficacy of different HIF mimetics in hyperglycaemic conditions and in the development of in vitro models to study these efficacy.

Table 1-3 Experimental evidence of HIF-mimetics used in wound healing.

HIF mimetic	Application	Model	Outcome
DFO	0.1% DFO ointment[198] - Control: ointment	Streptozotocin-induced diabetic male rat (2x2 cm^2dorsal excision)	↑↑ micro-vessel density in granulation tissue at days 3,7,14 &19 ↑↑ orientation of the collagen fibers & percentage of thicker collagen fibers from day 7 onward ↑↑Wound closure percentage: 7, 14 & 19 days mRNA: ↑↑ HIF-1α, VEGF, SDF-1α, TGF-β1 & IL-10 at 3, 7 & 14 days ↓↓ TNF-α, MMP-9 & IL-1β at 7, 14 & 19 days Protein expression; ↑↑ HIF-1α, VEGF, SDF-1α & TGF-β1 at 3, 7 & 14 days ↓ TNF-α ↑ IL-10 increase at 3, 7, 14 and 19 days ↑↑Wound closure percentage: 7, 14 & 19 days
DFO	DFO [208] Intraperitoneal injection (100 mg/kg, 10 mg/ml) Control: (-) Same PBS volume (+)VEGF treatment: 0.5 nM intradermal injection around wound site	Streptozotocin-induced diabetic male rats (8-mm punch biopsy, circular full-thickness cutaneous wounds)	↑ Re-epithelialization and granulation tissue formation in DFO- groups at day 7 ↑ Capillary density in DFO group at day 7 ↑ HIF-1α and SDF-1 protein levels in DFO- group at day 7 ↑↑ shortened healing time in DFO- group when compared to VEGF-treated and control groups at 16, 23 and 28 days
DFO DMOG	DFO (100 µL, 1mM) [165] DMOG (100 µL, 2mM) [165] (+) adenovirus expr. HIF-1α (-) vehicle solution Topical application after wounding and every other day	Genetically diabetic C57BL/KsJm/Lept db vs normoglycaemic heterozygous mice (6-mm biopsy punch, two full-thickness wounds -panniculus carnosus- on the dorsum.)	DMOG, DFO and (+) in diabetic mice at day 7: ↑ Re-epithelialization with thick well-structured granulation tissue ↑ mRNA HSP-90, VEGF-A, VEGF-R1, SDF-1α, SCF ***DMOG had higher proliferation than DFO (- control db) ↓ granulation tissue and neo-vascularisation ↓ HIF-1α, VEGFA and SDF-1 expression, mRNA HSP-90, VEGFA, VEGF-R1, SDF-1α
$CoCl_2$	$CoCl_2$ [209] In vitro(200 µM) for 6 hours In vivo:	Genetically diabetic mice B6.Cg- m1/1 Leprdb/J, Bar Harbor, ME) vs nondiabetic	↑ Wound closure rates comparison: acceleration in wound closure rate when compared with (-) control

	500µL of $CoCl_2$ after wounding CMV-Hif-1α^{DODD}	(2.0-cm-diameter open wound	
Copper: Ascorbic acid depletor	Copper oxide-impregnated dressings[210] composition: Internal: 3% cellulose copper oxide-plated fibers External: 2.3% (w/w) copper-oxide particles	Genetically engineered diabetic mice vs wild type - Treatment: Copper oxide-impregnated dressings - Control: (-) Dressing without copper (+) Silver particles-containing Commercially used absorbent wound dressing Wounding: Circular full-thickness single skin wound was created on the dorsum	↑ Mean wound size smaller in copper dressings-treated-mice compared with (-) control (6, 12 and 17 days) and (+) control (12 and 17 days) ↑Significant increase for PLGF, HIF-1α and VEGF compared to (-) control
Non-degradable active form of HIF-1α; stable in normoxia: Gene transfer	Gene transfer of murine active form of HIF-1α (CMV-Hif-1α ODDD) expression plasmid lacking the oxygen-dependent degradation domain [209,211]	- Animals: Lepr$^{db-/-}$ diabetic mice Lepr$^{db+/-}$ non-diabetic mice - Wounding: 2.0 cm-diameter full-thickness wound was excised - Treatment: CMV-Hif-1α DODD expression plasmid into skin Control: (-) empty vector control	↑Significantly up-regulated VEGF, Nos2, and Hmox1 - Wound closure rates comparison: ↑Treated group showed significant acceleration in wound closure rate ↑↑granulation tissue formation, angiogenesis, extracellular matrix deposition and epithelial regeneration) in treated mice compared with emptyvector control ↑PECAM-1 staining: Angiogenesis promotion in skin proximal to the wound bed, as revealed at day 7

↑↑ Significantly higher, ↑ higher, ↓↓ significantly lower, ↓ lower, ≈ no difference, (+) Positive Control (-) Negative Control. TDSS (transdermal drug delivery system)

1.8 **Ions that may have an effect of modulating HIF**

Cobalt (II)[131,212,221–223,213–220], nickel (II)[213,215,217,218,220,224], copper (II)[210,225–228], manganese (II)[213,218,229–231] and chromium (VI) [202,218,232,233] are metallic ions that have the ability of artificially stabilise HIF-1α. These elements along with iron, form part of the transition metals, with consecutive atomic numbers differing from 1-3 electrons with iron. For the purposes of this thesis, only cobalt will be discussed.

It is suggested that because of these similarities, Co^{2+} can substitute Fe^{2+} in the PHD 1-3 and FH-1, HIF-1α regulatory dioxygenases, inactivating the enzymes.[215,218,220,232] In addition, several mechanisms of HIF stabilisation trough cobalt are considered. It is proposed that cobalt binds to the HIF-α domain in the VHL binding region and preventing ubiquitination via the pVHL oxygen-dependant degradation pathway, inhibiting FIH hydroxylation of the HIF C terminal asparagine 803 residue.[131,214] It is proposed that Co^{2+} artificially stabilises HIF as it has a tighter bind to the membrane transporter DMT-1, suppressing the delivery of ferreous iron into the cell, thus causing depletion of intracellular iron. In this manner the PHDs -HIF-1α degrading molecule- are inhibited. Another suggested mechanism is that cobalt increase oxidative stress which depletes ascorbate, necessary for the functioning of the enzymes,[216,221] suggesting that this mechanism could happen also extracellularly, where the metallic ions avert the ascorbate from entering the cell.[234,235]

1.8.1 **Cobalt toxicity-awareness**

Cobalt is an essential trace element for humans. It is found in the heart, liver, kidney and spleen, and in smaller quantities in the pancreas, brain and serum. Cobalt forms part of vitamin B -hydroxycobalamin-, it is also a coenzyme for cell mitosis; it is involved in the forming of neurotransmitters and proteins to create myelin sheath in nerve cells; As well as a stimulant for the synthesis of erythropoietin by inducing hypoxia.[236] The normal levels for cobalt in serum is below 0.0085 µM and in urine between 15 and 85 µM.[237]

Cobalt is introduced to the body mainly by food and absorbed in the small intestine. The second source of intake is through breathing, being common the in heavy metal industry and lastly through skin.[238] In healthy closed skin, cobalt appears to have a relatively low rate absorption, which was dependent upon concentration. Following exposure, it is excreted through urine. It has been reported that after a cobalt-related burn accident, the levels of cobalt and plasma increased considerably, normalising as it was excreted in a period of 3 weeks.[237,239] A study comparing the distribution and

excretion of cobalt on skin versus intramuscular application, indicated that the elimination of the metal through urine was faster when this was applied intramuscularly. An evaluation of the full thickness skin application revealed that cobalt was still present after 48h, confirming the difference between the intramuscular and topical application in terms of the excreted cobalt.[240] It has been reported that circulating cobalt can accumulate in the myocardium, it can increase myocardial stiffness induced by chemical hypoxia, occasioning cardiomyopathy.[241,242]

High concentrations of cobalt can inflict cell damage through different mechanisms. ROS is increased when in presence of cobalt in a dose dependant manner.[216] Low concentrations of cobalt, such as 100 µM report to have a small increase in ROS production, meanwhile concentrations such as 300 µM cobalt induces a five-fold ROS increase compared to basal levels.[215,220] A reduction in glutathione has also been described as a result of excessive levels of cobalt, this mechanism could be through the increase in the ROS production. However, cobalt, having a high affinity to sulfhydryl groups, could diminish the production of the reduced GSH. Cobalt appears to inhibit enzyme mitochondrial dehydrogenase, fundamental for mitochondrial respiration.[234,241,243] Cobalt ions can increase damage to DNA under the presence of other oxidants, such as H_2O_2 or UV radiation.[244] Lipoic acid can also be chelated under aerobic conditions by cobalt. Lipoic acid is a cofactor of the oxidative decarboxylation of α-ketoglutarate to succinate and pyruvate to acetyl CoA.[234,245]

Hypoxia mobilises the calcium from intracellular stores- mitochondria and endoplasmic reticulum- it is suggested that this reorganisation of Ca^{2+} can increase the generation of ROS. Similarly, when cobalt blocks the calcium channels, by using the same transporting channels, a reduced calcium influx is observed triggering the relocation of intracellular calcium.[222,242] In the glucose metabolism, a dose-dependent reduction of ATP production has been reported in response to Cobalt,[222,234] although this mechanism could be through the artificial stabilisation of hypoxia.[234]

In terms of the dose range of safe cobalt usage, concentrations of ~500 µM $CoCl_2$ were found to decrease metabolic activity significantly and to produce impairment to the colony forming efficiency (CFE) test to 50%; a reduction to 73% was reported in 100 µM $CoCl_2$, while there was no effect at 10 µM. This is likely to be cell -type specific. The metabolic activity was seen to halve at a 620 µM Co (II), while inducing loss of membrane activity at 860 µM.[246] Literature has observed clear disparity between cobalt concentrations in conditioned mediums and the respective cellular uptake.[246,247] In HaCaT cells (a human keratinocyte-derived cell line) exposed to 40 µM Co (II), the

intracellular concentration was reported to be 0.21 nM Co/10^6 cells, whilst under 400 µM, 4.0 nM Co/10^6 cells. Further analysis at 400 µm Co (II) revealed that 77% of the cobalt ions were present in the cytosol, 22% in the nuclear fraction and 1% in the membrane fraction.[246]

The cobalt species may have different biological interactions (as reviewed by Tvermoes et al. (2015) and Paustenbach et al. (2013)) and occur predominantly in a +2 and +3 predominant oxidation states in cobalt compounds, however Co (II) is more stable.[248] Bioactive glasses allow for the controlled release of cobalt[249] by adjusting their composition and varying the surface area available. As the cobalt content in the bioactive glass structure is in the same phase as the rest of the ions, the release rate is dictated by the overall composition and degradation of the glass.

1.9 **Bioactive glasses as ionic therapy for wound healing**

To date, wound dressings have not fulfilled chronic wound patients' efficiency requirements, aiding into the revascularisation of the damaged site whilst remaining affordable. Bioactive glasses, however, have shown antibacterial capacity and increased angiogenesis under adverse conditions. The first bioactive glass was produced by Professor Hench in 1969, based on a composition of Na_2O-CaO-SiO_2-P_2O_5. This glass was produced with the intention to bond strongly with bone, replacing the bio-inert implant materials at the time, which provoked fibrotic encapsulation. The composition was termed 45S5 or Bioglass®, and with this, a new generation of biomaterials emerged. Bioactive materials evoke beneficial responses as a result of the interaction with the tissue with having bioactive properties, as opposed to bio-inert materials that usually serve with a mechanical purpose, usually having tissue/material miss-matching mechanical properties. Orthopaedic, cranial-facial, and dental-maxillofacial products have derived from the 45S5 composition.[250,251] As the research on the 45S5 evolved, different applications and new bioactive glass compositions surged. The incorporation into more complex systems and processing methods allowed the improvement of the mechanical properties of the glasses and/or enhancement of biomaterials, as well as the use of glasses as drug carriers,[252,253,262–265,254–261] eventually finding the way into soft tissue applications.[259,260,263,265–271]

In order to enhance wound healing, bioactive glass has been integrated into suture coatings, often the bioactive glass compositions enhanced with silver or copper ions.[272,273] Silver integration into the glass network has proven to increase antibacterial effect to multidrug resistant bacterial strains; however the silver, even at

low concentrations, has been seen to be toxic in different cell lines.[274] Bioactive glass have been used as antibiotic carriers, in collagen composites or as hollow fibres having a reducing effect on *staphylococcus aereus and epidermidis*, displaying no toxic effect on cells.[275–277] Cobalt bioactive glasses have been previously made by Acevedo et al. (2010), however the applications have been targeting bone regeneration. Three authors have reported the use of CoBG for wound healing. Raja et al. have reported incorporating cobalt into phosphate glasses for osteogenic purposes, due to the high importance of phosphorus in HA. They observed that the antimicrobial effect of the glasses were only seen when glass was present, as opposed to the ionic dissolution. It was also observed that by using the supernatant of monocyte cells (glass conditioned) HUVEC cells, induced tubule-like formation. However, it was required higher cobalt content in these phosphate-based glasses in order to release the cobalt therapeutic ion release.[278] Barrioni et al (2018) developed glasses that release low concentrations of cobalt, reporting chronic inflammation whilst forming new blood vessels.[279] Moura et al. (2017) created PCL/Co sol-gel BG electospun fibres, however non *in vitro* data was reported.[280]

However, the main focus is to restore the vascularisation in compromised wound healing processes. Borate-based glasses have demonstrated enhancement of VEGF expression and micro-vascularisation, which was improved with the incorporation of copper or zinc ions. Borate glasses displayed a faster degradation rate to silica-based ones. The ion dissolution product was found to promote cell migration, however toxicity due to borate accumulation is a concern among the use of these glasses [227,281,282]

Silica-based glasses possess antimicrobial capacity, as the pH rise when cations are released during glass dissolution,[251] nevertheless the antibacterial properties have reported to be augmented by silver and copper ions.[280,283] The calcium released from silica-based bioactive glasses has demonstrated to participate actively in a rapid blood-clot formation, which can aid in non-healing wounds. Calcium ions participate in the haemostatic response to wounding, that leads to fibrin polymerization and clot stabilisation.[284] Animal studies report that in diabetic rats, the granulation process when treated with silica glasses is observed at an earlier point, along with higher levels of VEGF and SDF-1 secretion[265,285] when compared to the control.[283] It is of interest not only promote VEGF secretion in impaired wounds, but to restore the microvascularisation and tissue closure and remodelling. HIF-1α mimetics can be incorporated into bioglass[260,262,278,280] to induce, in a controlled release manner, the stabilisation of the HIF pathway, effecting positively the injured site.

1.10 **Novelty and need for new approaches**

HIF-1 pathway is dysregulated under hyperglycaemic conditions and HIF-1α expression is reduced with age.[123,152,167,168,187,191] The advantage of targeting HIF specifically is the upregulation of the gene expression involved in the angiogenic process -as well as key regenerative events- under pathological environments where HIF stabilisation is impaired. Artificial HIF stabilisation under diabetic conditions has proven to increase angiogenesis, [120,286] however the response to hypoxia and HIF mimetics is cell specific[199] and prolonged HIF stabilisation or too high a concentration of HIF mimetic could have adverse effects. Furthermore, minimal research has been undertaken into the effect of HIF mimetics under hypoxia environment.

To develop a dressing with the control release of HIF mimetics, a better understanding of the biological interactions is needed in conditions that model chronic wounds. Currently there are direct comparison of the efficacy of different HIF mimetics in hyperglycaemic conditions for wound regenerative responses. To this end a hyperglycaemic model was developed in Chapter 3 and different HIF mimetics efficacy tested in Chapter 4.

Cobalt-releasing bioactive glasses for wound healing purposes were fabricated, incorporating zinc oxide to improve the cell response to hyperglycaemic increased ROS environments. The materials were characterised to corroborate their glass conformation and ionic release profile. The biological response of the 8 composition was evaluated in terms of metabolic activity, cell proliferation and VEGF expression.

1.11 **Hypothesis and Aims:**

HIF mimetics can restore the response to hypoxia under hyperglycaemic conditions. HIF mimetics can be control released in physiological-relevant concentrations for chronic wound healing.

Main Aim: Design a material that activates the HIF pathway under pathological conditions.

- Chapter 3: Develop a hyperglycaemic model for dermal cells.
- Chapter 4: Evaluate different HIF mimetics under hyperglycaemic conditions.
- Chapter 5: Develop a material that releases HIF mimetics in relevant concentrations.

Chapter 2. Materials and Methods

2.1 **Materials**

All cell culture reagents were obtained from GIBCO® Thermo Fisher.

Dulbecco's Modified Eagle Media (DMEM) was supplemented with 10% Foetal Bovine Serum (FBS) and 1% Penicillin/Streptomycin (P/S), this preparation will be referred as fully supplemented media.

DMEM was used at 1 g/L (5.5mM) and 4.5 g/L (25 mM) glucose concentration. In the experiments requiring 9 g/L glucose, 4.5 grs/L of D-glucose (Sigma Aldrich - Cat. No. G7021) was added to 4.5 g/L DMEM and filtered through a PES filter.

Methylglyoxal (Sigma Aldrich-Cat No.78-98-8) was diluted in a stock concentration of 50mM in DMEM and further diluted to the working concentrations.

Dimethyloxalylglycine (DMOG, Sigma Aldrich - Cat. No. D3695) was reconstituted in Dimethyl sulfoxide (DMSO anhydrous, ≥99.9%, Sigma Aldrich - Cat No. 276855) in a stock concentration of 142.74 mM, which was then aliquoted and preserved at -20ºC. It was further diluted in fully supplemented DMEM according to the experiment setting.

Desferoxamine (Deferoxamine mesylate salt DFO, Sigma Aldrich - Cat. No. D9533) was reconstituted in Dimethyl sulfoxide (DMSO anhydrous, ≥99.9%, Sigma Aldrich - Cat No. 276855) in a stock concentration of 76.127 mM, which was then aliquoted in vials and preserved at -80ºC. It was further diluted in fully supplemented DMEM according to the experiment setting.

Cobalt chloride hexahydrate (Sigma Aldrich - Cat. No. C8661) was diluted in a distilled water base of 200mM stock solution. The concentration was confirmed with ICP-AES and diluted as stated in each experiment in fully supplemented DMEM.

Trolox ((±)-6-Hydroxy-2,5,7,8-tetramethylchromane-2-carboxylic acid 97%, Sigma Aldrich Cat No. 238813) was obtained from Sigma Aldrich and dissolved in DMSO to form a stock concentration of 40 µM, which was aliquoted and kept at -80º C. For the experiments, it was further diluted in fully supplemented media.

2.2 **Methods**

2.2.1 **Cell Culture**

Human keratinocyte like cells (HaCaTs) and primary human dermal fibroblasts (HDFs) were obtained from ECACC and ATCC correspondingly and were used in the passage range of (4-20). Cells were cultured in Dulbecco's Modified Eagle Media (DMEM) (1g/L glucose), supplemented with 10% Foetal Bovine Serum (FBS) and 1% Penicillin Streptomycin under normoxic (20% O_2) conditions at 37º C in 150cm^2 flasks (all cell culture reagents were obtained from GIBCO® Thermo Fisher unless otherwise stated) and passaged prior to confluence (70-80%). For hyperglycaemic preconditioning cells were cultured in in high glucose DMEM 4.5 g/L (25 mM) purchased from GIBCO® Thermo Fisher. In the experiments requiring 9 g/L glucose, 4.5 grs/L of D-glucose (Sigma Aldrich - Cat. No. G7021) was added to 4.5 g/L DMEM and filtered through a PES (Polyethylene system) filter.

2.2.2 **Oxygen Exposure**

For standard normoxic cell culture (20% O_2, 5% CO_2) a Sanyo incubator at 37ºC was used. For hypoxia exposure cells were cultured in either 1 or 2% O_2 (5% CO_2 and the remaining nitrogen) oxygen regulating incubators (a New Brunswick Scientific Innova CO 48 and Binder CB 60 EG at 37ºC) were used. For the duration of the experiment, conditioned media was kept in flask at the same oxygen level as the plate where it would be added, in order to reduce the thermal and oxygenating stress that the change of media could produce

Hyperoxygen exposure (100%) - Hyperoxygen chamber construction.

For high oxygen pressure exposure (to measure cell survival) a custom oxygen chamber was created (Figure 2-1), whereby inlet and outlet butterfly valves (WPI Inc.) were inserted and sealed at opposite sides of a rectangular 5.5 L airtight 13" x 9" x 4" box (Lakeland®). An additional unidirectional valve was inserted to control interior pressure. Oxygen (100%) was then flushed into the box for 5 min at a flow rate of 5.5 L per minute. The interior oxygen percentage was measured with a MicroX 4 fiber optic oxygen meter (PreSens®), whilst the maintenance of atmospheric pressure after oxygen was confirmed by using a Comark®C9557 Pressure Meter.

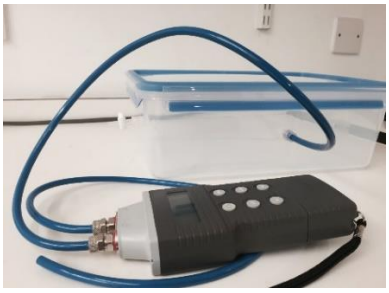

Figure 2-1 Hyperoxygen chamber. A 5.5 L airtight box was adapted to expose the cells to 100% O_2.

2.2.3 **Cell Viability and Metabolic Activity Quantification**

In order to assess cell metabolic activity an alamarBlue® Cell Viability Assay (ThermoFisher Scientific) was used. This assay was selected for its sensitivity and because it does not harm the cells, allowing continuing experimentation. The alamarBlue® assay is based on resazurin, which is a blue non-fluorescent cell permeable compound. After entering the cell reduces the resazurin to resorufin, a highly fluorescent red compound. This effect is due to the reducing environment of the cytosol in viable cells. The amount of fluorescence is proportional to the metabolic active of the cells. The assay was performed protected from direct light and under sterile conditions. Prior to the experiment, the alamarBlue® agent (as purchased) was diluted 1:10 in DMEM in sterile conditions. The dilution media used was conditioned to the testing variable/compound unless otherwise stated. The media present in the cell plate was gently removed and replaced with 500 microliters of alamarBlue® media. A no cell control sample was kept as an assay blank. Experiments with HDF were incubated for 4 hr, while HaCaT experiments were incubated for 3 hr due to their higher metabolic nature and cell number, in the correspondent oxygen condition unless specified. After the appropriate time period (3 or 4 hr) 200µl were transferred to a 96 black well plate and Fluorescence was read at an exaltation wavelength of 530 nm and emission wavelength of 620 nm using the microplate reader Fluoroskan Ascent FL, Thermo Labsystems, UK.

2.2.4 **DNA Quantitation and Cell Proliferation**

DNA present in the experimental wells was quantified as a determinant of cell number and overtime as a measurement of cell proliferation. This assay allowed the normalization of cell behaviour to cell number (e.g. metabolic activity/unit of DNA, HIF-1α stabilisation/unit of DNA and VEGF production/unit of DNA). The DNA Quantitation Kit from Sigma Aldrich was used as per manufacturer guidelines. The assay is based on Hoechst 33258 dye which binds to AT sequences of double stranded DNA. When excited at 360 nm, Hoechst emits fluorescence at 460 nm. The fluorescence

increases in a linear trend to the presence of DNA. Calf thymus DNA is provided for the DNA standard curve. The DNA stock solution (10 µgr/ml) is prepared according to the manufacturer's protocol by mixing 1% calf thymus DNA, 10% 10x fluorescent assay buffer and 89% molecular biology grade water. Multiple vials with were prepared and frozen to minimize experimental variation. The cells were prepared for DNA quantitation by removal of experimental media, washing with PBS followed by the addition of 200µl of molecular biology grade water to each well. The cells were then lysed by freeze and thaw method, prior to quantification.

On the experimental day, the cells were thawed once again. The DNA stock solution was serial diluted 1:1 in 250µl of 1x Assay Buffer to produce the standard curve. The Hoechst solution was prepared by diluting 1:1000 the Hoechst dye in 1x Assay Buffer. Then 50 microliters of the standard curve and sample were transferred to a 96 black well plate and 50 microliters of the Hoechst dye was added. The plates were read with the microplate reader (Fluoroskan Ascent FL, Thermo Labsystems, UK) at Ex. 355 nm and Em. 460 nm wavelengths. The standard curve was plotted against the relative fluorescence units. The least squares regression equation for the line was generated. The values were then converted to DNA concentration in relation to the standard curve.

2.2.5 **ELISA- Immunoassay analysis for MMP-9 and VEGF**

The ELISA Quantikine for Human VEGF and MMP-9 (Cat no. DVE00 and DMP900) were bought from R&D Biotechne® and used according to manufacturer's instructions. Cell supernatants were collected at the time points described in each experimental chapter and kept frozen at -20º C until analysed. Two hrs prior to analysis the samples were brought to room temperature and centrifuged for 5 min at 4º C at 250 x g.

The standard curves and assay were performed according to the protocol, and deionised water was used to prepare the washing buffer. The optical density was determined using a plate reader Tecan Infinite M200 PRO set to 450nm and with a wavelength correction of 540nm. The standard curve was plotted after subtracting the average zero optical density. The optical density of the samples was then converted in relation to the standard curve.

2.2.6 **Cytotoxicity- Toxilight Assay**

Toxilight™ bioassay kit and Toxilight™ 100% lysis reagent set were purchased from Lonza. The assay is based on measuring the adenylate kinase (AK) released from

damaged membrane cells, which will convert the added ADP into ATP. An enzyme luciferase then will catalyse the formation of light, which is linearly related to the AK concentration. An adaptation to the protocol was made in order to measure the intracellular AK and the one present in the supernatant.

HaCaT cells (Human, Adult, low Calcium, high Temperature, human skin keratinocyte) were seeded at a concentration of 20 000 cells per cm^2. Following attachment overnight, the cells were treated according to the oxygen and HIF mimetic conditions. At the defined time point, 50µL of the supernatant was transferred into another plate where 25µL of lysing buffer was added. The rest of the media was collected on a separate plate for later evaluation.

Then 100µL of lysing media were added to the experimental wells. The cells were incubated for 10 minutes to allow complete lysis and 50µL were transferred to a new plate, where 175µL of the balancing solution were added. At this stage a vial of the AK detection reagent was reconstituted in 12 ml of assay buffer. Finally, 20µL of the cell lysates or supernatant preparations were transferred into a white plate, where 100µL of the AK detection reagent was added and incubated for 10 minutes and luminescence read with the Tecan Infinite M200 PRO.

2.2.7 **Reactive Oxygen Species**

Reactive Oxygen Species are a by-product of the cellular respiration and are involved in cell signalling and homeostasis. ROS can be increased as a result of oxidative stress (in inflammation, disease and hypoxia). An excess of ROS production may result in lipid, DNA, RNA and proteins damage that can result in cellular dysfunction or death. Meanwhile healthy cells have different mechanisms through which they balance or ameliorate the possible damage occasioned by ROS.

The H2DCFDA dye (2′,7′-Dichlorodihydrofluorescein diacetate, SIGMA) was used to detect hydrogen peroxide, peroxyl radicals, and peroxynitrite anions. The acetate groups in the dye are cleaved intracellularly by the esterases and oxidation products converting the non-fluorescent H2DCFDA into fluorescent DCF. The dye was dissolved in methanol at stock concentration of 20 mM and aliquoted under nitrogen conditions. Cells were plated in 96 well plates at a concentration of 22500 cells/cm^2 for HDF and 48 000/cm^2 for HaCaT and allowed cell attachment overnight. As a positive control, a solution of Hydrogen Peroxide H_2O_2 (800µM for HDF and 400µM for HaCaT) was added 30 min before the time point. Briefly, before the reading, the

H2DCFDA dye stock was diluted in warm sterile PBS for a final concentration of 10µM and protected from the light.

The conditioned media was carefully removed and 100µl of the working H2DCFDA solution was added to each well and incubated in dark for 30 mins. Then, 90µl of each sample and control were transferred to a black 96 well plate. The assay was read with the microplate reader (Fluoroskan Ascent FL, Thermo Labsystems, UK) at Ex. 485nm and Em. 538nm wavelengths.

2.2.8 **Antioxidant Assay**

The Antioxidant Assay Kit was obtained from Sigma-Aldrich (Cat no. CS0790). The principle of the assay is measuring the total antioxidant through the formation of ferryl-myoglobin radical which oxidise ABTS. The radical is formed from the interaction between the sample, the metmyoglobin and hydrogen peroxide. The colour intensity is decreased proportionally to the antioxidant capacity and compared to the antioxidant capacity of Trolox, a water-soluble analogue for vitamin E.

HaCaT cells were seeded at a concentration of 100 000 cells/cm^2 in 1 ml of media. The cells were allowed to attach overnight in a normoxic incubator. The following day the cell media was replaced under the conditions described in each experimental chapter. The samples were prepared by adding 200 µL of cold lysis buffer after the removal of the supernatant. The cells were scratched with a pipette tip and sonicated on ice for 10 mins. The samples were then centrifuged at 12 000 x g for 15 min at 4ºC. The lysate was kept on ice while the Trolox standard curve was prepared. Ten microliters of the sample or standard curve were transferred into a clear plate, followed by the addition of 20 µL of the myoglobin working solution. Then 150µL of freshly prepared ABTS substrate working solution was added into each well. It was incubated for 4 min at room temperature and protected from light when 100µL of stop solution was added. The absorbance was promptly read at 405nm using the plate reader Tecan Infinite M200 PRO. The whole assay was run on ice to prevent degradation.

Table 2-1 Antioxidant assay solutions

Myoglobin Solution	The contents of the vial were diluted in 285 µL of ultrapure water and vortexed. It was aliquoted and stored at -20º C.
Working Solution:	The stock solution was diluted 100 times in 1X Assay Buffer.
Trolox Working Solution	Trolox was reconstituted in 2.67 ml of 1x Assay Buffer to obtain a 1.5 mM concentration. The standard curve

	was produced according to the dilution factors stablished in the protocol.
ABTS Substrate Solution	An ABTS substrate tablet and a Phosphate-citrate buffer tablet were dissolved in 100 ml of ultrapure water.
Working Solution:	25 µL of 3% H_2O_2 were added to 10 ml of ABTS substrate solution, this solution was freshly prepared for each experiment.

2.2.9 **Fluorescence staining**

The cells were seeded on glass at 15 000 cells/cm^2 and incubated overnight at 37º C under normoxic condition. The following day, the media were replaced and conditioned according to the experiment. At the time point, medium was removed, and the cells were washed twice with PBS, then fixed for 20 min with 4% formaldehyde in 1X PBS pH 7.4. The formaldehyde was removed, and the cells were washed twice with PBS.

The membranes were stained by incubating at room temperature for one hour with wheat germ agglutinin Alexa Fluor™ 594 conjugate (10µg/mL) in PBS (pH 7.4, Sigma). The cells were washed twice with PBS (0.5 mL each) and then mounted by inverting the cover-glasses cells-side-down onto a rectangular glass slide containing a droplet of Prolong™ Diamond Antifade mountant with DAPI. The glass slides were stored flat, in the dark overnight, allowing the mountant to solidify. The edges of the coverglass were sealed with enamel. The samples were imaged using a Nikon Eclipse Ti microscope. HaCaTs were imaged using a 60X oil immersion lens and HDFs at 40X objective.

2.2.10 **Cell size measurement and analysis**

HaCaT cell size area (µm^2) in euglycaemic and hyperglycaemia (normoxia) was quantified after fluorescence staining and imaging using the ImageJ software from the National Institutes of Health and the Laboratory for Optical and Computational Instrumentation and freely available. The single cellular bodies (red- wheat germ agglutinin Alexa Fluor™ 594) were identified manually. Cells that were in the edges of the images or when the borders not were clearly defined were excluded.

To evaluate the variance in the cell size, student t-test of unequal variance was performed.

2.2.11 **HIF-1α protein quantification**

2.2.11.1 *Sample Preparation*

To determine HIF-1α stabilisation, the amount of functionalised HIF-1α within the nucleus was determined. To obtain a sufficient amount of HIF-1α for detection cells were grown in 75 or 150cm^2 flasks. The Nuclear Extract Kit (Active Motif Cat No. 40010) was used for nuclear extraction according to the manufacturers' protocol. All the steps were performed on ice with cold reagents and tubes. Cells were firstly washed with the PBS/Phosphatase Inhibitor Solution and collected in the same solution by cell scraping. The cell suspension was then centrifuged 200*g* for 10 min in a pre-chilled centrifuge at 4°C. The supernatant discarded and the pellets were frozen at -80°C.

Cytoplasmic Fraction Collection

After collection of all time points, cell pellets were re-suspended in 1X Hypotonic buffer, transferred into pre-cooled vials and incubated for 20 min before the addition of the detergent. Cells were vortexed for 10 secs at the highest speed and later centrifuged at 4°C in at 14000*g* for 30 sec. The cytoplasmic fraction –supernatant- was transferred to a second vial and frozen at -80°C.

Nuclear Fraction Collection

The resulting cell pellets were resuspended in Complete Lysis Buffer followed by high speed vortexing. The samples were incubated on ice on a shacking platform for 30 min. The samples were centrifuged at 14000 x *g* for 10 min at 4°C. The nuclear fraction –supernatant- was transferred into a pre-cooled vial and frozen.

Table 2-2 Nuclear extraction solutions

PBS/Phosphatase Inhibitor Solution	10% 10X PBS, 5% Phosphatase inhibitors 85% distilled water
1x Hypotonic Buffer	10% 10X Hypotonic Buffer 90% Distilled Water
Complete Lysis Buffer	9.7% 10 mM DTT 86% Lysis Buffer AM1 1% Protease Inhibitor Cocktail 3.3% Detergent

2.2.11.2 *HIF-1α ELISA*

The Human/Mouse Total HIF-1α Duo Set® IC ELISA (R&D Cat No. DYC1935) was used to determine HIF-1α stabilisation after nuclear extraction. The principle of the assay is the sandwich ELISA, which specifically binds to the protein of interest with an immobilized capture antibody. The assay was performed according to the manufacturer's protocol, with the slight modification the samples and standard curve were incubated for 4hr to increase sensitivity. The samples were added at a proportion of 1:1 to the Reagent Diluent.

After the Stop Solution was added, the plate optical density was determined using the Tecan Infinite M200 PRO at a wavelength of 450 nm with a correction wavelength of 540 nm. The standard curve was fitted to a four-parameter logistic curve with the aid of www.mycurvefit.com. The sample dilution was taken into consideration in the calculation of the results.

2.2.12 **Cell-cycle flow cytometry**

Cells were treated with conditioned media and exposed to the relevant oxygen, supernatant was removed at the end of the time point and placed in a FACS tube (to include floating dead cells in the analysis). The cells were washed with PBS and removed with trypsin/EDTA and added to the corresponding FACS tube. Samples were centrifuged for 5 min at 1700 rpm. The supernatant was carefully removed with a pipette and cells were washed again with 1m l of PBS. The cells were re-centrifuged at the same parameters. The PBS was removed once again and 2 ml of ice cold 70% ethanol (in deionised water) was added in a dropwise manner while vortexing and the samples were placed back in ice. The samples were centrifuged at 2 000 for 5 min. The supernatant was removed and 1 ml of PBS was added. Cells in each tube were counted and corrected to a density of 100 000/vial. Cells were centrifuged at 2 000 for 5 min and the PBS was gently removed. The cells were stained with 500µl of FxCycle™ PI/RNase Staining Solution (Invitrogen, Cat. No. F10797) and incubated at room temperature for 30 min.

Samples were analysed using BD LSRII Flow Cytometer. Only single cells were analysed and a number of with 30 000 events were recorded. The data was processed with FLowJo_V10.

Chapter 3. Diabetic wound model

3.1 **The diabetic model**

Improved *in vitro* models are needed to determine the validity of new treatments, improve translation, and help our understanding of disease and to reduce animal testing. There are a number of different in vitro diabetic models described in the literature but little consensus on which model is most appropriate, or in determining measures of successful mimicry of in vivo hyperglycaemic conditions. In vitro models for chronic, hyperglycaemic wounds, include various different cell types (keratinocyte,[287] fibroblast[288] or inflammatory cell), different origin of cells (primary, immortalised or cancerous), different glucose levels (1.98 g/ml to 18.015 g/ml),[289] differing durations of high glucose preconditioning,[290] whether osmolality is normalised or reflective of in vivo conditions, if insulin levels are reflective of the in vivo environment and if additional factors are added to induce the AGE products[291] found in diabetic (and elderly) patients (Figure 3-1 illustrates the number of differing in vitro parameters used to attempt to mimic the in vivo diabetic wound environment).

The variance of diabetic, hyperglycaemic in vitro models may partly reflect the differences observed in vivo, in diabetic patients with impaired wound healing. In vivo, fasting glucose levels above 7 mM are considered diabetic,[292] there is also greater fluctuations of glucose levels than in non-diabetic patients,[293] there is decreased response to hypoxia,[109] an increase in osmolality (275 to <295 mOsm/kg),[294] increased number of glycated molecules[295] and a range of insulin levels which also fluctuates (19±2 U/L in diabetics, 13±2 U/L in healthy patients)[296] (Figure *3-1*).

There is also a lack of standardisation within the literature in terms of appropriate measure to determine if the vitro environment induces a phenotype that is similar to native diabetic disease or not. Some measures include whether cells have similar metabolic profile[297] and if they normal adaptive responses to a drop in oxygen pressure by measuring VEGF[298,299] and HIF-1α stabilisation.[165,300]

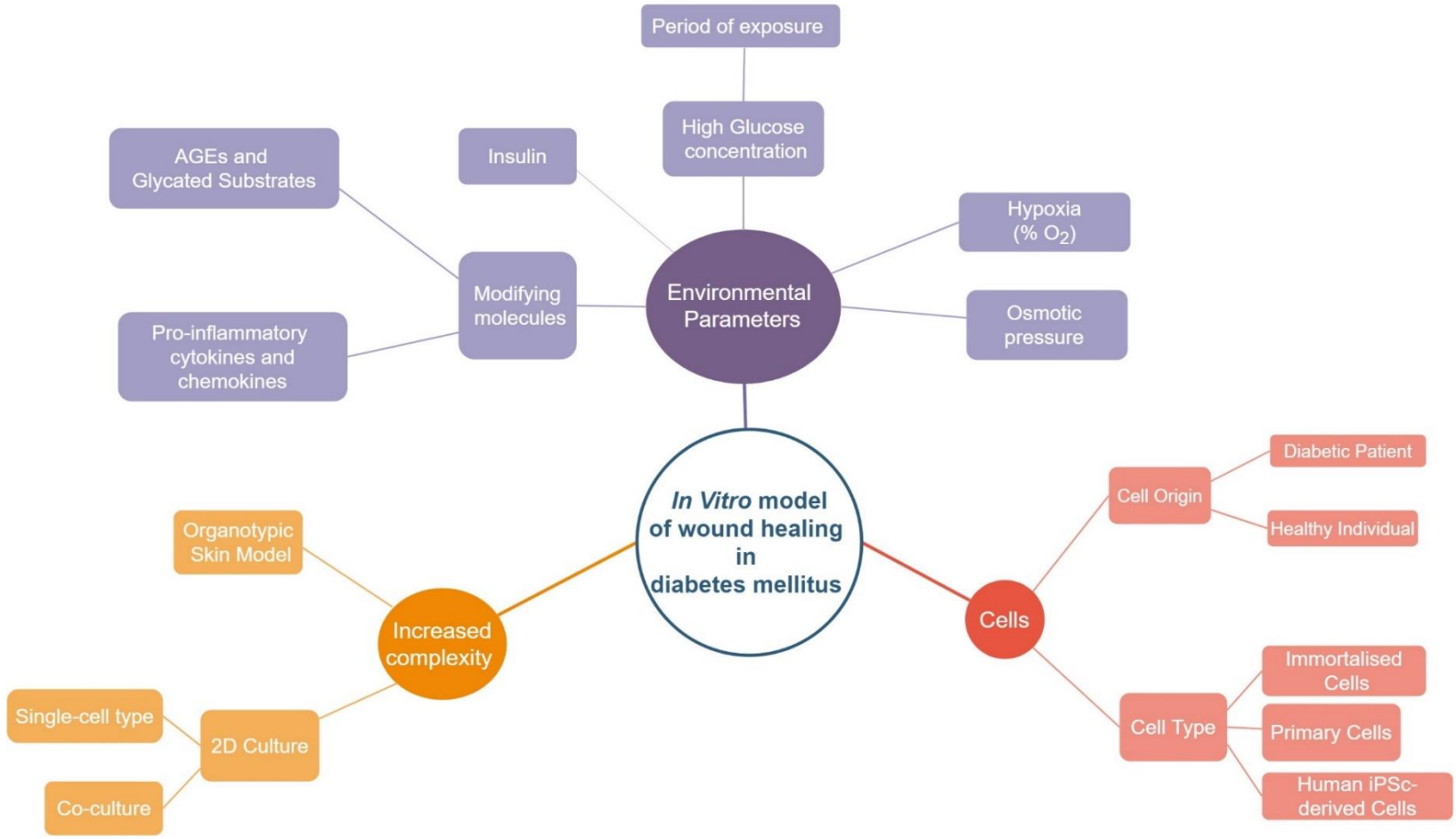

Figure 3-1 A summary of differing parameters used in vitro to mimic the diabetic in vivo wound environment. There are various parameters used to mimic differing aspects of the diabetic wound including, environmental parameters (glucose concentration and duration of high glucose exposure, insulin and osmotic pressure), types of cell (red) and complexity of in vitro model (orange). Oxygen pressure is often used to determine if cells have a normal cellular response to hypoxia.

3.1.1 **Cell type**

Fibroblasts and keratinocytes have been widely used in chronic wound healing *in vitro* models, as they are the major cellular components of epidermis and dermis. The use of keratinocytes is common to emulate wound healing and chronic inflammatory diseases as they represent 95% of the epidermal cells. They function as a barrier, a structure to the epidermis, and respond differently to a combination of stimuli as ROS, cytokines, calcium and oxygen gradients.[134,150,301–303] There is a wide variation in the cell species and origin of fibroblasts and keratinocytes in wound healing models. *In vivo* models of wound healing in mice are common, while numerous studies have used mouse cells *in vitro*. These models have contributed significantly to our understanding of skin pathologies and biology, and also allow the development of transgenic and knockout mice, which would not be possible with humans.[304–306] There are, however, differences between mouse and human wound healing responses, hypoxia response,[307] wound size, cell and epidermal proliferation and remodelling, and the species-specific interaction of the chemokines and cytokines,[308] as well as specific dendritic and epidermal cell subtypes and NK1.1$^+$ T cells present in mice skin -as reviewed by Mestas and Hughes 2004 and Gurtner et al. 2011. A major difference between human and mice healing is the presence of the panniculosus carnosus layer in mice skin, a thin muscle that produces a rapid wound contraction.[309] The presence of hair follicles is extensive in mice, whereas in human is highly variable; the hair cycle in mice is 3 weeks approximately, while in humans it can last several years.[310,311] For both fibroblasts and keratinocytes a number of host parameters have been shown to influence *in vitro* cell behaviour or wound healing response,[157,312] these include donor age,[313] underlying disease[156,157] anatomical location,[314] and if they smoke.[315] The method of isolation and purification may also determine if the population is a single cell type or a mixed population. There are, therefore, considerable advantages of using a well characterized immortalised cell line (such as HaCaTs), that have less variability than primary cell sources and enable grater comparisons with the literature (the difference between common cell lines used in skin studies as reviewed by Olschläger et al. (2009).

3.1.1.1 *HaCaT (Human, Adult, low Calcium, high Temperature, human skin keratinocyte)*

HaCaT keratinocyte cells, are a transformed aneuploidy immortalised cell line commonly used in wound healing studies.[145,301,322–326,302,303,316–321] The HIF response in HaCaT cells has been previously reported and they have been demonstrated to

respond to hypoxia,[134,228,300,327–333] and increase the expression of VEGF in response to hypoxia (less than 1% O_2).[153,162,177,290,321,326,334] HaCaT cells have been demonstrated to have a similar cytokine/chemokine profile to primary keratinocytes when cultured in sub-confluent low Ca^{2+} medium but have a different inflammatory secretome when cultured in different Ca^{2+} levels and different serum levels.[303] Although differences in transcriptome expression[335] and abnormal epidermal ECM production has also been reported in 3D skin models *in vitro*.[336]

3.1.1.2 *HDF (Human Dermal Fibroblasts)*

Human dermal fibroblast (HDF) are spindle-like primary cells, which are easy to isolate from skin biopsies, easily cultured and maintained *in vitro*.[337]They produce several growth factors for wound healing process, including VEGF and FGF,[299,338–344] responding to oxygen levels below 2% O_2.[345] They have also been used to study the effect of high glucose (as a diabetic model) on cell behaviour,[185,291,349,299,312,340,342,345–348] and have been demonstrated (in the presence of high glucose) to have diminished HIF-1α stabilisation[345] and reduced VEGF expression, including the production of collagen similarly to that observed diabetes and ageing –i.e.. loss of collagen type I and III, increased MMP-1and fragmentation of fibrils.[189,190,193,291,350,351]

3.1.2 **Hyperglycaemia- Glucose level**

The terms euglycaemia or normoglycaemia are defined as glycaemic levels associated with low risk of developing diabetes or cardiovascular diseases, with the normal fasting plasma glucose level defined by the World Health Organisation as lower than 5.6mM glucose.[292] In a cohort study of 820,900 patients, the non-diabetic fasting glucose level was determined as 5.2±0.6mM , while diabetic patients ranged between 8.6±3.6mM.[352] Fasting glucose levels exceeding 5.6mM were associated with excess risk of death when compared with 3.9 to 5.6mM (0.7-1g/l); with fasting levels of 7.0mM (1.26g/l) glucose or above linked to substansially increased risk for cancer, vascular and non-cancer nonvascular deaths.[352] The glucose concentration in the subcutaneous tissue and cutaneous (and therefore the glucose levels exposed to cells involved in wound healing) has been found to resemble that of the plasma.[353]

Glucose levels influence the metabolism and proliferation rate of the cells. Rheinwald and Green (1974) first describe in vitro that that a lack of glucose inhibit cell function and caused a “decline in cell state”.[354] A high glucose environment has also been observed to alter cell behaviour, growth factor release profile, ECM formation and phenotypical characteristics[170,355,356] and these have been reported to be similar to

those presented in cells from diabetic patients and diabetic animal models.[162,170,357] Others have shown that fibroblast and keratinocyte migration is inhibited by high glucose levels.[356,358,359] Which may (in part) be due to the reduced expression of integrin subunits αv and α5, which when interacting with fibronectin, enable migration.[317,357] Moreover, there is a decrease in the capacity of the fibroblasts to secrete and adhere to fibronectin[342,357,360] and the contraction of the collagen matrices is also reduced.[355] A hyperglycaemic environment has also been shown to impair cell responsiveness to hypoxia similarly to when mimicking hypoxia through $CoCl_2$.[361] Hyperglycaemia inhibits the proteosomal degradation of HIF-1α under normoxic conditions inducing a pseudohypoxia.[362] Whilst VEGF expression is increased under normoxic hyperglycaemic conditions[109,191,363] (possibly through a ROS mechanism since it has been demonstrated that oxidative stress is also increased in hypoxia) a decreased angiogenic response to hypoxia in hyperglycaemia has been demonstrated[191,363] to decrease VEGF response which may explain the re-vascularisation and re-epithelisation observed in chronic wounds.[109,156]

Across literature research, 55 studies were found to report the effect of high glucose as opposed to a euglycaemic control in epidermal keratinocytes and dermal fibroblasts.[f] Among these, 29 studies addressed the effect on fibroblasts[77,109,347–349,355,356,359,364–367,163,368–371,185,288,289,312,323,342,346], 21 on keratinocytes[162,169,325,358,372–379,287,290,301,318,320–323] and 5[299,319,351,380] in both cell lines. While most of the studies report using as a euglycaemic control media containing between 5-10mM glucose, (average =5.6 ±0.7 mM), this is slightly higher than the in vivo "normal levels" reported by WHO (5.2±0.6mM). There is, however, great difference and variance in the glucose level to mimic the characteristically high glycaemic environment of diabetic patients, ranging from 11.1 to 100mM glucose, with an average of 27.9 ±14.4mM. Some authors also further classify glucose levels as low, medium-high and high glucose (10-25mM and 26+mM glucose). The average concentration of medium-high glucose was 20.8 ±5.6 mM and high 39.4 ±17.4 mM glucose (Figure 3-2). These levels vary from those observed in diabetic patients in vivo, in terms of both the concentration (8.6±3.6mM) and in terms of the fluctuation of glucose levels observed in untreated (and to a lesser extent treated) patients.[381]

[f] Web of Science Core Collection, Scopus and Pubmed search from 1997 to 2017 years, using the search terms (diabet* OR hyperglycem* OR "high glucose" OR high-glucose) AND (wound* OR ulcer*) AND (keratinocyte* OR fibroblast*) Non primary research papers were excluded. This was a contribution from Eleni Balli as part of her MSc research project.

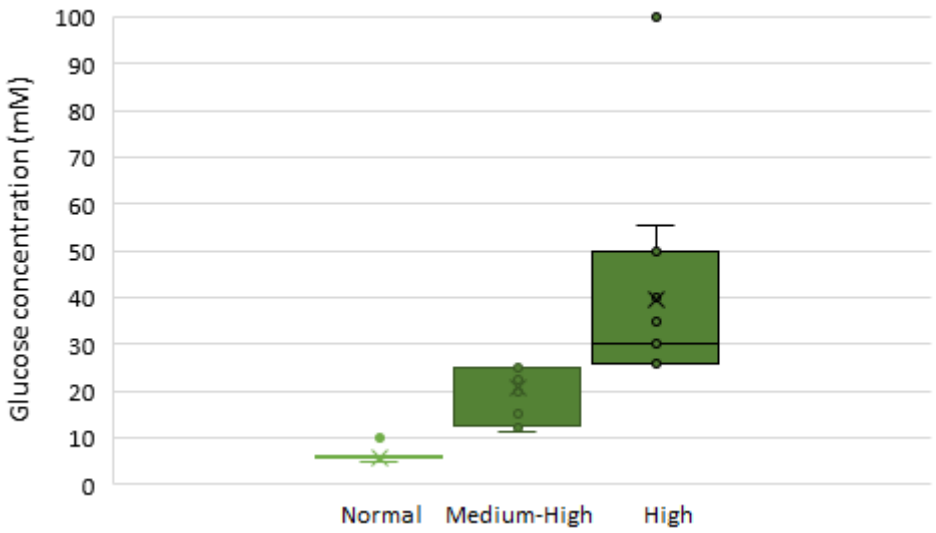

Figure 3-2 Box and Whisker plot representing the variance in glucose levels reported in the literature.[(f)] The average glucose levels used to mimic normal healthy individuals is 5.6±0.7mM, Medium-High 20.8 ±5.6 mM and High 39.4 ±17.4mM. The middle line represents the median, while the x represents the mean. The ◦ represents the different single values, while ● the outlier values. The bottom line represents the median of the 1st quartile, while the top line the median of the 3rd quartile. The whiskers represent the minimum and maximum value.

3.1.3 **Preconditioning period**

There is also considerable variance in the exposure period to high glucose concentrations, before evaluation (the preconditioning time). The preconditioning time allows cells to adapt to high glucose environments (change metabolic activity, gene and protein expression), and better mimic *in vivo* cellular diabetic responses. The preconditioning time varies from 0 to 30 days in high glucose conditions (average=6.4±6.6 days). The absence of a preconditioning period (less than 0-12hours) will not allow for the accumulation of AGE molecules or reflect the longer-term effects of oxidative stress experienced by cells in hyperglycaemic conditions *in vivo*. Yu et al. (2006) reported that under prolonged hyperglycaemic environment there is a change in the morphology of mitochondria which leads to ROS overproduction; this mimics the presence of high levels of glucose in patients suffering with chronic diabetes.[382]

3.1.4 **Osmolarity**

Hyperglycaemia is also characterised by an increase in osmolarity, in stable diabetic patients the osmoregulatory is similar to healthy patients (275 to <295 mOsm/kg) with a normal sensitivity, whilst in hyperglycaemia (>6 g/L) osmolarity can by >320 mOsm/kg and is accompanied with dehydration. An increase in osmolarity is a complication more common in patients with diabetes type II, but also observed in

diabetic ketoacidosis.[294,383–385] Keating et al. (2003) reported the increase of platelet reactivity in a model using isosmotic concentrations of mannitol and glucose. Both sugars increased the platelet aggregation and degranulation, which is consistent to what is seen in hyperosmolar hyperglycaemia patients. Mannitol being a metabolically inactive agent, suggests that osmolarity also contributes to hyperglycaemic cell behaviour impairment.[386] An increase of osmolarity (through mannitol and NaCl) has also been reported to induce endothelial cell apoptosis, activating tyrosine and stress kinases and intracellular free Ca^{2+}.[387] In contrast, Lamers et al (2011) observed a decrease in cell migration in HaCaT cells after hyperglycaemic preconditioning, which was not observed when cells were grown under the same osmotic conditions with L-glucose. Likewise, the increase in reactive oxygen species, generated by the high levels of glucose (D-Glc), were found to be independent of osmotic pressure.[359]

3.1.5 **Advance Glycation End-Products for in vitro modelling diabetic wound healing**

Advance glycation end products (AGE) are a post-transcriptional modification of proteins and macromolecules by reduced sugars, described by the Maillard reaction (see section 1.6.3). They are a result of normal metabolism and naturally occurring but increased under increased oxidative stress and hyperglycaemia. The levels of AGE accumulate with increasing age[388] and in diabetes[389] and can be used as a predictor of a number of diseases including vascular diseases.[390] Methylglyoxal (MGO) is considered to be one of the most important AGE precursors.[295,391,392] MGO is highly reactive di-carbonil-aldehyde by-product of the glycolysis that reacts with proteins, lipoproteins and DNA through the arginine, lysine and cysteine residues. While MGO accumulation is regulated through the glyoxalase system (GLO1), however endogenous formation of AGE occurs slowly and affecting mainly long-life molecules, and forming part of the ageing process.[393,394] The concentration for reduced glutathione is decreased by oxidative stress and under hypoxia, which allows MGO to accumulate, activating stress and several inflammatory pathways.

In diabetes, AGE levels are higher when compared to healthy subjects. The capacity for albumin to scavenge free radicals and bind to copper is reduced, as albumin is modified through MGO-induced factors.[395,396] The accumulation of MGO in the extracellular matrix can leads to the modification of the collagen, increasing fibrosis, thus impairing cell migration.[389] Bento et al. (2010) reported intracellular accumulation of MGO after hyperglycaemic conditioning, followed of the reduction of the half-life of

the HIF-1a. When cells were treated with MGO for a brief period under hypoxic conditions, a similar impairment of the HIF-1a stabilisation was observed,

There are different mechanisms involved, beyond the scope of this thesis, one of the possible mechanisms of MGO interference with HIF stabilisation under high glucose conditions, is the modification of the lysine and arginine terminals of the P300 protein reducing the binding to HIF-1α, therefore inhibiting translocation into the nucleus. [109,168] There is increased interest in the use of advance glycation end products and glycated substrates as models for ageing and diabetic complications, being the most common AGE-inducers methylglyoxal, glucosepane and AGE-modified bovine serum albumin. [193,195,397–399,291,298,362,375,390,393,394,396]

3.1.6 **Oxygen condition**

Normally cells are cultured *in vitro* under normoxic oxygen condition, consisting of 19.95% O_2 (95% atmospheric air supplemented with 5% CO_2) and an oxygen partial pressure (pO_2) of 150mmHg (normobaric).[138] This condition contrasts to the oxygen pressure *in vivo*, which varies greatly across tissues and depending on the distance from blood vessels. In the skin, the arterial and venous supply is located in the hypodermis.[400] As the oxygenation is increased in depth, the pO_2 above the sub-papillary plexus (100-120 µm from surface) is 35.2 ±8.0 mmHg, 24.0±6.4mmHg in the dermal papillae (45-65 µm) and 8±3.2mmHg in the superficial region (5-10 µm) of the skin.[137] A study by Scheid et al. (2000) reported that the foetal sheep subcutaneous average pO_2 was 8.3mmHg (1.2% O_2 in gas phase) and had stabilised HIF-1α, similarly to the maximal expression seen at 0.5% O_2 *in vitro*. Meanwhile the adult subcutaneous pO_2 was 36.3mmHg (5% O_2) and did not stabilise HIF-1α.[401] In chronic wounds, it has been reported that the pO_2 is 5–20 mmHg, however it can be lower in de-vascularised central wound regions. It has been previously established that hypoxia activates the initial response of wound healing, through stabilising HIF pathway (see section 1.5.2). Whilst cells in hyperglycaemic conditions have an impaired response to hypoxia, which may lead to impaired wound healing. This is of particular importance as the oxygen requirements of the region increase drastically due to the metabolic demand of the inflammatory cells and that the antimicrobial activities (mediated by ROS) of these inflammatory cells also requires oxygen. This event can be related to diabetic patients having a reduced bacteria killing capacity.[402] The oxygen requirements vary across the different stages of wound healing ranging from 25 to 100 mmHg. While fibroblast require at least 15 mmHg to proliferate, in order to synthesise collagen a pO_2 between 30-40 mmHg is required.

Several studies have reported *in vitro* models of wound healing under a hypoxic environment in normal glucose levels. The method of inducing hypoxia varies across the literature and so does the duration. Some report the use of chambers at constant gas-flow that create the effect similar to an atmospheric composition of 0.5% O_2,[140,156,403,404] whilst the use of anaerobic incubation systems –in the form of bags and jars- that interact chemically with the oxygen releasing CO_2 have been reported.[77,371,405] CO_2 incubators are also used, where the selected oxygen concentration is obtained from atmospheric air, CO_2 is maintained at 5% and the rest is replaced by nitrogen.[168,331,406,407]

3.1.7 **Measuring Success in Diabetic models**

Diabetes affects multiple molecular mechanisms resulting in several comorbidities, thus, complicating the modelling of the disease. Broad considerations are made to evaluate which factors would model better the disease. (Table 3-1) High glucose conditioning, depending on the degree and preconditioning time, will trigger different pathways, inducing AGE accumulation, increased oxidative stress that would mimic the diabetic phenotype. One method to establish whether the *in vitro* model is behaving in a similar way to diabetic wound cells, is to determine if the hyperglycaemic conditioned cells have a diminished response to hypoxia,[109] as observed *in vivo*.[408]

Table 3-1 Diabetic phenotypical characteristics evaluated in diabetic models across literature search.[g]

	Measure of diabetic phenotype	Relevant percentage from literature[g]
Cell behaviour	Proliferation	25.5%
	Metabolic Activity (Viability)	20%
	Cell Migration	27.3%
	ROS	12.7%
	Antioxidant Capacity / Production	5.5%
Angiogenic factors	VEGF	16.4%
	HIF-1α	7.3%
	TGF-β	10.9%
	PDGF	7.3%
	IGF-1	9.1%
	FGF (bFGF, FGF-1, FGF-2)	10.9%
	SDF-1	5.5%

[g] Ibid., p.42

Inflammatory response	TNF-α	7.3%
	IL-1	7.3%
	IL-8	7.3%
ECM interactions	MMP-9	12.7%
	Trans-membrane Proteins	9.1%
	Collagen (contraction & characterisation)	10.9%

3.2 Chapter Aims

Considering the lack of standardisation and often conflicting experimental methodologies reported in vitro, this chapter developed an in vitro hyperglycaemic model and will be used as a platform in future chapters to see if HIF mimetics can restore the normal hypoxia in hyperglycaemic condition.

This chapter investigated:

1. How hyperglycaemia and hypoxia effects the growth, metabolic activity and VEGF (and HIF stabilisation) production of cells important in wound healing (keratinocytes and fibroblasts).
2. The duration of hyperglycaemic pre-condition needed to diminish the hypoxic response (measured in terms of VEGF production and inhibited HIF-1α stabilisation).
3. The effect of Advance Glycation End Products in mimicking the effect of prolonged hyperglycaemia.

3.3 Methods

3.3.1 Does hyperglycaemia preconditioning create a model with an inhibited response to hypoxia in a similar manner to cells in diabetic patients?

HaCaT and HDF cells lines were grown and maintained in Dulbecco's Modified Eagle Media (DMEM) 1g/L glucose (4.5mM), supplemented with 10% Foetal Bovine Serum and 1% Penicillin Streptomycin under normoxia conditions (see 2.2.1). This glucose condition will be referred as euglycaemic and is comparable to a clinically chronic diabetic patient. [177,362,409] To mimic the hyperglycaemic environment cells were cultured in 4.5 g/L glucose DMEM for differing periods of time (6 hours to 28 days). This glucose level was selected based on *in vivo* diabetic conditions and to be comparable to previous hyperglycaemic models (see Figure 3-2). HDFs were also

cultured in 9 g/L glucose (high glucose) as previously used in other *in vitro* models (Figure 3-2).

HaCaT cells (passage number between 10 and 25) were seeded at a 20,000 cells/ cm^2, while HDFs (passage number between 10 and 20) were seeded at 10,000 cells/ cm^2. Cell number, metabolic activity and VEGF production (using the methodology described in sections 2.2.3, 2.2.4, 2.2.5) was examined in these glucose conditions in both normoxia and hypoxia. Cells were then preconditioned in 4.5 g/L or 9g/L glucose for different periods of time (Figure 3-3) under normoxic conditions, while cells kept at 1g/L glucose (euglycaemia) were used as controls. Cell culture media was replaced every 48 hours and cells were passaged during the preconditioning period when 80% confluence was reached.

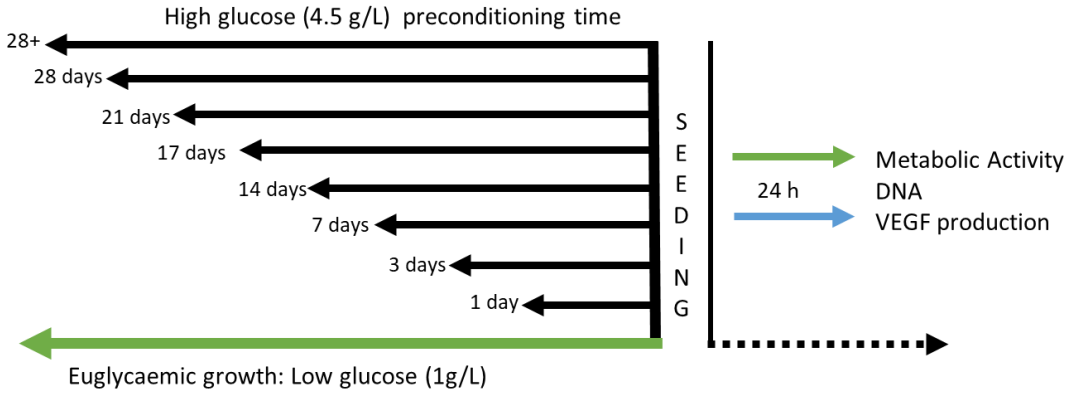

Figure 3-3 Experimental diagram for HDF diabetic model. Before seeding the experimental plates, cells were preconditioned in 4.5 g/L glucose for 28,21,14,7,3 and 1 days. Cells were allowed attachment overnight and media was replenished the following day. The plates were then seeded on to experimental plates and placed under normoxic or hypoxic conditions (1 and 2% O_2) for 24 hours and then the number of cells, metabolic activity, DNA quantification and VEGF expression was assessed.

3.3.2 **MMP-9 ELISA**

Cell culture supernatants were collected after 48 hours of oxygen conditioning to allow detectable levels of protein and frozen for later analysis. The samples were thawed, vortexed for 5 seconds and centrifuged at 250 x g for 5 minutes prior to MMP-9 quantification as described in section 2.2.5.

3.3.3 **Advance Glycation End Products as a model for Hyperglycaemia**

After modification of the protocol described by Bento et al (2010), in order to induce AGE formation, the precursor methylglyoxal was included. Cells were incubated with 500 µM MGO for a period of 4 hours. The supernatant was then replaced with 500 µL of glucose-conditioned DMEM. The media was collected after 6 and 24 hours for

VEGF measurement and plates were prepared for DNA quantification as described in sections 2.2.5 and 2.2.4.

3.3.4 **ROS activity and Antioxidant capacity**

Considering the known increase in ROS production and decrease in antioxidant capacity in cells within diabetic patients[176] these outcomes were also measured in the in vitro hyperglycaemic model described above Cell antioxidant capacity after high glucose preconditioning was measured with the Antioxidant Assay Kit (Sigma-Aldrich, UK) as described in section 2.2.8. Following preconditioning and hypoxia exposure, the antioxidant activity in the sample was assessed by the ability to supress the production of the radical cation after the addition of H_2O_2, a vitamin E analogue, was used as a standard antioxidant reference.

In order to test the effect of glucose and MGO (500µM) in ROS generation, the conditions evaluated were prepared in pyruvate-free DMEM and incubated at the normoxia incubator to allow stabilisation. The MGO applied and the cells incubated for 4 hours in hypoxia or normoxia. The ROS measurement was performed using a 2′,7′-Dichlorodihydrofluorescein diacetate dye (SIGMA) as described in Section 2.2.7.

3.3.5 **HIF-1α stabilisation assay**

In order to evaluate the impaired response to hypoxia HIF-1α was performed. Cells preconditioned to 4.5 g/L and 1/g/L glucose were seeded in a density of 4000 cells/cm^2 and placed in a normoxic (20% O_2) incubator for two days. The media was replenished, and the flasks were placed under normoxic or hypoxic (1% O_2) conditions accordingly. Nuclear extraction was done after 24 or 72 hours of oxygen exposure using Nuclear Extract Kit (Active Motif, US) described in section 2.2.11.1 and frozen at -80 ºC. The nuclear protein extracted (total) was measured with a Thermo Scientific NanoDrop™ Spectrophotometer to confirm successful nuclear extraction. HIF-1α protein quantitation by Human/Mouse Total HIF-1α Duo Set® IC ELISA (R&D, US) as described in section 2.2.11.2

3.3.6 **Fluorescence staining and cell size measurements**

The cells were seeded on glass at 15 000 cells/cm^2 and allowed attachment overnight at 37º C under normoxic condition. The following day, the media was replaced and cells were subjected to the corresponding oxygen condition for 24 hours. Cells were stained for cell membrane with wheat germ agglutinin Alexa Fluor™ 594 conjugate

and DAPI for nucleus as described in section 2.2.9. Glass slides were mounted on coverslips as described and imaged using Nikon Eclipse Ti microscope. HaCaTs were imaged using a 60X oil immersion lens and HDFs at 40X objective.

Cell size area was measured (6 photos taken from 3 replicates) with ImageJ (National Institutes of Health and the Laboratory for Optical and Computational Instrumentation).

3.3.7 **Statistical Analysis**

Experiments were repeated twice along with the controls, with 6 replicates each. In the case of the HIF-1α protein ELISA, the experiment was ran once with 3 repeats. Outliers were removed using the modified Thompson Tau test. Error bars represent standard deviation. The experimental data was analysed using Prism Graphpad. The data was checked to see whether it was required to use parametric or non-parametric tests by Pearson and Spearman's test. Comparison between two individual data sets, was made using Student's t-test. More dataset comparisons were made using the one-way Anova, or two-way Anova when appropriate, followed by Bonferroni. Mean and standard deviation were used. The representative experiments were selected for this chapter.

3.4 Results

3.4.1 Does short-term exposure to hyperglycaemia affect cell metabolism and VEGF expression?

Hyperglycaemia caused a moderate increase in metabolic activity in HaCaT's cultured in hypoxia (1% O_2) (p=0.01) but not in normoxia (Figure ***3-4***a). Hyperglycaemia culture caused a ~2.5-fold increase in VEGF production in both normoxia and hypoxia culture (Figure ***3-4***b). The increase of VEGF in hyperglycaemia normoxia was similar to hypoxia under euglycaemic conditions, however, hypoxia increased VEGF production in both glycaemic conditions (p=0.001) after 6 hours culture. VEGF data was normalised to cell number (total DNA) but there was no difference observed in total DNA after 6 hr culture (data not shown).

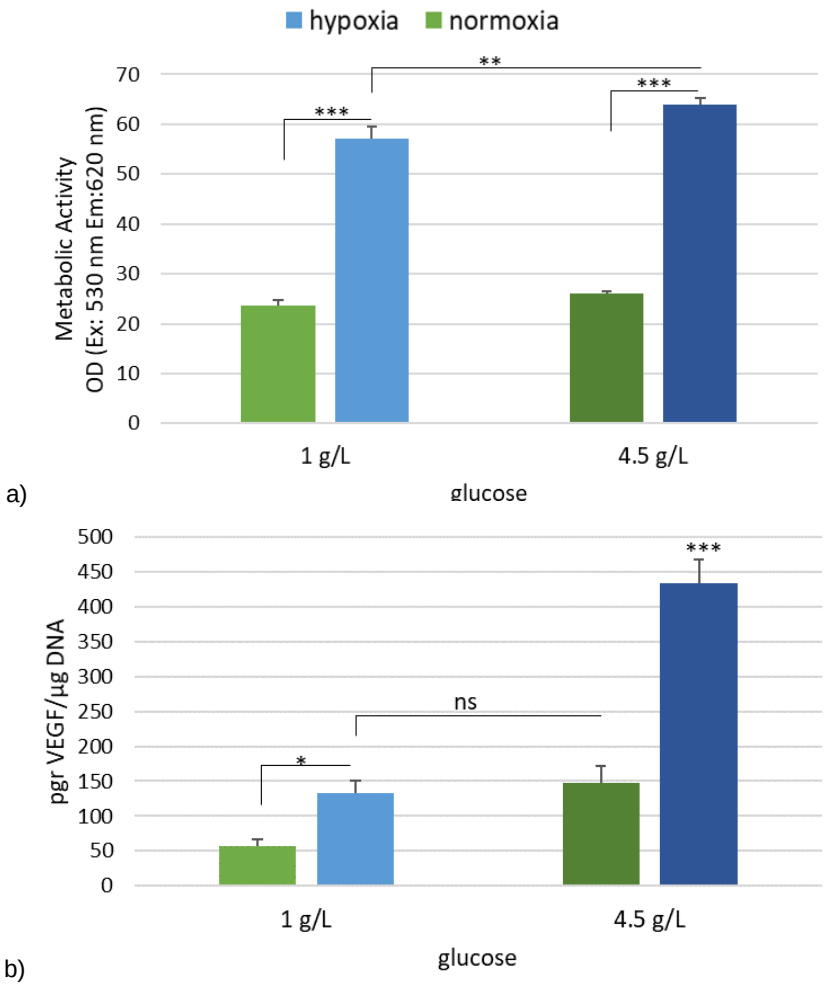

Figure 3-4 Hypoxia and hyperglycaemia increase VEGF secretion. Hypoxia (1% O_2) is represented by blue, whilst normoxia (20% O_2) with green. Hypoxia increased metabolic activity and VEGF production. After 6-hour hyperglycaemic treatment (4.5 g/L Glc) caused an increase in VEGF production in both normoxia and hypoxia (p=0.001) There were no differences in total DNA after 6 hours (data not shown). Error bars= SD, n=6, *p<0.05, ***p>0.001, ns=p>0.5.

3.4.2 Can hyperglycaemic preconditioning impair response to hypoxia in HaCaT cell line?

3.4.2.1 *Hyperglycaemia reduces cell proliferation and alters metabolic activity*

The metabolic switch is noticeable at day 3 (Figure 3-5a), where the metabolic activity of euglycaemic cells is decreased as a response to hypoxia ($p<0.01$), meanwhile hyperglycaemic hypoxic cells remain with an increased metabolic state, significantly higher ($p< 0.001$) than normoxic cells. As the glucose-conditioned media was replaced throughout the experiment, there is no glucose depletion due to high consumption.

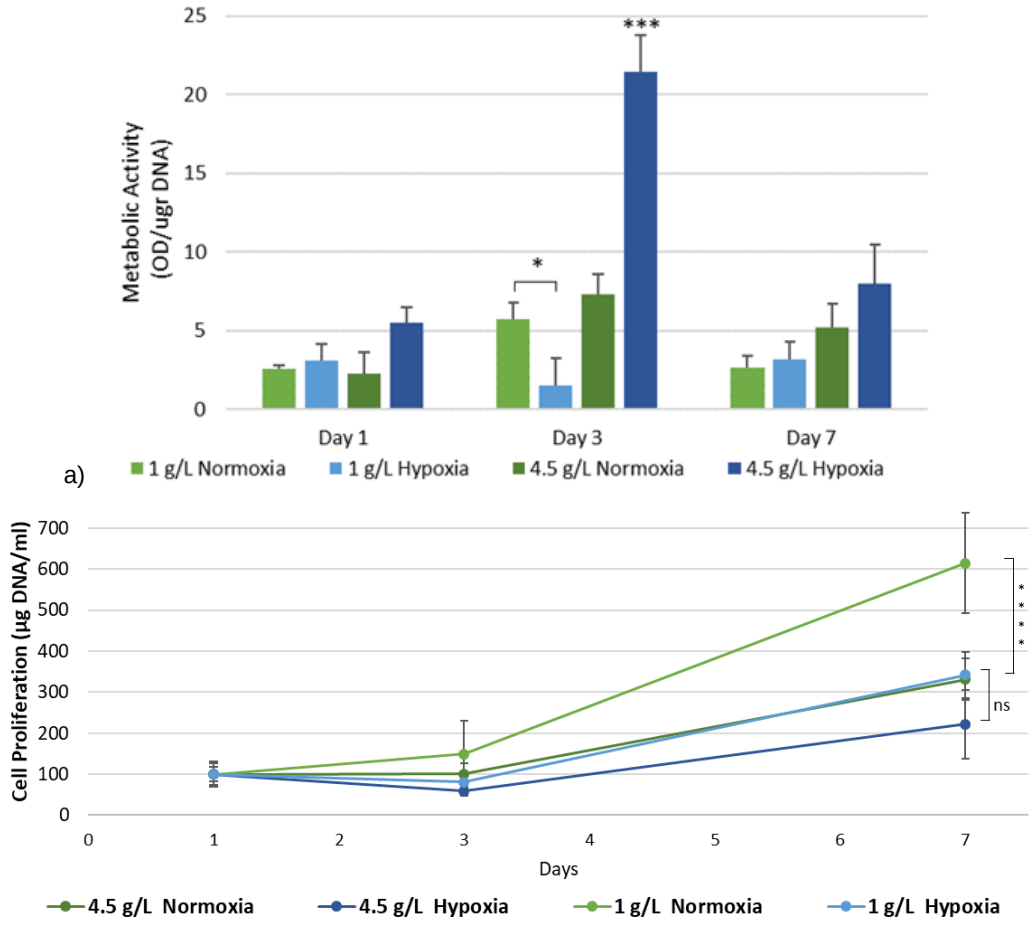

Figure 3-5 Hyperglycaemia reduces cell proliferation in normoxic and hypoxic environment as quantified by Hoechst dye. The chronic exposure to high glucose concentrations alters the metabolic state of HaCaT cells under low oxygen conditions, measured with Alamar Blue®. Error bars = Standard deviation, n=12, *p<0.05, *** p>0.0001.

Cells were able to proliferate in both glycaemic conditions and at normoxia and hypoxia. Euglycaemic cells were able to grow as normal (Figure 3-5b) and a significant decrease in cell proliferation was seen under a hypoxic environment by day 7 ($p<0.0001$). Cells preconditioned for 28 days at 4.5 g/L glucose had a lower

proliferation rate under normoxia conditions, similar to the hypoxic euglycaemic cells. Hyperglycaemic hypoxic cells had a lower proliferation rate, non-significant different to the ones with a reduced proliferation ratio.

3.4.2.2 *Hyperglycaemia decreases response to hypoxia*

HaCaT cells were able to replicate the dysfunctional response of hyperglycaemic cells to hypoxia. Cells were preconditioned for 28 days in 4.5 g/L glucose. The increase of VEGF (Figure 3-6) was seen to be significant under euglycaemic conditions ($p<0.05$), whilst under high glucose the VEGF increase was found non-significant.

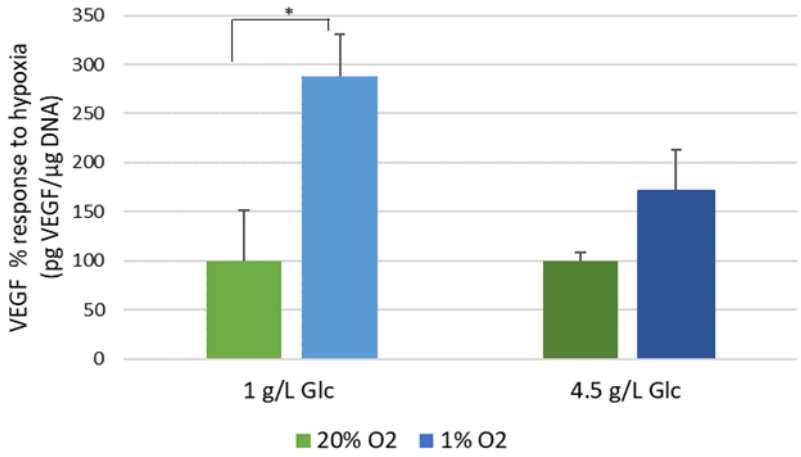

Figure 3-6 VEGF expression response to hypoxia was decreased in hyperglycaemic HaCaT cells as quantified by ELISA. Euglycaemic cells had an increase ($p<0.05$) in VEGF expression after 24 hours of hypoxic environment, meanwhile the hyperglycaemic cells (28 days preconditioning) did not increased VEGF production. Error bars = standard deviation, n=6, *$p<0.05$.

The stabilisation and activation of the HIF pathway is reflected in an increase in the VEGF expression, therefore the changes in VEGF will be used as a representation of the HIF pathway changes. Hyperglycaemic-preconditioned keratinocytes had a reduced response in HIF stabilisation after 3 days of exposure to 1% O_2 (Figure 3-6). Under normoxic conditions, nuclear HIF 1α molecule was increased in the hyperglycaemic condition when compared to the euglycaemic control (Figure 3-7), suggesting cellular hypoxia as a result of increased oxygen consumption in the mitochondria. Whilst the HIF protein level detected for euglycaemic cells remains constant at day 1 and day 3, there is a decrease at day 3 for hyperglycaemic cells. This decrease could be related to the consumption of the glucose due to the altered metabolic state. At day 1, both glycaemic conditions were able to stabilise HIF as a response to hypoxia. The increase of nuclear HIF protein for euglycaemic cells was higher than the diabetic model, seeing a reduction of HIF protein in hypoxia day 3 in

oxygen conditions; however, the HIF protein in high glucose hypoxic cells was lower than the normoxic pair.

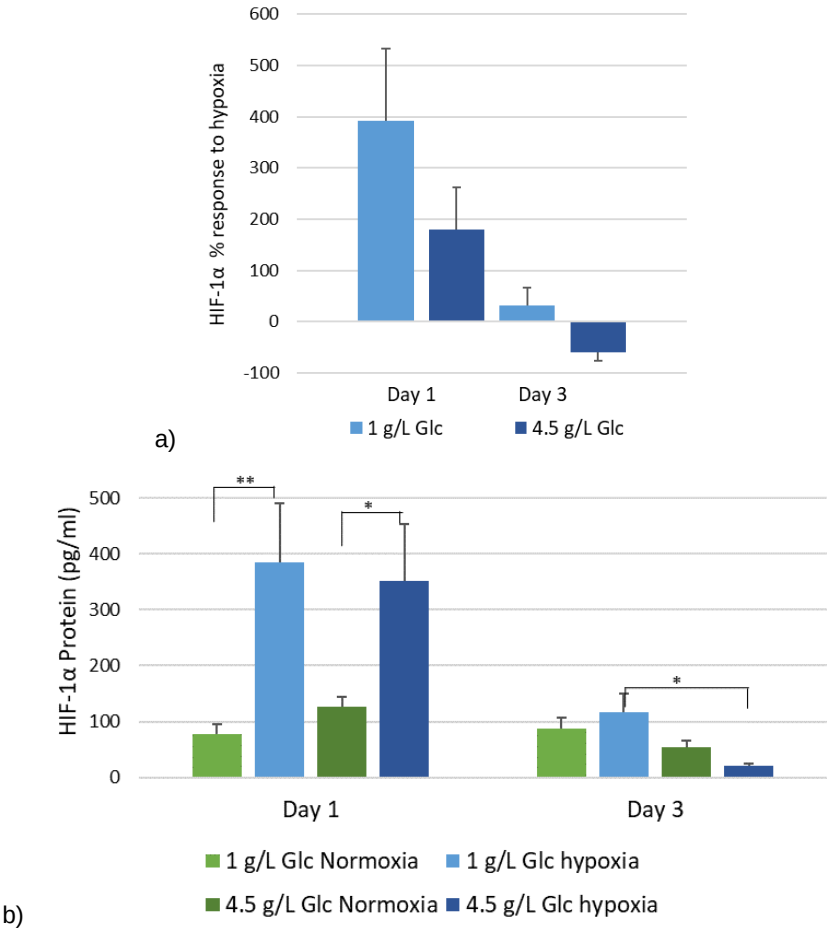

Figure 3-7 HIF-1α stabilisation as a response to hypoxia (1% O_2) was impaired following 28 days hyperglycaemic precondition. a) Nuclear HIF-1α, as quantified through HIF-1α ELISA, was increased in a four-fold manner as a response to hypoxia, whilst high glucose-conditioned saw a two-fold increase. Nuclear HIF-1α was decreased after 3 days in both glycaemic conditions. b) Nuclear HIF protein was increased in both glucose conditions as a response to hypoxia, there was no significant difference at day one. The amount of HIF expressed by normoxic euglycaemic cells remained constant across time. Higher levels of HIF protein were seen euglycaemic cells at day 3, where the expression of HIF-1α under hyperglycaemia was diminished. Error bars = Standard deviation, n=3, *p<0.05, **p>0.01.

3.4.2.3 *Antioxidant Capacity is reduced after hyper-glucose conditioning*

High glucose-conditioned HaCaT cells had a lower antioxidant capacity (Figure 3-8) response to hypoxia when compared to euglycaemic cells (p<0.01). The effect of hyperglycaemia and AGE precursors in ROS is discussed in Figure 3-13.

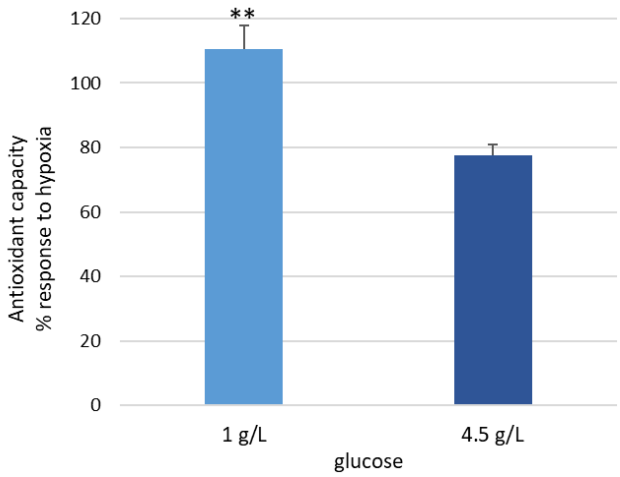

Figure 3-8 Antioxidant capacity response to hypoxia was reduced after prolonged high glucose exposure. The antioxidant capacity increased slightly after 24-hour exposure to hypoxia, whilst in high glucose conditions, the capacity fell below the normoxic levels, as quantified with the total antioxidant assay. Error bars = Standard deviation, n=6, **p<0.01.

3.4.2.4 *Hyperglycaemia increases MMP-9 production*

As a response to hypoxia in wound healing, an increase of MMP-9 aids the fragmentation of the extracellular matrix to allow cell migration. Hypoxia led to an increase in the MMP-9 expression in both glycaemic conditions (Figure 3-9). The MMP-9 expression under 20% O_2 was similar at both glycaemic conditions. A two-fold hypoxia-led increase was observed in euglycaemic cells in comparison to a 4.5-fold hyperglycaemic cells ($p<0.001$). The difference between normoxic conditions was not significant, which suggest an impairment in the MMP-9 regulation system driven by the excess of high glucose under hypoxia.

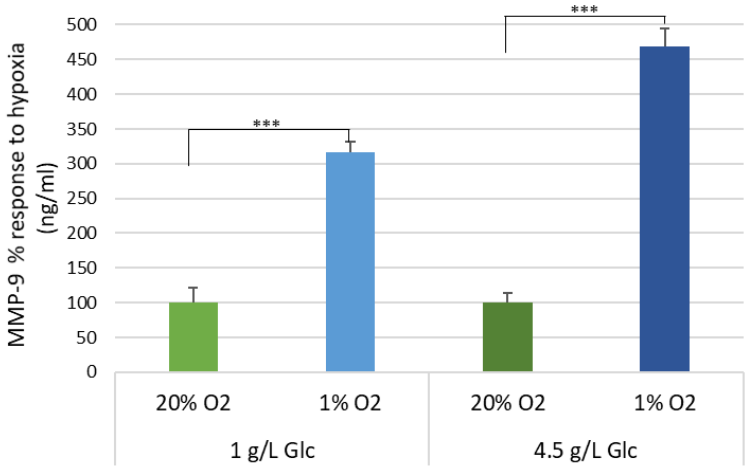

Figure 3-9 MMP-9 increases as a response to hypoxia in HaCaT cells. There is no difference in the MMP-9 expression, as measured with the MMP-9 ELISA, between euglycaemic and hyperglycaemic (4.5 g/L for a period of 28 days) MMP-9 in normoxic environment. Under euglycaemic hypoxia the increase is 2.8x, meanwhile in the hyperglycaemic the response is 4.5x higher. Error bars = Standard deviation, n=6, ***p<0.001.

3.4.2.5 *Morphological changes in HaCaT cells induced by hyperglycaemia*

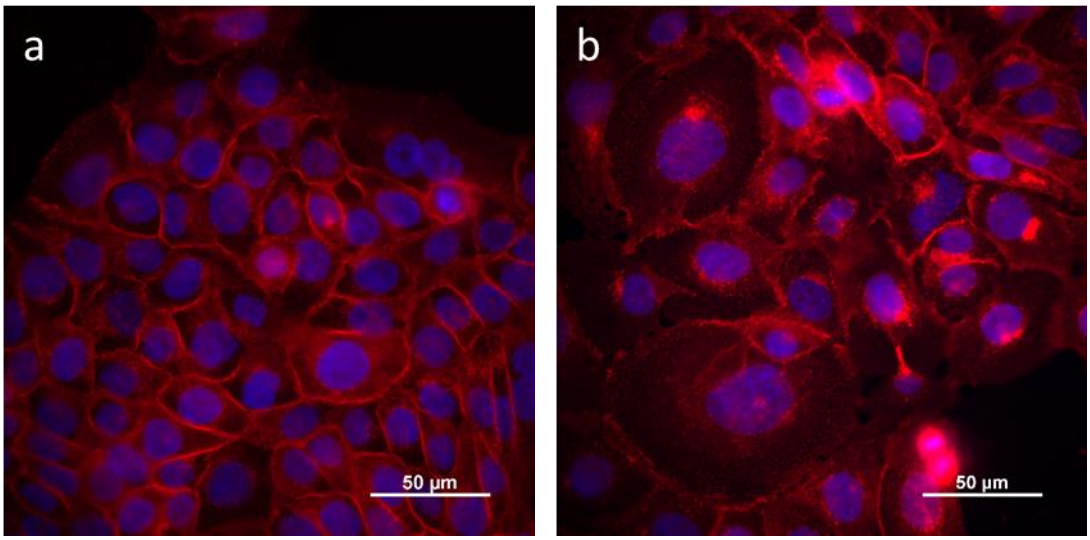

Figure 3-10 Fluorescence micrographs of hyperglycaemia-induced enlargement of HaCaT cells after 28 days of preconditioning. a) Euglycaemic cells maintained at 1 g/L glucose. b) Hyperglycaemic conditioning at 4.5 g/L Glc. Red: wheat germ agglutinin Alexa Fluor™ 594 for membrane, Blue: DAPI for nuclei.

HaCaT cells maintained their cobblestone shape (Figure 3-10) after high glucose conditioning, however morphological changes were observed in the diabetic-like phenotype. The presence of flattened and enlarged cells was observed during the experimental settings. Hyperglycaemia-cultured cells seem to have higher cell size area av. 1350±1487.67 μm^2 (n=101), while euglycaemic cells had an average size of 766.02±452.34 μm^2 (n=78) (Figure 3-11). The average cell size was not statistically different but the variance within the measured cell size (area) was found to be significant ($p<0.0009$, 1g/L n=78, 4.5g/L n=101).

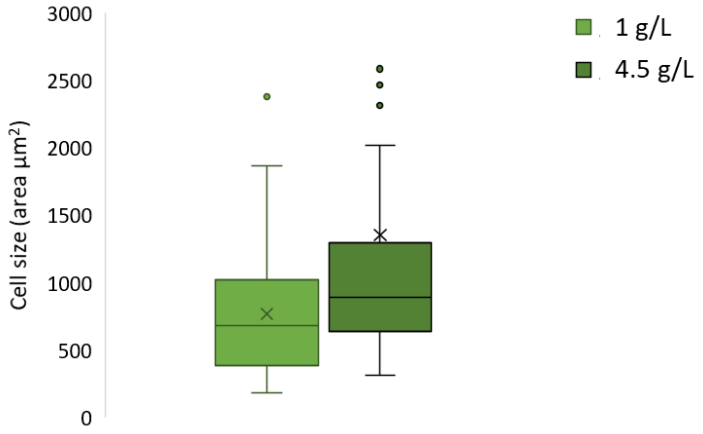

Figure 3-11 Cell size variability between euglycaemic (1 g/L Glc) and hyperglycaemic cells (4.5 g/L Glc for 28 days conditioning). Hyperglycaemic cells have higher cell size area variation than euglycaemic cultured cells. ($p<0.0009$, 1g/L n=78, 4.5g/L n=101) Error bars =SD

3.4.3 Impairment of hypoxia response through Advance Glycation End Products

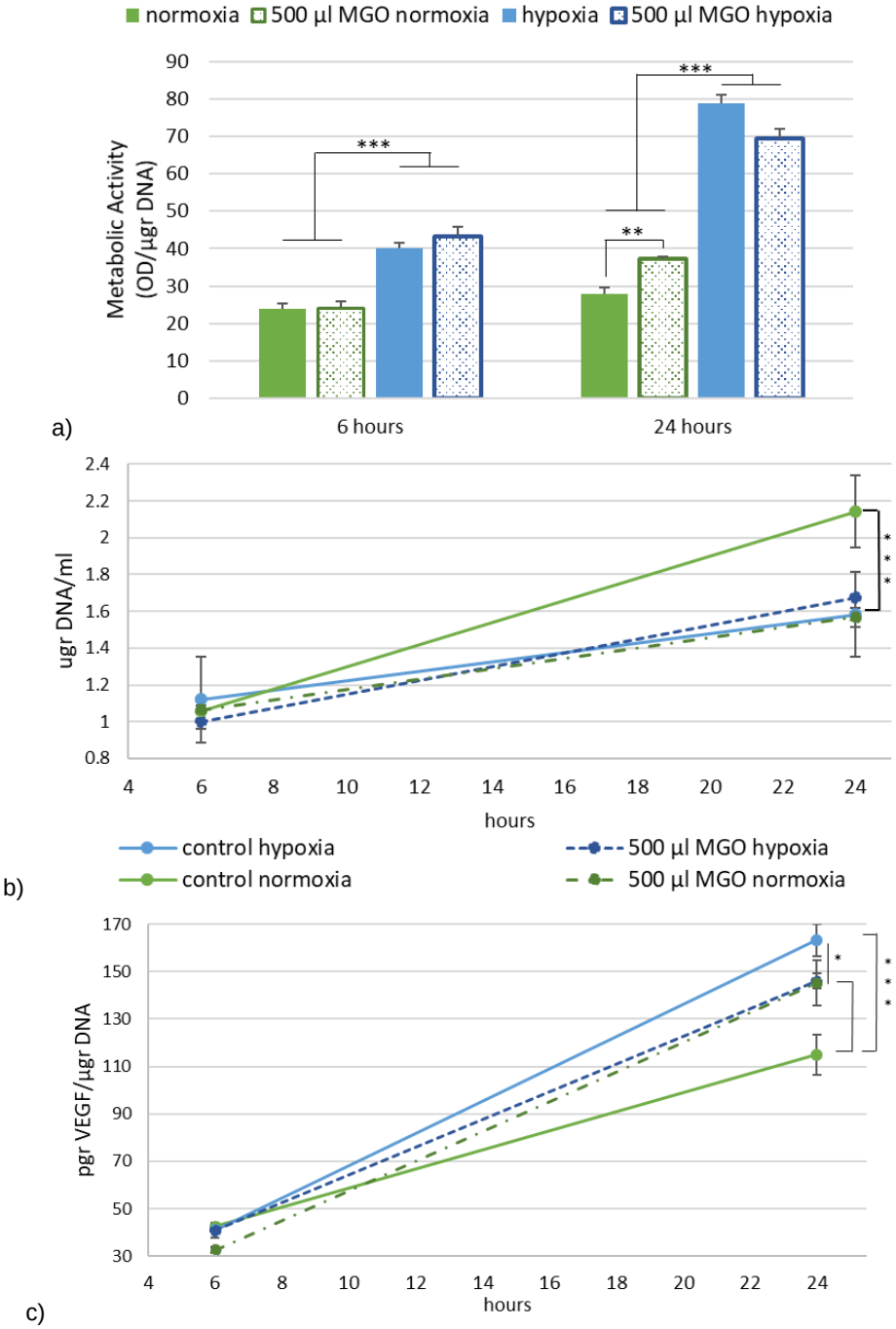

Figure 3-12 Methylglyoxal (MGO) mimicked impaired response seen after hyperglycaemic preconditioning. Euglycaemic cells were treated with MGO (500 µM) for 4 hours, after media replacement cells were evaluated at 6 and 24 hours. a) After 6 hours the metabolic activity increased as a response to hypoxia, as measured by alamar Blue®. At 24 hours there is a significant increase in the metabolic activity of MGO treated cells under normoxia ($p<0.01$). The difference between hypoxia was increased, meanwhile MGO treated cells had a lower metabolic activity ($p<0.005$). b) After 6 hours, there were no changes in cell number, after 24 hours non-treated normoxic cells doubled number. The hypoxic and MGO-treated cells had a similar lower proliferation, as quantified with Hoechst dye. After standardising the VEGF secretion to DNA, MGO in normoxia showed a decreased VEGF production after 6 hours ($p<0.001$). After 24 hours VEGF increased in the normoxia-MGO

treated cells, meanwhile the response to hypoxia was impaired in the MGO treated cells. The MGO conditioning was found to be not different to hypoxic control. VEGF was quantified by ELISA. Error bars = Standard deviation, n=6, *p<0.05, ***p>0.001

After preliminary experiments determining the toxicity of MGO, euglycaemic cells were incubated with 500uM of DMOG for 4 hours under normoxic conditions. Metabolic activity of the cells was evaluated under normoxia and hypoxia 6 and 24 hours after removal of MGO. After 6 hours, the metabolic activity of the cells was increased under the incubation in hypoxia (Figure 3-12a). Yet, after 24 hours in normoxia, increase of the metabolic activity was observed in the MGO-treated cells. The metabolic increase was more noticeable after 24 hours of hypoxia, where the MGO-treated cells had a lower metabolic activity than the hypoxia control. Cell proliferation was decreased after 24 hours exposure to hypoxia ($p<0.0001$). Normoxic cells previously exposed to MGO had a proliferation similar to those in hypoxia, with and without MGO treatment. ROS Production in under hyperglycaemia and response to AGE.

A non-significant increase in ROS production is observed (Figure 3-13) in euglycaemic HaCaT cells at normoxia with the addition of MGO (500 µM) for a period of 4 hours. Hypoxia induces ROS significantly higher in hyperglycaemic cells ($p< 0.005$), independently to the presence of MGO. The increase seen with the addition of MGO in euglycaemic cells under hypoxia, was not significant.

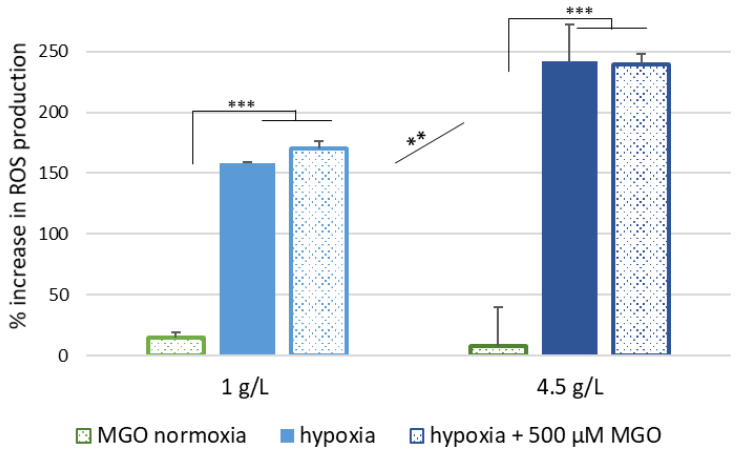

Figure 3-13 HaCaT's reactive oxygen species response to the addition of MGO as an AGE precursor. HaCaT 4.5 g/L cells were pre-conditioned for 28 days under normoxic conditions. The percentage increase in 4.5 g/L HaCaT cells was noticeably higher than the increase in euglycaemic cells. Although there is no significant difference under the presence of MGO at hypoxic levels (1% O_2), MGO increased ROS production at normoxic levels. ROS was quantified with DCFH-DA dye. Error bars = Standard deviation, n=4, **P<0.005, ***P>0.005.

3.4.4 **HIF stabilisation in HDF**

The amount of HIF 1α was significantly lower in HDF cells compared to HaCaT cell line. Multiple factors can have influenced the difference on HIF 1α expression, the cell origin, disparity in response to low oxygen, hydroxylation and degradation of the molecule, as well as cell number and confluency. Hyperglycaemic HDF were continuously grown at 4.5 g/L, while a normal glycaemic control (1 g/L) was grown in parallel. This experiment required seeding in T150 flask at a different density to the rest of the experiments, influenced by their larger size. The nuclear HIF 1α molecule was detected under low glucose conditions at normoxic level (Figure 3-14), meanwhile under hypoxia 1%, a large variation was observed. VEGF analysis suggested that HIF was stabilised as VEGF increased as a response to hypoxia ($p<0.0001$). After prolonged exposure to hyperglycaemia, HIF-1α was not detected under normoxic conditions, while at hypoxic conditions, HIF 1α was similar to the amount observed in low glucose normoxia. VEGF was secreted in both concentrations, although the increase to hypoxia was found to be not significant.

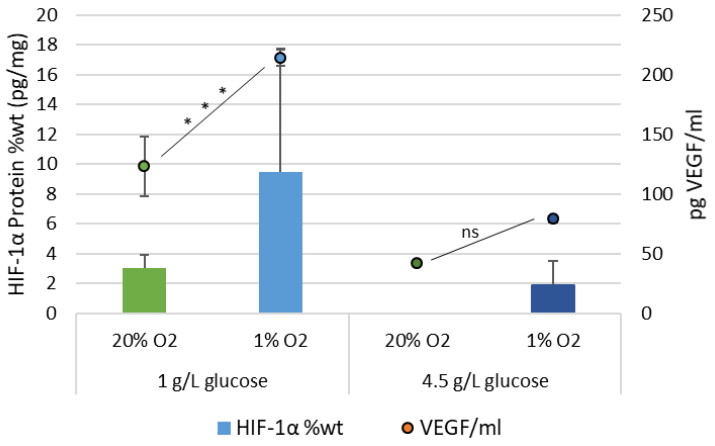

Figure 3-14 HIF-1α stabilisation and VEGF expression in low and high glucose conditions. Under normoxic conditions VEGF was detectable in euglycaemia, in response to hypoxia, HIF-1α was increased but high variability was observed. Under hyperglycaemia, HIF-1α was not detectable. VEGF expression increased under euglycaemia, but not significantly under hyperglycaemia. Both proteins quantified by ELISA. Error bars = SD, n=3, ***p>0.001.

3.4.5 Does hyperglycaemia preconditioning have an effect on response to hypoxia in HDF?

Cells grown under continuous high glucose had a decreased proliferation ($p<0.001$) when compared to euglycaemic cells (Figure 3-14). The proliferation rate was found to be not significantly different to the euglycaemic cells grown under 1% O_2. The proliferation rate of hyperglycaemic cells was further diminished under hypoxic stress ($p<0.001$).

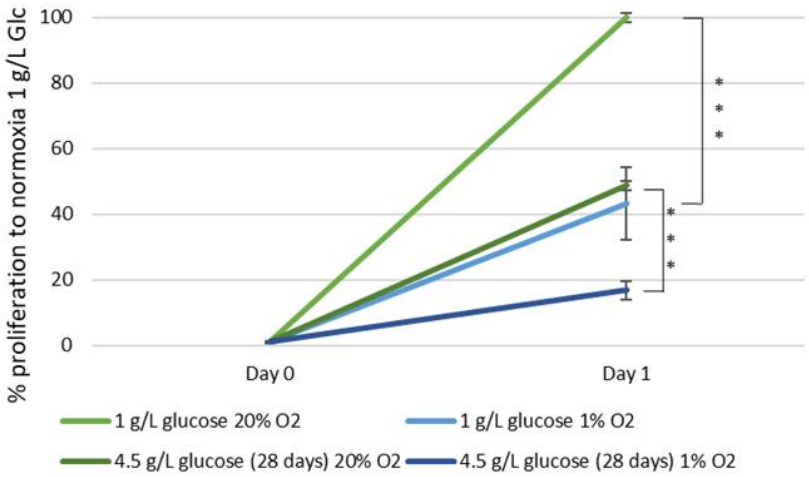

Figure 3-14 The effect of hyperglycaemia on cell proliferation. In normoxia, hyperglycaemia had a decrease cell proliferation, as DNA was quantified using Hoechst dye, similarly to the growth of euglycaemic cells under hypoxia. Error bars = SD, n=6, ***p>0.005.

Euglycaemic fibroblasts responded to the hypoxia stimuli -1 and 2% O_2- by increasing the metabolic activity (Figure 3-15a) when compared to normoxia ($p<0.0001$). There is no significant difference in the metabolic activity increase between 1 and 2% O_2 conditions, suggesting that 2% is enough to trigger the adaptive mechanism. Fibroblasts secreted higher amounts of VEGF ($p<0.0001$) following HIF-1α stabilisation as a result of the oxygen reduction (Figure 3-15b). VEGF was secreted in higher concentrations under lower hypoxia levels (1% O_2), this was observed in each experiment but because of experimental variation after grouping all experiments, the difference was not statistically significant.

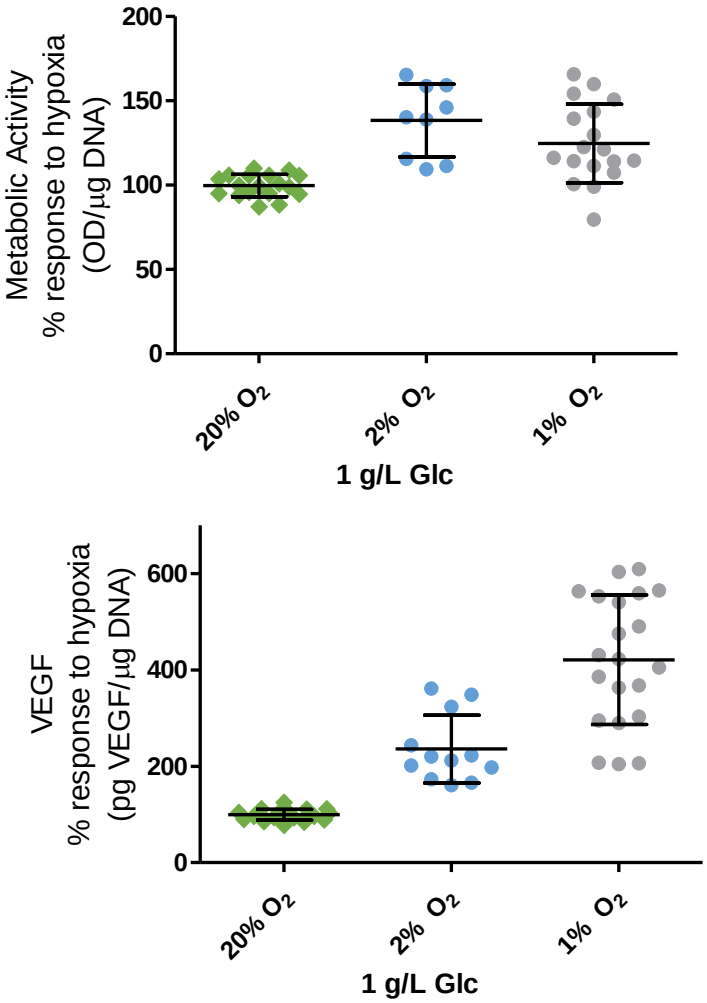

Figure 3-15 Euglycaemic fibroblast response to hypoxic environment. The graphs represent the variability of the euglycaemic cells as controls in the experimental repeats responding to hypoxia. Each dot represents a replicate from each experiment, the centre line the average from all experiments, while the error bars the standard deviation. a) Under euglycaemic conditions, the metabolic activity, as determined by alamar Blue®, increased significantly ($p<0.0001$) as a response to hypoxia, there was no significant difference between both hypoxic conditions. b) The VEGF secreted, quantified by ELISA, was directly related to the increase of the hypoxic stress. VEGF was increased under 2% O_2 ($p<0.001$) and further increased at 1% O_2 ($p<0.0001$). 20% O_2 n=24, 2% O_2 n=12, 1% O_2 n=24.

Cells were preconditioned to 4.5 g/L glucose for 1, 3, 7, 14, 17, 21 and 28+ days. (see Figure 3-3). After seeding and allowing attachment overnight, fresh media was replenished and determined as t=0. After 24 hours of hypoxia or normoxia, no significant metabolic activity variation across each pre-incubation period was observed (Figure 3-16). Glucose preconditioning had no effect in hindering the VEGF secretion at 2% hypoxia (Figure 3-17). Fibroblasts at 1 and 3 days of hyperglycaemic preconditioning had an increased VEGF production as a response to 1% O_2, when compared to euglycaemic fibroblasts. The response to 1% hypoxia decreases in a polynomial fashion (R^2=0.7870, df=32), describing the impaired response to the hypoxic insult of the cells after over 28 days of high glucose preconditioning.

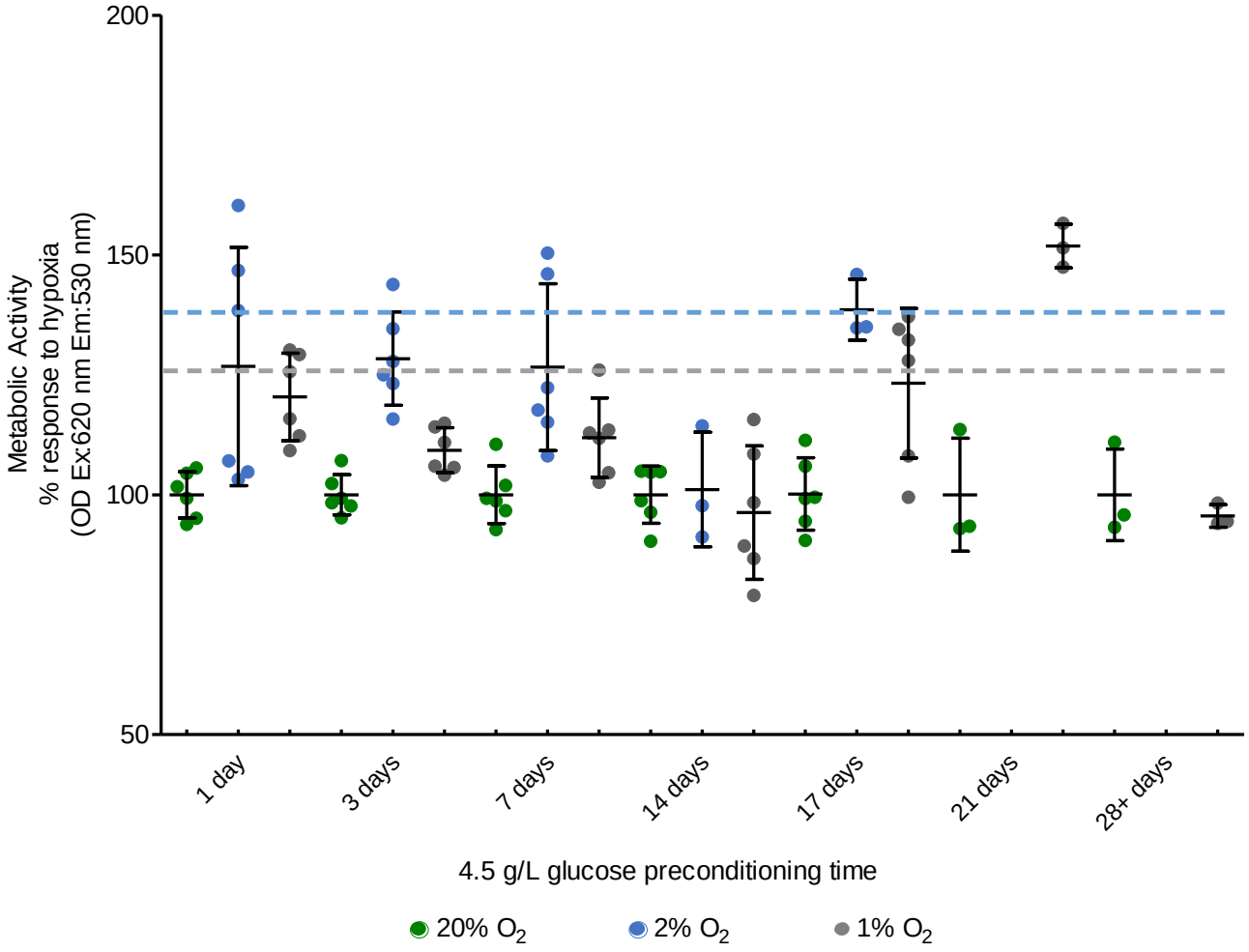

Figure 3-16 Cells responded to the oxygen deprivation by adjusting the metabolic activity. During the early preconditioning time-points, cells displayed an increased metabolism under 2% hypoxia, whilst at 1% the cell metabolism was decreased

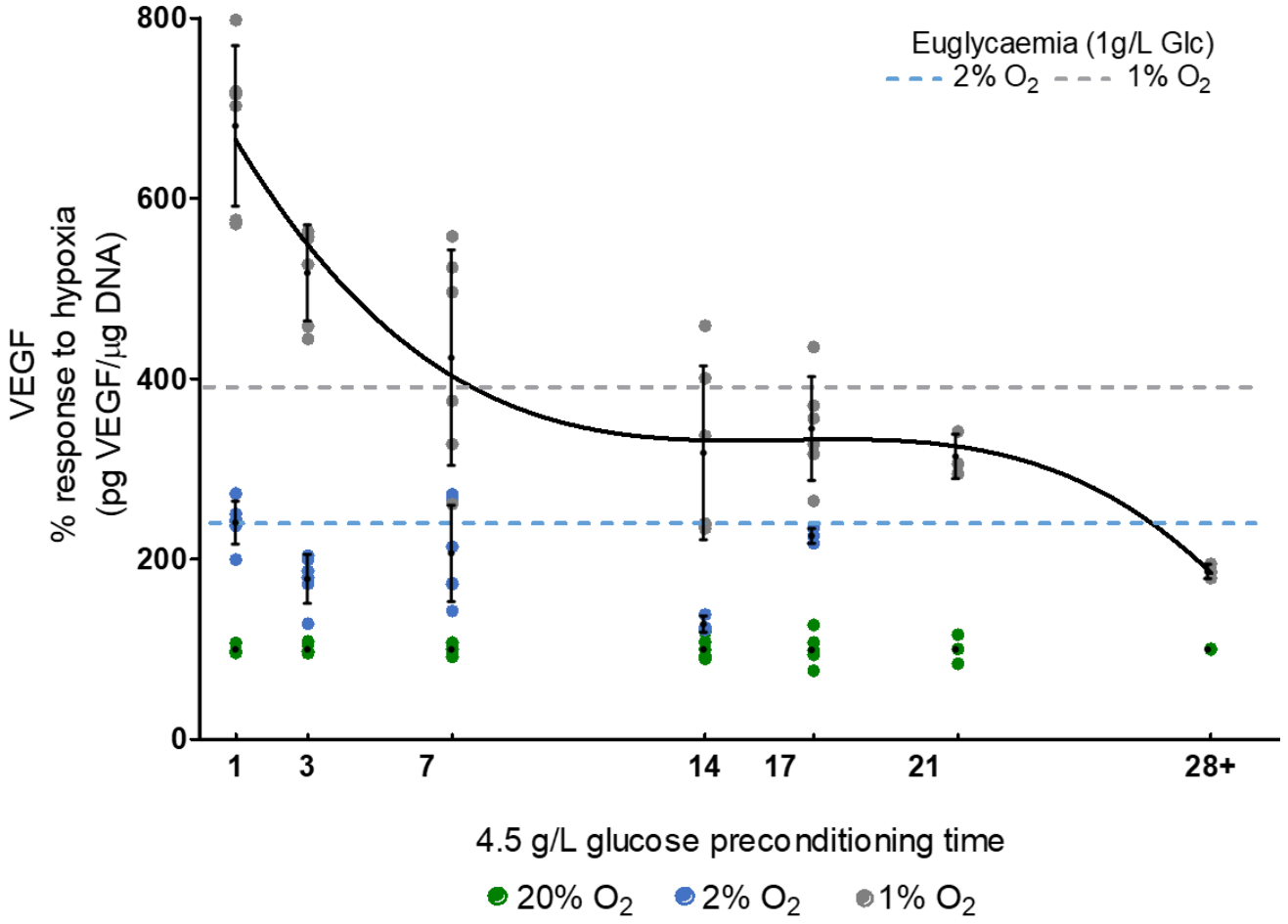

Figure 3-17 Prolonged high glucose preconditioning (28+ days) impaired VEGF secretion as a response to 1% hypoxia. As the conditioning period was extended, a decrease in the response to 1% hypoxia was observed. This was described by a third order polynomial curve (R2 = 0.7870, df=32). Short-term glucose preconditioning did not impaired VEGF expression as a response to low oxygen conditions Cells secreted VEGF proportional to the degree of hypoxia, secreting more VEGF in deeper hypoxic state. VEGF was quantified through ELISA.

3.4.6 **Does hyperosmotic hyperglycaemia inhibit hypoxia response?**

In order to elucidate the variation in these results, a glucose concentration similar to hyperosmolar hyperglycaemia (9g/L Glc) was evaluated following short-term exposure. As the cells had a reduced response at 2% O_2 in the previous experiment, this was selected for this experiment. The metabolic activity was evaluated after 3 and 7 days of preconditioning in both high glucose concentrations (Figure 3-18). There was a significant difference in the metabolic activity in the euglycaemic cells when exposed to hypoxia, which was also seen in the cells at 3 days preconditioning. The metabolic activity per unit of DNA was not significant between normoxia and hypoxia in the cells preconditioned for 7 days.

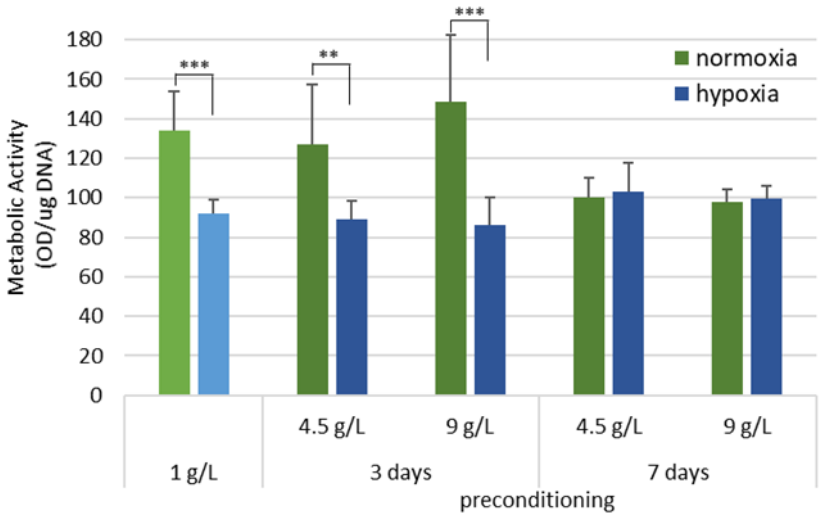

Figure 3-18 Effect of high glucose preconditioning in the HDF metabolic activity under normoxia and hypoxia (2% O_2). The metabolic switch to hypoxia, as determined by alamar Blue®, was observed at low glucose and 3 days preconditioning. The metabolic change was not seen at 7-day preconditioned cells in either high glucose level. Error bars = Standard deviation, n=6, **p<0.005, ***p>0.005

Two percent hypoxia increased significantly VEGF expression, suggesting HIF-1α stabilisation across all glucose levels. (Figure 3-19a) Under normoxic conditions, the cells with low glucose secreted higher levels of VEGF than the other normoxic conditions, except for the 3-day preconditioning at 4.5 g/L Glc.(Figure 3-19b) The euglycaemic VEGF secretion per DNA in hypoxia was significantly higher ($p<0.0001$), followed by 7 days precondition at 9 g/L Glc ($p<0.0001$). The glucose level of 4.5 g/L had a similar effect in both preconditioning times along with 9g/L Glc at 3 days of preconditioning. The effect seen on the 9 g/L 7 days precondition could be due to the decreased proliferation found in hyperglycaemia. After normalising the response to hypoxia to the VEGF secreted under each glucose level at normoxia (Figure 3-19a), 9 g/L had a 7-fold increase compared to euglycaemia, which had a 3.5-fold increase.

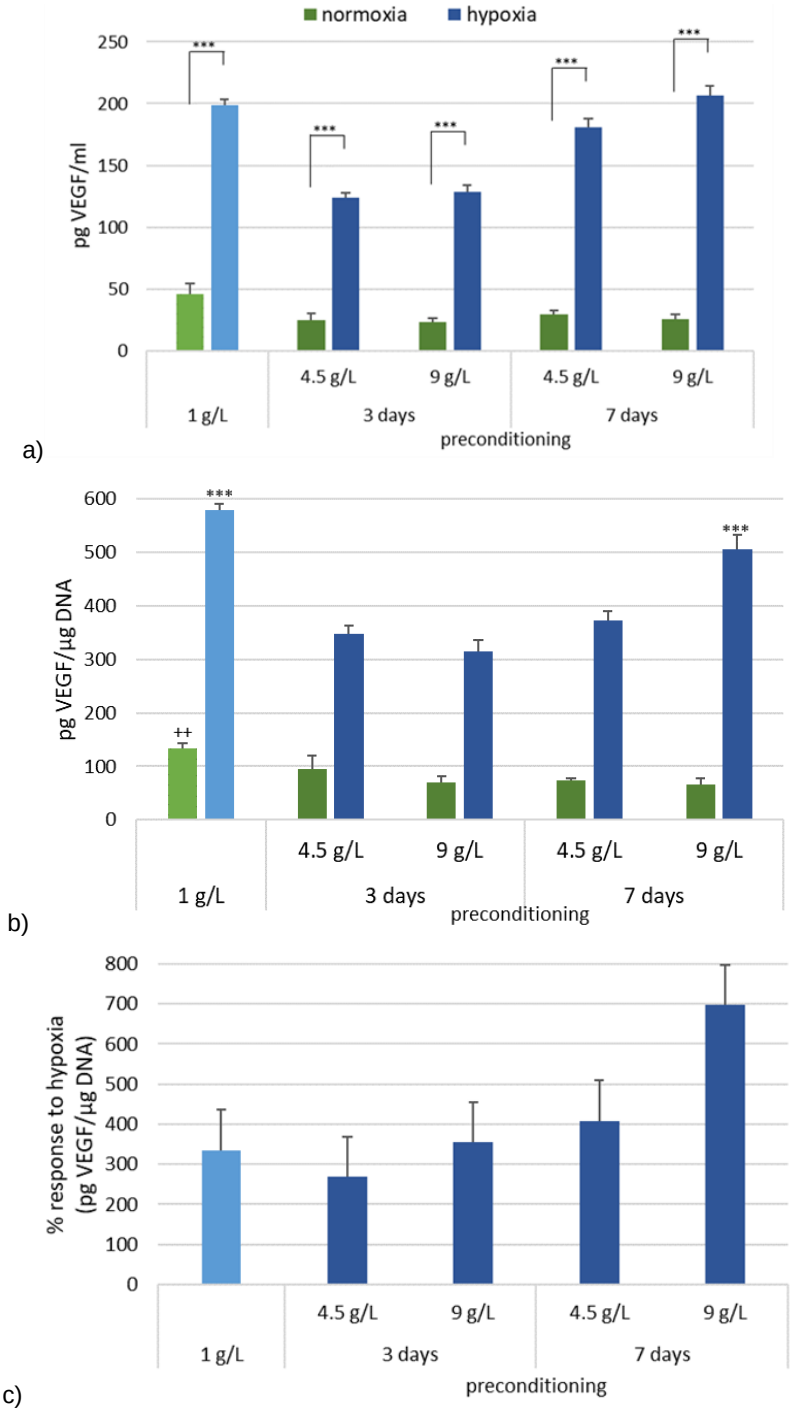

Figure 3-19 Short-term hyperglycaemia and hyperosmolarity did not inhibit the response to hypoxia. a) A significant increase of VEGF, as determined by ELISA, was seen in all the glucose conditions at 2% hypoxia. b) Euglycaemic HDF secreted a higher amount of VEGF ($p<0.0001$) followed closely by 7-day 9 g/L condition ($p<0.0001$), whilst the difference across the other conditions was found to be no significant. c) The increase is mayor in 9 g/L Glc 7-day conditioning, possibly due to a low proliferation under intense hyperglycaemia. The increase between the low glucose control and the other conditions. Error bars = Standard deviation, n=6, **$p<0.005$, ***$p>0.005$.

For the hyperglycaemic condition, HDF cells were continuously grown (28+ days) in high glucose (4.5 g/L Glc). Cells were exposed for 4 hours to hypoxia, where ROS

production was observed to increase in both glucose conditions ($p<0.001$), although hyperglycaemia saw a two-fold increase to healthy cells (Figure 3-20). The capacity of MGO (500 µM) to induce ROS was also evaluated. MGO did not increase ROS production under hypoxia in either glucose condition.

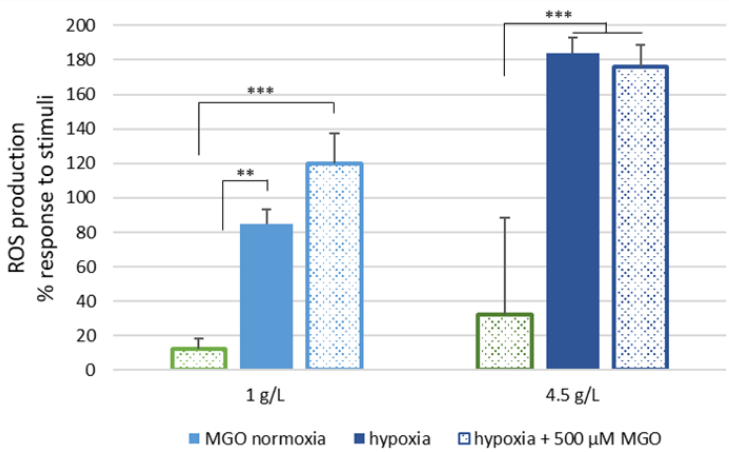

Figure 3-20 HDF's reactive oxygen species response to methylglyoxal in 1 g/L and 4.5 g/L glucose continuous preconditioning. After 4 hours of exposure to hypoxia (1% O_2), there is an increase in ROS production, as quantified by DCF-DA dye. The magnitude of the increase is higher in 4.5 g/L cultured HDFs ($p<0.005$), meanwhile there is no difference with the addition of MGO in both glucose levels. Error bars = Standard deviation, n=4, **$p<0.005$, ***$p>0.005$.

3.4.6.1 *Morphological changes in HDF induced by hyperglycaemia*

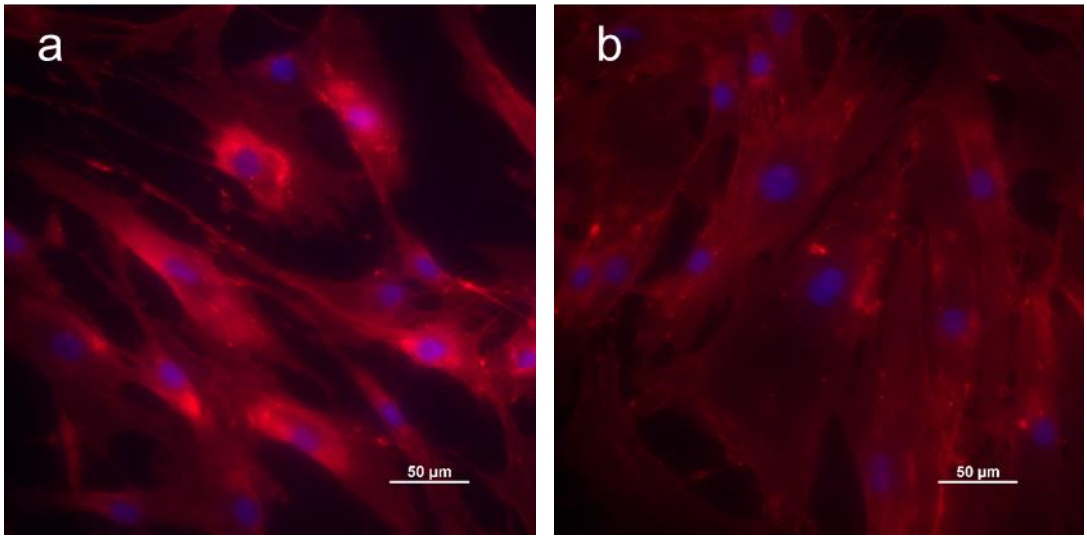

Figure 3-21 Fluorescence micrographs of high glucose-induced enlargement of HDF cells after prolonged conditioning. a) Euglycaemic cells maintained at 1 g/L glucose. b) Hyperglycaemic conditioning at 4.5 g/L Glc. Red: wheat germ agglutinin Alexa Fluor™ 594 for membrane, Blue: DAPI for nuclei

HDF cells in low glucose conditions present the spindle shape characteristic of fibroblast, however cells under high glucose although elongated, appeared to be larger and wider. The cell membranes were stained with wheat germ agglutinin Alexa Fluor™ 594 and the nuclei with DAPI.

3.5 **Discussion**

A limitation in the current *in vitro* models is the high variance in the hyperglycaemic conditions used to mimic a diabetic wound. In this work, a stable model of impaired wound healing in keratinocytes (HaCaT) has been characterised. After 28-day hyperglycaemic (4.5 g/L Glc) preconditioning, HaCaT cells for replicated the impaired response of diabetic keratinocytes to hypoxia. The decrease of nuclear HIF protein (Figure 3-7) was followed by an impairment in the VEGF increase as response to hypoxia (Figure 3-6). Followed by a lack of a metabolic switch as a response to the hypoxic environment and decreased cell proliferation in both oxygen environments (Figure 3-5); the increase of ROS production and MMP-9 expression, as well as the decreased antioxidant capacity are present in diabetic conditions. Aside of the glucose concentration, the duration of exposure to high levels of glucose plays a mayor effect on the cellular response.

3.5.1 **The response to the level of hypoxia is cell line specific**

HaCaT and HDF (euglycaemic) responded differently to hypoxia 2% and 1% O_2. HaCaT cells required a lower concentration of oxygen (1% O_2) to increase VEGF production. A response in VEGF expression on HDF cells was observed at 2% O_2, while the VEGF secretion was higher under 1%O_2, cell type specificity to hypoxia response has been previously reported.[410]

3.5.2 **High glucose preconditioning cells inhibits HIF-1α stabilisation**

There was an increase in HIF expression at the normoxic hyperglycaemic condition at day 1 concordant with Sada (2016) and Catrina (2004) et al. that hyperglycaemia induces a pseudohypoxia state in which HIF is stabilised. [176,362] The response to the hypoxic insult was impaired in high glucose cells, with a further decrease in HIF expression at day 3, mimicking what would be a prolonged inflammation process. The amount of HIF-1α accumulated under hypoxia at day 3, was significantly higher to that in hyperglycaemia. Euglycaemia under normoxia remained constant between day 1 and 3, however hypoxia was downregulated by day 3. This could be as HIF1 stability can be modulated post-transcriptionally by hormones and growth factor dependant pathways.[300]

HDFs had a decreased response to hypoxia after a prolonged conditioning to high glucose (28+ days). Different time points were evaluated in the 28 days period, where no significant decrease of the VEGF response to hypoxia was noted. The decrease

in the HIF-1α expression was seen after 24 hours of hypoxia when compared to euglycaemic cells. This impairment due to high glucose was also observed in the reduced VEGF expression.

3.5.3 Angiogenic factors driven by HIF-1α stabilisation are decreased under high glucose conditions

VEGF response to hypoxia was decreased in hyperglycaemic conditions. Thangarajah et al. (2009) reported that VEGF expression was reduced in diabetic patient-derived fibroblast as a response to 0.5%O_2. The cellular impairment was replicated after prolonged preconditioning healthy fibroblasts under 25 mM of glucose (4.5 g/L).

After conditioning HaCaT cells with 4.5 g/L glucose, an impairment in the VEGF response to hypoxia (1% O_2) was observed when compared to cells grown at 1g/L Glc. In dermal fibroblasts, the impairment in the VEGF response to hypoxia was seen after a prolonged exposure (28+ days) to 4.5 g/L glucose. Fibroblasts demonstrated rapid adaptation to hypoxia at earlier time points, when the capacity to stabilise HIF was reflected in the significant increase of VEGF at 2% O_2 and further increase at 1% O_2. The higher VEGF secretion at 1 and 3 days could be related to the availability of high glucose in a period where the cell has not accumulated damage from the excessive ROS production, AGE formation and cellular damage that come along with age and diabetes. As the cells are exposed to hyperglycaemic conditions for longer periods, is possible that AGE accumulates and glycation occurs[195]. This relates to the decrease in the response to hypoxia in terms of VEGF expression. A permanent damage in cells is observed in diabetic patients, where the cell proliferation is decreased even if the cells are obtained from a non-lesion area. [312]

3.5.4 High glucose reduces cell proliferation and alter metabolic activity through cellular pseudohypoxia

A significant difference in cell proliferation in HaCaT between hypoxia, normoxia and the glycaemic conditions can be observed at day 3 as hypoxia leads to a reduction in the cell proliferation orchestrated by HIF1.[411] The low proliferation in hyperglycaemic HaCaT under normoxic conditions suggest that hyperglycaemia is inducing pseudohypoxia, which can be related to the higher metabolic activity shown by HaCaT cells at day 3 and 7, when in euglycaemic cells the metabolic activity is regulated under hypoxia. Sada et al. (2016) proposed that as high glucose increased, so did mtROS, while also increasing O_2 consumption in the mitochondria, leading to cellular

hypoxia under normoxic conditions.[176] Conversely, Terashi et al. and Nakai et al. have previously described the decrease in cell proliferation at high glucose concentrations, proposing that high glucose decreases the replicative life span of HaCaT similar to observations in clinic where diabetic patient-derived keratinocytes have a reduced mobility.[287,321] The decrease in cell proliferation under hyperglycaemia was also observed in fibroblasts. A reduction in cell proliferation has been described by Seagroves et al. (2001) with HIF-1α-null fibroblasts under hypoxia, while Baracca et al. (2013) described the relation of HDF proliferation to oxygen condition, being reduced in high glucose levels.[133,345]

3.5.5 Diabetes, hypoxia and ROS generation: effect of hyperglycaemia in MMP-9 and antioxidant capacity

The amount of ROS production measured under normoxic conditions was not significantly different between both glucose conditions. An increase in ROS production under similar high glucose conditions (30 mM Glc) as opposed to euglycaemic conditions of 5 mM was reported by Nishikawa et al. (2000) By inhibiting the pyruvate -derived from the glycolysis- ingress to the mitochondria, suggesting the TCA cycle as the source of increased ROS through hyperglycaemia.[412] A disparity in ROS production as a response to hypoxia was observed in both cell conditions, where the ROS increase was higher under high glucose conditions. The response in ROS detection and production was higher in HaCaT cell line when compared to the HDFs. The increase of ROS in low glucose condition as a response to hypoxia was 158% meanwhile HDF response was 86%. The high ROS production under hypoxia in hyperglycaemic cells results are supported by the total antioxidant capacity assay performed in HaCaT cells, where a decrease in the response was observed under the same conditions. A reduction in the antioxidant capacity is reduced particularly in diabetic patients with microvascular complications.[395] Hypoxia increased significantly MMP-9 production, however the increase in hyperglycaemia was greater. Uemura et al. (2007) observed a 70 percentage increase of ROS under high glucose conditions and a decrease of MMP-9 with the addition of antioxidants, elucidating the role of oxygen-derived free radicals in MMP-9 production and regulation.[413]

The relevance in evaluating MMP-9 in wound healing lays on MMP-9 being upregulated under hypoxia promoting keratinocyte migration to the wound bed for re-epithelialization, also having an effect in angiogenesis, by releasing and activating VEGF and TGF-β from the ECM,[414,415] however, MMP-9 is not solely regulated by HIF-1α, but also mediated through the PKC pathway and ROS.[413,416] The MMP-9

profile results resemble what Liu et al. (2009) observed in diabetic foot ulcers. They found an increase of the MMP-9 and a decrease of the MMP-9 to TIMP-1 ratio in non-healing wounds at 4 weeks. As a factor of prediction of wound healing, they found this difference to be more noticeable at 12 weeks when comparing the healed ulcers (37%) to those who had not.[417] These results were similar to those described by Li et al. (2013), who observed a five-fold decrease in the MMP-9 serum concentration 4 weeks in healing patients. There was non-significant difference across time in the non-healing patients[142]. In hyperglycaemic murine models, a reduction of VEGF in response to hypoxia, a threefold increase in MMP9 and a decreased migration in diabetic cells. [418]Contrasting to these observations, Lan et al. (2008) report a decrease in the MMP-9 expression under high glucose conditions with a high level of TIMP-1, to which they attribute the low migration rate seen in hyperglycaemic cells. An important difference with their research is they measure the MMP-9 expression *in vitro* under normoxic conditions after a short period of exposure to high levels of glucose.[169]

3.5.6 **Use of Advance Glycation End Products to reduce HIF stabilisation**

MGO as a diabetic wound model was evaluated following the experiment by Sena et al. (2012) which was done on retinal pigment epithelial cell line ARPE-19. In HaCaT cells, after 6 hours of exposure to MGO (1 and 3mM), a decrease in the metabolic activity, VEGF expression and cell number was observed dependent upon the concentration, suggesting toxicity. Bento et al. (2010) reported using similar MGO concentrations as Sena, stating that even if these concentrations are higher than those seen in vivo, the accumulation of intracellular MGO are similar to those observed in pathological conditions. Treatment and removal of MGO after 4 hours in HaCaT cells, at lower concentrations than reported by Sena et al. (2012) and Bento et al (2010) decreased VEGF, and affected cell proliferation and metabolic activity similarly as the effect of 28 days of hyperglycaemic conditioning. HaCaT cell line appear to be more sensitive to the effect of MGO, as they report not detecting MGO in ARPE-19 after 3 hours of exposure, while in HaCaT cells an endure effect was observed, even upon removal of the MGO.[168,298] Four hour preconditioning with MGO did not increase ROS production under hypoxia or normoxia, however an increase of ROS through AGE-forming methylglyoxal under hyperglycaemia has been demonstrated by Nishikawa et al. (2000, 2016). These results demonstrate the potential of MGO chronic wound heal modelling with in a shorter incubation period.

3.5.7 **Hyperosmolarity under hyperglycaemia**

As high osmolarity (through mannitol) has been found to induce endothelial cell apoptosis, along with increasing stress markers, leading the activation of multiple disease pathways.[385] The experiments containing 1 and 4.5 g/L glucose DMEM had an osmotic pressure of 304-336 mOS/kg and 313-346 mOS/kg accordingly, as specified by Gibco. The variance in the osmolarity overlaps and are consistent to the osmolarity present in controlled diabetic patients. However, patients can have critical periods of hyperosmotic hyperglycaemia, where the glucose level can rise up to 9 g/L Glc.[384] In order to evaluate the effect of a higher glucose levels and the effect of the imbalance of the osmotic pressure, 4.5 g/L of glucose was added to media already containing 25 mM glucose. Unexpectedly, the VEGF under supra-high levels of glucose (9 g/L Glc) for 7 days preconditioning at normoxic conditions was lower than the euglycaemic control ($p>0.01$). The supra-high level of glucose had an increase of VEGF secretion under hypoxia per cell after 7 days of conditioning, when compared to the effect of 4.5 g/L at the same preconditioning time. Although the amount of VEGF per DNA was higher in euglycaemic cells in low oxygen conditions, the percentage increase in the supra-glycaemic cells was higher. This effect could be attributed to the hyperosmotic conditions of having the double amount of glucose, but to the glucose as well. In order to explain this, 4.5 g/L mannitol or *L*-glucose can be added to the high glucose media condition.

3.5.8 **Morphological changes in hyperglycaemia**

It has been reported that in diabetic and elderly patients, the morphological and biomechanical changes in not injured skin exist.[157,419] Some of the changes are attributed to the extensive glycation in the collagen fibres,[193,420] and the inflammatory and ECM changes induced by ROS.[157,162,318,416] An enlargement and flattened changes in HaCaT cells after conditioning the cells to 12 mM Glc (2.16 g/L) for 28 days was reported by Terashi et al. (2005) Moreover, Spravchikov et al. (2001) has also described these changes as well as the lack of orientation between them. They observed that under high glucose, HaCaT cells were more sensitive to calcium, a driving factor of terminal differentiation.[301] Furthermore, Okano et al (2016) described an increase of the tight junction protein (ZO-1) in diabetic epidermal mouse models.[106,170,356] which could be associated with the strong attachment -between the cells and towards the flask- observed through the experimental settings. HDF cells had similarities to the changes associated with ageing in a model with increased oxidative stress, where the collagen lattices were fragmented and dystrophic.[190]

3.6 **Conclusion**

The model presented in this work considers the effect of hyperglycaemia as the main driving factor in diabetic-associated complications. Through high glucose preconditioning, HDF and HaCaT cells replicated the high oxidative stress present in the disease, reflecting the changes in the metabolic activity, cell proliferation and increased VEGF expression. Moreover, the hypoxic insult exacerbated the damage by the hyperglycaemic condition. The impaired response to hypoxia and HIF stabilisation, common in chronic wounds. The high oxidative stress –seen in measurement of ROS production and reduction in the antioxidant capacity- translated to the over-expression of MMP-9 under hypoxic conditions.

The model reflects the damage in keratinocytes (HaCaT cells) and fibroblasts (HDF cell line) produced by a hyperglycaemia of 25mM Glc (4.5 g/L), consistent to the high glucose level used in 31% of the literature previously described. The hypoxic insult was induced through a CO_2 incubator in 1% O_2. The HDF were subjected at 2% O_2 hypoxia in order to evaluate their responsiveness and adaptability to oxygen variations. The effect of the impairment in the cells as a co-culture, or by using the supernatant with the growth factors from the other cell line is proposed, given the strong crosstalk between fibroblast and keratinocytes in the body.

It was also of interest to evaluate the effect of AGE glycation, described in patients with chronic diabetes and the elderly. This was assessed in HaCaT cell line in conjunction to hypoxia state. It is proposed that a similar model is made in HDF, which should include the effects of the MMP-9 and characterisation of the collagen produced.

To evaluate the effect of osmolarity in HDF, a two-fold glucose condition consisting of 50 mM (9 g/L) was used, having early time points of precondition. Although an effect in VEGF was observed, it remains unclear if this was driven by the HIF pathway or other pathway related to hyperglycaemia.

The assessment of cell migration under hyperglycaemic and hypoxic conditions remains to be addressed.

Chapter 4. HIF mimetics in wound healing

4.1 **Introduction**

Diabetic and elderly patients are more prone to develop chronic wounds (see 1.6 and 3.1). These patients also have an impaired response to hypoxia and this has been implicated in the enhanced risk of chronic wound development.[123,152,167,298,421] Artificial stabilisation of the hypoxia pathway has been shown to enhance wound repair in both diabetic[198,200,208,422] and elderly[365,423] *in vivo* wound models. HIF stabilisation has been shown to promote angiogenesis, cell migration and wound closure.[109,209,409] There are, however, limited studies comparing the effect of different HIF mimetics in high glucose in vitro models. There is also a need for the controlled delivery of these HIF within the chronic wound environment.

In hypoxia -and in the presence of DFO,[424] DMOG[423] and cobalt[216]- HIF is stabilised and translocated into the nucleus, binds to the HRE (Figure 1-4), and activates a host of different genes important in wound healing (Figure 1-2). HIF-1 stabilisation activates a number of angiogenic genes (including angiopoietin 2 (ANGPT2), bFGF, SDF-1 and PDGF, important for restoring oxygen haemostasis and wound healing. VEGF is one of the most potent angiogenic factors, VEGF increases endothelial cell proliferation, vascular permeability, cell survival, cell migration and microvasculature tube formation, (as reviewed by Rey and Semenza (2010)). While HIF-1α is a potent inducer of VEGF, VEGF expression can also be upregulated through non- HIF-1α mediated pathways such as ROS, MAPk and other inflammatory related transcription factors.[363]

4.1.1 **The importance of controlled delivery of HIF stabilisation factors – and the risks of excessive or prolonged HIF stabilisation**

Several diseases are characteristic of hypoxia-driven inflammation and/or inflammation-related hypoxia, caused by sudden metabolic requirements that cannot be covered by the oxygen supply. Chronic diabetic patients develop a pseudo-hypoxic stage in which HIF -1α can be stabilised through pro-inflammatory molecules or infection preventing degradation of the molecule.[362]

HIF stabilisation is essential for normal repair and remodelling; however, artificial HIF stabilising factors requires delicate dosage and delivery. In a healthy wound, HIF-1α is initially upregulated and later decreases following the restoration of the neo-

vascularisation (see Figure 1-5). Prolonged exposure to HIF mimetic factors would cause chronic inflammation and resemble the profile of tumour tissue[175,425] with the continuous expression of inflammatory mediators (e.g. IL-1, IL-2, IL-6, TNFα, Phosphoglycerate Kinase (PGK-1)) and a range of early angiogenic factor initiators (e.g. VEGF).[425] Prolonged HIF stabilisation has been associated with granulomatous tissue formation and neoplasia.[426,427] Prolonged inhibition of PHD inhibitor FG 4095 (HIF inducer) led to increased vascular leakage, resembling a sepsis-like syndrome.[428] Likewise PHD2 dysregulation can induce erythropoiesis or erythrocytosis.[175,203,429,430]

4.1.2 **HIF mimetics: mode of action and interaction**

While the mechanism of impaired stabilisation of diabetic HIF-1α is not fully understood, it is thought to occur through increased HIF-1α degradation through the increased hydroxylase activity,[109] an impaired HIF-1α/p300 association, protein modification and polyubiquitination and proteosomal mediated by CHIP (Carboxy terminus of Hsp70-Interacting Protein), and an increased sensitivity of HIF-1α to von Hippel-Lindau dependant degradation.[168] In diabetic (or other conditions where cells are not responding to hypoxia) HIF-1α can be stabilised through different artificial mechanisms (Table 4-1) through Fe^{2+} substitute ions, induced cellular iron deficiency, 2-oxoglutarate analogues, or small molecular inhibitors of HIF degradation pathway.

Table 4-1 HIF-mimetic factors stabilise HIF pathway through different mechanisms.[h] (DHB- Dihydrobenzoic acid; Ft1-Notoginsenoside; Concentrations out of range: *2 mM,[431] **100 µM[423] for 4 days)

Mechanism of Action	HIF-mimicking factors		Range of concentrations (*in vitro* studies)
Fe^{2+}-substitute ions	Co^{2+}	131,214,436,437,216,218,219,235,432–435	10-300 µM
	Ni^{2+}	213,215,218,232	0.5 – 1 mM
	Cu^{2+}	210,218,225–228	100 µM
	Cr^{6+}	202,218,232,233	5-20 µM
	Mn^{2+}	218,229–231	100 – 200 µM
Induced iron deficiency	DFO	131,165,436–441,203,206,208,235,327,330,332,431	10 -250 µM *
	AKB-4924	442	10-100 µM
2-Oxoglutarate analogue	DMOG	131,165,445,446,267,327,423,430,432,439,443,444	0.5 – 3 mM **
	L-mimosine	447–449	0.3 – 1mM
	DHB	439,450	10 -1000 µM
Small molecular inhibitors of HIF degradation	FG4497	130,131	-
	BAPTA	451	-
	Ft1	141,452	2.5 – 10 µM

4.1.2.1 *Fe^{2+}-substitute ions*

Iron is an essential metal in the body and is a cofactor for multiple enzymes, being fundamental in the electron transport and redox reactions (as reviewed by Emerit et al. 2001). Several transition metal ions alter cellular iron homeostasis by competing with the iron transporters and/or the iron regulated enzymes mimicking a hypoxia response in the cells under normoxic conditions.[218,453] Ions like Co^{2+}, Ni^{2+}, Cu^{2+}, Cr^{6+}, and Mn^{2+} have similitudes with iron and can bind in substitution to iron and inhibit the reaction. Several mechanisms of inhibition of HIF-1α degradation have been proposed (see section 1.8) being the most accepted that Co^{2+} can substitute Fe^{2+} in the PHD 1-3 and FH-1, HIF-1α regulatory dioxygenases, inactivating the degradation.[215,218,220,232]

[h] Literature search using (HIF mim* OR Cobalt Chloride* OR CoCl* DFO OR DMOG OR iron chelat*) AND (wound* OR ulcer*). Search through Web of Science Core Collection, Scopus, Google Scholar and Pubmed.

Copper naturally is present in the body and an essential trace element, participating in wound healing and in the Copper Chaperone for Superoxide Dismutase (CCS). The sensitivity and ability to induce HIF activation through copper ions has been reported with opposing results. While 100 µM Cu (II) induced HIF-1α stabilisation in Hep3B cells and Hep G2, a higher amount was required to stabilise in HeLa cells, however 100 µM Cu II was toxic in A549 cells. Copper did not increase the HRE-driven luciferase reporter activity, however demonstrated a delay in the degradation of HIF-1α by inhibiting the PHD, allowing stabilisation but not inducing the production of the molecule. Nevertheless, a high exposure to copper, in dose or prolonged exposure, can lead to haemolytic anaemia, kidney and liver failure and gastrointestinal bleeding.[218,225,226]

4.1.2.1.1 Cobalt

The effect of therapeutic cobalt-induced hypoxia in healthy tissue has demonstrated an increase in ROS production (in rats), where the levels of lipid peroxidation were decreased and a rise of the GSH/GSSG ratio (reduced glutathione/oxidised glutathione), demonstrating an increased antioxidant capacity.[243] As it has been previously described (see section 1.8), cobalt may prevent the degradation of HIF-1α by inhibiting the interaction between HIF-1α and von Hippel Lindau, by directly binding to the HIF-1α[214] and also possibly by inducing HIF-1α expression through ROS generation. The effect of cobalt in HIF stabilisation is specific to the HIF-1α isoform not HIF-2α.[219,432]

The concentration of $CoCl_2$ used to stabilised HIF-1α varies widely across the literature ranging from 10 to 300 µM $CoCl_2$.[131,214,216,218,219,235,432–435] Previous studies have reported the cellular uptake of cobalt ions in keratinocytes and fibroblasts, however toxicity is cell-type specific. Keratinocytes have been shown to have a higher uptake of cobalt ions than fibroblasts[240] (for toxicity see 1.8.1) It has been observed that cobalt accumulates at the peri-nuclear cytosol of HaCaT cells. This accumulation was suggested to happen in the Golgi apparatus and the endoplasmic reticulum, and possibly through the same systems for divalent cation transport used by zinc.[454]

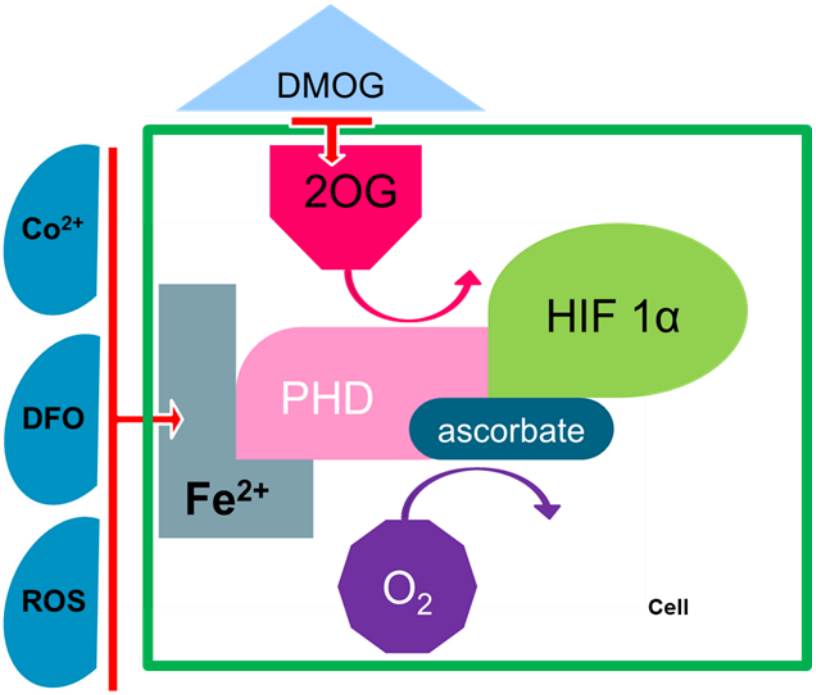

Figure 4-1 The mechanism of HIF stabilisation under normoxia by using HIF mimetics Co, DMOG, DFO and ROS. Co has been known to stabilise HIF-1α for over 25 years.[455] Co stabilises HIF1a by interaction with the HIF1a binding site of the von Hippel-Lindau protein (VHL)[214] and it has also shown that the action of Co to VHL is only specific to the HIF-1α protein not HIF 2α and 3α proteins.[432] DMOG is an analogue of 2OG, however, it lacks of binding to iron.[127] and strongly binds to 2OG active binding site of both PHD and FIH thus stabilises HIF-1a (competitive inhibitor). [456] DFO is a general iron chelator, which inhibits the binding of iron to PHD, thus stabilises HIF1a. ROS are hydrogen peroxide and oxygen free radicals, which inhibits the hydroxylation of PHD and FIH stabilising HIF consequently.

4.1.2.2 *Iron chelation*

Siderophores are small iron-chelating compounds with high affinity for soluble ferric ions in living systems. These compounds aid the organisms in uptake of iron in a soluble form from naturally occurring bound mineral forms like oxides and hydroxides by forming stable, hexadentate, octahedral co-ordination complexes (Figure 4-2).[457] AKB-4924 (Akebia Therapeutics) contains an α-hydroxycarbonyl that binds to iron, allowing HIF stabilisation.[442] AKB-4924 has been reported to reduce the inflammatory response and to improve epithelial barrier function, moreover in skin abscess model it reduced the lesion size resulting from *Staphylococcus aereus and* stimulated the killing capacity of keratynocites.[130,442]

4.1.2.2.1 DFO (Deferoxamine)

Deferoxamine (DFO/DFX) is a siderophore produced by the actinobacter *Streptomyces pilosus*, clinically used for iron overload and non-specific to the HIF pathway, due to the iron chelating nature.[127,424] As the PHD2 molecule uses iron as a cofactor and the FIH has an iron-core in its active site, therefore under the presence of DFO, the unavailability of iron would inhibit the degradation of HIF-1α.[203,424] Paller

and Hedlund (1994) proposed that the main site of action of DFO occurs extracellularly, thus depleting the iron from the cell, resulting in the inhibition of the PHD. Conversely DFO may also be able to penetrate some cell membranes, possibly through endocytosis (560 mw) and can protect the cells from lipid peroxidation.[458,459] DFO has been widely investigated for its promotion of angiogenesis, even under pathological conditions[208,438,441] and has been incorporated to different scaffolds and hydrogels to control the stable release.[206,460]

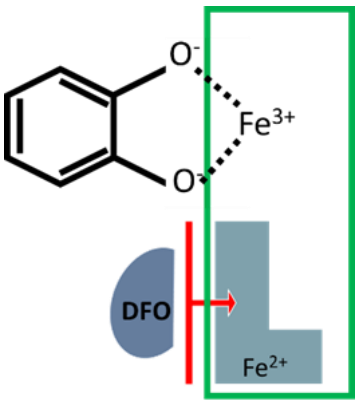

Figure 4-2 Siderophores sequestration of iron. Desferoxamine, a type of siderophore, disables the PHD2 and FIH molecules, as the first one uses iron as a cofactor; meanwhile the latter has an iron-core in in its active site.[457]

4.1.3 **2-Oxoglutarate analogue**

The existence of chemical compounds mimicking structurally 2-oxoglutarate inhibit PHD and FIH by blocking the binding to the iron-containing catalytic domain, which would initiate HIF-1α degradation.[127,175] L-mimosine (L-Mim) is a hypoxia mimetic agent that inhibits the prolyl and asparagyl hydroxylation, acting as a 2-oxoglutarate analogue, inhibiting prolyl 4-hydroxylase inhibitor. Although L-Mim has proved efficiency in mimicking HIF 1-α, by activating the HIF-1 target reporter, increasing the production of angiogenin, VEGF and reduction of PHD2, it has been reported the suppressed cell proliferation by inhibiting factors enabling cell cycle transition.[439,447–450] Dihydrobenzoic acid (DHB), is a less effective HIF mimetic, inhibiting the PHDS with respect to ascorbate depletion.[439,450]

4.1.3.1.1 DMOG

Dimethyloxalylglycine (DMOG) is a small molecule (MW 175.1g/Mol) non-specific analogue of 2-OG, it easily permeates into the cells and converted into N-oxalylglycine (NOG) by esterases and accumulates.[431,443] Due to its competitive binding to the PHD and FIH but lack of iron binding site, it stabilises HIF-1α.[127,431] A number of researchers have demonstrated that DMOG stabilises HIF in number of different cell types including (endothelial cells,[446] fibroblasts[165,365] and keratinocytes[327,461] in normoxia (See Table 4-1). Whilst it is assumed that the *in vivo* chronic wounds were hypoxic,

there is a lack of evidence that DMOG can further enhance HIF stabilisation in low oxygen conditions, certainly no in vitro data. The capacity of DMOG to mimic hypoxia under normoxia conditions in terms of gene transcript was well described by Elvidge et. al (2006), after observing that 190 HRE genes were significantly upregulated compared with 246 upregulated by actual hypoxia. Conversely, from the 191 transcripts that were downregulated by hypoxia, just 69 were downregulated by DMOG.[431] Zhdanov et al. (2015) observed a rapid suppression of NOG on mitochondrial respiration, which decreases the production of NADH and state 3 respiration and decrease of histone acetylation. These cascade of processes of DMOG affecting respiration happens before interaction of HIF-α proteins by PHD.[443] Thus the effect of DMOG may not be specific to the HIF pathway.

4.2 **Chapter Aims**

As shown in chapter 3, hyperglycaemia impairs the response of HIF pathway. This chapter tested the use of HIF mimetics to restore HIF functionality in the diabetic model.

Aim of this chapter:

1. To compare the effect of different HIF-mimetics (at different concentrations) on the restoration of wound healing responses (HIF stabilisation, cell metabolism and VEGF response) in response to hypoxia.
2. To determine if HIF mimetics causes changes in cell proliferation and cell survival.

4.3 **Materials and Methods**

The cell response to the HIF mimetics was evaluated in keratinocytes (HaCaT) and fibroblasts (HDF). Following a pre-selection of dose response in the HDF in terms of VEGF expression and metabolic activity, the response was evaluated in keratinocytes, as fibroblasts are more responsive to the oxygen variations. The response of fibroblasts was evaluated at days 1 and 3, keratinocytes were only evaluated at day 1.

HaCaT and HDFs were grown in fully supplemented DMEM with 10% FBS and 1% Penicillin/Streptomycin under normoxic conditions (see Methods section Cell Culture). HaCaT cell were seeded in a density of 20 00 cells/cm^2, while HDF were seeded at 10 000 cells/cm^2 in 48-well plates due to their nature in size and sensitivity to the assays. The cells were seeded and allowed to attach overnight, followed by the addition of the HIF mimetic and hypoxic conditions (1% O_2). After 24 hours, the media was collected and frozen for future VEGF measuring and metabolic activity was measured (see section 2.2.3). The cells were gently washed and 200µL of water were added. The plates were then placed in the freezer for future cell number quantification (see DNA Quantitation in 2.2.4). For the HDF, the media as replaced at day 2 in order to collect the VEGF response produced in 24 hours. The same measurement procedures were followed at day 3.

The HIF mimetic media were prepared in fully supplemented media (see above) before each experiment. Stock solutions of DMOG, DFO were prepared in DMSO and stored at -80ºC (see Materials in Chapter Methods). Cobalt chloride was diluted in distilled water at 200 mM concentration and kept at 4ºC. The specific ionic concentration was measured through ICP-AES and diluted accordingly.

4.3.1 **HIF stabilisation assay**

To confirm the HIF stabilisation, HaCaT cells –in euglycaemic and hyperglycaemic (28 days-preconditioned at 4.5 g/L Glc) were seeded in T150 flasks at a 4000 cells/cm^2 density with 25 ml of correspondent glucose media and allowed to attach and proliferate for 2 days. The media was replaced with HIF-mimetic conditioned media and the flasks were placed under normoxic and hypoxic (1% O_2) conditions for 24 hours. The HIF mimetic concentrations were selected from their capacity of increasing VEGF expression in the previous experiments, resulting in 50 µM of $CoCl_2$, 10 µM DFO and 250 µM for DMOG.

Nuclear HIF-1α molecule was measured with the Human/Mouse Total HIF-1α Duo Set® IC ELISA (see section HIF-1α protein quantification in Chapter Methods). Previously, nuclear extraction was performed using the Nuclear Extract Kit Active Motif. The nuclear protein extracted (total) was measured with a Thermo Scientific NanoDrop™ Spectrophotometer to confirm successful nuclear extraction.

4.3.1.1 *HIF stabilisation under hyperoxygen conditions*

In the cells exposed to 100% O_2, cells were seeded at 4000 cells/cm^2 density (as samples tested in hypoxia and normoxia), however T75 flasks were used with 12.5 ml of correspondent glucose media due to size restrictions of the hyperoxia chamber. The samples were placed in a constructed hyperoxygen chamber (see 2.2.2) and re-perfused with 100% O_2 for 5 min to allow air replacement. The nuclear HIF-1α was quantified using the same protocol as previously described; however, the volumes were halved to avoid dilution of the samples.

4.3.2 **Cell cycle flow cytometry**

In order to elucidate the effect of DMOG and 100% O_2, euglycaemic HDF cells were seeded in a concentration of 12 500 cells/cm^2 in a 6-well plate with 2.5 ml of 1g/L Glc media. Following overnight cell attachment, media was replaced with fresh or DMOG-conditioned (250 µM) media and placed under hyperoxygen conditions (as described in section 0). Cells were gently collected and stained (see section 2.2.12) using Propidium Iodide (FxCycle, Invitrogen) and flow cytometry was performed on LSRII and analysing 30 000 events.

4.3.3 **Statistical Analysis**

The experimental data was analysed using Prism Graphpad. The data was checked to see whether it was required to use parametric or non-parametric tests by Pearson and Spearman's test. Comparison between two individual data sets, was made using Student's t-test. More dataset comparisons were made using the one-way Anova, or two-way Anova when appropriate followed by Bonferroni. Each condition was repeated n=6, while the HIF assay had n=3. Mean and standard deviation were used. The representative experiments were selected for this chapter.

4.4 **Results**

Different concentrations of HIF mimetics were evaluated in fibroblasts and keratinocytes. The optimal concentrations were chosen based on the capacity to induce VEGF expression in fibroblasts and then used to test the VEGF release in keratinocytes. In order to confirm the stabilisation of the HIF pathway through the mimetics, HaCaT cells were used. Following the hypothesis that HIF mimetics can increase cell survival under hyperoxygen conditions, 85 and 100% O_2 conditions were tested. As an alternative, the preconditioning of the cells to HIF mimetics and/or hypoxia was also evaluated.

4.4.1 **Cobalt Chloride as a HIF mimetic: Biological response**

Fibroblasts were treated with 100, 75, 50 and 25 µM of cobalt chloride (Figure 4-3). After 24 hours, there was no significant difference in metabolic activity (SD ns, n=6). After 3 days, the metabolic activity of the cells in normoxia with cobalt have a significant increase to the control (***p<0.0001, n=6). Cells in hypoxia, under the presence of cobalt also had an increase of metabolic activity. VEGF secretion was increased in all the cobalt concentrations. In normoxic conditions, 75 and 100µM CoCl2 secreted VEGF similar to the level induced by 1% O_2 after 24 hours (***p<0.0001, n=6). After 3 days all conditions but 25 µM CoCl2 had an increased VEGF production. Under hypoxic conditions, the cobalt induced almost a two-fold increase of VEGF. At day 3 the VEGF production was increased in all the cobalt conditions, however 100 µM $CoCl_2$ had a threefold VEGF secretion (***p<0.0001, n=6).

In HaCaT cells, the metabolic activity was increased as a response to hypoxia (Figure 4-4), however, the metabolic activity with 50 µM $CoCl_2$ was significantly decreased, nevertheless, it was still higher than its normoxic pair (*** p< 0.0001, n=6). VEGF was increased in both oxygen conditions at 50 µM (**p<0.0014, n=6), which suggests HIF stabilisation. The cell number was not affected based in the DNA quantification after 24 hours, as there was no significant difference in all the conditions (SD ns, n=6), demonstrating that the cobalt chloride concentrations used were not toxic.

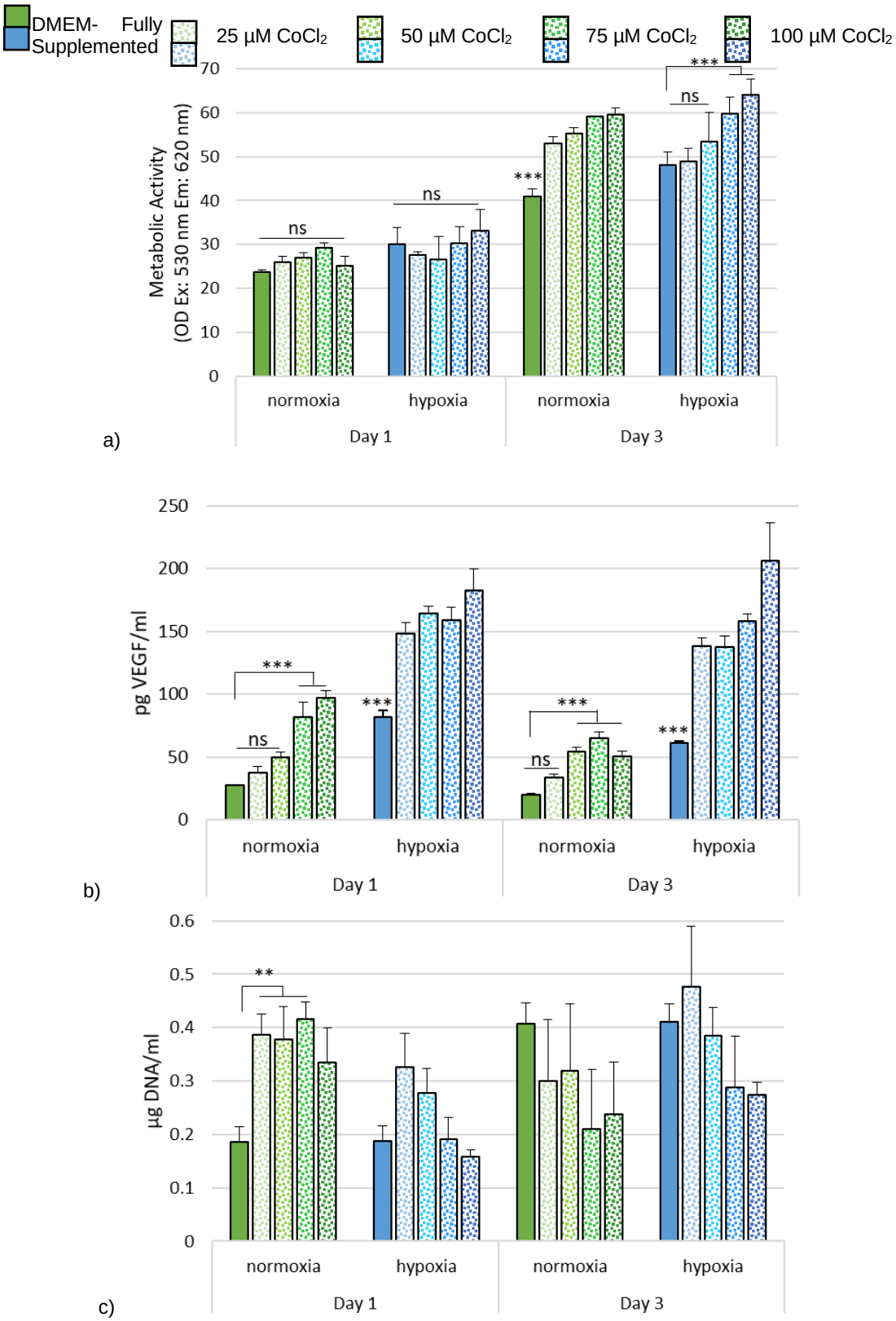

Figure 4-3 Cobalt induced VEGF expression under normoxia and hypoxia conditions in HDF cells. a) The metabolic activity of the cells remained constant after 24 hours of exposure to $CoCl_2$, as determined by alamar Blue®, however at day 3 the metabolic activity was increased. In hypoxia, changes were also observed by day 3, when the metabolic activity increased at 75 and 100 µM $CoCl_2$. b) A two-fold increase in VEGF secretion in normoxia is observed at 75 and 100 µM by day 1, similar to the hypoxia control. In day 3, 50-100 µM $CoCl_2$ increased significantly the VEGF production. $CoCl_2$ in combination with hypoxia further increased the VEGF secretion in both time points (Error bar= SD, ***p<0.0001, n=6).

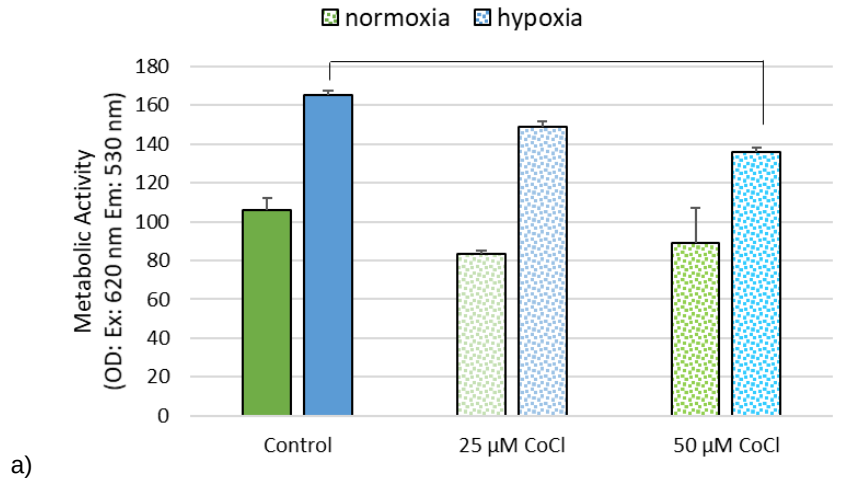

a)

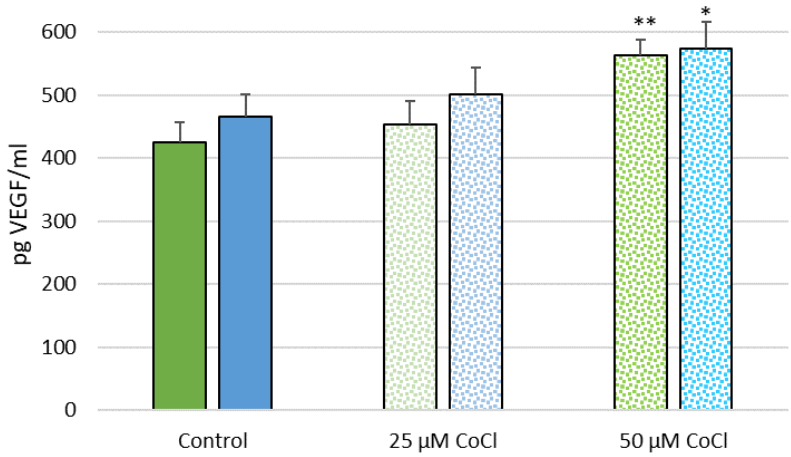

b)

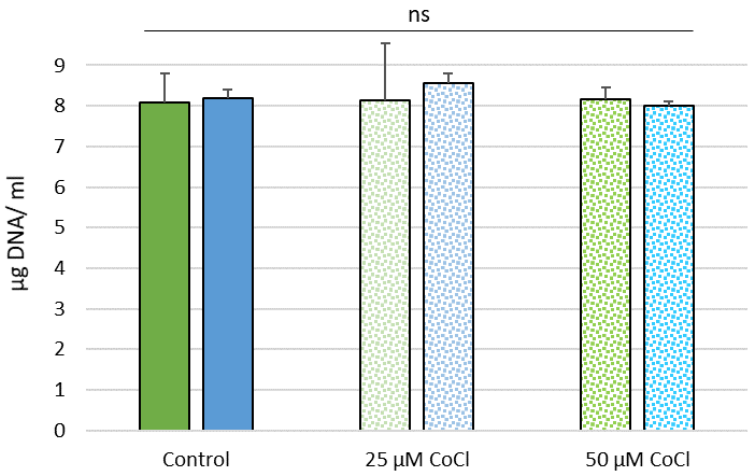

c)

Figure 4-4 Cobalt increased VEGF secretion in HaCaT a) The metabolic activity at normoxic levels was not affected by cobalt as measured by alamar Blue™, however, under hypoxia the activity decreased with 50 µM $CoCl_2$ (*** $p< 0.0001$, n=6). b) Cobalt chloride (50 µM) increased VEGF secretion at normoxic conditions and at 1% O_2 enhanced VEGF production resulting from hypoxia (** $p<0.0014$, n=6). c) Cell number, quantified using Hoechst dye, was not compromised under the presence of cobalt. Error bar= SD

4.4.1.1 *Cobalt: Nuclear HIF-1α stabilisation*

Cobalt chloride at 50 µM stabilised nuclear HIF-1α protein under hyperglycaemic normoxic conditions (Figure 4-5), being not significantly different to hypoxia or even hypoxia in euglycaemia. However this effect is reduced after day 3 and the HIF-1α is not significantly different to the basal level. This is contrary to what was observed under euglycaemic conditions, where HIF-1α was stabilised by day 1 and furtherly increased after 3 days (*** p <0.0001, n=3). Under hypoxic conditions at day 1, the addition of cobalt did not have an effect on the amount of HIF-1α detected, however under normal glucose conditions at day 3, the levels were higher than expressed in hypoxia (*** p <0.0001, n=3). In the same time point in hyperglycaemic conditions, the nuclear level of HIF-1α protein was below the basal level of hyperglycaemic normoxic cells.

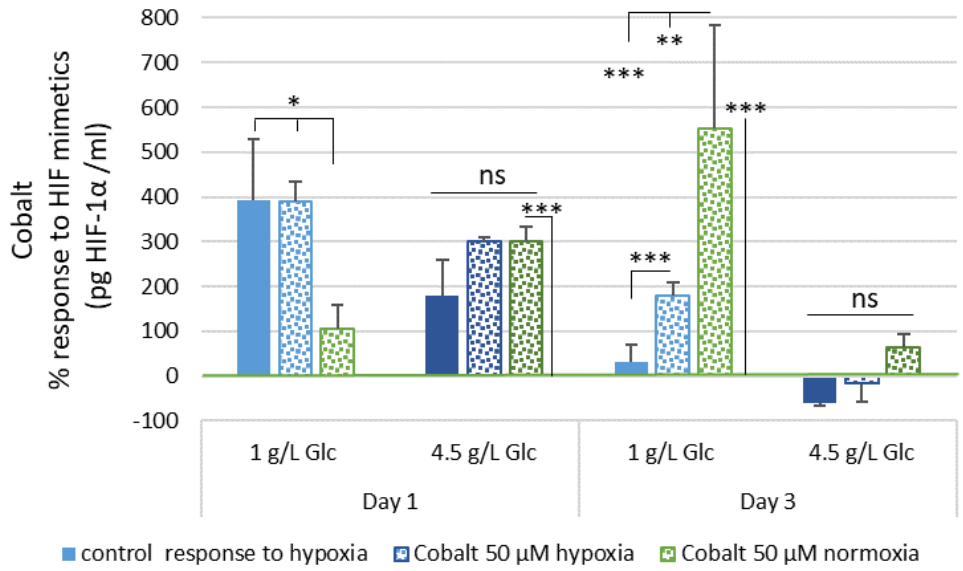

Figure 4-5 Cobalt stabilises nuclear HIF-1α, even under hyperglycaemic conditions. $CoCl_2$ successfully increased HIF-1α in both glucose conditions after 24 hours of exposure compared to basal normoxic levels as measured by HIF-1α ELISA. At day 3 the expression in euglycaemic conditions remained elevated similarly to the effect of hypoxia at day 1 –the green line represents the basal level in each glucose condition- (*** p <0.0001, n=3). In euglycaemia day 1, there is no difference between the HIF-1α expressed under hypoxia with or without the presence of cobalt, however at day 3, it was significantly increased (*** p <0.0001, n=3). Under hyperglycaemia in day 3, HIF-1α in hypoxia was at similar levels to the basal protein expressed in normoxia or even lower, the differences were found to be not significant. Error bar= SD

4.4.2 **Deferoxamine as a HIF Mimetic: Biological Response**

DFO had no effect on the metabolic activity of fibroblast at low concentrations (10-25 µM) at day 1, nevertheless a reduction in the metabolic activity was observed at day 3. The metabolic activity of cells in normoxic conditions was decreased significantly (***p<0.0006, n=6) compared to the control. Under hypoxia, the metabolic activity of the DFO conditioned cells (Figure 4-6) was compared to that in the normoxic control, however it was significantly decreased in a dose dependent manner (***p<0.0006, n=6). When the metabolic activity was compared to their pair under normoxia, all the conditions were significantly increased (***p<0.0006, n=6), which is commonly observed under hypoxia. DFO increased significantly VEGF expression under normoxia after 24 hours in a concentration-dependent manner, where 5 µM induced a 2.4-fold increase, whilst 25 µM a 4.5-fold (***p<0.0001, n=6)). The effect of the 5 µM concentration was reduced by day 3, when the VEGF secreted was no significantly different to the control (SD ns, n=6). However, in the other concentrations, VEGF remained elevated (***p<0.0001, n=6). DFO in normoxia in the concentrations between 10-25 µM had a higher VEGF expression than the hypoxic control. In hypoxia, the increase of VEGF was not significant at 5 and 10µM at day 1 when compared to the VEGF increased induced by hypoxia by itself, however, with 25 µM the VEGF secreted was doubled (p). At day 3 the production of VEGF by 10 µM was significantly higher than the control (***p<0.0001, n=6), and so were the higher concentrations evaluated, reaching a 1.5-fold increase at 25 µM DFO. Cell number remained constant, not increasing after 3 days under the effect of DFO, being significantly lower to the control (***p<0.0001, n=6, ** for 5 µM in both oxygen conditions).

In HaCaT cells DFO demonstrated to have a greater effect on metabolic activity (Figure 4-7**Error! Reference source not found.**), where the metabolic activity was observed to halve under normoxia (***p<0.0001, n=6). However, under hypoxia, the metabolic activity was not significantly decreased. The cell number was affected under the presence of DFO in a dose-dependent manner, a higher cell reduction number was observed at 25 µM of DFO. Hypoxia appeared to offer a mechanism of protection to the presence of DFO, as the cell number was reduced, however to a lesser extent (***p<0.0001, n=6). DFO had an increase in the VEGF production in normoxia at 25 µM DFO, due to the HIF stabilisation of the iron chelating compound, however this particular condition had a greater decrease in cell number, potentially due to toxicity.

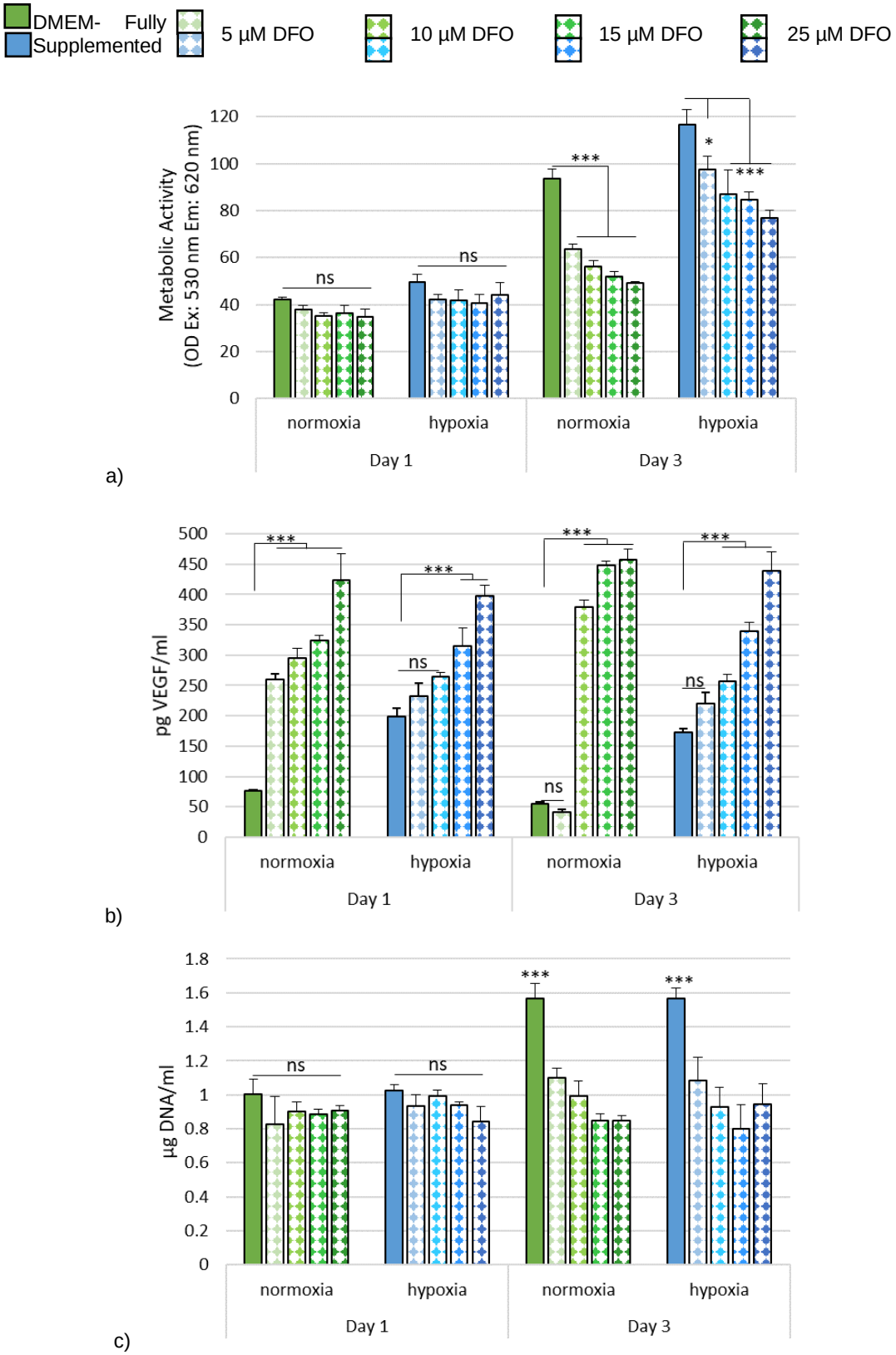

Figure 4-6 DFO induced toxicity in fibroblasts at low concentrations. a) DFO (5 to 25 µM) decreased metabolic activity, as determined by alamar Blue®, after 3 days of exposure in a dose-dependent manner. b) VEGF secretion was increased under the presence of DFO. The VEGF expression was similar between normoxia and hypoxia, as quantified using VEGF ELISA, under the effect of DFO. However, the 5µM failed to increase VEGF expression at day

3 on normoxia. c) Cell number remained constant, failing to increase number after 3 days when DFO was present. (Error bars= Standard deviation, n=6, ***p<0.0001)

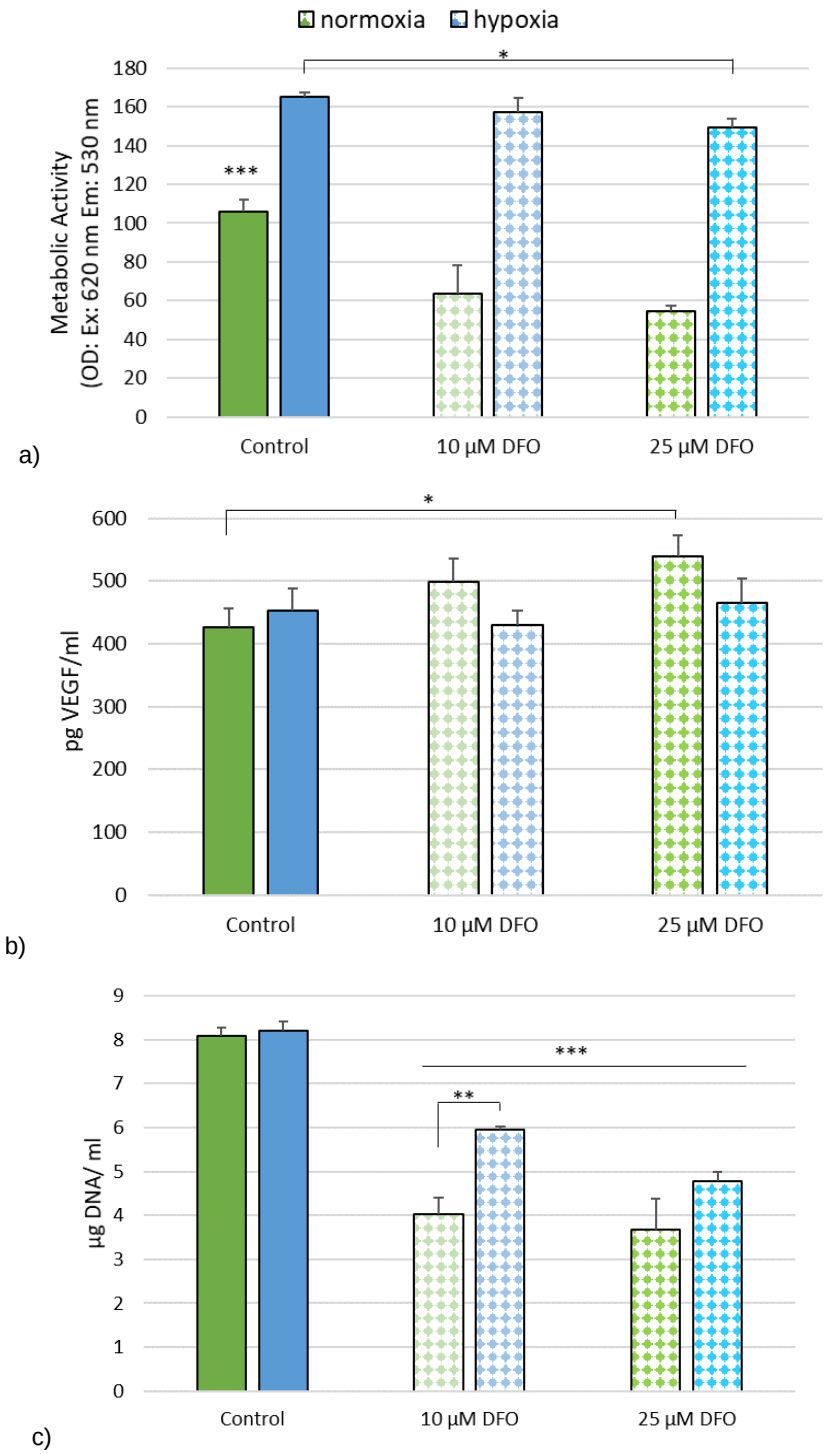

Figure 4-7 DFO had a toxic effect on HaCaT cells at low concentrations. a) DFO at 25 and 10 µM a significant reduction in cell metabolic activity, this decrease was more noticeable under normoxic conditions. b) DFO increased slightly VEGF production at 25 µM (*p=0.0107, n=6) c) Cell number was halved under the effect of DFO in normoxia; however, hypoxia had a protective effect in the observed toxicity from DFO as the cell number reduction was less. Error bars= Standard deviation, n=6, ***p<0.0001. Error bar= SD

4.4.2.1 *Deferoxamine: Nuclear HIF-1α stabilisation*

DFO at a 10 μM concentration has the capacity to stabilise HIF-1α under normoxic conditions in euglycaemic (1g/L Glc) conditions (Figure 4-8). The stabilisation of the HIF-1α under hypoxic conditions, was not significantly different to the one caused by the decrease of oxygen. However, by day 3, the expression of the HIF-1α is sustained, remaining equal for the normoxic condition and higher than the control under hypoxia.

Under hyperglycaemic conditions (see Diabetic model section 3.4.2), DFO is able to stabilise HIF at normoxic conditions in the same manner as the hypoxic hyperglycaemic control ($p>0.05$, $n=3$). The DFO under hypoxia does not have an effect in the protein regulation at day 1. DFO had no effect in increasing HIF-α expression under the wound model, nor in normoxia or in hypoxic conditions.

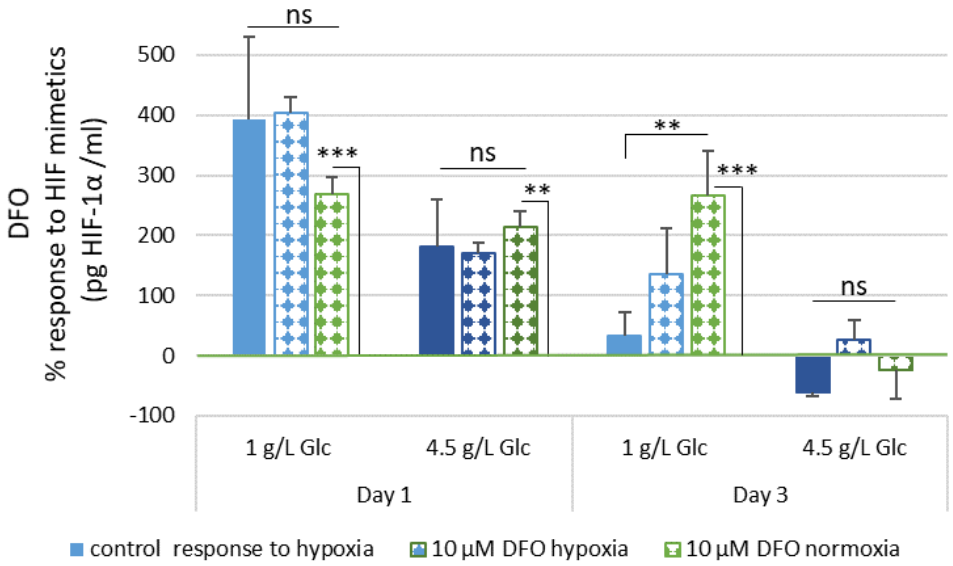

Figure 4-8 DFO stabilised HIF-1α under normoxic conditions in both glucose levels. The amount of HIF protein, as measured by HIF 1α ELISA, under normoxic conditions was non-significantly different to the one in the hypoxic control for each glycaemic condition, but it was significantly higher than the basal normoxic level (*** $p<0.0001$, $n=3$). DFO had no significant effect when in combination with hypoxia at day one. By day 3, HIF-1α was stabilised by DFO only under low glycaemic conditions, and under normoxia was expressed at a higher concentration than the hypoxia control (***$p<0.0001$, $n=3$). Under high glucose, the HIF-1α expression was not significant among them, or to the basal level. Error bars= Standard deviation, $n=3$, ***$p<0.0001$

4.4.3 **DMOG as a HIF mimetic: Biological Response**

DMOG had no significant effect on the metabolic activity of fibroblast at day one under normoxia conditions (Figure 4-9), however a decrease was observed under hypoxia conditions as the concentrations increased (*p<0.05, n=6). At day three, the metabolic activity of 100 µM DMOG in normoxia increased to the same level as the hypoxic control suggesting HIF stabilisation. The metabolic activity of the other concentrations remained similar to the normoxia control; however, a decrease was observed at the highest concentration-1 mM (*p<0.05, n=6), which was also observed under hypoxic conditions at both time points (***p< 0.0001, n=6), and to a lesser extent with the other DMOG concentrations. VEGF was significantly increased with all the concentrations of DMOG, particularly at day 1. A concentration of 100 µM was sufficient to have a four-fold increase in VEGF secretion under normoxic conditions while 1mM increased VEGF in a fifteen-fold. The response of VEGF secretion under hypoxia was further increased under the presence of DMOG, for the 100 µM concentration, a four-fold increase was observed; whilst at 1mM an increase of five-fold was seen. At day 3, the response of DMOG at normoxia was diminished while the trend remained. The VEGF secretion was doubled at the lowest DMOG concentration (***p<0.0001, n=6), whilst 1 mM induced a thirteen-fold increase. Under 1% O_2, the VEGF secretion remained elevated in a four-fold in 1 mM and 500 µM, when compared to the hypoxia control. There was no significant difference across the concentrations of DMOG.

In HaCaT cells, DMOG did not affect metabolic activity in concentrations between 100-500 µM (Figure 4-10). Cells responded to the hypoxic stimuli by increasing the metabolic activity (***p<0.0001, n=6), there was no significant difference across the DMOG concentrations and under normoxia. VEGF was increased in hypoxic conditions, however only 250 µM DMOG increased VEGF significantly under normoxic conditions (*p<0.0039, n=6). Cell number did not varied significantly (SD, n=5). When normalising the VEGF per cell number (data not shown), 250 µM DMOG under normoxia had a similar expression to the hypoxic control (SD ns, n=6), however it was significantly higher to the normoxic control (*p<0.05, n=6).

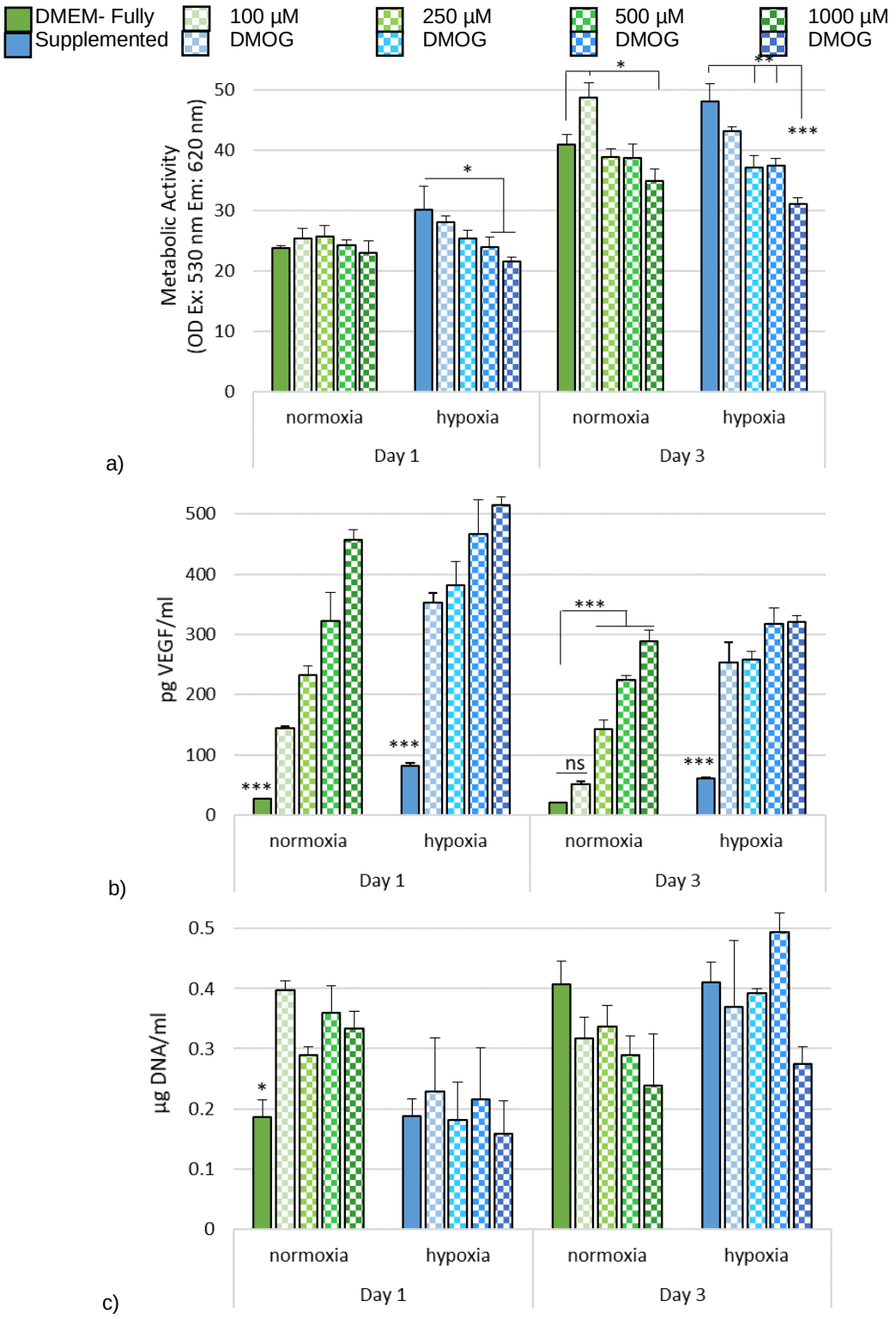

Figure 4-9 DMOG induces a VEGF increase in HDF cells. a) Metabolic activity was not significantly affected after 24 hours of exposure to DFO, after 3 days the metabolic activity decreased in a dose-dependent manner under hypoxia. b) DMOG induced a significant 15-fold of VEGF expression in normoxia at 1mM DMOG, and a 4-fold increase at 100 µM DMOG, which was the lowest concentration. In conjunction to hypoxia, DMOG increased VEGF between a three and 5-fold. At Day 3, the VEGF DMOG continued inducing VEGF expression, however in a lesser quantity. In normoxia, the highest amount was induced by 1mM of DMOG, and the effect of 100 µM was reduced to a 1.5x increase. There was no significant difference in the release of VEGF in DMOG-hypoxic cells; however, it remained increased 3.5x higher than the control. Error bars= SD, n=6, ***p<0.0001

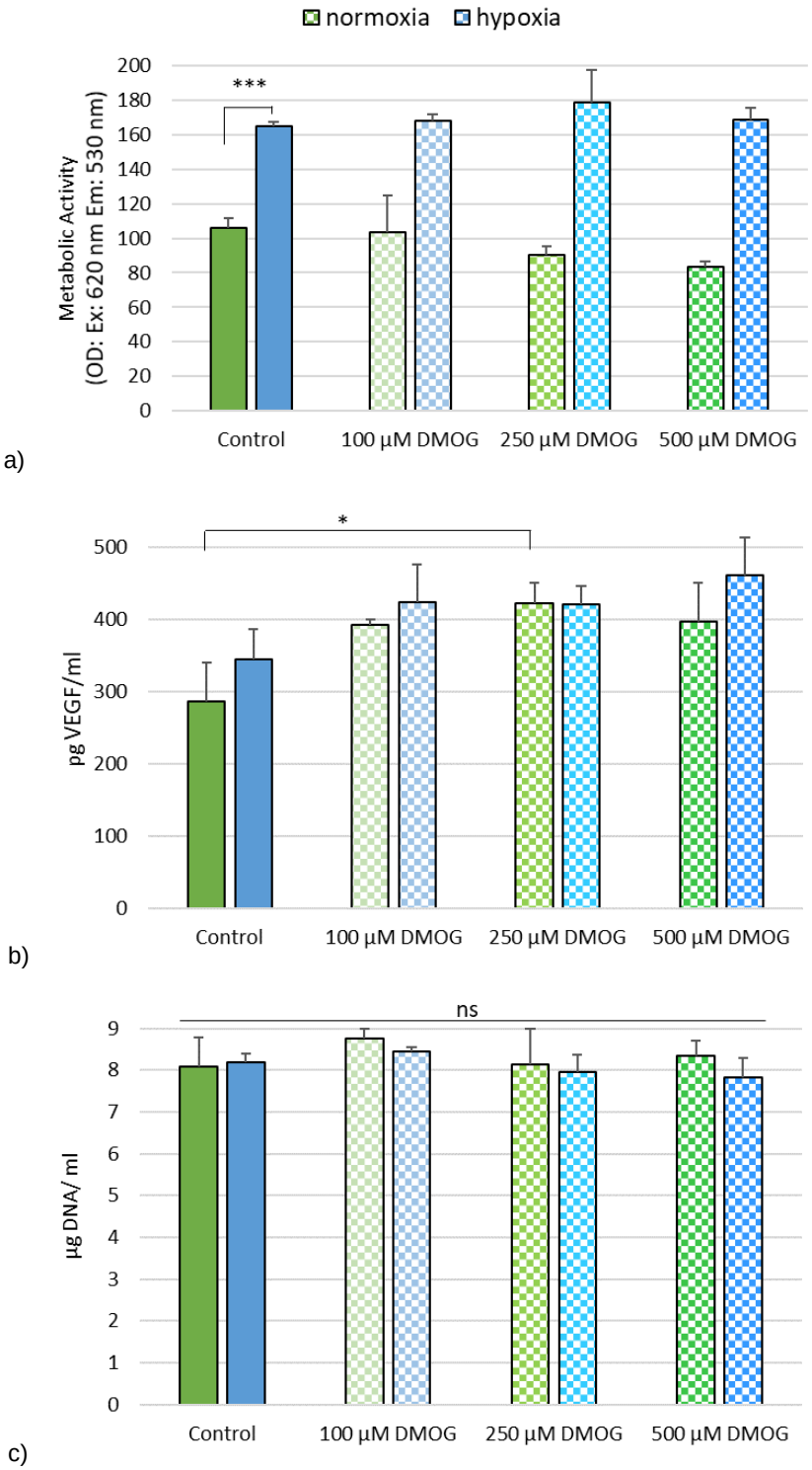

Figure 4-10 DMOG increases VEGF expression in HaCaT cells. a) Metabolic activity was not affected by DMOG. In all the concentrations HaCaT increased the metabolic activity as a response to hypoxia (***p<0.0001, n=6), while the metabolic activity did not varied across concentrations. b) DMOG increased VEGF secretion at 250 µM under normoxia (*P<0.0039, n=6) c) DMOG did not affect cell number after 24 hours (ns- no significant). Error bars= SD, n=6.

4.4.3.1 *DMOG: Nuclear HIF-1α stabilisation*

DMOG at a 250 µM was evaluated for the ability to stabilise nuclear HIF-1α based on the VEGF expression in fibroblast and keratinocytes (Figure 4-9b, Figure 4-10b). DMOG significantly decreased the HIF-1α after 24 hours of hypoxia in euglycaemic cells (Figure 4-11), halving the response induced by hypoxia (*p< 0.05, n=3). However in hyperglycaemia hypoxic cells, HIF-1α was found not to be significant higher than the basal level. At day 3, the hypoxic control was not significantly higher than the basal level in any glycaemic condition, and in combination with DMOG, the levels were even lower than the basal HIF-1α protein produced (**p<0.001, n=3). Under normoxia, DMOG did not increased HIF-1α in any glycaemic conditions in both time points; furthermore, in the hyperglycaemic cells it was significantly decreased when compared to the basal level. (***p<0.0001, n=3).

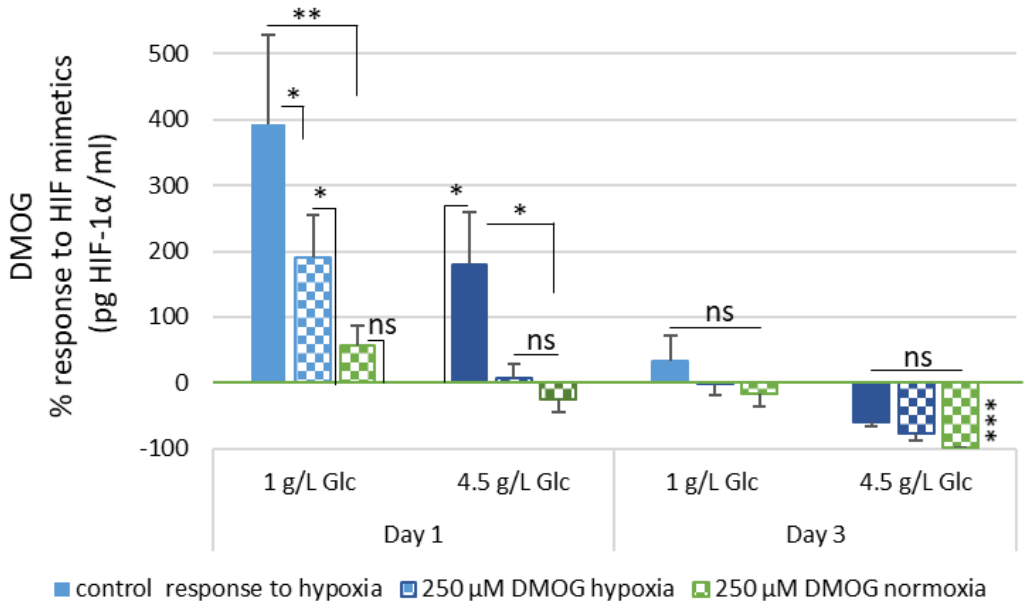

Figure 4-11 DMOG at low concentrations (250 µM) did not stabilised HIF-1α. The response to hypoxia at day 1 in both glycaemic conditions stabilise HIF-1α significantly compared to the basal level expressed in normoxia (represented as a green line), however, this response was diminished by day 3, as determined by HIF 1α ELISA. DMOG under hypoxia decreased the amount of nuclear HIF-1α, it was halved in euglycaemic cells (*p<0.05, n=3), however it was significantly increased compared to normoxia (*P<0.05, n=3), whilst in hyperglycaemia the protein was null. At day 3, DMOG had no effect in HIF-1α at either oxygen condition in euglycaemia, moreover in the hyperglycaemic conditions, the presence of DMOG significantly reduced the amount of HIF-1α below basal levels (***p<0.000, n=3). Error bars = standard deviation.

4.4.3.2 *Does DMOG (HIF-mimetics) enhance cell survival?*

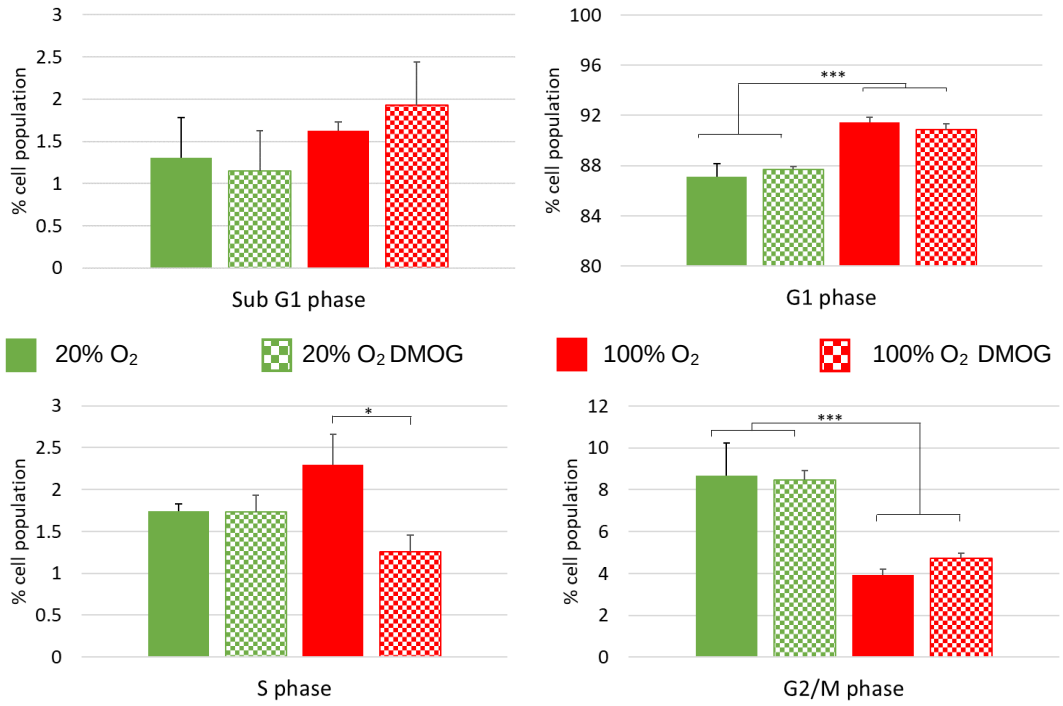

Figure 4-12 Hyperoxia (100%) induced cell cycle changes, independently of DMOG, as determined by flow cytometry. Cells with or without DMOG (250 µM) were incubated for 24 hours under normoxic or 100% O_2. Under normoxia, there is no difference in cell cycle progression, as determined by flow cytometry- cell cycle assay, between DMOG treated and non-treated cells. Under hyperoxygen conditions (100% O_2), a higher percentage of the cell population (3%) remained in G1 phase, and the cell population at G2/M phase was significantly lower under high oxygen conditions. DMOG however, had a significant effect under hyperoxia in the S phase ($p<0.05$, n=30 000 events).

Cell cycle flow cytometry was done in HaCaT cells to evaluate if 250 µM DMOG exerted a protective effect in cell survival under 100% O_2 conditions (Figure 4-12). In normoxic conditions, DMOG did not have any influence in the cell cycle progression after 24 hours of exposure ($p>0.05$, n=30 000). The number of events measured in G1 increased 4% under hyperoxia (***$p<0.001$, n=30 000), this increase was also observed in hyperoxic cells with DMOG. In the S phase, there was no significant difference from hyperoxia to normoxia, however a difference with hyperoxia DMOG was observed (*$p<0.05$, n=30 000). A lower number of events was observed in both hyperoxic conditions in the G2/M phase (***$p<0.001$, n=30 000).

4.4.3.3 *Can DMOG reduce cellular damage from oxidative stress?*

DMOG at 500 and 250 µM decreased basal ROS production (Figure 4-13) after 5 hours incubation (***$P<0.0001$, n=4). The ROS production was similar to the

decreased ROS under antioxidants 2 mM N-Acetylcysteine and 10 mM sodium pyruvate (ns SD p>0.05, n=4).

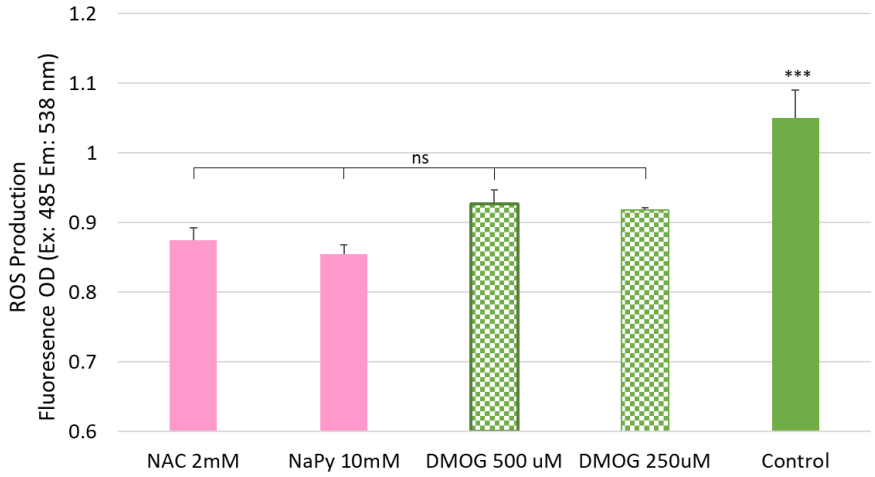

Figure 4-13 DMOG increases the cell antioxidant capacity. Basal ROS, as determined using DCF-DA dye, in normoxia was reduced under the presence of DMOG at 250 and 500 µM concentrations in normoxic conditions, similarly to the effect that antioxidants as N-acetylcysteine (NAC) and sodium pyruvate (NaPy) have. (p<0.001, n=3) Error bars=standard deviation

4.4.3.4 *Relation between oxygen, glucose level and cell survival*

HaCaT and HDF respond differently to different levels of oxygen (Figure 4-14 describes HDFs). Both cell lines were able to proliferate and were metabolic active at 85% O_2 (see HDF images in Figure 4-15 and HaCaT in Figure 4-16) however hyperglycaemia had an effect cell proliferation and cell survival. By day 3, euglycaemic fibroblasts had a higher proliferation rate than hyperglycaemic; however, after 7 days of 85% hyperoxia, the cell number in the hyperglycaemic condition was higher (***p<0.0001, n=5). The hyperglycaemic DMOG-treated cells were significantly less than the non-treated ones. Cells under 100% O_2, rapidly decreased in cell number. After 24 hours, the number of cells was significantly decreased compared to the rest of the conditions (***p<0.0001, n=5). DMOG did not have an effect on cell survival (ns SD, p>0.05, n=5).

The metabolic activity was decreased under hyperoxygen conditions. After 24 hours, the metabolic activity of cells at 100% O_2 was almost zero. The metabolic activity at 85% O_2 did not varied significantly between day 1 and 3, however at day 7, the metabolic activity of hypoglycaemic cells was significantly reduced (***p<0.0001, n=5). In the hyperglycaemic cells at 85% O_2, there was a significant difference between DMOG treated cells, with a decreased metabolic activity (***p<0.0001, n=5).

a)

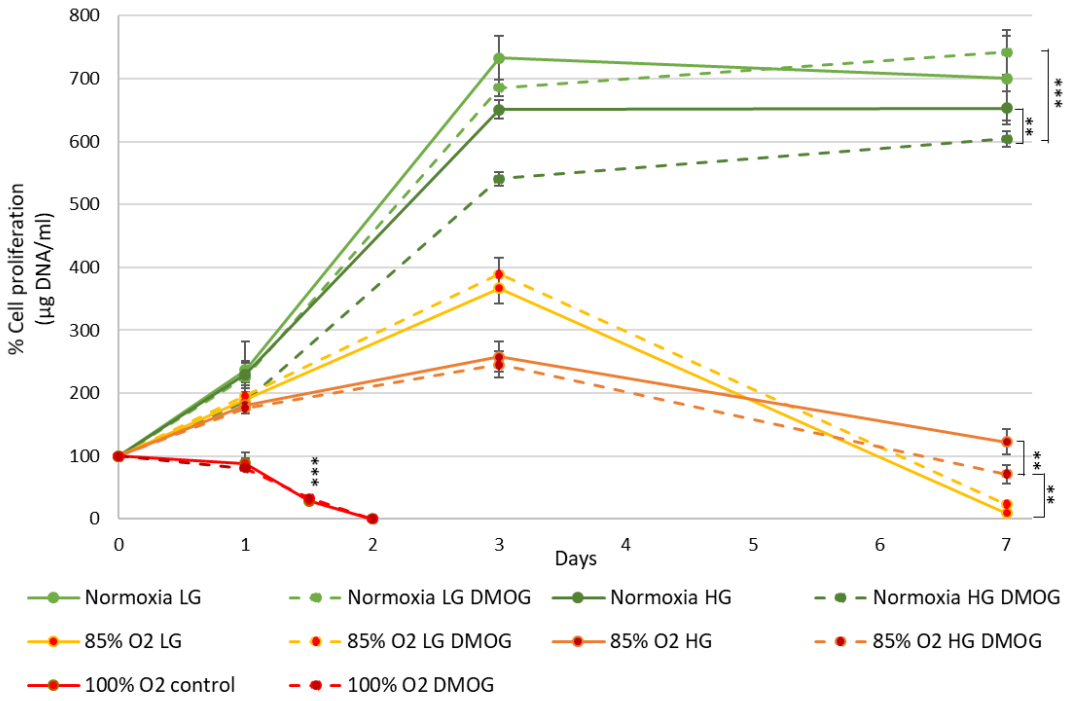

b)

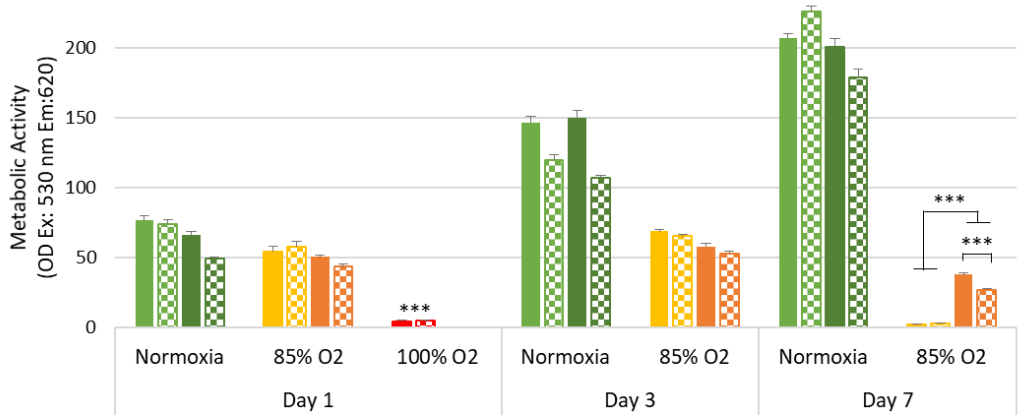

Figure 4-14 Hyperoxia reduces cell proliferation and survival in HaCaT cells, whilst cells are able to proliferate at 85% O_2. a) Cells under 85% O_2 had a reduced cell proliferation, as quantified with Hoechst dye, after 24 hours ($p<0.05$ n=5), where the glucose level had no effect. DMOG had no effect in the cell proliferation in euglycaemic cells, but in hyperglycaemic cells a reduction in cell proliferation was observed by day 3 ($p<0.0001$ n=5) After 3 days, euglycaemic cells had a higher proliferation rate 100% when compared to hyperglycaemic cells, nevertheless the cell number halved the one observed in normoxic conditions. The cell survival/proliferation observed in euglycaemic cells in 85% O_2 was reversed by day 7, were the cell number was notably reduced in hyperglycaemic conditions, DMOG having less cell survival ($p<0.0005$ n=5), and a very reduced number for the euglycaemic cells ($p<0.0005$ n=5). After 36 hours of exposure, 100% O_2 had a detrimental effect in cell number ($p<0.0001$ n=5), DMOG having no effect in cell survival. b) Cell metabolic activity, as determines by alamar Blue®, was affected by the increase of oxygen concentration. At 85% O_2, the metabolic activity was decreased, having a higher impact under hyperglycaemic conditions. This was observed also in the 3rd day. At day 7, only hyperglycaemic cells were metabolically active, however, cells with DMOG had a lower level ($p<0.0001$, n=5).

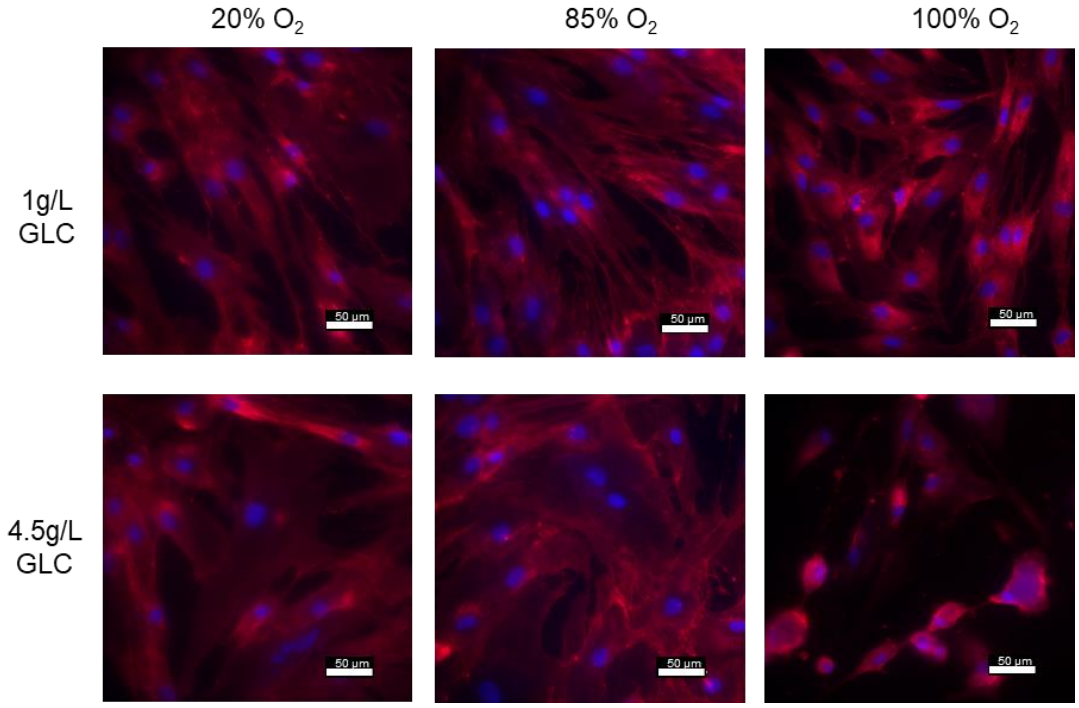

Figure 4-15 Fluorescence micrographs of euglycaemic and hyperglycaemic HDFs under hyperoxygen (85 and 100% O_2) exposure. Immunofluorescence of the cellular body (Red: wheat germ agglutinin Alexa Fluor™ 594 for membrane, Blue: DAPI for nuclei) and body shrinking after oxygen increases. A higher number of euglycaemic HDF at 100% O_2 (top-right) were observed when compared to hyperglycaemia. However, cell number decreased when compared to 85% O_2 (central images). Scale bar 50 µm.

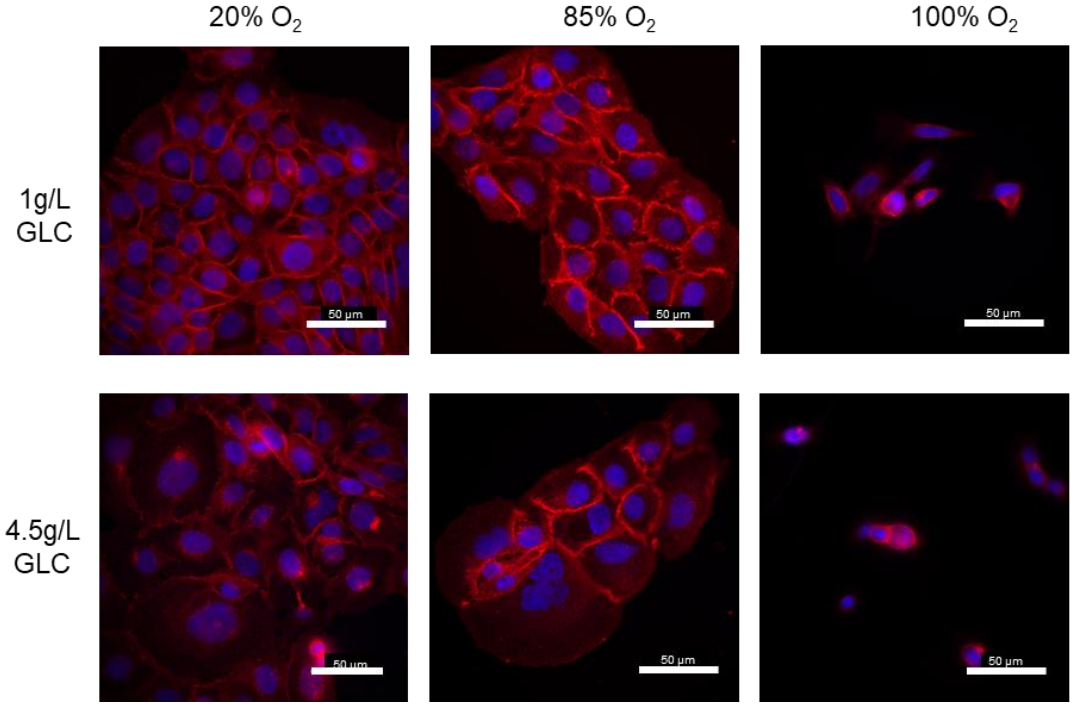

Figure 4-16 Fluorescence micrographs of the effect of hyperoxia (24 hours under 85 and 100% O_2) in euglycaemic and hyperglycaemic HaCaT cells. Cell size was affected by the glucose level. (Red: wheat germ agglutinin Alexa Fluor™ 594 for membrane, Blue: DAPI for nuclei.) At 85% O_2, cells maintained their characteristic cobblestone shape under both glucose conditions (central images). After 24 hours of hyperoxygen (100% O_2) the cells have reduced bodies (right column). Scale bar 50 µm.

4.4.3.5 *Can HIF-1α be stabilised through 100% O_2?*

Euglycaemic cells did not stabilise HIF-1α under 100% oxygen (Figure 4-17). There was no significant difference under the presence of DMOG in either glucose lever (ns SD p>0.05). However hyperglycaemia increased significantly (***p<0.0003, n=3) HIF-1α accumulation. VEGF under hyperglycaemia cells was increased significantly when compared to the control (*p<0.005, n=3), while DMOG did not increase VEGF production.

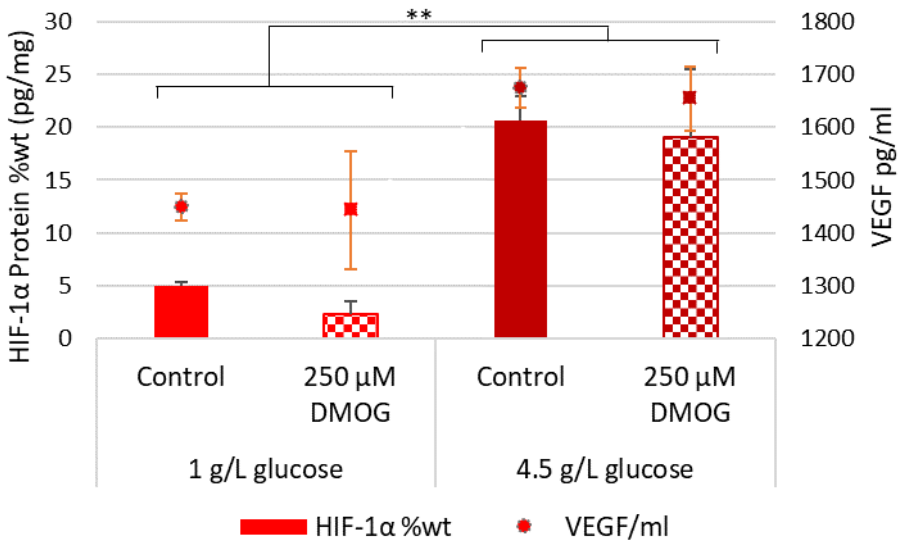

Figure 4-17 HIF-1α stabilisation under 100% O_2 was mediated through high glucose. Euglycaemic cells had a reduced HIF-1α protein level, as quantified with HIF 1α ELISA, compared to hyperglycaemic cells (p<0.000, n=3), DMOG did not influence HIF-1α stabilisation. VEGF determined with VEGF ELISA. Error bars= SD

4.5 **Discussion**

The cell response between fibroblasts and keratinocytes is not only different to hypoxia, but also to the HIF mimetics.[199] HDF appeared to be more sensitive to the variations of the oxygen condition and the response to the HIF mimicking factors was also more noticeable than in HaCaT cells. The HIF mimetics $CoCl_2$, DFO and DMOG were selected as their use as HIF mimetics is widely reported (see Table 4-1). The biological response to the mimetics was evaluated in euglycaemic cells to select effective doses that can induce an increase in VEGF response. The capacity to stabilise nuclear HIF was assessed under hyper- and euglycaemic conditions. This was only performed in HaCaT cells, due to the difference in the cell size and the high number of cells required; taking also in consideration the stability of the preconditioning in the diabetic model. It is important to consider the effect of the HIF mimicking factors under hypoxia. Whilst there is heterogeneity in the oxygenation of skin and wounds, it is exaggerated in diabetic environments.

4.5.1 **Can Cobalt Chloride restore the HIF functionality under hyperglycaemic conditions?**

Cobalt chloride successfully stabilised nuclear HIF-1α at a 50 μM concentration in normoxia in both glucose conditions. However, the increase of HIF-1α accumulation after 24 in euglycaemic cells was not significant when compared to the amount of molecule expressed at basal levels in normoxia. By day three, the levels had reached the same amount of protein that is induced in hypoxia after only 24 hours, significantly higher than the basal level. Interestingly, cobalt could induce the HIF accumulation in the same extension as in hypoxia in the hyperglycaemic environment. Even if this response is characterised as an impaired response to hypoxia, it was significantly higher than the basal hyperglycaemic level and higher than the accumulation in euglycaemic cobalt pair. The amount of HIF-1α measured in hyperglycaemia by day 3 was not considered to be higher than the basal level and was significantly decreased when compared to the previous time point. Cobalt in hypoxia did not had a significant effect in increasing HIF-1α at day 1, in both glycaemic conditions there was no significant difference. However, in day 3 in the euglycaemic condition, HIF-1α in hypoxia remained significantly higher than the basal level, although the amount of protein halved. Nevertheless, the amount of protein in the normoxic euglycaemic cobalt condition was significantly higher than the hypoxia and cobalt+hypoxia condition.

Similarly to these results, it has been reported that in HeLa cells the accumulated HIF-1α induced by cobalt chloride and DFO were sustained for a prolonged period, in comparison to the hypoxia itself.[235] While it has been reported that cobalt can mediate a similar HIF1-gene expression than hypoxia.[462,463] Concomitantly with the results, Milosevic et al. (2009) described HIF-1α stabilisation after 3 days of exposure to 50 and 100 µM $CoCl_2$, without affecting the metabolic activity of NPC (human Neuroprogenitor) cells.[131] Furthermore, cobalt chloride and DFO induce the transactivation domains (TAD) in HIF-1α inducing gene expression.[464] Cobalt chloride has also been reported to induce HIF stabilisation in diabetic murine models, preventing diabetic nephropathy.[422]

Cobalt did not significantly influence cell number or growth at the concentrations evaluated within 72 hours incubation period, consistent to what has been reported previously in NPC cells.[131] Although in normoxia an increase was observed after 24 hours, cell number did not changed compared to day 3. Bresson et al. (2006) reported that concentrations at 100 µM decrease the colony forming efficiency of HaCaT cells in a 73%, whilst it was halved at ~500 µM Co (II). However, 620 µM Co (II) reduced the metabolic activity of the cells to 50% (EC_{50}).[246] Here, in HDF the metabolic activity of the cells increased after 3 days of exposure to $CoCl_2$, corresponding to the Warburg effect induced by HIF stabilisation.[465,466] Under cobalt+hypoxia treatment the metabolic activity was increased at 75 and 100 µM $CoCl_2$, but was not significant different to the paired normoxic condition. In HaCaT cells at day 1, cobalt did not have an effect on the metabolic activity in normoxia. Under hypoxia, cobalt 50 µM reduced the metabolic activity compared to the hypoxic control, however it remained elevated compared to the normoxic pair and control.

VEGF secretion was significantly increased with 50 µM $CoCl_2$ in both cell lines under normoxic conditions. Cobalt induced a further secretion of VEGF under hypoxic conditions, this could be possibly through the influence of cobalt in the HIF-1α TAD.[125,436,437] When VEGF was normalised to the cell number (data not shown), the positive effect of cobalt+hypoxia in VEGF secretion was more noticeable.

As discussed previously (1.8.1) cobalt can accumulate intracellularly, possibly leading to toxicity;[246,286,454,467] although the accumulation is not linear.[246,247] Nevertheless, the capacity of cobalt to induce a regenerative response in a chronic wound may outweigh the negative effects it could produce. One of the major events in wound closure is the migration of keratinocytes into the wound bed. Fitsialos et al. (2008) observed that under normoxic conditions, when HIF-1α was silenced, the

migration of HaCaT cells was reduced by 50% in a scratch wound and trans-well models, meanwhile the cell proliferation was not affected. In addition they showed that inducing the stabilisation of HIF-1α with $CoCl_2$ under normoxic conditions, keratinocyte adhesion and motility increased.[300] Cobalt demonstrated the capacity to stabilise HIF-1α under hyperglycaemic conditions under normoxia, furthermore in hypoxia it did not affect negatively the reduced response to the low oxygen tension. Thus, ionic cobalt and incorporation to delivery systems for chronic wound healing is a promising area of research. The incorporation of cobalt (II) to bioactive glass as a delivery system is discussed in Chapter 5.

4.5.2 Can DFO restore the HIF functionality under hyperglycaemic conditions?

DFO stabilised HIF-1α under hyperglycaemic and euglycaemic conditions after 24 hours of exposure at a concentration of 10 µM. The amount of accumulated HIF-1α was similar between both glucose conditions and significant to the basal production in normoxia. HIF-1α was non-significantly different to the expression under hyperoxia in the presence of DFO or with hypoxia as stimuli. DFO did not affect HIF expression in conjunction with hypoxia, moreover in day 3 under euglycaemic conditions, it allowed further accumulation of the protein –however it was not statistically significant. By day 3, HIF-1α remained sustained under euglycaemic normoxic conditions.[235] The amount expressed was significantly different to the hypoxic expression at the same time point and similar to day 1. This effect of prolonged HIF stabilisation was also observed under cobalt chloride HIF stabilisation (see previous section).

DFO concentrations were selected based on initial experiments with 100-50 µM, which had a toxic effect seen as a decrease in metabolic activity by ~50% (Appendix 1). Under lower concentrations DFO, fibroblasts had a significant increase in VEGF secretion in both oxygen conditions. While 25 µM DFO had an increase of 4.5-fold increase in VEGF production in normoxia and a two-fold in hypoxia, which remained elevated by day 3. DFO 10 µM -which was used for the HIF-1α assay- had an increase of almost a three-fold at day 1 and almost six-fold by day 3, however under hypoxia it increased VEGF production in a lesser extension. The lowest concentration evaluated, 5 µM only had an effect in VEGF increase for the first 24 hours under normoxic conditions. In the keratinocytes cell line, the increase was less significant, happening at a concentration of 25 µM after 24 hours. DFO had an important effect in metabolic activity in both cell lines and oxygen conditions. In fibroblast by day three, the metabolic activity under DFO had decreased when compared to the control. It is

interest to observe that the fibroblasts did not significantly increased the cell number under the influence of DMOG in any oxygen condition, possibly explaining the metabolic activity response. It remains unclear if this phenomenon was due to a reduced cell proliferation resulting from HIF stabilisation –although the hypoxia control proliferated- or could be possibly attributed to toxicity.

Under DFO, fibroblasts had an important increase in VEGF secretion in both oxygen conditions. While 25 µM DFO had an increase of 4.5-fold increase in VEGF production in normoxia and a two-fold in hypoxia, which remained elevated by day 3. DFO 10 µM -which was used for the HIF-1α assay- had an increase of almost three-fold at day 1 and almost six-fold by day 3, however under hypoxia it increased VEGF production to a lesser extent. The lowest concentration evaluated, 5 µM only had an effect in VEGF increase for the first 24 hours under normoxic conditions. In the HaCaT cell line, the increase was less significant, happening at a concentration of 25 µM after 24 hours. DFO had an effect in metabolic activity in both cell lines and oxygen conditions. In fibroblast by day three, the metabolic activity under DFO had decreased when compared to the control. It should be noted that fibroblasts not significantly increase the cell number under the influence of DMOG in any oxygen condition, possibly explaining the metabolic activity response. It remains unclear if this phenomenon was due to a reduced cell proliferation resulting from HIF stabilisation –although the hypoxia control proliferated- or could be attributed to toxicity. In the HaCaT cells the reduction in metabolic activity was more noticeable, a reduction of ~47% was observed with 25 µM DFO in normoxia, however in hypoxia it was not significant. The cell number was also significantly increased under the presence of DFO, suggesting this decrease was due to toxicity. It was hypothesised that under artificial HIF stabilisation, the metabolic activity would increase due to the Warburg effect –anabolic respiration.[125,465] However, Botusan et al. (2008) have reported the anti-proliferative effect of 30 µM DFO *in vitro* in mouse fibroblasts and in *in vivo* models at 1 mM.[165]

DFO has been shown to induce angiogenic growth factors production and vascularisation in murine models[109,200,406,438] and previously has been used for in vitro experiments in concentrations ranging from 10-250 µM, increasing VEGF and HIF stabilisation (see Table 4-1). However as discussed in section 3.5.1, the response to HIF mimetics and even hypoxia is cell specific.[199,332] In this work, DFO had an effect in the cell number and metabolic activity in HaCaT at day 1 when in HDF the effect was observed at day 3. Habryka et al. (2015) reported that DFO at 100 and 250 µM for 24 hours decreased ~30% the metabolic activity of HaCaT cells and decreased

cell number, which was not observed under the effects of cobalt chloride and hypoxia.[332]

4.5.3 Can DMOG restore the HIF functionality under hyperglycaemic conditions?

DMOG displayed an increase in VEGF secretion in euglycaemic fibroblasts at 100 µM in both oxygen conditions, a low concentration compared to what has been previously reported (see Table 4-1). However, in day 3, a significant increase in normoxia was observed at 250 µM. In HaCaT cells this concentration also increased VEGF secretion after 24 hours. Thus, this concentration was used for the HIF-1α assay. DMOG at a concentration of 250 µM did not stabilise HIF-1α under any condition. Moreover, in euglycaemic hypoxia, it significantly reduced the expression of HIF-1α similar to the impaired HIF stabilisation under hyperglycaemic conditions. By day 3, DMOG did not have any effect under euglycaemic conditions, whilst under hyperglycaemia a significant decrease to the basal expression of HIF-1α was observed under both oxygen conditions. The decrease of HIF-1α at 250 µM suggests, that in HaCaT cells, it might induce hydroxylation of HIF-1α molecule, although the mechanism remains unclear. Milosevic et al. (2009) reported HIF-1α stabilisation at 500 µM DMOG in hNPC cells, however this dose reduced the metabolic activity.[131] Zhadanov et al. (2015) have also reported a decrease of HIF-1α on under hypoxia DMOG treated cells (1mM in H4K16ac cells). They observed within minutes that DMOG decrease the cellular respiration by inhibiting mitochondrial function, and associated to a decrease in the NADH production and OxPhos with activation of glycolysis.[443]

As the increase of VEGF was not preceded by HIF stabilisation, or it was not detected, the increase could possibly be attributed to other signalling pathways as DMOG is not specific to the HIF pathway. The increase could be related to the AMPK (Activated Protein Kinase)[443] as it is involved in metabolic response to oxidative stress.[468,469] It has also been reported that the PKC (Protein Kinase Pathway), which precedes inflammatory reactions, can induce HIF-1α protein by translational up-regulation.[225,470] Both pathways stimulate VEGF expression and thus the effect observed in the upregulation of VEGF could be through this mechanism.[471]

The concentrations evaluated are similar to the ones reported to Milosevic et al. (2009) who reported DMOG-induced HIF-1α stabilisation under normoxic conditions in HEK-DAT cells (human embryonic kidney cells expressing human dopamine transporter) at 500 µM and 1 mM, however the concentrations demonstrated to be cytotoxic. As reported by them, DMOG induced an LDH release above 30% at 1mM

concentration, whilst 500 µM DMOG showed no significant LDH release, but a decrease in cell viability when evaluated with MTT. A concentration of 100 µM was not cytotoxic; however, it did not induce HIF stabilisation.[131]

4.5.4 DMOG did not influence cell survival or proliferation under 100% hyperoxia

DMOG had no effect in the cell cycle progression under normoxic conditions. Cells under normoxic conditions progressed in a timely manner; however, cells under 100% oxygen had a delayed cell cycle transition to S phase. This may be due to the ROS increase induced by the high oxygen conditions, in which the cell activates a survival mode avoiding replication. Deng et al. (2003) attributed the cell cycle transition retardation between G1/S through Bcl2, which can function as an antioxidant, reducing intracellular ROS. Bcl2 is also involved in the apoptosis regulation.[472] The difference between cell cycle progression in normoxia and hyperoxia was also observed in the G2/M phase, where the cells have duplicated the chromosomes, preparing for mitosis. It has been reported that the delay in the cell transition due to hyperoxia can be overcome with the use of antioxidants.[473] The DMOG concentration used however was unable to stabilise HIF, and did not have any effect in cell cycle progression compared to the hyperoxia control. It has been reported that the use of antioxidants do not prevent cell death under hyperoxygen conditions, even when preventing the increase of mitochondrial ROS.[473] It is suggested that the cell death under high oxygen can be regulated by Bcl-2 proteins and resulting from cytoplasmic ROS.[472] In a separate experiment, DMOG at 250 µM decreased the basal ROS production in a similar amount as NAC and NaPy –antioxidants- did. An increased concentration of 500 µM DMOG did not decrease further the basal ROS production in normoxia. ROS is involved in the stabilisation of HIF-1α under cobalt ions, in the presence of 5 mM NAC inhibited the HIF stabilisation with CoCl2, however it had no effect in DFO.[235]

It has been reported that HIF mimetics can influence the cell cycle. Milosevic et al (2009) reported that at 50 µM CoCl2 decreased cell population in G0/G1 phase in NPC cells and an increase in the S and G2/M phases, whilst in 100 µM $CoCl_2$ - considered to be toxic.[131] Triantafyllou et al. (2006) reported similar results at 150 µM $CoCl_2$ and 150 µM DFO in HeLa, where the HIF mimetics inhibited cell cycle and proliferation.[235] While the HIF mimetic FG-4497 had an increase in the S phase population in NPC cells after a week of conditioning under normoxic conditions to

concentrations between 5-30 µM, which previously had demonstrated HIF stabilisation after 3 days of exposure to 5 and 10 µM.[131]

Previous experiments from our group had shown an increase of VEGF production under hyperoxygen conditions (100%O_2) in conjunction with DMOG. To define if this increase was due to DMOG-driven HIF stabilisation, HIF-1α was quantified, including hyperglycaemia. DMOG had no effect in HIF stabilisation, however a significant increase was observed under hyperglycaemia, with corresponding VEGF release. Previously, Milosevic et al. (2008) reported HIF stabilisation on NPC cells at 100 %O_2, however it was under hyperbaric conditions (1.5 atmospheric absolute).

4.6 **Conclusion**

Hyperglycaemic conditions inhibit the response to hypoxia by increasing hydroxylation of the HIF-1α protein.[362] The HIF mimetics act through different mechanisms and although they inhibit PHDs activity on HIF-1α, they can modulate different pathways, resulting in different cellular responses. DFO and DMOG can activate also both SOD2 and PGK promoters – regulated through HIF-2, while cobalt only induces HIF-1α.[432] $CoCl_2$ stabilised HIF-1α under normoxic and hypoxia conditions, and under hyperglycaemia in normoxic conditions, increasing VEGF secretion without compromising cellular metabolism or cell number. DFO although reduced significantly the metabolic activity and inhibited cell proliferation, significantly increased VEGF expression in fibroblasts. DFO also stabilised HIF-1α in both glycaemic and oxygen conditions. On the other hand, DMOG had a significant initial effect on VEGF expression, which was reduced by day three. However, others have shown that DMOG further stimulates HIF stabilisation in hyperglycaemic *in vitro* murine wound healing models using higher concentrations of DMOG compared to the ones used in this study. Cobalt chloride demonstrated an increase HIF-1α expression under hyperglycaemic conditions in keratinocyte cells, suggesting a potential for incorporation in wound healing dressings.

Chapter 5. The controlled release of ions from Si bioactive glasses for wound regeneration.

5.1 Introduction

5.1.1 Ion release for wound healing properties

Bioactive glasses (BGs), originally created by Larry Hench 50 years ago, can release ions that can be beneficial to chronic wound healing. For the creation of HIF stabilising material, Co release from BGs has the advantage of precise control of the release profile (through initial glass composition and particle size) together with the simplicity of manufacture and low relative cost. Multiple ions can also be simultaneously released from BGs with beneficial wound healing properties. Previous studies using bioactive glasses for wound healing purposes include the release of; silver (Ag) for antimicrobial properties,[273] zinc (Zn) for its anti-oxidative properties,[474] Boron[282] (B) which has an unknown cellular mechanism but may involve phosphylation and MMP activation[475] and Cobalt for its ability to stabilise the HIF pathway.[280] BGs also contain Si and Ca, these ions themselves have also been reported to have wound properties in terms of increased metabolic activity (Ca – as reviewed by Bikle et al (2012)) and increased proliferation and migration (Si –Quignard et al. (2017)). Whilst a few other papers have investigated the use of HIF stabilising CoBGs for bone (e.g Azevedo et al. 2010, 2015) only three other publication has investigated the use of CoBGs for wound healing. Furthermore, this is the first study to investigate and create HIF stabilising Co BGs that also release other ions (Zn and Mg) that may provide beneficial wound healing and to compare the relative wound healing effect of these ions in vitro.

5.1.1.1 *Cobalt*

Cobalt through the stabilisation of the HIF pathway (see section 4.4.1.1), can activate over 300 hypoxia responsive element genes (HREs) important for wound healing including; 1) enhanced cell survival,[476] 2) recruitment of stem cells,[152] 3) enhancement of the antimicrobial response,[134] 4) enhanced keratinocyte/fibroblast proliferation and migration[219] and (importantly) neovascularisation.[477] HIF stabilisation has also been demonstrated to enhance wound healing in populations most at risk of generating chronic wounds, the elderly[191] and diabetic.[109] These patients have a diminished cellular ability to sense a drop in oxygen pressure.

Cobalt chloride is the most common form of ionic *in vitro* HIF mimetic. $CoCl_2$ has shown previously to have a systemic effect[478] mimicking hypoxia; however $CoCl_2$ has a strong affinity with oxygen, hence decreases its dissolution and oxygenation of aqueous solutions, depleting the available oxygen.[479] Moreover, could replace Fe^{2+} in haemoglobin, behaving as a chelator.[480] Cobalt has been first incorporated into bioactive glasses by Jell et al. (2009) as a HIF mimetic[481] and the use of CoBG is mainly focused on bone tissue engineering.[482–484] Cobalt has also been incorporated in magnetic nanoparticles for magnetic resonance and as a drug delivery mechanism,[485] however the toxicity remains as a concern as the nanoparticles can up taken and exert a gene expression.[462]

For the successful translation of Co therapies for HIF stabilisation and chronic wound healing the controlled release of Co is needed. High concentrations of Co have been shown to be toxic,[486] (see 1.8.1) whilst prolonged HIF stabilisation will also cause chronic inflammation and also possibly carcinogenic.[220] Metal salts are also retained in the skin for an extended period of time and could lead to prolonged antigen processing and consequent immune responses in the dermal tissue.[240]

5.1.1.2 *Zinc*

Zinc is a trace element present in all tissues, the human body contains between 1.5 and 2.5 g of zinc,[487] while the skin accounts for the 11% of the body's total amount. At a cellular level, its importance relies in the involvement of serving as a catalyst for enzymes responsible for DNA replication, gene transcription and protein synthesis.[488–490]

It is often described as an important antioxidant due to its capacity of protecting the cells against lipid peroxidation and DNA fragmentation. It is an essential element for over 300 Zn-metalloenzymes participating in cell metabolism, DNA repair, the intracellular antioxidant defences and the regulation of apoptosis among other important cell process.[491]

It is hypostatised that the presence of zinc protects the thiol groups from ROS oxidation and maintains the GSH scavenging activity, through its ability to induce methallothionenis as they serve as cofactors. Methallothionenins (MTs) are a ubiquitous family of low molecular weight binding proteins involved in the homeostatic function of essential metals. MTs are responsive to a variety of stimuli, including glucocorticoid hormones, IL-1 and -6, tumour necrosis factor and oxidative stress. In wound healing the zinc-induced metalloproteinases enhance autodebridement and keratinocyte migration.[492]

Extracellular Zn^{2+} has also demonstrated inhibition of pneumococcal growth in vitro locking the PsaA, a protein that plays a major role in pneumococcal attachment to the host cell and virulence, in a closed state. As Zn^{2+} has a higher affinity to the PsaA, than Mn^{2+}, its physiological ligand.[493]

A decrease in the body zinc has been strongly linked to diabetes, possibly through hyperzincuria –loss of zinc through urine – or a decrease gastrointestinal absorption of zinc. Both of them related to the hyperglycaemia and decreased insulin production and its low efficiency in diabetic patients.[494–496]

For these reasons it is of interest analysing the effect of zinc in low oxygen conditions and the possible effect that can bring to a wound environment when incorporated in a controlled release system, with and without the presence of cobalt as a HIF stabilising ion.

5.1.2 **Bioactive glasses as a drug releasing mechanism**

Bioactive glasses and in particular Bioglass®-45S5- was invented by Larry Hench in 1969. It is a glass network formed of Na_2O-CaO-P_2O_5-SiO_2, which has shown a strong mechanical bond with bone through the release of ions (Ca, P and Si) and the formation of a layer of hydroxyapatite (HA).[250] The focus in bioactive glasses has been predominantly in the field of bone regeneration, but the ability to incorporate different ions and the ability to control the release of these ions have meant that a number different applications have been suggested including cartilage repair,[261] nerve repair[259] and for wound healing.[260,283,497]

The glass properties of silicate-based bioactive glasses, including the degradation rate, can be varied by altering the molar composition of the glass (Figure 5-1) and through the addition of additional ions that may disrupt the glass network.[498,499] For example, magnesium and zinc ions have been shown an inhibition of the calcite nucleation rate and thereby diminish apatite formation.[500]

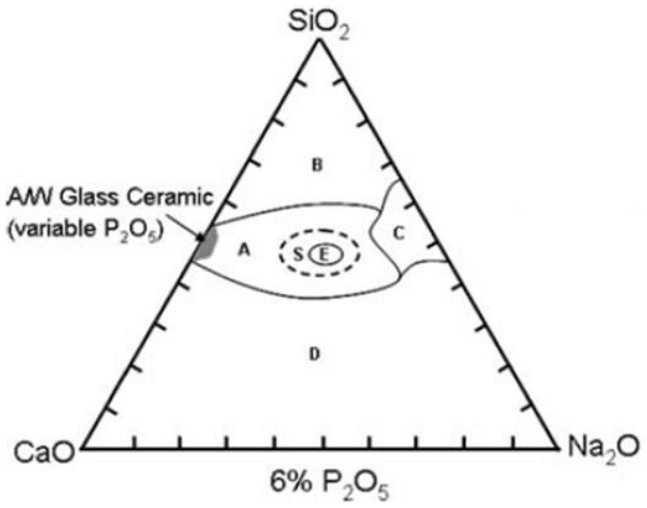

Figure 5-1 Tissue/glass interaction in relation to the composition as described by Hench,[501] Region A is described as bone bonding, region B and C as non-bonding due to low and high reactivity, whilst the region D does not allow glass formation. Region E is the Bioglass® composition. (Image from Hench 2016)

5.1.3 **Structural definition of a glass and synthesis**

For the controlled release of ions from bioactive glasses for therapeutic purposes, it's important to understand the Si bioactive glass network. Glasses have an extended three-dimensional network and are amorphous without a regular arrangement of its molecular constituents. Glasses are considered energetically unstable, keeping the same interatomic forces that a corresponding crystal network would have. The composition and therefore the network structure will confer the physical characteristics to the glass, transition temperature, rigidity and solubility.

Goldschmidt found that the radius ratio of oxides able to form glass is between 0.2-0.4, corresponding to a tetrahedral arrangement of oxygen atoms around atom A, thus conferring silica the ability to form glasses. The network connectivity (NC) of the glass is calculated considering the relative numbers of the network forming oxide species and the network modifiers species, which would form non-bridging species. As the network connectivity is reduced, the solubility is increased.

As the tetrahedron has a triangular shape, the network properties change as determined by the size of the cations occupying them. The silica network is disrupted by Na_2O and CaO by creating non-bridging oxygens (NBO) thus defined as network modifiers.[502] Univalent cations will have higher migration rate than divalent cations and smaller cations than larger ones. Therefore, Na^+ will migrate more easily than

Ca^{2+}. The substitution of Ca^{2+} with Na^{2+} decrease the glass transition temperature and the peak crystallisation temperature.[503]

The addition of other oxides such as cobalt, zinc and magnesia can further disrupt the glass network, altering the network connectivity, ion release rate and HA formation. They might not possess the ability to form a glass on their own and depending on the amount and the composition, they can behave as network modifiers or intermediate oxides within a glass network depending to the charge to size ratio. In example, in the glass ICIE-1, the calculated NC is 2.13, when substituting 6% CaO with a metal oxide that can possibly act as a bridging oxide, the NC increases to 2.76, i.e. the glass structure is more rigid, or less soluble. In the case of cobalt, forming $[CoO_4]^{2-}$ when entering the network as an oxide intermediate and as Co^{2+} when participating as modifier of the silicate network (Figure 5-2).[205]

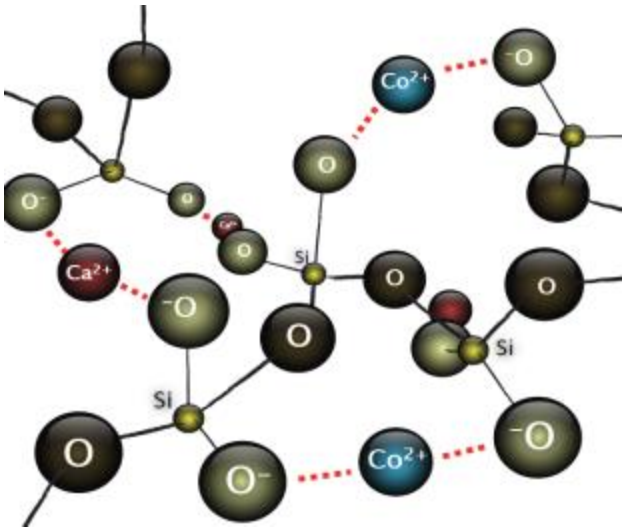

Figure 5-2 Incorporation of cobalt ions to the glass network as modifiers. The basic structure of the silicate glass is the SiO_4 tetrahedral where alkali and alkaline oxides modify the network structure by replacing bridging oxygens by non-bridging oxygen, reducing the degree of interconnectivity (Image taken from Azevedo et al. 2010) [205]

5.1.4 **Dissolution of the BG**

The dissolution products and rate of dissolution can be tuned by varying the molarity of the glass precursors and the network connectivity. The glass dissolution is initiated by the rapid exchange of alkaline cations, Na^+ and Ca^{2+} with H^+ or H_3O^+ from solution. The rate is dictated by the cations functioning as network modifiers by forming non-bridging oxygen bonds and are not forming part of the glass network. This reaction increases the pH, leading to the network dissolution by breaking the Si-O-Si bonds through the hydroxyl (OH^-) ions release soluble silica in the form of silicic acid $[Si(OH)_4]$.[500,504,505]

5.2 **Chapter Aims**

Following the ability of Cobalt to restore the hypoxia response in hyperglycaemic environments, this chapter's aim was to develop a means for the controlled delivery of HIF-1α stabilising factor; to create HIF-1α stabilising glasses and assess their ability to cause desirable wound healing responses. Furthermore, taking advantage of the ability to incorporate multiple ions into the BG network, other ions were also investigated. Future experiments are planned to test these HIF modulating BGs in hyperglycaemic models as developed in 4.4.1.1.

The specific aims of the chapter are to:

1. Develop silica-based bioactive glasses that release Co and Zn ions in a controlled manner in physiological relevant concentrations.
2. Determine the biological effects of the silica-based Co BG in dermal cells by evaluating VEGF expression, metabolic activity and proliferation.

5.3 **Materials and methods**

5.3.1 **Bioactive glass synthesis**

Si-based bioactive glasses were created via the melt derived route based on the Mg series originally created by Prof. R. Hill and Iman Elgayar (2005 - ICIE-1 Imperial College). In order to study the effect of cobalt and zinc, the ions were substituted for CaO in a molar basis, with and without the presence of MgO. The bioactive glasses were designed according to the model of soda-lime–phosphosilicate glasses with the general formula of $3SiO_2{\cdot}0.07P_2O_5{\cdot}(1.4\text{-}X)CaO{\cdot}1.6Na_2O{\cdot}XAO$ (A = Co, or Zn) keeping constant the network connectivity calculated with the Equation 2 (Figure 5-3). The network connectivity considering the cobalt, zinc and magnesium as intermediate oxides (NC2) was calculated with the Equation 3 assuming the whole molar % for these oxides participated as a network forming. The glasses are not charge balanced as the substitution was made on the CaO, a network modifier.[502,506]

Equation 1
$$NC = \frac{BO - nonBO}{NF}$$

Equation 2
$$NC1 = \frac{4nSi_20 - 2(nCaO + nNa_2O + nCoO + nMgO + nZnO) + 6nP_2O_5}{nSi_2O}$$

Equation 3
$$NC2 = \frac{4nSi_20 + 6(nCoO + nMgO + nZnO) - 2(nCaO + nNa_2O) + 6nP_2O_5}{nSi_2O + nCoO + nMgO + nZnO}$$

NC — network connectivity
BO — bridging oxygens
nonBO — non-bridging oxygens
NF — network formers
*NC1*network connectivity considering Co^{2+}, Mg^{2+} and Zn^{2+} are considered network modifiers
NC2 — network connectivity considering Co^{2+}, Mg^{2+} and Zn^{2+} are considered network forming
n — number of moles in the composition

Figure 5-3 The network connectivity of the bioactive glasses can be described by the equation 1. The network connectivity varies depending upon the participation of the oxides as network modifiers or forming

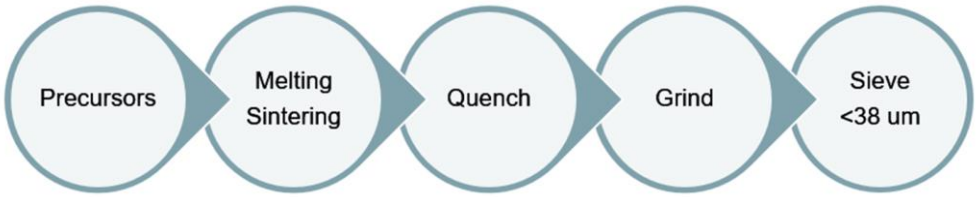

Figure 5-4 Glass synthesis process: Oxide precursors are mixed, calcined and molten gradually. The mixture is quenched rapidly in water. The frits are grinded and finally sieved.

The glass making has evolved through different techniques, although melt derived remains the most common method. The powder compositions were prepared by mixing the mole/weight fraction of the oxide precursors according to Table 5-1. The composition was transferred into a platinum crucible and placed in a preheated furnace at 1350ºC for 90 minutes. During this period, the glass mixture was calcined at 500 ºC, where the gaseous substances are released out of the composition. The powders' temperature increased to melting point, remaining at high temperature to facilitate the uniform fusion and achieve a homogeneous molten material. The crucible was taken out and the molten glass was quenched in tap water at room temperature as the glass formation depends critically on the cooling rate, to avoid nucleation and crystallisation.[507,508] The glass frit was collected and dried in an oven at 60º-C. The frits were grinded using Planetary Micro Mill PULVERISETTE 7 from Fritsch at 500rpm for 6 minutes. Particles of size less than 38µm were obtained after sieving the bioactive glasses with a mechanical shaker at an amplitude of 2 mm for 5 min.

Table 5-1 Theoretical Mol percentage composition and network connectivity of the bioactive glasses. %MS represents percentage molar calcium substitution. The grey boxes are the oxides substituted in the compositions.

	Theoretical Mol%							Network Connectivity		
	SiO_2	Na_2O	P_2O_5	CaO	CoO	ZnO	MgO	%MS	NC1	NC2
ICIE1	49.46	26.38	1.07	23.08	-	-	-	-	2.13	2.13
0Zn 4Mg 0Co	49.46	26.38	1.07	19.08	-	-	4	4	2.13	2.57
1Zn 0Mg 0Co	49.46	26.38	1.07	22.08	-	1	-	1	2.13	2.25
1Zn 4Mg 0Co	49.46	26.38	1.07	18.08	-	1	4	5	2.13	2.67
1Zn 0Mg 0.3Co	49.46	26.38	1.07	21.78	0.3	1	-	1.3	2.13	2.28
1Zn 4Mg 0.3 Co	49.46	26.38	1.07	17.78	0.3	1	4	5.3	2.13	2.70
2Zn 2Mg 0.3Co	49.46	26.38	1.07	18.78	0.3	2	2	4.3	2.13	2.60
1Zn 4Mg 1Co	49.46	26.38	1.07	17.08	1	1	4	6	2.13	2.76
0Zn 4Mg 2Co	49.46	26.38	1.07	17.08	2	-	4	6	2.13	2.76

5.3.2 **Glass characterisation**

5.3.2.1 *XRD Analysis and FTIR*

To understand the role of the ions (Co, Zn, Mg) in the glass network FTIR and XRD were performed. Glass crystallisation was determined by X-ray diffraction (XRD) was performed using a Bruker D2 PHASER. XRD was done through step scanning with Cu radiation, at 30kV and 10 mA. Data were collected in the range 10° to 70° 2θ with a times step of 10 s and step size of 0.034°.

Fourier transform infrared spectroscopy (FTIR) were applied to the bioactive glass powders before dissolution studies to determine the functional groups within the glass structure. FTIR spectra were collected in absorbance mode using in the range of 600-2400 cmFin $^{-1}$.

5.3.2.2 *Ion release rate tests*

To mimic the amount of ions present in cell culture, the ion release rate of the BG was conducted in DMEM. In the study, 375mg of the different compositions of the bioactive glass particles were immersed in 250mL of DMEM, and placed in a rotating shaker at 37°C. A quantity of 4 mL of DMEM supernatant from each sample was collected at each time point (0.25, 0.5, 1, 4, 8, 24 hours) and 4mL of fresh DMEM was added to keep the volume of the solution constant. The sample was filtered with a 0.2µm polymer filter (Corning, UK) and added to 9ml of distilled water. The solutions were analysed using the Vista MPX Inductively Coupled Plasma-Optical Emission

Spectrometer (ICP-OES) (Varian, USA) analysis to determine the following elements Ca (3179nm analytical line), Si (2516 nm), Na (5895nm), Co (2286nm), Zn (4810nm), Mg (2795nm) and P (1859nm). During the ICP it was observed an interferance between the zinc and the cobalt spectra line (2062nm).

5.3.2.3 *Lithium Metaborate*

In order to measure the composition of the glasses produced, acid digestion compositional analysis was carried out by the lithium metaborate fusion dissolution method as described by Barrioni et. al 2018. 50mg of finely ground BG particles was mixed carefully with 250 mg of anhydrous lithium metaborate (80% w/w) and lithium tetraborate (20% w/w) in a clean and dry platinum crucible using a glass rod. The mixture was fused in a furnace for 20 min at 1050°C and later dropped to room temperature. The mixture was subsequently dissolved in 2M nitric acid. The elemental concentration in the solution was measured using inductively coupled plasma optical emission spectroscopy (ICP-OES).

5.3.3 **Effect of ionic release on HaCaT cells**

In order to evaluate the effect of the bioactive glass compositions in wound healing experimental analysis in hypoxic and normoxia conditions. HaCaT cells were seeded at a density of 2000 cells/cm^2 in 48 well plates and allowed to attach overnight. The following day, at Day 0, the media was replaced with 500µL of full supplemented BG conditioned media () and full supplemented DMEM as a control. The cell viability was assessed at Day 1, 3 and 7 as mentioned in section 2.2.3 in both oxygen conditions. On Day 2, 4 and 6 the media was replenished and in all times the supernatant was collected and preserved at -20°C for future analysis.

5.3.3.1 *Bioactive glass conditioned media*

HaCaT cells were grown in fully supplemented media as described in section 2.2.1, the BG conditioned media was prepared by mixing 750mg of the BG in 500 ml of DMEM and placed in a rotating shaker at 37°C for 4 hours. Then the media containing the BG particles was filtered using a 0.20µm pore size PES Filtration System (Corning). The media was kept in the fridge. The required BG condition media was aliquoted and supplemented with 10% FBS and 1% Penicillin/Streptomycin prior to the experiment.

5.3.3.2 *Biological Responses*

The media was collected at day 1, 3 and 7, and frozen at -80 ºC until analysis. The VEGF ELISA Human VEGF Quantikine ELISA Kit was performed following manufacturer's instructions[509] and as described in section 2.2.5.

Total DNA quantification was performed on days 1,3 and 7 using Hoechst binding (DNA Quantitation Kit, Sigma Aldrich), following cell lysis (PBS wash followed by addition of 200 µL of DI water and 6 freeze thaw cycles) and quantitative assessment at absorbance Ex. 355 nm and Em. 460 nm (previously described in section 2.2.4).

5.3.3.3 *Reactive Oxygen Species*

To evaluate the influence of the glass ions in the reduction of ROS, the cells were incubated with 50µM CoCl, 10 µM ZnO, 2mM sodium metasilicate and 80µM Trolox, an antioxidant, as a control. After 4 hours of incubation, the cells were stimulated with 800 µM of H_2O_2. The ROS detection was performed 30 minutes later, following the protocol in section 0.

5.3.4 **Statistical Analysis**

Statistical analysis was done with GraphPad Prism. The correlation analysis for the ICP ion release at 4 hours to the % Mol Ca substitution was done using the Pearson method after evaluating normal distribution with Shapiro-Wilk test. Cobalt had a nonnormal distribution which was confirmed through D'Agostino & Pearson test. The ionic release by the different compositions after 4-hour dissolution in DMEM was analysed with One Way Anova.

For the biological samples, the ROS production was evaluated with One Way Anova and Tukey as a post test. The metabolic activity, cell proliferation and VEGF secretion were analysed with a Two Way Anova with the Bonferroni post-hoc test to compare between multiple samples.

5.4 Results

5.4.1 Characterisation of the Bioactive Glasses

The glasses were characterised by different methods to confirm an amorphous structure and the ionic release profile.

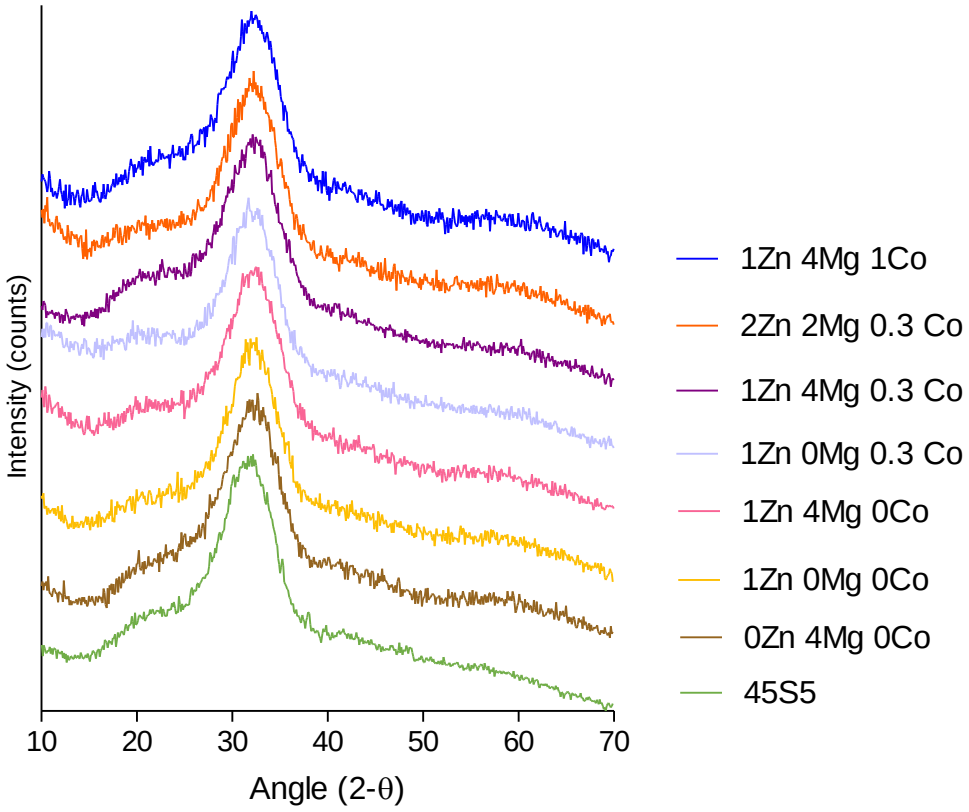

Figure 5-5 XRD spectra of the bioactive glasses. The glasses display an amorphous structure with no particular crystallisation peaks.

5.4.1.1 *XRD and FTIR analysis*

The addition of ions did not caused crystallisation as determined by XRD (Figure 5-5). All glasses had an amorphous structure with no evidence of crystallisation. The presence of cobalt, zinc and magnesium did not affect the XRD patterns, and in all cases a broad band centred at ≈31-32º (2θ range) was observed.

FTIR displayed the characteristically peak band of silica-based glasses (Figure 5-6) at 1000– 1100 cm^{-1} for the main Si-O-Si stretching mode. The band present at 860-975 cm^{-1} with high intensity about 910 is associated with the presence of a large number of non-bridging oxygens (NBO) forming bonds with the network modifying ions (Si-O-NBO).

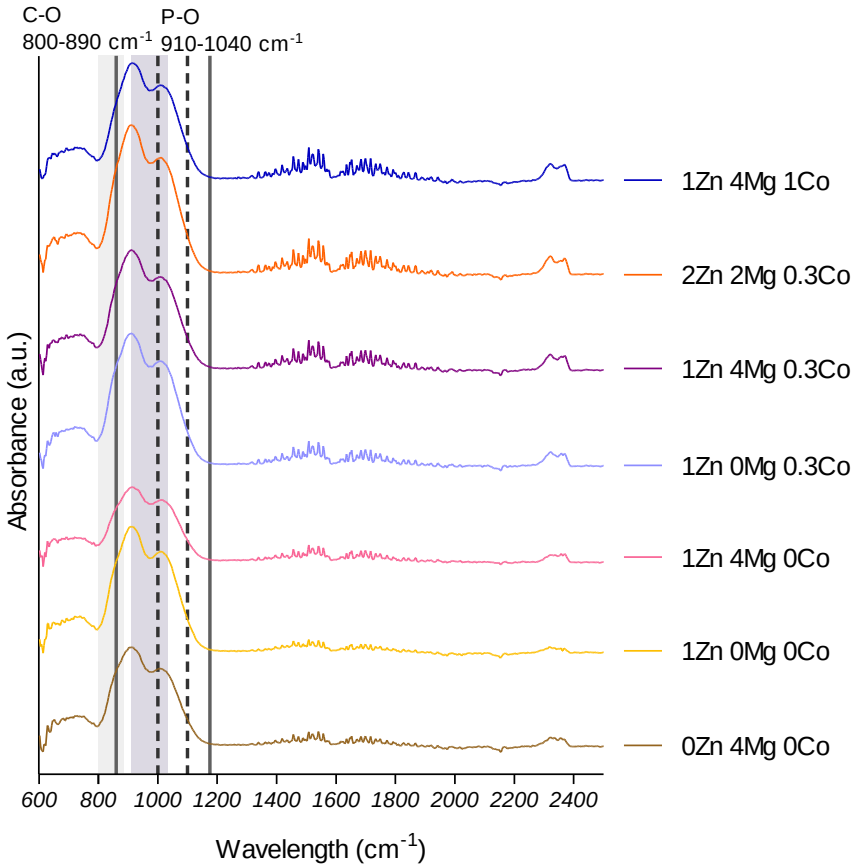

Figure 5-6 FTIR characterisation of the glasses. The glasses had a similar conformation. The region between the solid lines (860-1175 cm^{-1}) shows the Si-O-Si bonds, while the region between the doted lines the Si-OH bonds. The grey band (800-890 cm^{-1}) represents the C-O stretch bonds, whilst the darker band (910-1040 cm^{-1}) the P-O stretch. (n=4)

5.4.1.2 *Lithium Metaborate Assay- Glass Molar Composition*

The molar composition of the glasses was determined through the lithium metaborate method (see 5.3.2.3). All the glasses contained higher amounts of silica than expected (when compared to Table 5-1), however the modified ionic content –Co, Zn & Mg- reflected values similar to the calculated molarity.

Table 5-2 Bioactive glass percentage Mol composition. The *grey italic* numbers refer to the difference between the theoretical and real Mol composition. The grey boxes are the oxides substituted in the compositions.

Lithium Metaborate calculated Mol %							
	SiO_2	Na_2O	P_2O_5	CaO	CoO	ZnO	MgO
0Zn 4Mg 0Co	63.2 *+13.7*	5.5 *-20.9*	2.5 *+1.5*	23.7 *+4.6*	- *-*	0.1 *-*	5.0 *+1*
1Zn 0Mg 0Co	62.8 *+13.3*	5.7 *-20.7*	2.6 *+1.6*	27.5 *+5.5*	- *-*	1.3 *+0.3*	- *-*
1Zn 4Mg 0Co	61.7 *+12.2*	6.9 *-19.4*	1.8 *+0.7*	23.0 *+4.9*	- *-*	1.3 *+0.3*	5.3 *+1.3*
1Zn 0Mg 0.3Co	62.8 *+13.4*	6.9 *-19.5*	2.7 *+1.6*	26.0 *+4.2*	0.3 *0.0*	1.2 *+0.2*	0.0 *-*
1Zn 4Mg 0.3 Co	62.7 *+13.2*	6.9 *-19.4*	2.4 *+1.4*	21.2 *+3.4*	0.3 *0.0*	1.3 *+0.3*	5.1 *+1.1*
2Zn 2Mg 0.3Co	61.0 *+11.5*	5.6 *-20.8*	2.6 *+1.5*	25.4 *+6.6*	0.4 *+0.1*	2.6 *+0.6*	2.5 *+0.5*
1Zn 4 Mg 1Co	60.2 *+10.7*	6.9 *-19.5*	2.6 *+1.5*	22.4 *+5.3*	1.2 *+0.2*	1.5 *+0.5*	5.3 *+1.3*

5.4.1.3 *ICP release Profile*

The glass network is altered by the addition of additional network modifiers (NM) as indicated by changed release of Si (Figure 5-7a). –For the ionic dissolution and SD at four hours see Appendix 2- The addition of the NM marginally reduced Ca (apart from 1Zn 0Mg 0.3Co) which is anticipated considering the substitution of NM for Calcium (see Figure 5-8). The glass compositions were grouped by the present ions and compared among them section 5.1.4.

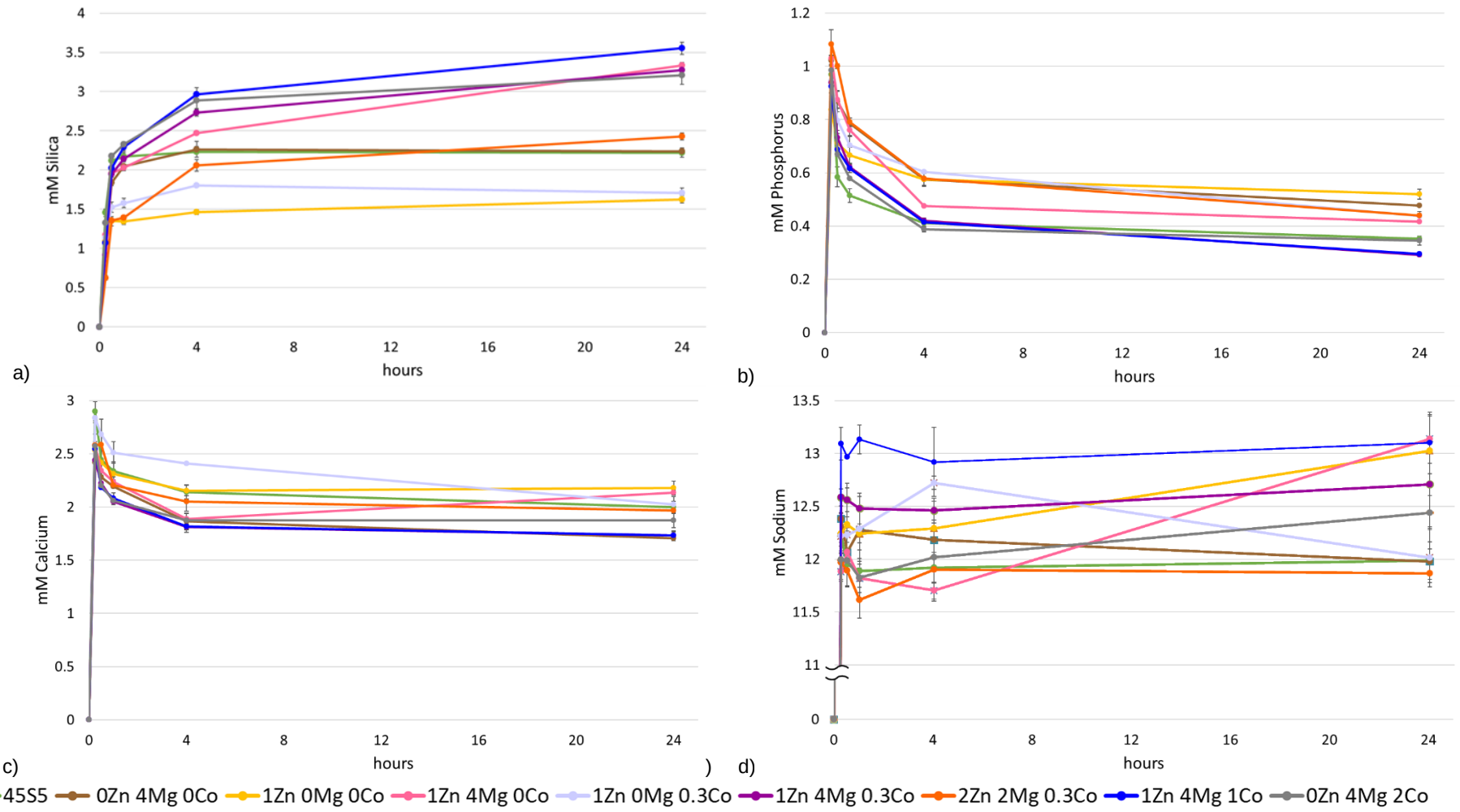

Figure 5-7 Concentration of the different cations in DMEM as determined by ICP-OES as a function of time after incubation of BGs for up to 24 hours. Differences in silica, calcium and sodium release were observed in relation to the calcium substitution. (n=6) (for values and SD see Appendix 2).

Silica profile release

The silica release profile (Figure 5-7) was strongly influenced by the calcium substitution degree (p value <0.0001 & r^2 0.9440) at four hours (Figure 5-8). The glasses with lower than 4% Mol Ca substitution had a slight increase in the silica release between 1 hour and 4 hours, plateauing afterwards. Interestingly the addition of Mg increased the Si release rate, whilst the addition of Zn reduced Si release (most obvious after 1 hour). The glasses with a higher substitution percentage had a fast release rate up to the four-hour time-point. The lowest silica release at 4hours was seen in the 1Zn 0Mg 0Co composition (1.47 mM), observing a two-fold increase in the glasses 0Zn 4Mg 2Co and 1Zn 4Mg 1Co (2.86 and 2.96mM).

Sodium profile release

The sodium ionic (Figure 5-7d) concentration and profile is similar among all compositions after a burst release. The sodium plateaus after after 1 hour of exposure of the bioactive glasses to DMEM with the concentration ranging between 13.14 mM ± 0.23 and 11.62 ± 0.18 mM. However, the release of the sodium ion release decreased (Figure 5-8**Error! Reference source not found.**) as the % molar Ca s ubstitution increased (p=0.005, r^2 0.8842).

Calcium profile release

Calcium release is similar in all the compositions (Figure 5-7c) eventhough is the substituted ion. The variation in the calcium release at four hours varies in 0.59 mM. The glasses containing the less amount of calcium substitution (more calcium) had a slight higher release of calcium (p=0.0140, r^2 0.6618) which can be directly related to their NC (see Table 5-1).

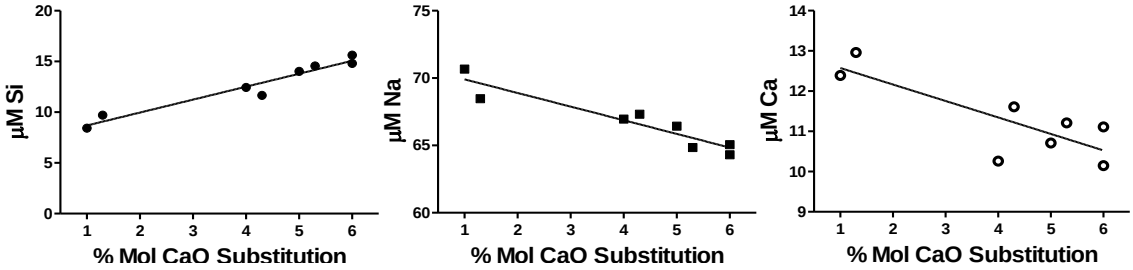

Figure 5-8 Correlation between the Si, Na and Ca ion release and the % Mol Substitution. The molarity of the ions released after incubation in DMEM at 37 ºC was analysed in relation to the % Mol calcium substitution, where Si had a p value <0.0001 and r^2 0.9440. The sodium and calcium release decreased as the % Mol calcium substitution increased (Na p=0.005 r^2 0.8842, Ca p=0.0140 r^2 0.6618). (See appendix 3) There was not a significant relation for the other ions.

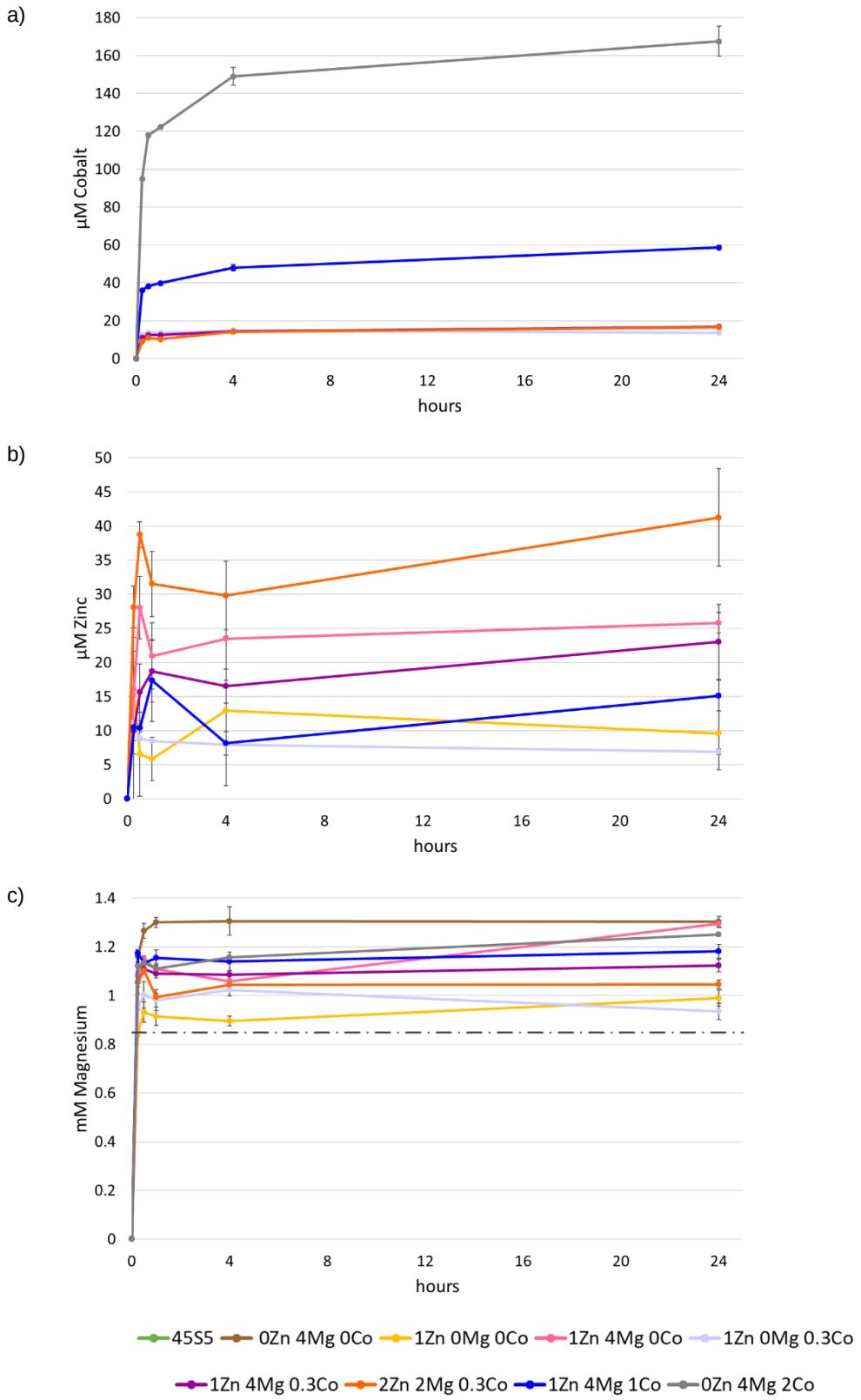

Figure 5-9 Concentration of Co (a), Zn (b) and Mg (c) cations in DMEM as determined by ICP-OES as a function of time after incubation of BGs for up to 24 hours. The dotted line in the magnesium profile represents the magnesium molarity present in DMEM.

Cobalt profile release

For the glasses containing 1 and 2% Mol Co, the ion release rate slowered after 4 hours of exposure to DMEM. At 4 hours there is a three-fold increase between the 0.3% Mol glasses and the 1% Mol. There is a threefold increase in the ion release between the glasses 1Zn 4Mg 1Co and the 0Zn 4Mg 2Co, although there is a two-fold increase in the cobalt molar concentration in the glasses. This difference in the ionic release can be related to the presence of zinc modifying the network connectivity, which will be discussed in section 5.4.2.

Zinc profile release

The grade of calcium substituition did not seemed to have an effect on the zinc release. The release at 4 hours varied from 23.44 mM to 7.94 mM at 1% Mol Zn depending on the composition. There was not a significant correlation between the zinc and silica release, although for the sample containing 2%M Zn the silica release was 2.06 ± 0.073 mM compared to 1Zn 4Mg 0.3Co was 2.73 ± 0.0423, whilst the cobalt ion release remained constant. Accordingly to the increase of percentage molarity of the sample, the 2%M Zn composition released the highest amount of zinc ions (29.84 ±5.044). There was no correlation between the % Mol Calcium substitution and the zinc ionic release.

Magnesium profile release

The highest amount of magnesium was, as expected, released by the glass that contained 4% Mg (Figure 5-9). However, the addition of Zn also apeared to influence Mg release, where 1% Zn inceased the release of 4% Mg (Appendix 3), indicating a further disruption of the glass network and a reduction in NC.

Phosphorus profile release

The phosphorus decreases rapidly during the first 30 min after a burst release. After 4 hour the slope tends to plateau. There is a distinguishable fashion in the compositions. The upper band shows the compositions with lower calcium substituition. The lower band consists the compositions with the higher %Mol calcium substituition (>5.3 %Mol Ca subst). There is a composition that sits between both bands, with 5% calcium substituition, which joins the upper band (lower substituition) after 24 hours. There was no correlation between the phosphorus ion release and the % Ca Mol substitution.

5.4.2 Analysis of bioactive glass release at 4 hours

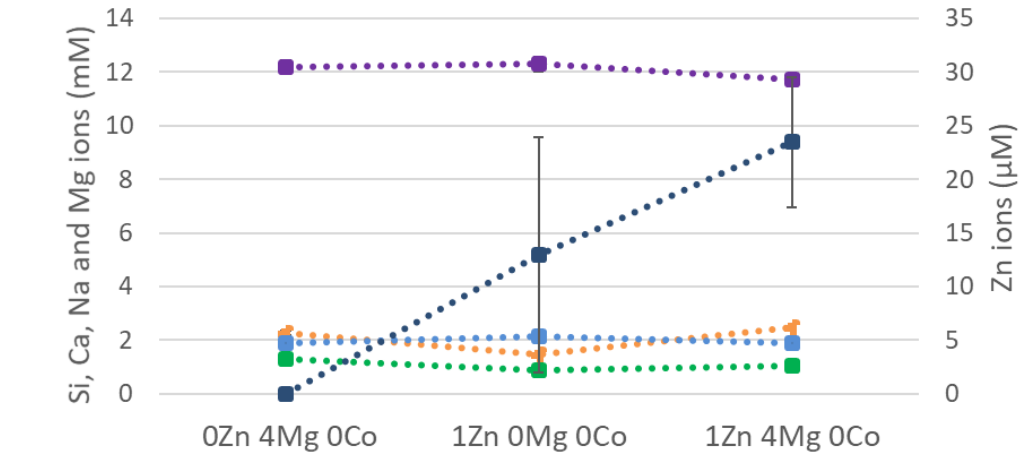

a)

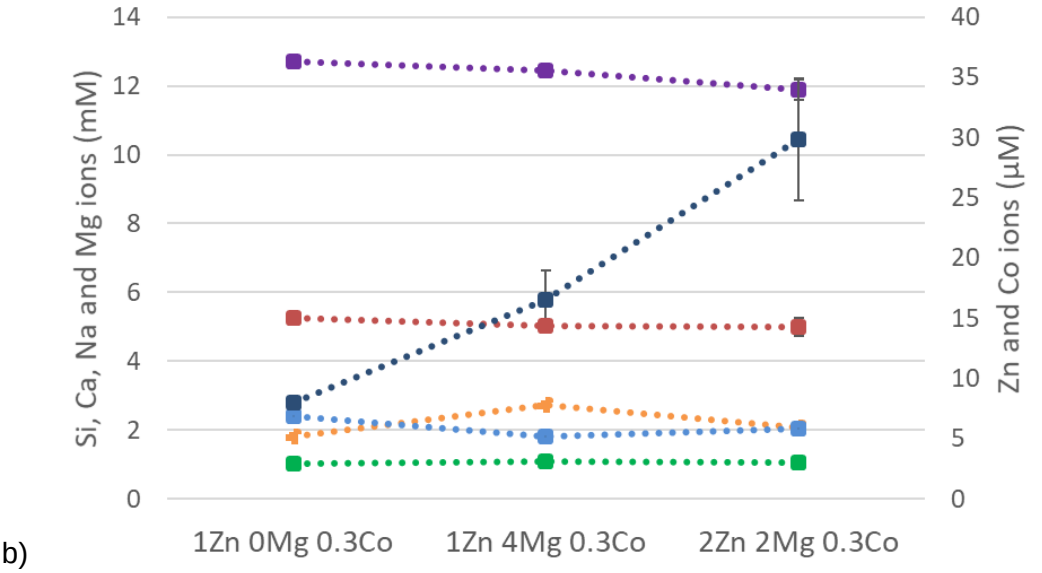

b)

Figure 5-10 Zinc-Magnesium effect in BG. (a) ion profile release (determined by ICP-OES) of non- cobalt bioactive glasses (b) ion profile release of 0.3% Mol cobalt containing bioactive glasses.

Although there are observable changes in the release of the calcium and silica, these differences were found to be not significant among all the glass compositions. The sodium, phosphorus and magnesium were all released with any noticeable difference, and if any, resulted not significant.

The zinc measurement resulted with high standard deviation for some samples during the ICP procedure (Appendix 2) as the zinc channel was interfering with the cobalt detection channel. There is an obvious trend in the release of the zinc in the glasses without cobalt (Figure 5-10 a), but because of the reason previously explained, no

significant difference can be determined. It can only be confirmed the presence of zinc in 1Zn 0Mg 0Co and 1Zn 4Mg 0Co.

Among the samples containing a different ratio between magnesium and zinc with constant 0.3% Mol Co (Figure 5-10b), it can be observed that the presence of magnesium increased the release of the zinc ions ($p<0.0001$). This result could possibly be extended to the previous comparison, with the similar trend but not significant difference due to the large standard deviation. There was also a significant difference in the release of the zinc ions with double the amount of %Zn Mol.

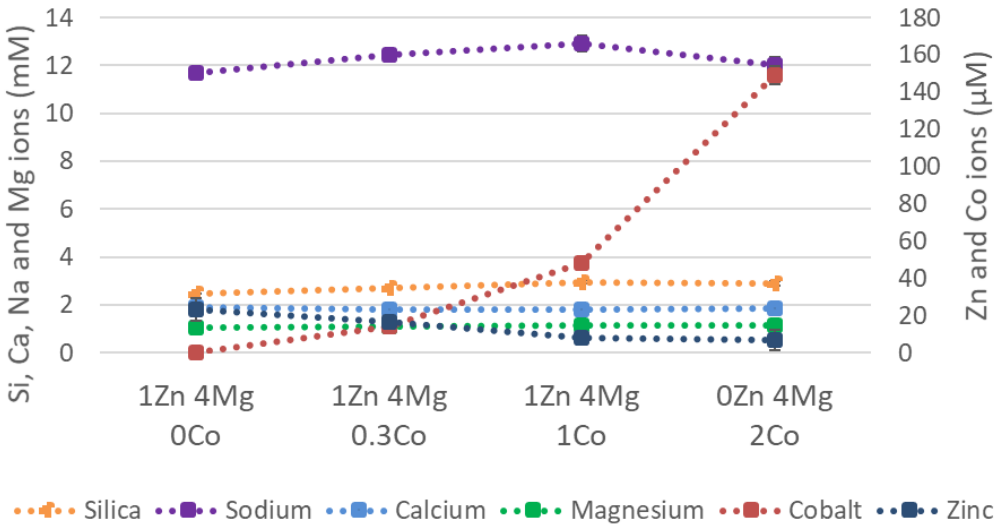

Figure 5-11 Cobalt effect in ion profile release of 0.3% Mol bioactive glasses, as determined by ICP-OES.

The cobalt ions were released following (Figure 5-11) the increase in the cobalt content ($p<0.0001$). There was a three-fold increase in the cobalt release when the % Mol cobalt was tripled in the 1Zn 4Mg glasses, meanwhile in the glass that did not contained zinc, the cobalt release was tripled with a two-fold increase of cobalt. Interestingly, as the cobalt release increased, the zinc ion release decreased ($p<0.001$).

5.4.3 **Cell Studies**

The cellular (HaCaT) response to bioactive glass releasing ions (Zn and Co) were studied individually (for cobalt see section 4.4.1) and as released from bioactive glasses (see dissolution media methodology section 5.3.2.2), in both normoxia (20% O_2) and hypoxia (1% O_2) to mimic oxygen levels in a chronic wound (discussed in section 0).

5.4.3.1 *Effect of zinc in hypoxia and normoxia conditions*

Zinc appeared to enable cell survival, as determined by metabolic activity ($p \leq 0.001$, n=6) and number of cells present ($p \leq 0.0001$, n=6), after 7 days culture in hypoxia but did not affect cell metabolic activity or cell number in normoxia (Figure 5-12).

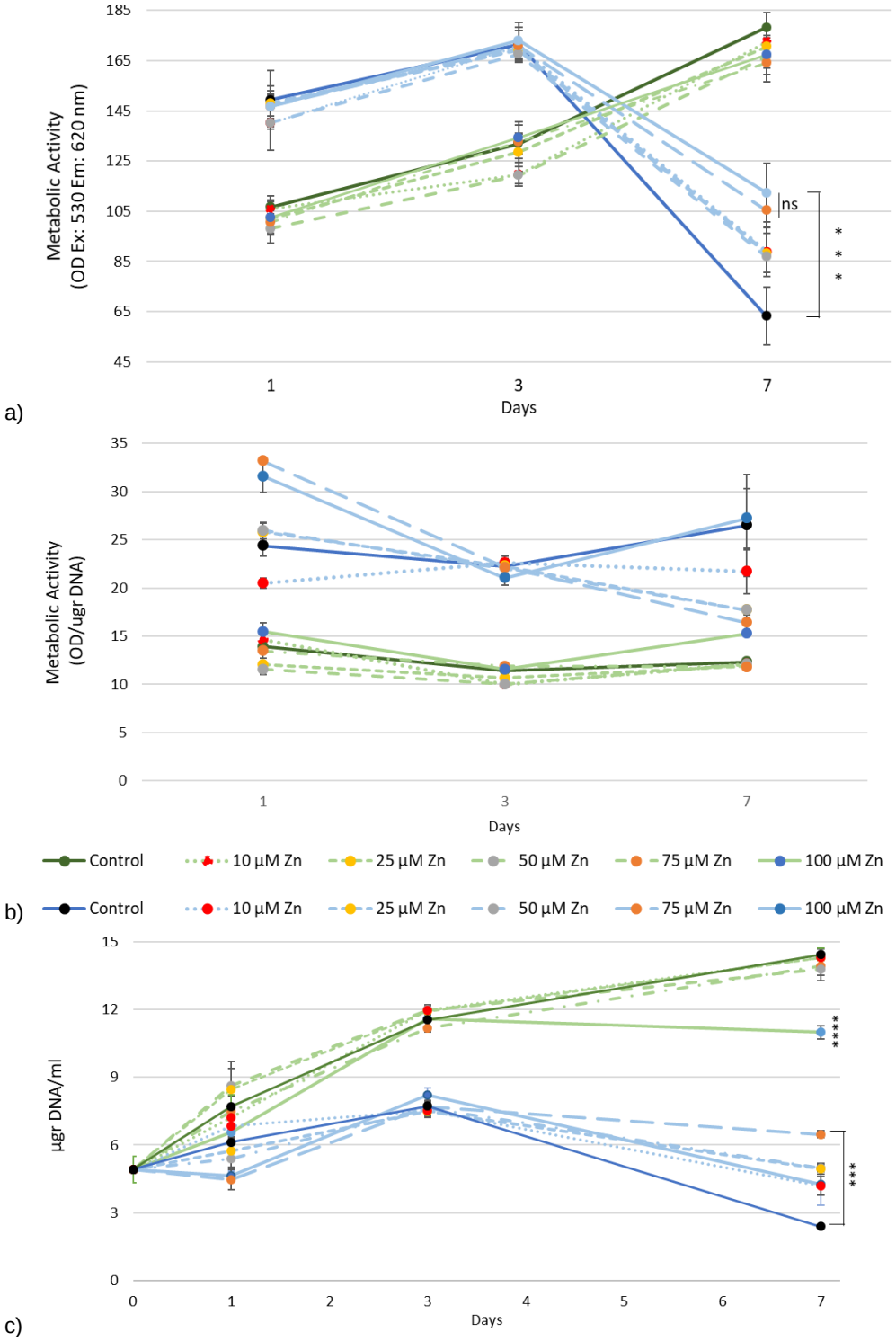

Figure 5-12 Effect of Zinc in cell metabolism and proliferation under normoxia and hypoxia. a) Zinc alters the metabolic activity during hypoxia, as determined by alamar Blue® b) When the metabolic activity is normalised to DNA, as quantified using Hoechst dye, the effect of different zinc concentrations.

Zinc also increased total VEGF production but this is likely to be because of the increased cell survival (Figure 5-13a), indeed when normalised to DNA only the highest concentration of Zinc (100µM) increased VEGF production (p≤0.01, n=6).

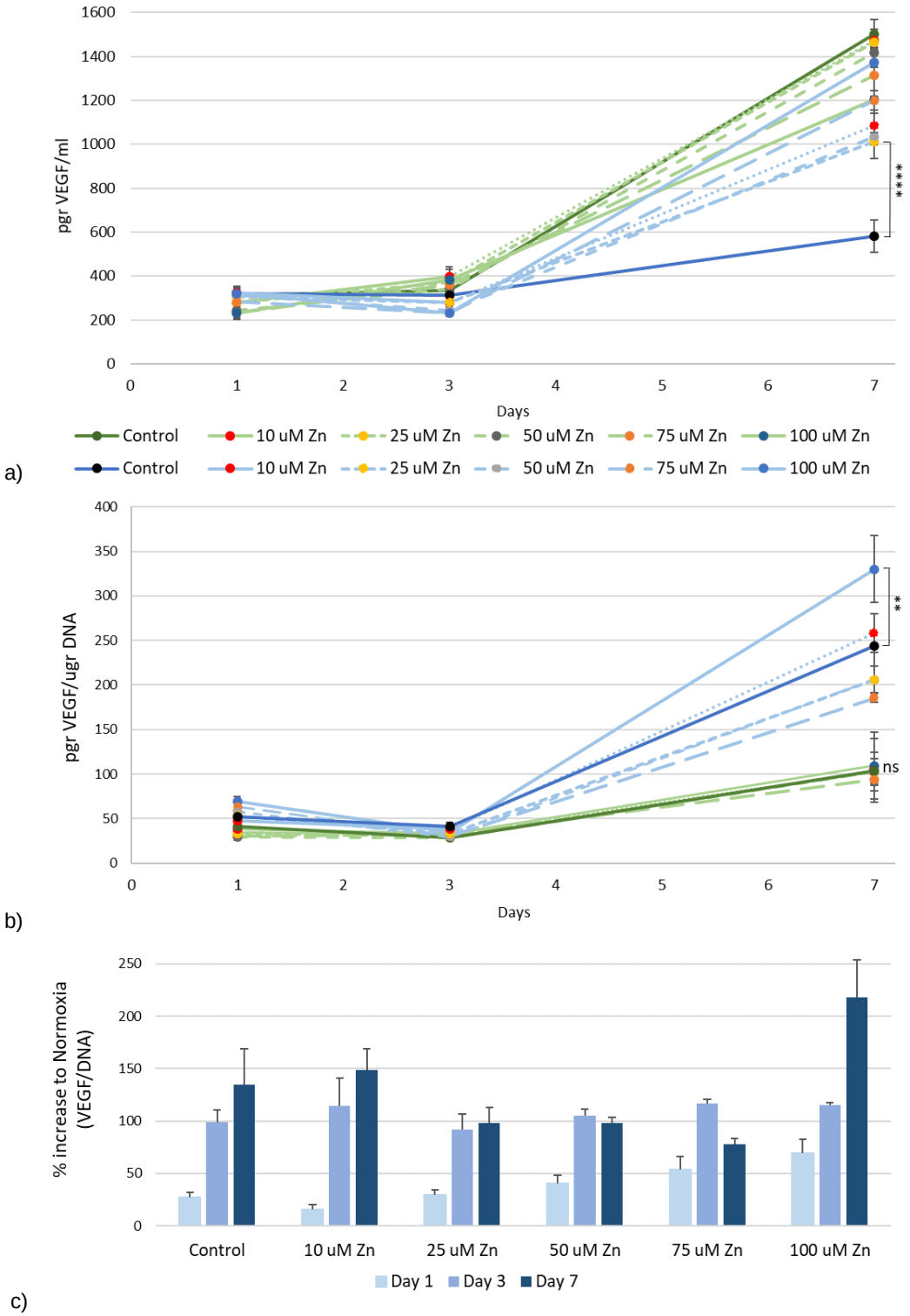

Figure 5-13 VEGF expression under zinc conditions. a) Hypoxic cells under zinc influence were able to secrete VEGF, as determined by ELISA, in a similar fashion to the normoxic cells with higher cell number, in higher amounts than hypoxia (***p<0.0001, n=6). b) High levels of zinc increased VEGF secretion response under hypoxia (**p<0.01, n=6). Zinc did not had a VEGF effect in normoxia.

The metabolic activity was increased after 24 hours under hypoxia conditions. The increase in the metabolic activity in the hypoxia cells is independent to the effect of the zinc, as it was significantly increased in all conditions. The difference in cell proliferation between the two oxygen conditions is increased at day 3 and day 7. The supplementation of zinc had no effect on the cell proliferation at day 3, but plays an important role in the number of cells present after 7 days of culture.

Zinc seems to play an important role in hypoxia, whilst in normoxia the metabolic activity is similar across all concentrations. At Day 7, 100 µM Zinc appears to be having an effect on the metabolic activity of the cells/DNA, but this could be related to the lower cell proliferation in this condition.

5.4.3.2 *Do cobalt and zinc increase antioxidant capacity?*

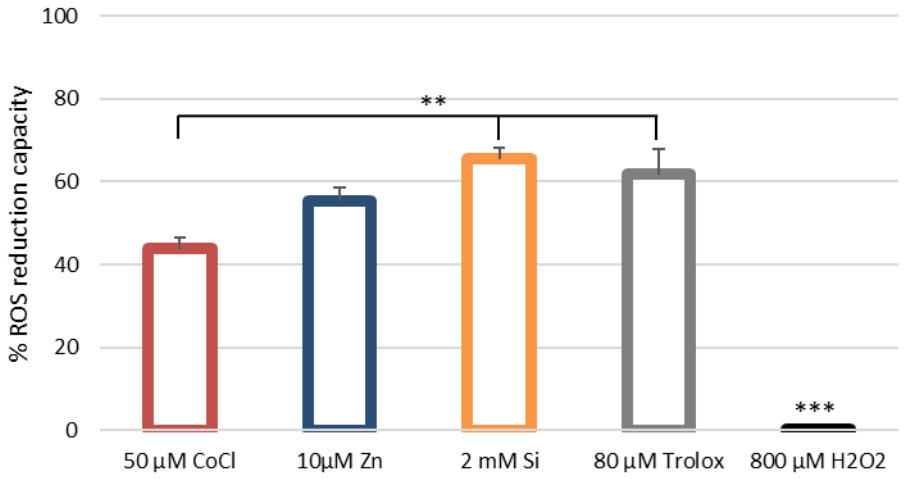

Figure 5-14 Capacity to inhibit produced ROS by the ions present in the glasses compositions. The capacity of reduction of ROS, as determined by DCF-DA dye, produced after HaCaT cells were stimulated with 800 µM of H_2O_2, the cells were previously incubated for 4 hours with the different conditions. A reduction of the ROS was seen in all the conditions.

Cobalt, zinc and silica ions had an effect in suppressing the ROS increase in HaCaT cells after being stimulated with 800 mM H_2O_2 (Figure 5-14). Trolox, an antioxidant known as a cytoplasmic ROS scavenger [415], was kept as a negative control. The basal cellular ROS production was 12.35% ± 0.39. The increase of ROS production was significant in all the samples compared to the basal level, and also significantly decreased when compared to the maximum production. The effect of silica and zinc were similar to the reduction produced by the use of Trolox, where there was not significant difference observed. There was a significant difference in the reduction capacity of the cobalt to the other agents ($p < 0.01$).

5.4.3.3 *Effect of zinc-containing bioactive glasses in HaCaT cells*

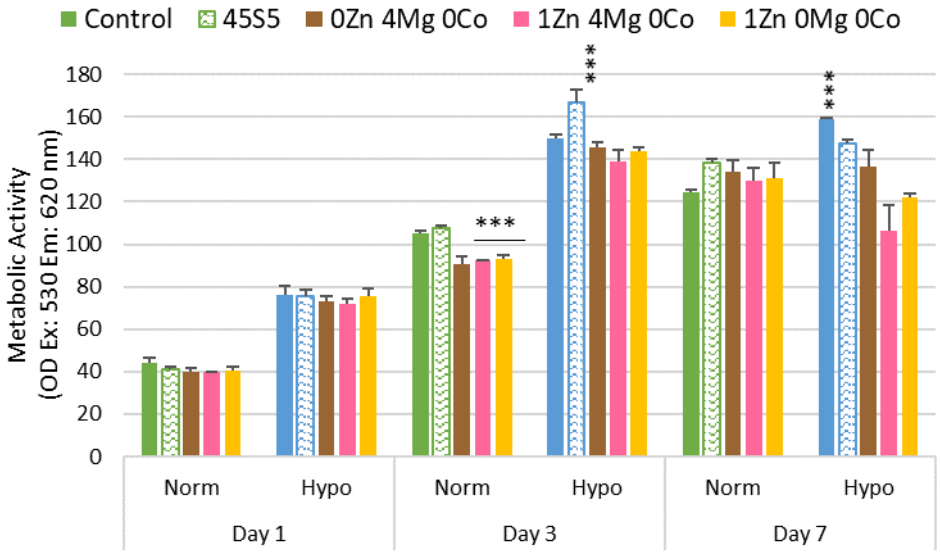

a)

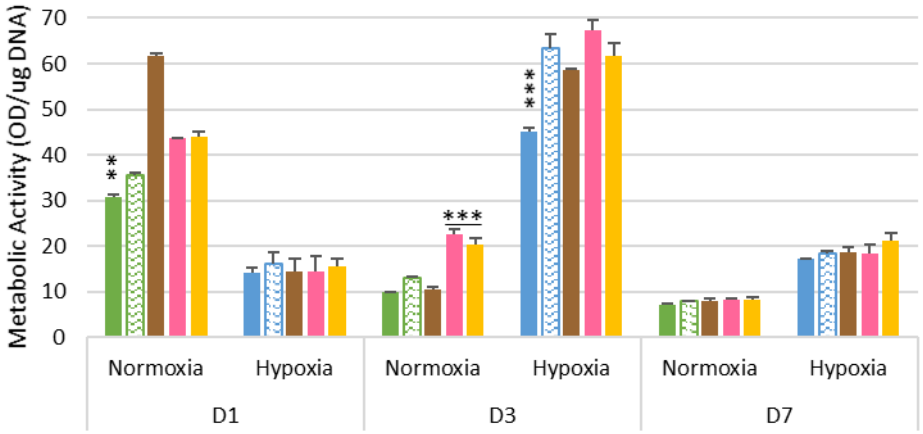

b)

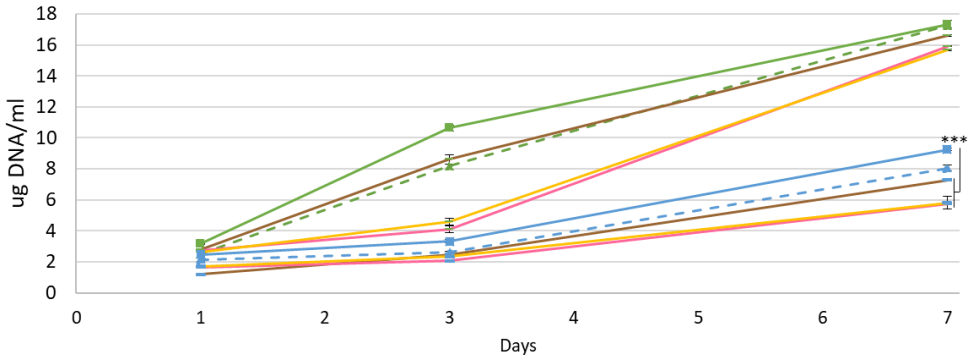

c)

Figure 5-15 The effect of Zinc and Magnesium ions released by bioactive glasses. Glasses containing zinc had an initial slower cell proliferation rate, as quantified using Hoechst dye, under normoxia and slightly decreased cell proliferation after 7 days of hypoxia. The same compositions induced a higher metabolic activity per cell, measured using alamar Blue®, under normoxic conditions at day 1 and 3.

The metabolic activity is higher in all the glasses at normoxic levels (Figure 5-15) with the BG without zinc (Mg only) being the highest, there is not much difference between the ones containing zinc, regardless of the presence of Mg. whist hypoxia has not noticeable effect. The difference in the metabolic activity in normoxia day 3 is reduced. The 0Zn 4Mg 0Co, had the highest metabolic activity at day 1, now is similar to the one in the control. The metabolic activity in the zinc containing glasses remains higher, but to a less extent than Day 1. At day 7 all of them have a similar metabolic activity.

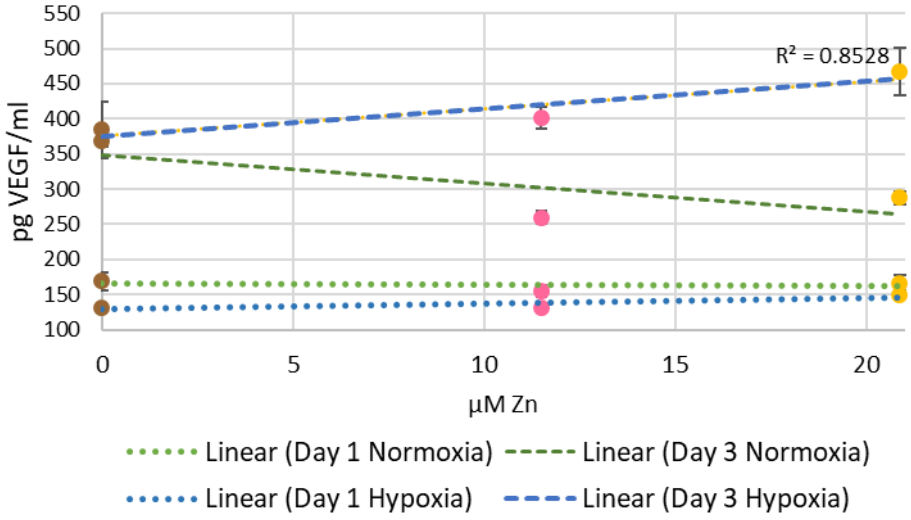

a)

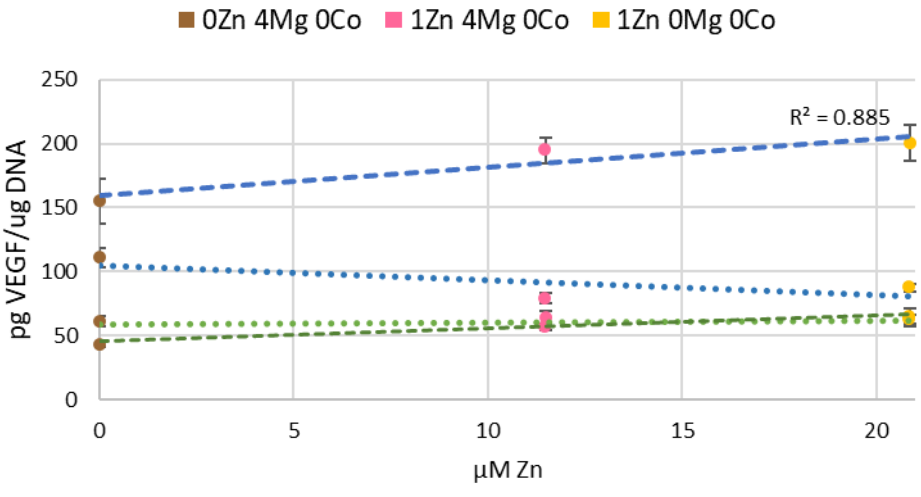

b)

Figure 5-16 Effect of Zinc in VEGF production under hypoxic conditions. Zinc increased VEGF production (r^2=0.8528, normalised to DNA r^2=0.885), as determined by VEGF ELISA and Hoechst dye accordingly, under hypoxia at day 3.

Control and 45S5 did not had an increase of VEGF/cell as a response to hypoxia. Hypoxia D1 0Zn 4Mg 0Co had a significant higher VEGF/DNA compared to all. Followed by 1Zn 0Mg0Co and 1Zn 4Mg 0Co. With no statistical difference between

them. There is an increase on VEGF production at normoxia Day 3 in the 1Zn 0Mg 0Co and 1Zn 4Mg 0Co, suggesting an effect from the zinc ions.

5.4.3.4 *Zinc/Magnesium ratio effect in cobalt-containing glasses*

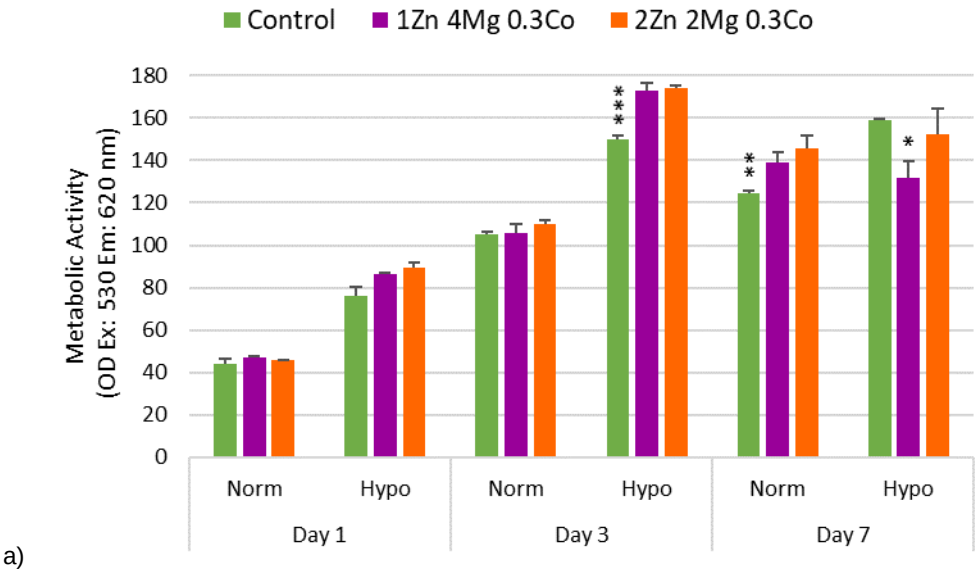

a)

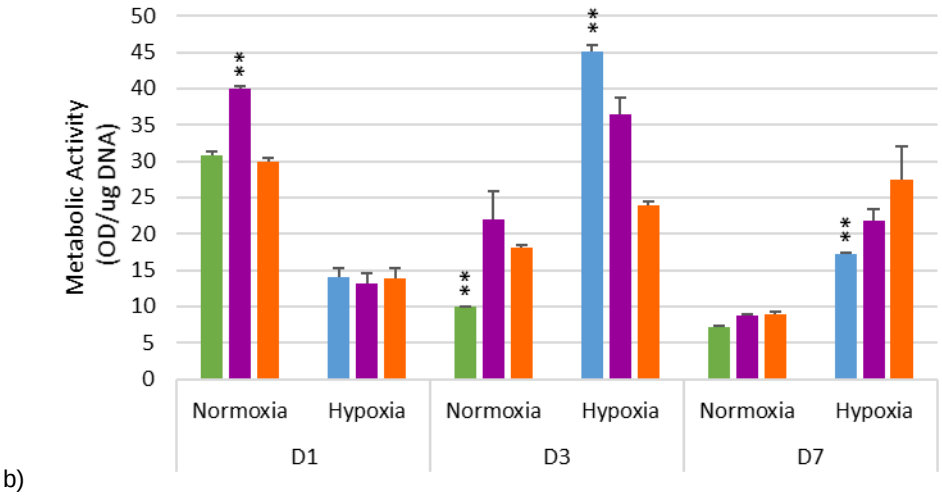

b)

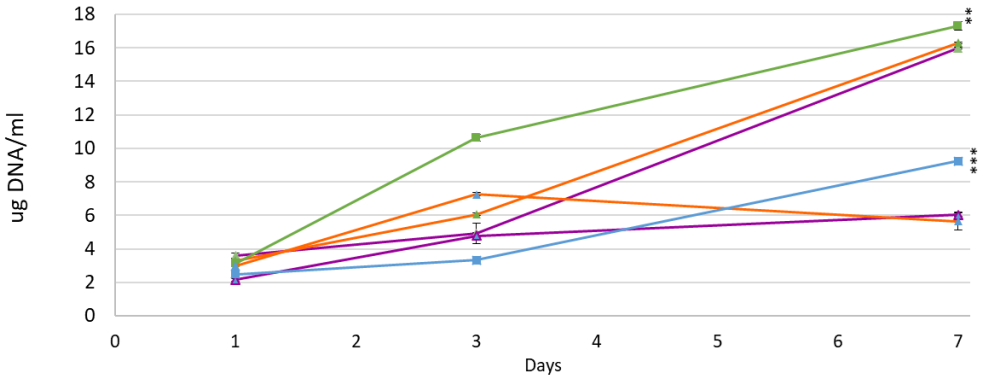

c)

Figure 5-17 Effect of Magnesium and Zinc rates in bioactive glasses. Zinc influenced cell growth, as determined by Hoechst dye, under hypoxia by day 3 ($p<0.01$, n=6). The proliferation was decreased by day 7 in both CoBG due to the presence of the HIF mimetic ($p<0.001$, n=6). Metabolic activity was quantifies using alamar Blue®. N=6, Error bars= Standard deviation

The CoBG had an influence in the metabolic activity of HaCaT cells (Figure 5-17a). The composition 1Zn 4Mg 0.3Co had a higher metabolic activity under normoxia at day 1 and 3 possibly as a result of HIF stabilisation induced by the Co ions, although the VEGF increased was observed until day 3 (Figure 5-18a). The metabolic activity per cell for the 2Zn 2Mg 0.3Co was similar to the control at day one, and so was the VEGF expression. By day 3 the metabolic activity significantly increased and so did the VEGF per cell as a result of the cobalt. The metabolic increase induced by Co ions in normoxia was observed at day 3 ($p<0.001$, $n=6$) (Figure 5-17b). The metabolic activity under the glass conditions was higher than the control in hypoxia at day 7, although the cell proliferation was significantly lower.

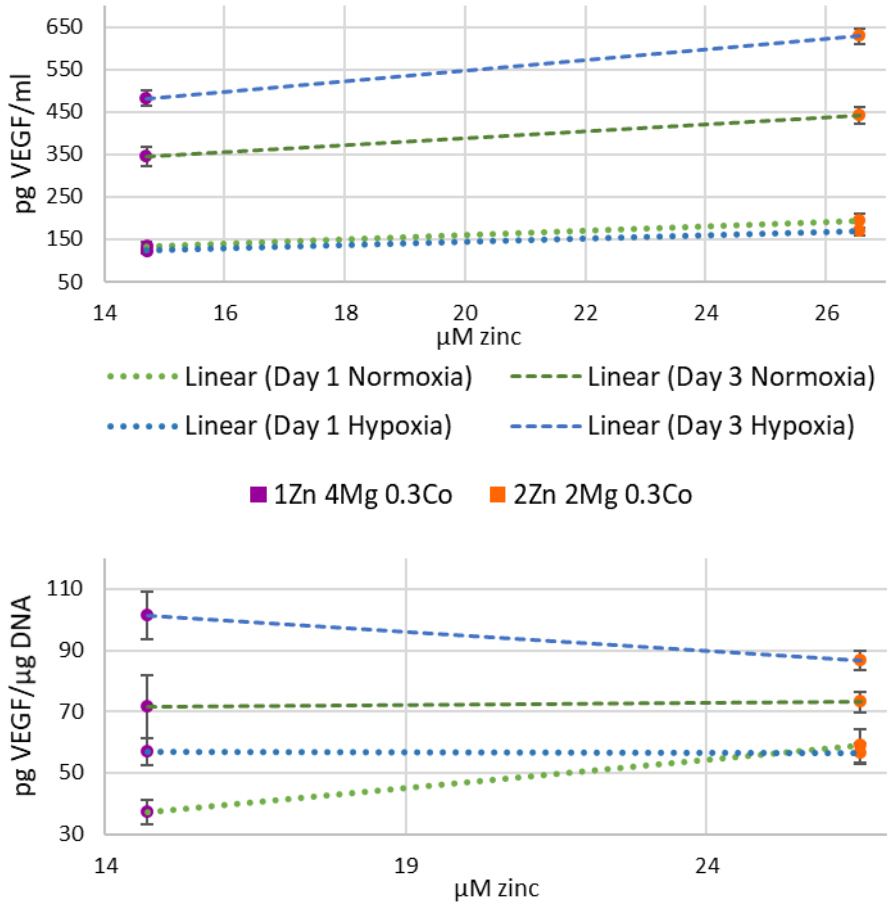

a)

b)

Figure 5-18 Zinc/Magnesium ratio effect on cells. a) The VEGF, as determined by VEGF ELISA, was increased at day 3 under hypoxia and normoxia a higher amount of zinc ($p<0.001$, $n=6$). The effect of increased VEGF as zinc increased was observed only at normoxia day 1 ($p<0.001$, $n=6$). DNA was quantified using Hoechst dye. Error bars=Standard deviation.

The BG-treated cells had a lower cell growth at normoxic conditions (Figure 5-17c) when compared to the control. Whilst hypoxic control resulted in a higher cell proliferation until day 7 ($p<0.001$, $n=6$), being significantly lower than 1Zn 4Mg 0.3 Co

at day 3 ($p<0.001$, n=6). When comparing between the two compositions, 2Zn 2Mg 0.3Co had a higher cell growth under hypoxic conditions after 24 hours of exposure, while in day 3 it was higher than the normoxic pair. This cell growth rate was reduced by day 7 under hypoxia, when the cell population decreased for the 2% Mol Zn. This initial effect could be possibly related to the zinc that can enhance the DNA synthesis, and for the last stage cell proliferation inhibition the effect could be related to the decreased ROS production during prolonged hypoxia.

The VEGF/DNA expression is higher (Figure 5-18b), as expected under hypoxia conditions, being not significantly different by day 3. The increase of VEGF/DNA at normoxia conditions in the 2Zn 2Mg 0.3Co at day 1 can be related to the higher presence of zinc ($p<0.001$, n=6), meanwhile this effect is not significant at day 3 and can be attributed to the Co component (14.3 µM) of the glasses.

5.4.3.5 *Cobalt glasses in HaCaT cells*

Under normoxia conditions, the metabolic activity of the zinc-containing glasses was influenced by the CoBGs (Figure 5-19a). At day 3 the metabolic activity in normoxia was increased at the glass containing 1%Mol Co ($p<0.05$, n=6), by day 7 the CoBGs had a higher metabolic activity than the control ($p<0.05$, n=6). These results suggest the metabolic was increased through the glass cobaltous ions.

The glass-conditioned cells had a lower proliferation rate (Figure 5-19c) during the first time points, but were able to reach confluence similar to the normoxia control at day 7, with the exception of 0Zn 4Mg 2Co ($p<0.001$), which contained 148 µM of Co and no zinc. Interestingly under hypoxia, the same composition had a similar profile to the 1Zn 4Mg 0Co and 1Zn 4Mg 0.3Co, whilst the 1Zn 4Mg 1Co had a decline in cell population after day 3 ($p<0.001$). The cells with only fully supplemented media had the highest cell proliferation among hypoxia.

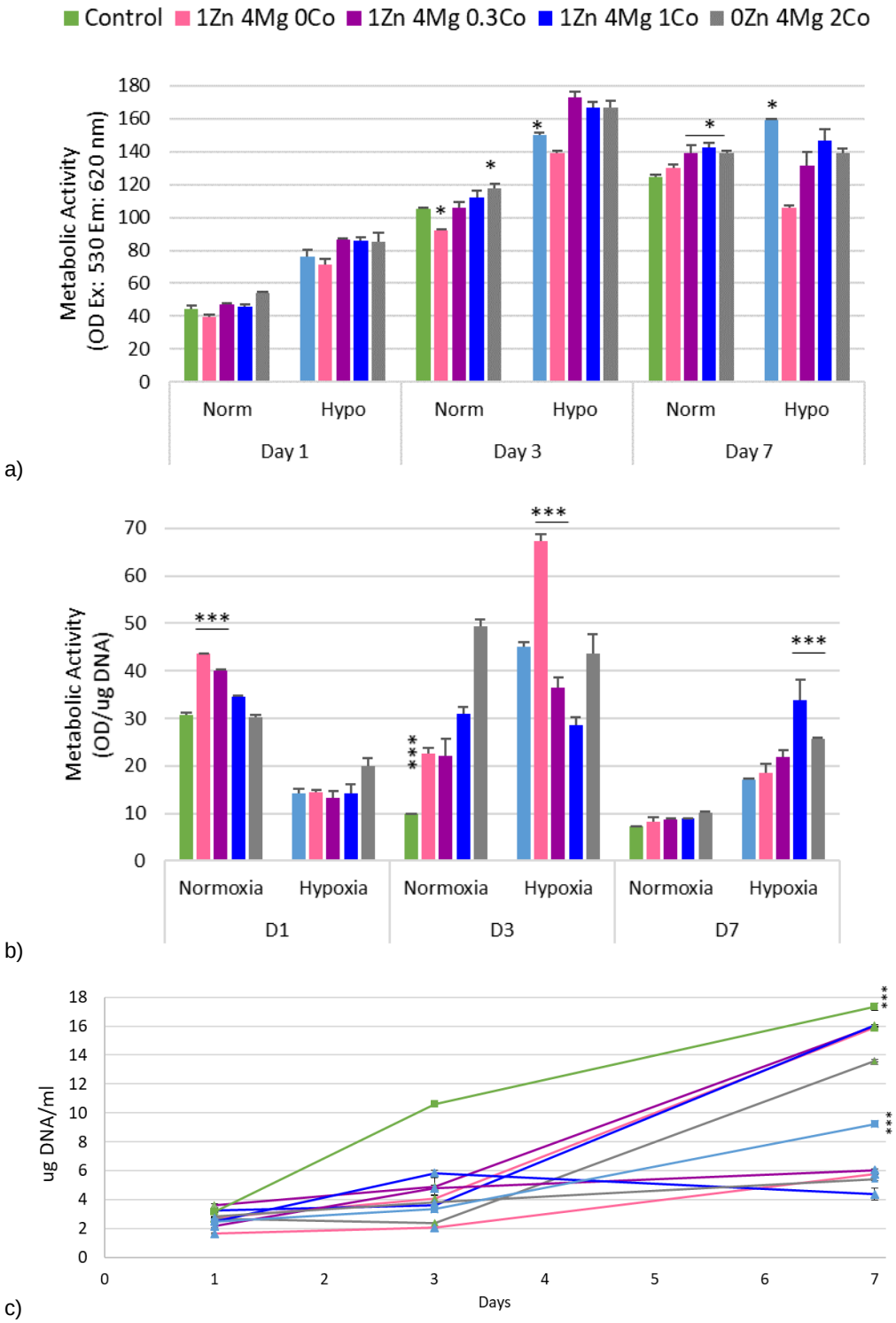

Figure 5-19 Effect of cobalt-bioactive glasses in HaCaT cells. a) Metabolic activity was affected by the presence of the different ions, as determined by alamar Blue®. Cell growth was reduced with the bioactive glasses, as quantified using Hoechst dye, independently of the amount of cobalt in both oxygen conditions ($p<0.001$, $n=6$) Error bars=Standard deviation.

As the cobalt concentration increases, so does the VEGF expression ($r^2=0.9953$) (Figure 5-20 a). This can be seen in VEGF/ml and normalised to total DNA values (Figure 5-20b). The amount of VEGF secreted at 1% Molar at normoxia levels was

the same as the hypoxic control (SD ns, n=60. The HIF inducing effect of cobalt was greater under normoxic conditions at 1 and 2% Mol. The effect of the 0Zn 4Mg 2Co was slightly seen from Day 1 on a 0.55X and Day 3 by a 6.25X increase. The effect of the 0Zn 4Mg 2Co on hypoxia was seen at Day 3, with a 0.4x increase than the hypoxia control. At Day 3 in the 1Zn 4Mg 0.3 Cobalt there is no difference in the cell proliferation between the two oxygen levels. The VEGF is 2.5x higher than normoxia control by day 3, whilst in hypoxia it decreased at both time points.

a)

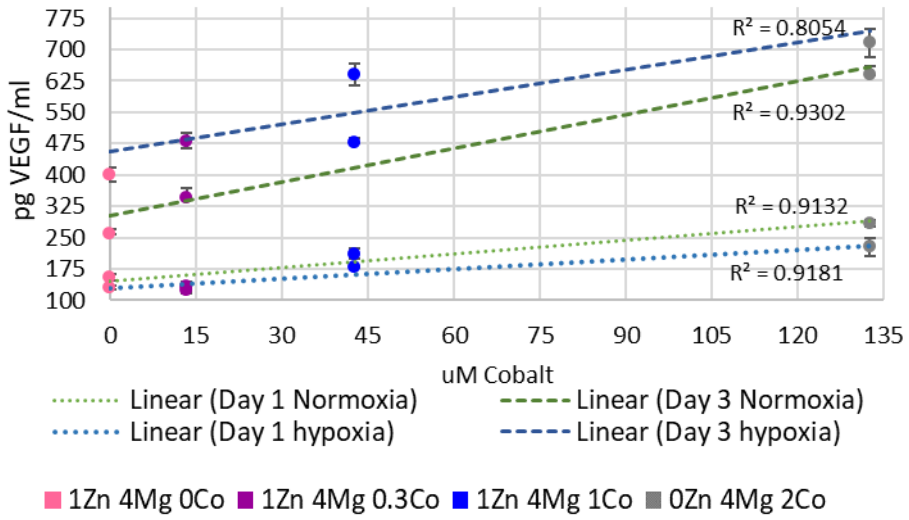

b)

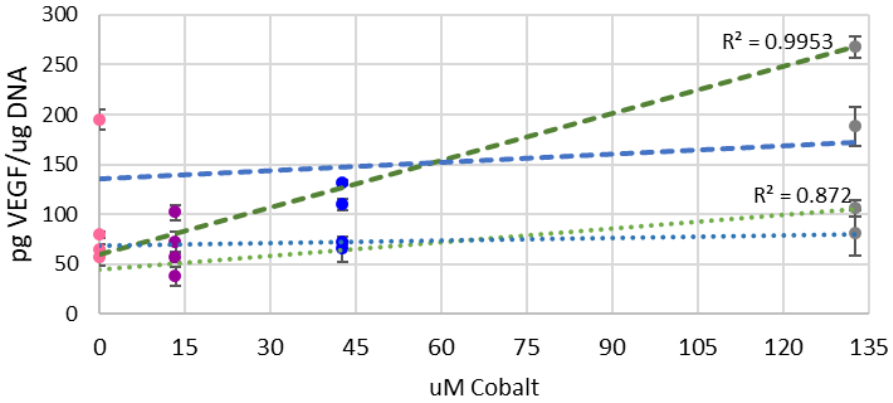

Figure 5-20 The effect of Cobalt incorporation in bioactive glass. VEGF secretion was increased linearly to the cobalt content in the glasses, as expected with the use of a HIF mimicking ion. VEGF was quantified by VEGF ELISA and DNA using Hoechst dye.

Cobalt increased VEGF/cell secretion directly related to the molarity in the glass dissolution (Figure 5-20b), however the glass only containing magnesium and zinc had increased VEGF expression under hypoxia at day 3.

5.5 **Discussion**

In this chapter Si-based hypoxia bioactive glasses were created for chronic wound healing. Cobalt has been previously incorporated to melt derived glasses for bone engineering purposes,[249,483,510] however, this thesis is the first investigation into the effect of CoBGs for wound healing purposes. There are no (to our knowledge) previous publications on the effect of CoBGs on keratinocytes or in hypoxia conditions. Here we demonstrated that CoBGs can be created that release cobalt ions in a controlled manner and at physiologically relevant ranges that were previously demonstrated to stabilise HIF (Figure 4-5). The dissolution products of these BGs were also found to dramatically increase VEGF production dependant on the concentration of cobalt within the glass. Other ions known to have wound healing properties (Zn and Mg) were also investigated and the Zn was found to have a promoting effect on VEGF expression under hypoxia and a higher cell number after prolonged exposure to hypoxia.

5.5.1 **The role of the ions in the glass network**

Zn, Mg and Co were added to the BG via calcium substitution, if these ions had the same role within the glass structure as calcium then it would be expected that the release of the other ions (e.g. Ca, Si, P or Na) would remain the same. This was not, however, the case. As Ca substitution increased Si release also increased (Fig. 5.8), suggesting that these ions are affecting the glass network differently to Ca and causing increased disruption of the network. Others have also reported that increased number of different ions, substituted for calcium, causes increased glass network disruption and higher Si release rates.[503,511]

The lower release of silica in the 1Zn 0Mg 0Co (8.43 %Mol Si) and 1Zn 0Mg 0.3Co (9.71 %Mol Si) compared to the other compositions (av. 12.65 %Mol Si) notes the rigidity of the glass network at low calcium substitution degree. A fraction of the zinc molar percentage possibly forms part of the network, as the amount of silica released decreases with its inclusion into the composition whilst the release of the cobalt is the same. This was not observed in the glasses containing magnesium, suggesting Mg is behaving as a network modifier of the BG network.[492]. The electrostatic attraction of negative charged Zn restrains the mobility of the Na ions, which initiate the ion exchange and hydrolysis of the silicate network.[474]

The cobalt can play a similar role in the glass network due to the size to charge ratio, the incorporation to the network has shown to delay bioactive glass dissolution and

alter ion release, as an intermediate oxide would.[205] However to define the specific role that the cobalt, zinc and magnesium played in the conformation of the glass network, NMR studies need to be done.

Watts et al. (2009)) reported that the incorporation of magnesia to BG changed the Si/Na release in ICIE-1 glasses, increasing the network connectivity (NC) as quantified by NMR.[511] They kept the predicted NC molarity constant by considering the MgO acts as a network modifier (as performed in this chapter). Their result suggest the MgO is participating as network forming oxide, as it increases the NC with the increase of the %Mol, as described in NC2 equation (see *Equation 3*) .[511] The cobalt can play a similar role in the glass network due to the size-to-charge ratio, the incorporation to the network has shown to delay bioactive glass dissolution and alter ion release, as an intermediate oxide would.[205] However to define the specific role that the cobalt, zinc and magnesium played in the conformation of the glass network, NMR studies need to be performed.

Relatively few studies investigate the ion release in DMEM, however, to evaluate the effect of the glasses in the cells and the real dissolutions to which the cells would be exposed to, this was necessary. Differences between the ion release in different media compositions may influence the glass dissolution,[512] and thus altering the ionic concentrations to which the cells are subjected to. Differing media have different amounts of ions, which may cause further changes to the release rates or to spontaneous precipitation (apatite formation), for example DMEM media contains 1.80 mM calcium and 0.81 mM magnesium,[513] whilst RPMI 0.42 mM Ca and 0.41 mM magnesium.[514]

5.5.1.1 *Cobalt*

The ions released by the cobalt containing glasses were able to increase of the VEGF production per cell under normoxia conditions, suggesting the stabilisation of the hypoxia pathway as discussed previously (Section 4.4.1.1). The VEGF production was directly correlated to the cobalt released (% molarity). The glasses with the 0.3% Co were found to release the same amount of cobalt ions. The glass 0Zn 4Mg 2Co showed significantly lower cell proliferation, characteristically of hypoxia stabilisation, nevertheless had higher proliferation and VEGF expression than the hypoxia control. The increase in the concentration of cobalt in the 1Zn 4Mg xCo compositions had an effect in the zinc ion release. As the cobalt concentration increased, the zinc ion release was decreased, suggesting that a portion of cobalt could be participating as a network modifier. Meanwhile, Bresson et al. (2006) reported that under the presence

of cobalt ions, the intracellular concentrations of zinc increased.[246] It would be interesting to observe the mechanism in which this phenomenon occurs and if the presence of zinc ions in conjunction with cobalt have an effect.

Although CoBG have been previously developed, the effects in chronic wound healing remains unanswered. Moura et al. (2017) developed a composite of PCL electrospun fibres with CoBG (via sol-gel) for wound healing purposes, however they reported the material characterisation and not included *in vitro* evaluation.[280] Raja et al. (2019) evaluated the antimicrobial properties of BG in gram positive and gram negative bacteria, as well as in fungal colonies for future wound healing applications. They reported antibacterial properties only under the presence of the glasses and not in the BG-ion dissolution, this could be possible due to the pH changes happening during glass dissolution.[278]

5.5.1.2 *Zinc*

Zinc functions as a site-specific antioxidant through binding competition with Fe and Cu, to bind to ferritin and metallothionein (reviewed by Bettger 1992). Prolonged exposure to hypoxia or HIF stabilisation mimetics leads to increased ROS production and activation of the apoptotic pathway.[444] Zinc has been shown to have geno-protective properties.[490] Parat et al. (1997) demonstrated that pre-incubation of HaCaT cells with 100 µM zinc chloride, reduced DNA fragmentation after UVB irradiation. The reduction of the ROS production seen in Figure 5-14 by Zn BGs is comparable to the reduction produced by the potent anti-oxidant Trolox (an analogue of vitamin E). It has been also reported that even in glutathione cell depletion, zinc-methallothionein has the ability to protect the DNA from ROS damage in HaCaT cells functioning as sacrificial site for antioxidant attacks.[490] The higher cell proliferation under hypoxic conditions resulting from the exposure to ionic zinc can be related to these anti-oxidant and anti-apoptotic properties. This has been previously reported by Kontargiris et al. with 15uM and 30µM Zn.[516]

As discussed before, zinc can act as a network modifier, while in higher amounts it can act as an intermediate oxide. Oki et al. (2004) reported that the incorporation of zinc to bioactive glasses did not reduced the biocompatibility, but aided in buffering the pH of simulated body fluid.[492,517,518] The zinc-containing ion glass dissolution had an effect in the increase of VEGF under hypoxic conditions, even when cobalt was not present. The addition of 0.3% Mol cobalt to the similar composition had no significant effect. This increase in VEGF is in contrast to the reduction on VEGF and HIF-1α downregulation described by Nardinocchi et al (2010) described in human

prostate cancer cells and glioblastoma in hypoxia[519] and a reduction in astrocyte HIF-mediated migration under hypoxic conditions under the presence of $ZnSO_4$ (50µM).[520] However, a spliced variant of HIF-1α induced by $ZnCl_2$ (500 µM) has been identified.[521] Although HIF-1α stabilisation with cobalt has been quantified, the capacity of the Co-containing glasses and the effect of zinc incorporation remained pending.

5.5.1.3 *Magnesium*

Between the different glass compositions, the magnesium release concentration was within a narrow range (0.46 mM range), however the magnesium in the BG may have disrupted the glassy network,[511,522] affecting the ion degradation profile. Therefore, the cell behaviour difference across the glass compositions containing magnesium could be attributed to the variation in the concentration release of the other ions. Magnesium has proved to have a stimulating effect HUVECS in terms of proliferation and increasing the motogenic (migration) response to angiogenic factors at low concentrations and in keratinocytes. Besides stimulating proliferation it can also improve cell-matrix interactions.[523,524] These results were supported by the addition of magnesium in bone culture systems having an increased vascularisation effect. [524,525]

5.5.1.4 *Silica*

The results indicate that the bioactive glass compositions released silica ions in a similar fashion and that they did not affected negatively the cell proliferation or metabolic activity; these was also observed in the compositions that did not contained cobalt. The glasses released ions that could activate angiogenic-related processes and could have therapeutic outcomes for impaired wound healing.

It was also observed that silica, at the concentration released by the glasses, had the capacity of decrease ROS induced by H_2O_2. The mechanism could be through the iron chelating capacity of silicate. Silicate is widely used in the paper-making industry as a stabiliser of H_2O_2; it interacts with the metal ions present in the bleaching process.[195,526,527] As ROS is a major cause of tissue injury in inflammatory conditions, including diabetes type 2, the regulation capacity of high levels of ROS can be found beneficial.

Amorphous silica is considered as a low toxicity agent, as opposed to the crystalline silica, which has been found to be cyto- and genotoxic. Barnes et al. made a meticulous investigation with two independent laboratories to assess the toxicity of silica particles and found that the particles investigated dis not caused genotoxicity. [528] This has been supported by Busch et al. (2010) where they found that the most of

the gene expression observed by the cobalt- containing nanoparticles was coinciding with the cobalt control gene expression and not in the simple form of the particles. Whilst Nabeshi et al. found an increased ROS production and DNA damage induced by amorphous nanoparticles.[529]

5.5.1.5 *Sodium*

The dissolution of the glass is initiated by the sodium interaction with the DMEM. In the glass formation, the increase of the % molarity of sodium will decrease the glass transition temperature and peak crystallisation temperature.[503] in our compositions, the sodium release remained constant throughout the time evaluated and showed no significant difference across samples. Although the effect of the sodium released by the glasses was not evaluated and being the highest ion released, the cells were able to proliferate as the media control, consisting with Tennenbaum et al, who evaluated the addition of sodium to magnesium-containing media and observed no negative effect in the DNA synthesis. [524]

5.5.1.6 *Calcium*

Cell proliferation and metabolic activity is influenced by Ca^{2+} gradients in *in vitro* and *in vivo* models, functioning as a cue for basal and stratum corneum differentiation; as well as regulating adherent and tight junctions which would affect the cell migration, vital in wound healing.[530] Although calcium has an effect on HaCaT behaviour, Colombo et al. (2017) reported that the cellular density has a major regulation factor under low variations of calcium. The particular effect of calcium was not analysed in this thesis.

5.6 **Conclusion**

Zinc demonstrated to have an effect in cell survival and VEGF production under prolonged hypoxic conditions, whilst under normoxic conditions it had no effect in VEGF production or proliferation. Silica and zinc showed ROS reduction capacity similar to Trolox, a widely used antioxidant analogue to vitamin E. Diabetic patients generally had an increase ROS production, also characteristic of impaired healing due to the prolonged inflammation conditions.

The non-cobalt containing glasses had no significant effect on cell survival, the proliferation under hypoxic conditions was reduced slightly, but an increase in the VEGF per unit of DNA was positively related to zinc under hypoxic conditions by day 3. When comparing the magnesium/zinc ratio, no significant effect was observed, as

the VEGF production and reduction of cell proliferation was driven by the presence of the cobalt in the glass compositions.

As the cobalt content in the glass increased, so did the VEGF per DNA unit under normoxic conditions. This was particularly observed under normoxic conditions, suggesting the effective HIF stabilisation which resulted in the VEGF increase. This was also seen under hypoxic conditions, although surprisingly the glass without cobalt, but containing zinc and magnesium, had also an increase on the VEGF production.

The cobalt-zinc glasses demonstrated potential for wound regeneration. It was in the limits of this thesis to evaluate their performance under hyperglycaemic conditions. Fibroblast characterisation and cell migration need to be addressed.

As HaCaT are able to accumulate metallic ions and the toxicity of cobalt is dose dependant. It would of interest to evaluate the intake and accumulation of cobalt ions during and after exposure to the glass dissolutions.

Chapter 6. General Discussion

This thesis addresses new treatments for chronic wounds via the artificial stabilisation of the HIF-1α pathway. An in vitro hyperglycaemic model was created that demonstrated that prolonged culture in high glucose conditions caused a diminished response to hypoxia (as determined by VEGF production). Using this model, commonly used HIF mimetics (with differing modes of action) were investigated for their ability to stabilise HIF-1α and restore a wound healing response. In addition, the controlled delivery of cobalt, at physiological relevant concentrations, was achieved through the use of silica-based bioactive glasses. This chapter discusses the importance, impact and limitations of the thesis.

6.1 **Diabetic Model**

An in vitro model of hyperglycaemic wound healing was developed using two dermal cell types, keratinocytes (HaCaT cells) and fibroblasts (HDF). The studies were made in HaCaT cells, a keratinocyte immortalised cell line with similar cytokine/chemokine profile to primary keratinocytes- and HDF, primary dermal cells. These two cell lines were selected as they are majorly involved in the inflammatory and remodelling stages of wound healing, cell recruitment and activation of other cells through their secretome following HIF stabilisation/hypoxia sensing.[145] The diabetic model consist on a 28-day exposure to high glucose conditions, based on Terashi et al. (2005). Euglycaemia was determined as 1 g/L (5.5 mM) glucose, being physiologically relevant (non-diabetic fasting glucose level is 5.2±0.6mM)[292] and concordant to what others have used as low/normal glycaemic conditions, as reviewed in section 3.1.2. There is no consensus in the use of high levels of glucose; therefore, hyperglycaemia was determined as 4.5 g/L (25 mM) as it is close to the average of the literature review (27.9 ±14.4mM) and it is commercially available at this concentration, decreasing variability in the experiments.

The diabetic model in HaCaT cells is similar to what is observed in chronic wounds; a decrease response to hypoxia, which translates to a low level of HIF-1α stabilisation observed in day 3. The inhibition in HIF stabilisation is mirrored to a reduced VEGF expression, which would initiate angiogenesis,[407] reduced cell proliferation, involved in re–epithelialisation, and increased ROS production[382] and decreased antioxidant capacity, which increases the oxidative stress and DNA damage and MMP-9 overexpression[413] degrading ECM. Hyperglycaemic HaCaTs are appeared to be

larger and flattened concomitant with literature.[287,321] Moreover, a significantly higher variation in cell size was measured under hyperglycaemia. This morphological change could be translated to impaired skin barrier function, as described in murine models, due to an increased tight junction protein-1 (ZO-1) level in diabetes-1.[170]

In vitro modelling of chronic wounds is important in creating new treatments and in improving the translation of these new treatments. Hyperglycaemia clearly does not account for all the differences observed within diabetic patients (as discussed in section 3.1) but does allow for mimicking of some key behavioural responses. Surprisingly the human fibroblasts (HDF cells, 28 days of hyperglycaemia) did not consistently have a significantly response to hypoxia, whilst keratinocytes did. This may indicate cell-type variations in glucose metabolism[531] or highlight other experimental variations. Indeed, others have demonstrated that fibroblasts do have a diminished response to 0.5% oxygen when cultured in 25 mM (4.5 g/L) glucose conditions.[109] The reason for this difference may be due to adaptation of the cell line to high glucose. The cells obtained were p4-20, it is likely the cells (prior to obtainment) were cultured in “normal” glucose DMEM (4.5g/L) which is classed within hyperglycaemic environment as high (Figure 3-2). Others have reported that exposure prolonged exposure high glucose-mediated cell growth, become unresponsive to further glucose changes inhibition.[350,532]

MGO (as a means of introducing AGE products) was investigated as an alternative to prolonged hyperglycaemia[298,393], as a means of creating a simpler model. After MGO treatment the cells had a diminished response to a change in oxygen pressure (decreased VEGF production and metabolic adaption). These characteristics were initially similar to those observed under 28 days of hyperglycaemic condition; however, ROS was not increased, as was observed with prolonged hyperglycaemia. Yu et al. (2006) has reported that ROS overproduction in a diabetic environment is preceded by mitochondrial morphological changes[382]. The effect of MGO in antioxidant capacity, MMP-9 production and cell proliferation further 24 hours after exposure remains to be answered. However, the data suggest that MGO has potential to reduce the preconditioning period of diabetic models.

In the HaCaT cells diabetic model, cell migration -which is reduced in diabetic and elderly patients) and temporal characterisation of the evolution under hyperglycaemia (as represented in Figure 3-16 and Figure 3-17 in HDFs) remain as future research.

6.2 **HIF mimetics in wound healing**

The efficacy of Cobalt, DMOG and DFO to induce HIF-1α stabilisation and VEGF secretion in HDF and HaCaT cells was evaluated. The concentrations were firstly evaluated in fibroblast and based on VEGF expression, several concentrations were then evaluated in HaCaT cells. It is of interest to note that the study of HIF mimetics under hypoxic conditions. The synergistic effect, or possibly detrimental, of enhancing HIF stabilisation under already hypoxic conditions is not commonly investigated under wound models. Rey et al. (2009) investigated the effect of adenoviral HIF-stabilisation factor and DMOG in a ischemic rat limb, observing an increased limb salvage in a mouse critical limb ischemia, with higher perfusion and functionality restoration.[423]

DFO had a significant increase in VEGF expression in fibroblasts, however the doses used in these experiments fall on the lower limit of what it has been reported in the literature as reviewed in section 4.1.2.2.1. The initial concentrations evaluated (100-50µM) decreased metabolic activity significantly and cell number, however VEGF was increased significantly ~10 fold. In the lower doses, DFO decreased metabolic activity and cells did not proliferated after 3 days, nevertheless VEGF was significantly increased. The effect of DFO in cell metabolic activity and cell proliferation was firstly considered as a toxic effect. However, iron is a co-factor for DNA synthesis and due to the iron-chelator nature, DFO reduces cell proliferation after depleting iron from the cells as shown by Siegers at al. (1991). Although as mentioned DFO decreases cell proliferation shown in this study in vitro and others[235,533] its positive effect on wound healing *in vivo* has been previously proven.[200,438]

As mentioned before, the concentrations of the HIF mimetics were based on the increased of VEGF, hypothesising that this was a result of the HIF stabilisation. DMOG at the selected concentration did not increased HIF-1α stabilisation. A limitation of the research is that the concentrations were selected based on the response in HDF cells and then evaluated in HaCaT cells. This was based on the sensitivity of the assay to cell number and cell size difference between HaCaT and HDF (fibroblasts are bigger and basal HIF was not detected hyperglycaemic normoxia), thus it was considered sensible to evaluate first the VEGF expression response in HDF and later in HaCaT. However, as discussed previously, the response to hypoxia and HIF mimetics is cell specific, fibroblasts respond to lower hypoxia changes, as they increased their metabolism and their VEGF release at 2% O_2, whilst in HaCaT it was only observed at 1% O_2. In hyperoxygen conditions, DMOG did not protect the cells from damage, even if VEGF increased. At 85% of oxygen cells under

high glucose have a reduced proliferation rate compared to euglycaemic cells at day 3, however they survived to the constant exposure to high levels of oxygen. Moreover, HIF-1α was accumulated in hyperglycaemic hyperoxia, whilst in euglycaemia it was comparable to the levels of normoxic expression.

Cobalt stabilised HIF-1α under normoxia in hyperglycaemic cells, this increase was found to be similar to the one exerted by hypoxia in euglycaemia and higher to that one in euglycaemia normoxia. However, it was a short-term effect, as in day 3 hyperglycaemia there was no significant effect. The BGs released cobaltous ions in physiological relevant concentrations. Cobalt increased VEGF release in a dose/dependent manner, in $CoCl_2$ and in the ionic release of the BGs. HIF-1α quantification remained pending, however Co interaction with HIF pathway is specific the HIF-1α isoform. The materials were evaluated in euglycaemic conditions, in order to preselect BG compositions that elucidate relevant responses. All cobalt containing glasses increased VEGF expression, and surprisingly so did a composition with no cobalt but zinc. It is of interest evaluate the effect of the CoBG in MMP-9, as MMP-9 is strongly related to cell migration and ECM remodelling. Cobalt ions may induce ROS production whilst zinc ions could possibly serve as antioxidant.

6.3 **Development of HIF mimicking wound dressings**

Here we found that HIF mimetics (cobalt and DFO) restored the HIF-1α pathway in dermal cells and (some) of the normal wound healing responses to hypoxia. Wound dressings that release HIF mimetics would could therefore be a commercial target for improved chronic treatments. Currently there are no commercially available HIF mimicking wound dressings, but several recent publications have developed materials for the release of DMOG from borosilicate BG and mesoporous BG with poly(3-hydroxybutyrate-co-3-hydroxyhexanoate) polymers [264,534] and DFO from cross-linked gelatine and injectable hydrogels loaded with BG [206,260]. The strength of evidence that these materials stabilise HIF or increase wound healing in vivo is poor. The release of HIF mimicking ions from bioceramics have a number of advantages over DMOG and DFO in terms of control of the release, cheapness of manufacture and by incorporating other ions that may also benefit wound healing. Similar work in Cu BG was independently published, however copper had a lower effect in VEGF secretion.[535] Indeed, recently borate fibrous glass scaffolds (Mirragen™) has been granted FDA approval for chronic wound healing (although the cellular mechanism remains unknown), these could be incorporated with cobalt.

There are however, a number of considerations in the design of this wound dressing in terms of delivery mechanism (concentration and duration of release), toxicity – prolonged HIF stabilisation – biofilm / penetration of drug (debridement would still be required) and carrier (provide barrier, allow gaseous exchange and retain moisture).

6.4 **Future areas of research**

1. Is hyperglycaemia leading to intracellular AGE accumulation? The prolonged exposure to high glucose concentrations led to a reduced response to hypoxia (see 3.4.2). It is also considered that in ageing, the reduced response to hypoxia is associated to intracellular AGE accumulation (see 1.6.3). Prolonged hyperglycaemia may induce AGE accumulation, which possibly would be the mechanism of HIF-1α impairment[168]. If true, hyperglycaemia preconditioning can also be translated into an ageing model for HIF-1α impairment. The measurement of intracellular advance glycation protein after high glucose preconditioning could provide insight towards this approach.
2. Is the MGO effect specific to HaCaT cells?
   Bento et al. (2010) reported the inhibition of the hypoxia response in Retinal pigment epithelial (RPE) cells, however this inhibition was observed under the presence of MGO.[168] Here, HaCaT cells had a decrease VEGF secretion 24 hours after treatment and removal of MGO. HIF-α stabilisation/inhibition after MGO treatment remains to be assessed in HaCaT cells and if this effect is only observed in HaCaT, or if similar in fibroblasts/
3. Can MGO decrease the preconditioning time of hyperglycaemia? Several pathological responses are activated through ROS production, however 4-hr preconditioning with MGO did not increase ROS in euglycaemic cells, whilst affecting VEGF production. Sequential treatment with MGO or MGO treatment in combination with short-term high glucose could potentially reduce the hyperglycaemia conditioning (28 days), as single longer exposure of the cells to MGO (6 hours) and higher doses induced cell death.
4. Can HIF mimetics prevent/restore the damage of AGE accumulation? The restoration of the oxygen sensitivity (HIF pathway) in diabetic and ageing *in vitro* models using high glucose, osmotic variations and some gene knockouts have been widely reported; and whilst MGO has been used in several diabetic models as an AGE precursor, inhibiting HIF stabilisation,[168] there were no reports of HIF mimetics in methylglyoxal diabetic models.

Chapter 7. Conclusion

In this work a diabetic model of chronic wound healing has been developed, that mimics the complex environment in diabetic patients. The model had a reduced response to hypoxia, showing a decrease accumulation of HIF-1α, a reduced increase of VEGF expression, increased ROS production, decreased antioxidant capacity, and increased MMP-9 production. HIF-mimetics were able to increase HIF-1α stabilisation in hyperglycaemic conditions, showing a potential incorporation into active wound dressings. The glasses released cobalt in relevant physiological concentrations that were shown to increase HIF stabilisation.

Appendix

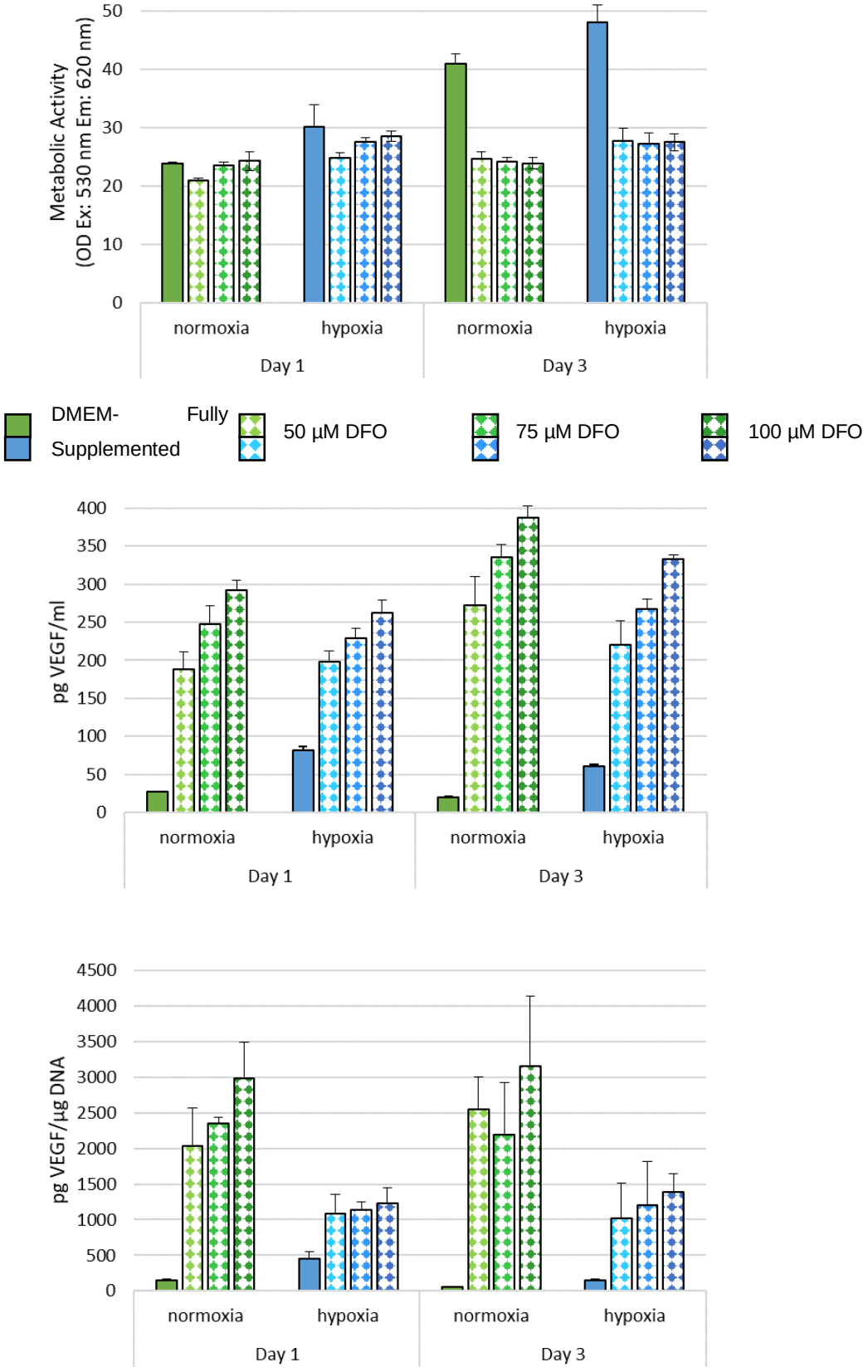

Appendix 1 DFO can induce cell toxicity at high concentrations. DFO at 50 µM and higher concentrations reduced the metabolic activity of the cell and decreased cell number; however, the cells continued to express VEGF under these toxic concentrations.

Appendix 2 Bioactive glass Mol release at 4 hours in DMEM.

Molar release at 4 h							
	Si (mM)	**Na** (mM)	**P** (mM)	**Ca** (mM)	**Co** (µM)	**Zn** (µM)	**Mg** (mM)
45S5	2.23 ±0.07	11.92 ±0.14	0.41 ±0.02	2.14 ±0.07	0.45 ±0.02	5.09 ±4.36	0.85 ±0.03
0Zn 4Mg 0Co	2.26 ±0.10	12.18 ±0.26	0.57 ±0.02	1.87 ±0.07	0.01 ±0.01	-	1.31 ±0.06
1Zn 0Mg 0Co	1.47 ±0.02	11.70 ±0.08	0.48 ±0.01	1.89 ±0.02	-	23.45 ±6.03	1.06 ±0.01
1Zn 4Mg 0Co	2.47 ±0.03	12.29 ±0.28	0.58 ±0.02	2.15 ±0.05	-	12.91 ±10.98	0.89 ±0.02
1Zn 0Mg 0.3Co	1.80 ± 0.01	12.72 ±0.06	0.60 ±0.01	2.41 ±0.01	15.02 ±0.03	7.95 ±0.014	1.02 ±0.01
1Zn 4Mg 0.3 Co	2.73 ±0.04	12.46 ±0.09	0.42 ±0.01	1.81 ±0.03	14.39 ±0.19	16.52 ±2.49	1.09 ±0.02
2Zn 2Mg 0.3Co	2.06 ±0.07	11.90 ±0.30	0.58 ±0.03	2.05 ±0.09	14.25 ±0.76	29.84 ±5.04	1.04 ±0.04
1Zn 4 Mg 1Co	2.96 ±0.09	12.92 ±0.33	0.41 ± 0.02	1.82 ±0.06	47.93 ±1.83	8.16 ±1.71	1.14 ±0.04
0Zn 4Mg 2Co	2.89 ±0.10	12.02 ±0.32	0.39 ±0.01	1.873 ±0.07	148.97 ±4.76	6.97 ±5.43	1.16 ±0.05

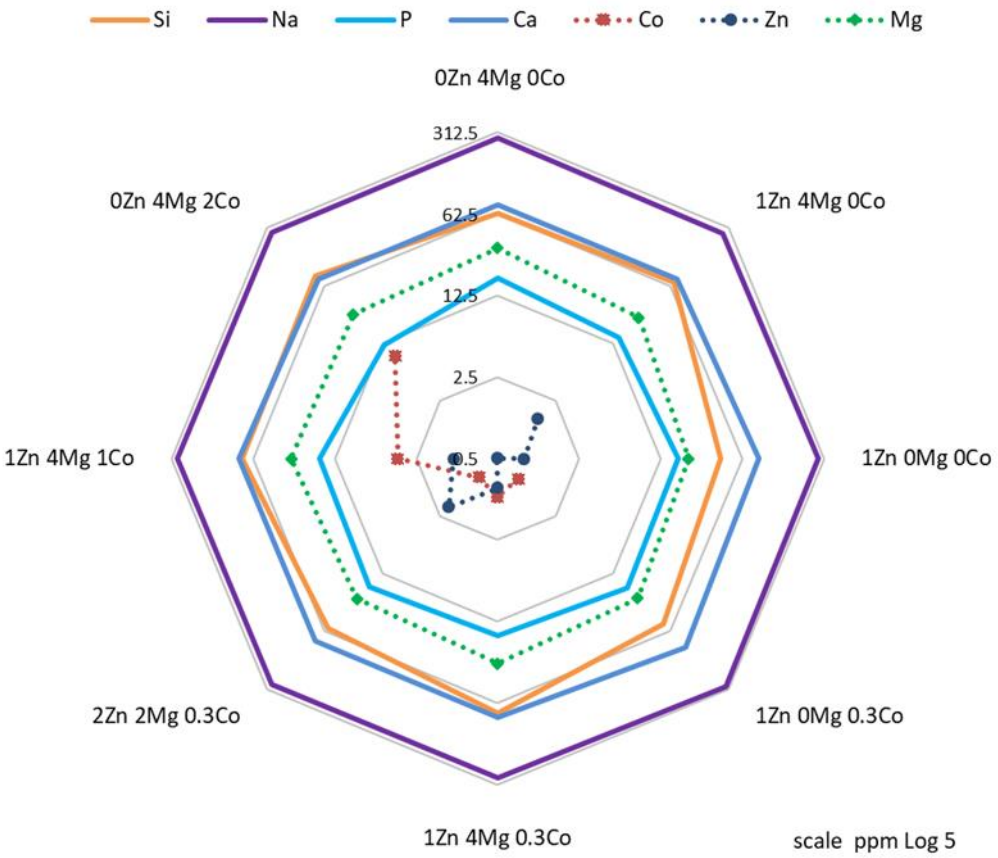

Appendix 3 Relationship glass composition and ion release (ppm) after 4 hours in DMEM. The ratio of silica/calcium ion release varies according to the presence and amount of zinc, magnesium and cobalt, proposing the active involvement in the glass conformation. The magnesium and sodium release does not present any significant fluctuations. The solid lines represent the ions present in ICEI-1. The dotted lines show the ions modifying the glass network. The substitution was made in % molar of calcium. The scale represents the ions released (ppm) by the glasses.

References

1. Lazarus, G. S. *et al.* Definitions and guidelines for assessment of wounds and evaluation of healing. *Wound Repair Regen.* **2**, 165–170 (1994).

2. Bjarnsholt, T. *et al.* Why chronic wounds will not heal: A novel hypothesis. *Wound Repair Regen.* **16**, 2–10 (2008).

3. Zhou, K., Ma, Y. & Brogan, M. S. Chronic and non-healing wounds: The story of vascular endothelial growth factor. *Med. Hypotheses* **85**, 399–404 (2015).

4. Agency for Healthcare Research and Quality. *Skin Substitutes for Treating Chronic Wounds*. *Technology Assessment Program, Agency for HealthCare Research and Qualtiy* (2019).

5. Sen, C. K. *et al.* Human Skin Wounds: A Major and Snowballing Threat to Public Health and the Economy. *Wound Repair Regen.* **17**, 763–771 (2009).

6. Posnett, J. & Franks, P. . The burden of Chronic wounds in the UK. *Nursing Times* 44,45 (2008). Available at: http://www.nexis.com/search/homesubmitForm.do. (Accessed: 4th February 2016)

7. Posnett, J., Gottrup, F., Lundgren, H. & Saal, G. The resource impact of wounds on health-care providers in Europe. *J. Wound Care* **18**, 154–161 (2009).

8. Apelqvist, J., Bakker, K., van Houtum, W., Nabuurs-Franssen, M. & Schaper, N. What is the most effective way to reduce incidence of amputation in the diabetic foot? *Diabetes. Metab. Res. Rev.* **7560**, (1999).

9. National Cardiovascular Intelligence Network (NCVIN). Diabetes Foot Care Profiles. (2019).

10. Armstrong, D. G., Boulton, A. J. M. & Bus, S. A. Diabetic Foot Ulcers and Their Recurrence. *N. Engl. J. Med.* **376**, 2367–2375 (2017).

11. Alavi, A. *et al.* Diabetic foot ulcers: Part I. Pathophysiology and prevention. *J. Am. Acad. Dermatol.* **70**, 1.e1-1.e18 (2014).

12. Iversen, M. M. *et al.* History of foot ulcer increases mortality among individuals with diabetes: Ten-year follow-up of the Nord-Trøndelag health study, Norway. *Diabetes Care* **32**, 2193–2199 (2009).

13. Diabetes UK. *Diabetes UK 2015 Facts and Stats*. (2015).

14. Wagner, F. W. The Dysvascular Foot: A System for Diagnosis and Treatment. *Foot Ankle* 64–122 (1981).

15. Lavery LA, Armstrong DG, H. L. Classification of Diabetic Foot Wounds. *J Foot Ankle Surg* **35**, 528–531 (1996).

16. Ince, P. *et al.* Use of the SINBAD Classification System and Score in Comparing Outcome of Foot. *Diabetes Care* **31**, 964–967 (2008).

17. Oyibo, S. O. *et al.* A Comparison of Two Diabetic Foot Ulcer Classification Systems. *Diabetes Care* **24**, 84–88 (2001).

18. National Institute of Clinical Excellence. *Diabetic foot problems: prevention and management*. (2015).

19. Edmonds, M., Foster, A. & Vowden, P. *Wound bed preparation in practice*. *European Wound Management Association* (2004).

20. Lebrun, E., Tomic-Canic, M. & Kirsner, R. S. The role of surgical debridement in healing of diabetic foot ulcers. *Wound Repair Regen.* **18**, 433–438 (2010).

21. Baltzis, D., Eleftheriadou, I. & Veves, A. Pathogenesis and Treatment of Impaired Wound Healing in Diabetes Mellitus: New Insights. *Adv. Ther.* 817–836 (2014). doi:10.1007/s12325-014-0140-x

22. Schultz, G. S., Barillo, D. J., Mozingo, D. W. & Chin, G. A. Wound bed preparation and a brief history of TIME. *Int. Wound J.* **1**, 19–32 (2004).

23. NICE, N. I. for H. and C. E. Chronic wounds: advanced wound dressings and antimicrobial dressings. 1–43 (2016).

24. Werdin, F., Tennenhaus, M., Schaller, H.-E. & Rennekampff, H.-O. Evidence-based management strategies for treatment of chronic wounds. *Eplasty* **9**, e19 (2009).

25. Smiell, J. M. *et al.* Efficacy and safety of becaplermin (recombinant human platelet-derived growth factor-BB) in patients with nonhealing, lower extremity diabetic ulcers: A combined analysis of four randomized studies. *Wound Repair Regen.* **7**, 335–346 (1999).

26. Martinez-Zapata, M. *et al.* Autologous platelet-rich plasma for treating chronic wounds (Cochrane Review). *Cochrane Database Syst. Rev.* (2016). doi:10.1002/14651858.CD006899.pub3.www.cochranelibrary.com

27. Aljghami, M. E., Saboor, S. & Amini-Nik, S. Emerging Innovative Wound Dressings. *Ann. Biomed. Eng.* **47**, 659–675 (2019).

28. Shabunin, A. *et al.* Composite Wound Dressing Based on Chitin/Chitosan Nanofibers: Processing and Biomedical Applications. *Cosmetics* **6**, 16 (2019).

29. National Institute for Health and Care Excellence. Pressure ulcers: prevention and management. (2014).

30. National Institute for Health and Care Excellence. *Putting NICE guidance into practice Costing statement : Challenging behaviour and learning disabilities Implementing the NICE guideline on challenging behaviour and learning*. (2015).

31. Fonder, M. A. *et al.* Treating the chronic wound: A practical approach to the care of nonhealing wounds and wound care dressings. *J. Am. Acad. Dermatol.* **58**, 185–206 (2008).

32. Bharambe, S. V., Darekar, A. B. & Saudagar, R. B. Wound healing dressings and drug delivery systems: A review. *Int. J. Pharm. Technol.* **5**, 2764–2786 (2013).

33. Wu, L., Norman, G., Dumville, J. C., O'Meara, S. & Bell-Syer, S. E. M. Dressings for treating foot ulcers in people with diabetes: An overview of systematic reviews. *Cochrane Database Syst. Rev.* **2015**, (2015).

34. Dumville, J. C., Deshpande, S., O'Meara, S. & Speak, K. Foam dressings for healing diabetic foot ulcers. *Cochrane Database Syst. Rev.* (2011). doi:10.1002/14651858.CD009111

35. NICE. Wound care products. *National Institute for Health and Care Excellence* (2019). Available at: https://www.nice.org.uk/advice/ktt14.

36. Kim, P. J. & Steinberg, J. S. Wound care: Biofilm and its impact on the latest treatment modalities for ulcerations of the diabetic foot. *Semin. Vasc. Surg.* **25**, 70–74 (2012).

37. Su, N., Tong, N., Du, L., Wu, B. & Xu, T. Heparin and related substances for treating diabetic foot ulcers (Protocol). *Cochrane Database Syst. Rev.* (2014). doi:10.1002/14651858.CD011087.www.cochranelibrary.com

38. Kalani, M. *et al.* Effect of Dalteparin on Healing of Chronic Foot Ulcers in Diabetic Patients. *Diabetes Care* **26**, 2575–2580 (2003).

39. Richard, J.-L. *et al.* Effect of Topical Basic Fibroblast Growth Factor on of the Foot. *Diabetes Care* **18**, 64–69 (1995).

40. Hui, Q., Jin, Z., Li, X., Liu, C. & Wang, X. FGF Family : From Drug Development to Clinical Application. *Int. J. Mol. Sci.* (2018). doi:10.3390/ijms19071875

41. Ohura, T. *et al.* Clinical efficacy of basic fibroblast growth factor on pressure ulcers : Case-control pairing study using a new. *Wound Repair Regen.* **19**, 542–551 (2011).

42. TSANG, M. W. *et al.* Human Epidermal Growth Factor Enhances Healing of Diabetic Foot Ulcers. *Diabetes Care* **26**, (2003).

43. Henemyre-harris, C. L., Adkins, A. L., Chuang, A. H. & Graham, J. S. Addition of Epidermal Growth Factor Improves the Rate of Sulfur Mustard Wound Healing in an In Vitro Model. *Open Access J. Plast. Surg.* 136–150 (2008).

44. Mohan, V. K. Recombinant human epidermal growth factor (REGEN-D TM 150): Effect on healing of diabetic foot ulcers. *Diabetes Res. Clin. Pract.* **78**, 405–411 (2007).

45. Rollman, O. *et al.* Platelet derived growth factor (PDGF) responsive epidermis formed from human keratinocytes transduced with the PDGFβ receptor gene. *J. Invest. Dermatol.* **120**, 742–749 (2003).

46. Rees, R. S. *et al.* Original articles Becaplermin gel in the treatment of pressure ulcers : a phase II randomized , double-blind , placebo-controlled study. *Wound repair Regen.* 141–147 (1999).

47. Takzaree, N., Hadjiakhondi, A., Hassanzadeh, G. & Rouini, M. R. Wounds After Topical Application of Aloe Vera Gel. **1290**, 1285–1290 (2016).

48. Robson, M. C. *et al.* Safety and effect of transforming growth factor?????2 for treatment of venous stasis ulcers. *Wound Repair Regen.* **3**, 157–167 (1995).

49. Yang, L., Qui, C. X., Ludlow, A., Ferguson, M. W. J. & Brunner, G. Active transforming growth factor-β in wound repair: Determination using a new assay. *Am. J. Pathol.* **154**, 105–111 (1999).

50. Hirshberg, James BS; Coleman, James MD; Marchant, Beverly RN; Rees, R. S. TGF-β3 in the Treatment of Pressure Ulcers: A Preliminary Report. *Adv. un Ski. Wound Care* **14**, 91–95 (2001).

51. Hu, X., Sun, H., Han, C., Wang, X. & Yu, W. Topically applied rhGM-CSF for the wound healing: A systematic review. *Burns* **37**, 729–741 (2011).

52. Marques Da Costa, R., Jesus, F. M., Aniceto, C. & Mendes, M. Double-blind randomized placebo-controlled trial of the use of granulocyte-macrophage colony-stimulating factor in chronic leg ulcers. *Am. J. Surg.* **173**, 165–168 (1997).

53. RW, J., L, W., GF, P. & TA., M. Granulocyte-macrophage colony-stimulating factor and granulocyte colony-stimulating factor: differential action on incisional wound healing. *Surgery* **115**, 325–334 (1994).

54. Galiano, R. D. *et al.* Topical Vascular Endothelial Growth Factor Accelerates Diabetic Wound Healing through Increased Angiogenesis and by Mobilizing and Recruiting Bone Marrow-Derived Cells. *Am. J. Pathol.* **164**, 1935–1947 (2004).

55. Kusumanto, Y. H. *et al.* Treatment with Intramuscular Vascular Endothelial Growth Factor Gene Compared with Placebo for Patients with Diabetes Mellitus and Critical Limb Ischemia : A Double-Blind Randomized Trial. *Hum. Gene Ther.* **691**, 683–691 (2006).

56. Springer, M. L., Chen, A. S., Kraft, P. E., Bednarski, M. & Blau, H. M. VEGF Gene Delivery to Muscle: Potential Role for Vasculogenesis in Adults. *Mol. Cell* **2**, 549–558 (1998).

57. Attia, E. A. S., Belal, D. M. I., El Samahy, M. H. & El Hamamsy, M. H. A pilot trial using topical regular crystalline insulin vs. aqueous zinc solution for uncomplicated cutaneous wound healing: Impact on quality of life. *Wound Repair Regen.* **22**, 52–57

(2014).

58. Apikoglu-Rabus, S., Izzettin, F. V., Turan, P. & Ercan, F. Effect of topical insulin on cutaneous wound healing in rats with or without acute diabetesOriginal article. *Clin. Exp. Dermatol.* **35**, 180–185 (2010).

59. Lima, M. H. M. *et al.* Topical insulin accelerates wound healing in diabetes by enhancing the AKT and ERK pathways: A double-blind placebo-controlled clinical trial. *PLoS One* **7**, 1–13 (2012).

60. Greenway, S. E., Filler, L. E. & Greenway, F. L. Topical insulin in wound healing: a randomised, double-blind, placebo-controlled trial. *J. Wound Care* **8**, 526–528 (1999).

61. de Leon, J. M. *et al.* The clinical relevance of treating chronic wounds with an enhanced near-physiological concentration of platelet-rich plasma gel. *Adv. Skin Wound Care* **24**, 357–368 (2011).

62. Roubelakis, M. G. *et al.* Platelet-Rich Plasma (PRP) Promotes Fetal Mesenchymal Stem/Stromal Cell Migration and Wound Healing Process. *Stem Cell Rev. Reports* **10**, 417–428 (2014).

63. Edmonds, M., Apligraf, A., Foot, D. & Study, U. Apligraf in the Treatment of Neuropathic Diabetic Foot Ulcers. *Int. J. Low. Extrem. Wounds* **8**, (2009).

64. Singer, A. J. & Clark, R. A. F. Cutaneous Wound Healing. *N. Engl. J. Med.* 738–746 (1999).

65. Veves, A., Falanga, V., Armstrong, D. G. & Sabolinski, M. L. Graftskin, a Human Skin Equivalent, Is Effective in the Management of Noninfected Neuropathic Diabetic Foot Ulcers. *Diabetes Care* **24**, 290–295 (2001).

66. Sams, H. H., Chen, J. & King, L. E. Graftskin treatment of difficult to heal diabetic foot ulcers: One center's experience. *Dermatologic Surg.* **28**, 698–703 (2002).

67. GENTZKOW, G. D. *et al.* Use of Dermagraft, a Cultured Human Dermis, to Treat Diabetic Foot Ulcers. *Diabetes Care* **19**, (1996).

68. MARSTON, W. A., HANFT, J., NORWOOD, P. & POLLAK, R. The Efficacy and Safety of Dermagraft in Improving the Healing of Chronic Diabetic Foot Ulcers. *Diabetes Care* **26**, 1701–1705 (2003).

69. National Institute for Health and Care Excellence. NATIONAL INSTITUTE FOR HEALTH AND CARE UrgoStart for treating leg ulcers and diabetic foot ulcers. 1–12 (2018).

70. Augustin, M. *et al.* Cost-effectiveness of treating vascular leg ulcers with UrgoStart®and UrgoCell®Contact. *Int. Wound J.* **13**, 82–87 (2016).

71. Betts, A., Yeowell, G., Odeyemi, I. & Fatoye, F. Pmd41 - the Budget Impact and Cost-Consequence of Treating Diabetic Foot Ulcers With Urgostart. *Value Heal.* **21**, S249 (2018).

72. Gibbons, G. W. Grafix ® , a Cryopreserved Placental Membrane, for the Treatment of Chronic/Stalled Wounds . *Adv. Wound Care* **4**, 534–544 (2015).

73. Lavery, L. A. *et al.* The efficacy and safety of Grafix® for the treatment of chronic diabetic foot ulcers: Results of a multi-centre, controlled, randomised, blinded, clinical trial. *Int. Wound J.* **11**, 554–560 (2014).

74. Driver, V. R. *et al.* A clinical trial of Integra Template for diabetic foot ulcer treatment. *Wound Repair Regen.* **23**, 891–900 (2015).

75. Yao, M., Attalla, K., Ren, Y., French, M. A. & Driver, V. R. Ease of use, safety, and efficacy of Integra bilayer wound matrix in the treatment of diabetic foot ulcers in an outpatient clinical setting: A prospective pilot study. *J. Am. Podiatr. Med. Assoc.* **103**, 274–280 (2013).

76. Wang, H. T. *et al.* Phototherapy for treating foot ulcers in people with diabetes. *Cochrane Database Syst. Rev.* **2017**, (2017).

77. Sekhejane, P. R., Houreld, N. N. & Abrahamse, H. Irradiation at 636 nm positively affects diabetic wounded and hypoxic cells in vitro. *Photomed. Laser Surg.* **29**, 521–530 (2011).

78. Ngo, Q. D., Vickery, K. & Deva, A. K. The effect of topical negative pressure on wound biofilms using an in vitro wound model. *Wound Repair Regen.* **20**, 83–90 (2012).

79. Nuutila, K., Yang, L., Broomhead, M., Proppe, K. & Eriksson, E. Novel negative pressure wound therapy device without foam or gauze is effective at −50 mmHg. *Wound Repair Regen.* 162–169 (2018). doi:10.1111/wrr.3

80. Morykwas, M. J., Argenta, L. C., Shelton-Brown, E. I. & McGuirt, W. Vacuum-assisted closure: A new method for wound control and treatment: animal studies and basic foundation. *Annals of Plastic Surgery* **38**, 553–562 (1997).

81. Hess, C. L., Howard, M. a & Attinger, C. E. A review of mechanical adjuncts in wound healing: hydrotherapy, ultrasound, negative pressure therapy, hyperbaric oxygen, and electrostimulation. *Ann. Plast. Surg.* **51**, 210–218 (2003).

82. Mittermayr, R. *et al.* Extracorporeal shock wave therapy (ESWT) for wound healing: Technology, mechanisms, and clinical efficacy. *Wound Repair Regen.* **20**, 456–465 (2012).

83. Qureshi, A. A., Ross, K. M., Ogawa, R. & Orgill, D. P. Shock wave therapy in wound healing. *Plast. Reconstr. Surg.* **128**, 721–727 (2011).

84. Byl, N. N., Mckenzie, A., Wong, T. & Hunt, T. K. Incisional Wound Healing: A controlled study of low and high dose ultrasound. *JOSTP1* **18**, (1993).

85. Hakim, E. W. & Heitzman, J. Wound management in the presence of peripheral arterial disease. *Top. Geriatr. Rehabil.* **29**, 187–194 (2013).

86. Medicare Learning Network. CMS National Coverage, Electrical Stimulation (ES) and Electromagnetic Therapy for the Treatment of Wounds. *MLN Matters* 2009–2011 (2004). Available at: https://www.cms.gov/Outreach-and-Education/Medicare-Learning-Network-MLN/MLNMattersArticles/downloads/MM3149.pdf. (Accessed: 29th September 2019)

87. Kloth, L. C. Electrical stimulation for wound healing: A review of evidence from in vitro studies, animal experiments, and clinical trials. *Int. J. Low. Extrem. Wounds* **4**, 23–44 (2005).

88. Arenbergerova, Monika; Engels, Peter; Gkalpakiotis, Spyros; Dubska, Z. A. P. Effect of topical haemoglobin on venous leg ulcer healing. *Ewma* **13**, 25–30 (2013).

89. Arenberger, P. *et al.* Clinical results of the application of a hemoglobin spray to promote healing of chronic wounds. *GMS Krankenhhyg. Interdiszip.* **6**, Doc05 (2011).

90. Li, J. *et al.* A topical aqueous oxygen emulsion stimulates granulation tissue formation in a porcine second-degree burn wound. *Burns* **41**, 1049–1057 (2015).

91. P. S. Grim et al *et al.* Hyperbaric Oxygen Therapy. *Jama* **263**, 2216–2220 (1990).

92. Mutluoglu, M., Cakkalkurt, A., Uzun, G. & Aktas, S. Topical Oxygen for Chronic Wounds: A PRO/CON Debate. *J. Am. Coll. Clin. Wound Spec.* **5**, 61–65 (2013).

93. Gordillo, G. M. *et al.* Topical oxygen therapy induces vascular endothelial growth factor expression and improves closure of clinically presented chronic wounds. *Clin. Exp. Pharmacol. Physiol.* **35**, 957–964 (2008).

94. Dissemond, J., Kröger, K., Storck, M., Risse, A. & Engels, P. Topical oxygen wound therapies for chronic wounds: a review. *J. Wound Care* **24**, (2015).

95. Blackman, E., Moore, C., Hyatt, J., Railton, R. & Frye, C. Topical wound oxygen therapy in the treatment of severe diabetic foot ulcers: a prospective controlled study. *Ostomy. Wound. Manage.* **56**, 24–31 (2010).

96. Lavery, L. A. & Ryan, E. C. Does Continuous Diffusion of Oxygen Improve Diabetic Foot Ulcer Healing? *J. Diabetes Sci. Technol.* **11**, 892–893 (2017).

97. Davison-Kotler, E., Sharma, V., Kang, N. V. & García-Gareta, E. A Universal Classification System of Skin Substitutes Inspired by Factorial Design. *Tissue Eng. - Part B Rev.* **24**, 279–288 (2018).

98. Zhang, Z. & Michniak-Kohn, B. B. Tissue engineered human skin equivalents. *Pharmaceutics* **4**, 26–41 (2012).

99. Boyce, S. T. & Lalley, A. L. Tissue engineering of skin and regenerative medicine for wound care. *Burn. Trauma* **6**, 1–10 (2018).

100. Organogenesis Inc. *Dermagraft-Directions for USE*. (2014).

101. Karu, T. I., Pyatibrat, L. V. & Afanasyeva, N. I. A Novel Mitochondrial Signaling Pathway Activated by Visible-to-near Infrared Radiation. *Photochem. Photobiol.* **80**, 366 (2004).

102. Sunkari, V. G. *et al.* Hyperbaric oxygen therapy activates hypoxia-inducible factor 1 (HIF-1), which contributes to improved wound healing in diabetic mice. *Wound Repair Regen.* **23**, 98–103 (2015).

103. Schreml, S. *et al.* Oxygen in acute and chronic wound healing. *Br. J. Dermatol.* **163**, 257–268 (2010).

104. LL, Z., JD, D., SC, W., SI, R. & TA., M. Effect of hyperbaric oxygen and growth factors on rabbit ear ischemic ulcers. *Arch. Surg.* **129**, (1994).

105. Kang, T. S., Gorti, G. K., Quan, S. Y., Ho, M. & Koch, R. J. Effect of hyperbaric oxygen on the growth factor profile of fibroblasts. *Arch. Facial Plast. Surg.* **6**, 31–5 (1966).

106. Huang, Y. L., Chang, M. L. & Chiu, C. J. *Glycemic Index and Age-Related Macular Degeneration*. *Handbook of Nutrition, Diet and the Eye* (Elsevier, 2014). doi:10.1016/B978-0-12-401717-7.00022-8

107. Mirza, R. E., Fang, M. M., Ennis, W. J. & Kohl, T. J. Blocking interleukin-1β induces a healing-associated wound macrophage phenotype and improves healing in type 2 diabetes. *Diabetes* **62**, (2013).

108. Lukashev, D. *et al.* Cutting Edge: Hypoxia-Inducible Factor 1α and Its Activation-Inducible Short Isoform I.1 Negatively Regulate Functions of CD4 + and CD8 + T Lymphocytes . *J. Immunol.* **177**, 4962–4965 (2006).

109. Thangarajah, H. *et al.* The molecular basis for impaired hypoxia-induced VEGF expression in diabetic tissues. *Proc. Natl. Acad. Sci. U. S. A.* **106**, 13505–13510 (2009).

110. Abaci, A. *et al.* Effect of diabetes mellitus on formation of coronary collateral vessels. *Circulation* **99**, 2239–2242 (1999).

111. Liao, H., Zakhaleva, J. & Chen, W. Cells and tissue interactions with glycated collagen and their relevance to delayed diabetic wound healing. *Biomaterials* **30**, 1689–1696 (2009).

112. Quondamatteo, F. Skin and diabetes mellitus: What do we know? *Cell Tissue Res.* **355**, 1–21 (2014).

113. Britton, K. a *et al.* Insulin resistance and incident peripheral artery disease in the Cardiovascular Health Study. *Vasc. Med.* **17**, 85–93 (2012).

114. James, G. A. *et al.* Biofilms in chronic wounds. *Wound Repair Regen.* **16**, 37–44 (2008).

115. Gardner, S., Hillis, S. L., Heilmann, K., Segre, J. A. & Grice, E. A. The Neuropathic DFU microbiome is associated with clinical Factors. *Diabetes* **62**, 923:930 (2013).

116. Rey, S. & Semenza, G. L. Hypoxia-inducible factor-1-dependent mechanisms of vascularization and vascular remodelling. *Cardiovasc. Res.* **86**, 236–242 (2010).

117. Provot, S. *et al.* Hif-1α regulates differentiation of limb bud mesenchyme and joint development. *J. Cell Biol.* **177**, 451–464 (2007).

118. Beegle, J. *et al.* Hypoxic preconditioning of mesenchymal stromal cells induces metabolic changes, enhances survival, and promotes cell retention in vivo. *Stem Cells* **33**, 1818–1828 (2015).

119. Zou, D. *et al.* In vitro study of enhanced osteogenesis induced by HIF-1α-transduced bone marrow stem cells. *Cell Prolif.* **44**, 234–243 (2011).

120. Boutin, A. T. *et al.* Epidermal Sensing of Oxygen Is Essential for Systemic Hypoxic Response. *Cell* **133**, 223–234 (2008).

121. Peyssonnaux, C. *et al.* HIF-1 a expression regulates the bactericidal capacity of phagocytes Find the latest version : HIF-1 α expression regulates the bactericidal capacity of phagocytes. *J. Clin. Invest.* **115**, 1806–1815 (2005).

122. Rezvani1, H. R. *et al.* Loss of epidermal hypoxia-inducible factor-1a accelerates epidermal aging and affects re-epithelialization in human and mouse. *Journal of cell science* 4172–4183 (2011). Available at: http://jcs.biologists.org/content/joces/124/24/4172.full.pdf. (Accessed: 20th January 2016)

123. Bento, C. F. & Pereira, P. Regulation of hypoxia-inducible factor 1 and the loss of the cellular response to hypoxia in diabetes. *Diabetologia* **54**, 1946–1956 (2011).

124. Semenza, G. L. HIF-1 and mechanisms of hypoxia sensing. *Curr. Opin. Cell Biol.* **13**, 167–171 (2001).

125. Semenza, G. L. Hypoxia-inducible factor1: oxygen homeostasis and disease pathophysiology. *TRENDS Mol. Med.* **7**, 345–350 (2001).

126. Marín-Hernández, A. EL FACTOR INDUCIDO POR LA HIPOXIA-1 (HIF-1). **28**, 42–51 (2009).

127. Smirnova, N. A. *et al.* Catalytic mechanism and substrate specificity of HIF prolyl hydroxylases. *Biochem.* **77**, 1108–1119 (2012).

128. Berra, E., Roux, D., Richard, D. E. & Pouysségur, J. Hypoxia-inducible factor-1α (HIF-1 escapes O2-driven proteasomal degradation irrespective of its subcellular localization: Nucleus or cytoplasm. *EMBO Rep.* **2**, 615–620 (2001).

129. Weidemann, a & Johnson, R. S. Biology of HIF-1alpha. *Cell Death Differ.* **15**, 621–627 (2008).

130. Chan, M. C., Holt-Martyn, J. P., Schofield, C. J. & Ratcliffe, P. J. Pharmacological targeting of the HIF hydroxylases – A new field in medicine development. *Mol. Aspects Med.* **47**–**48**, (2016).

131. Milosevic, J. *et al.* Non-hypoxic Stabilization of Hypoxia-Inducible Factor Alpha (HIF-α): Relevance in Neural Progenitor/Stem Cells. *Neurotox. Res.* **15**, 367–380 (2009).

132. Semenza, G. L. Hypoxia-inducible factors in physiology and medicine. *Cell* **148**, 399–408 (2012).

133. Seagroves, T. N. *et al.* Transcription factor HIF-1 is a necessary mediator of the pasteur effect in mammalian cells. *Mol. Cell. Biol.* **21**, 3436–44 (2001).

134. Peyssonnaux, C. *et al.* Critical Role of HIF-1a in Keratinocyte Defense against Bacterial Infection. *J. Invest. Dermatol.* **128**, (2008).

135. Kalani, M., Brismar, K., Fagrell, B., Östergren, J. & Jorneskog, G. Transcutaneous Oxygen Tension and To e of Diabetic Foot Ulcers. *Diabetes Care* **22**, 147–151 (1999).

136. Tsai, A. G., Johnson, P. C., Intaglietta, M. & Pittman, R. N. Oxygen gradients in the microcirculation. *Acta Physiol. (Oxf).* **202**, 311–322 (2011).

137. Wang, W., Winlove, C. P. & Michel, C. C. Oxygen partial pressure in outer layers of skin of human finger nail folds. *J. Physiol.* **549**, 855–863 (2003).

138. Carreau, A., Hafny-Rahbi, B. El, Matejuk, A., Grillon, C. & Kieda, C. Why is the partial oxygen pressure of human tissues a crucial parameter? Small molecules and hypoxia. *J. Cell. Mol. Med.* **15**, 1239–1253 (2011).

139. Cramer, T. *et al.* HIF-1α is essential for myeloid cell-mediated inflammation. *Cell* **112**, 645–657 (2003).

140. Schneider, G., Bubel, M., Pohlemann, T. & Oberringer, M. Response of endothelial cells and pericytes to hypoxia and erythropoietin in a co-culture assay dedicated to soft tissue repair. *Mol. Cell. Biochem.* **407**, 29–40 (2015).

141. Shen, K. *et al.* Notoginsenoside Ft1 promotes angiogenesis via HIF-1α mediated VEGF secretion and the regulation of PI3K/AKT and Raf/MEK/ERK signaling pathways. *Biochem. Pharmacol.* **84**, 784–792 (2012).

142. Li, Z., Guo, S., Yao, F., Zhang, Y. & Li, T. Increased ratio of serum matrix metalloproteinase-9 against TIMP-1 predicts poor wound healing in diabetic foot ulcers. *J. Diabetes Complications* **27**, 380–382 (2013).

143. Stadelmann, W. K., Digenis, A. G. & Tobin, G. R. Physiology and Healing Dynamics of Chronic Cutaneous Wounds. *Plast. Reconstr. Surg.* **79**, 657 (1987).

144. Walter, M. N. M., Wright, K. T., Fuller, H. R., MacNeil, S. & Johnson, W. E. B. Mesenchymal stem cell-conditioned medium accelerates skin wound healing: An in vitro study of fibroblast and keratinocyte scratch assays. *Exp. Cell Res.* **316**, 1271–1281 (2010).

145. Koivisto, L., Jiang, G., Häkkinen, L., Chan, B. & Larjava, H. HaCaT keratinocyte migration is dependent on epidermal growth factor receptor signaling and glycogen synthase kinase-3α. *Exp. Cell Res.* **312**, 2791–2805 (2006).

146. Baum, C. L. & Arpey, C. J. Normal cutaneous wound healing: clinical correlation with cellular and molecular events. *Dermatol. Surg.* **31**, 674–686; discussion 686 (2005).

147. Grimshaw, M. J. & Balkwill, F. R. Inhibition of monocyte and macrophage chemotaxis by hypoxia and inflammation - A potential mechanism. *Eur. J. Immunol.* **31**, 480–489 (2001).

148. Sen, C. K. & Roy, S. Redox signals in wound healing. *Biochim. Biophys. Acta - Gen. Subj.* **1780**, 1348–1361 (2008).

149. Niethammer, P., Grabher, C., Look, A. T. & Mitchison, T. J. A tissue-scale gradient of hydrogen peroxide mediates rapid wound detection in zebrafish. *Nature* **459**, 996–999 (2009).

150. Wojtowicz, A. M. *et al.* The importance of both fibroblasts and keratinocytes in a bilayered living cellular construct used in wound healing. *Wound Repair Regen.* **22**, 246–255 (2014).

151. Takahashi, K. *et al.* Induction of Pluripotent Stem Cells from Adult Human Fibroblasts by Defined Factors. *Cell* **131**, 861–872 (2007).

152. Loh, S. a *et al.* SDF-1 alpha expression during wound healing in the aged is HIF dependent. *Plast. Reconstr. Surg.* **123**, 65S-75S (2009).

153. Jazwa, A. *et al.* Effect of heme and heme oxygenase-1 on vascular endothelial growth factor synthesis and angiogenic potency of human keratinocytes. *Free Radic. Biol.*

Med. **40**, 1250–1263 (2006).

154. Deschene, K., Céleste, C., Boerboom, D. & Theoret, C. L. Hypoxia regulates the expression of extracellular matrix associated proteins in equine dermal fibroblasts via HIF1. *J. Dermatol. Sci.* **65**, 12–18 (2012).

155. Werner, S., Krieg, T. & Smola, H. Keratinocyte-fibroblast interactions in wound healing. *J. Invest. Dermatol.* **127**, 998–1008 (2007).

156. Schwarz, F. *et al.* Soft tissue fibroblasts from well healing and chronic human wounds show different rates of myofibroblasts in vitro. *Mol. Biol. Rep.* **40**, 1721–1733 (2013).

157. Brandner, J. M., Zacheja, S., Houdek, P., Moll, I. & Lobmann, R. Expression of matrix metalloproteinases, cytokines, and connexins in diabetic and nondiabetic human keratinocytes before and after transplantation into an ex vivo wound-healing model. *Diabetes Care* **31**, 114–120 (2008).

158. Blakytny, R. & Jude, E. The molecular biology of chronic wounds and delayed healing in diabetes. *Diabet. Med.* **23**, 594–608 (2006).

159. Blakytny, R. & Jude, E. B. Altered Molecular Mechanisms of Diabetic Foot Ulcers. *Int. J. Low. Extrem. Wounds* **8**, 95–104 (2009).

160. Galkowska, H., Wojewodzka, U. & Olszewski, W. L. Chemokines, cytokines, and growth factors in keratinocytes and dermal endothelial cells in the margin of chronic diabetic foot ulcers. *Wound Repair Regen.* **14**, 558–565 (2006).

161. Yue, D. K. *et al.* Abnormalities of Granulation Tissue and Collagen Formation in Experimental Diabetes, Uraemia and Malnutrition. *Diabet. Med.* **3**, 221–225 (1986).

162. Lan, C. C. E., Wu, C. S., Huang, S. M., Wu, I. H. & Chen, G. S. High-Glucose environment enhanced oxidative stress and increased interleukin-8 secretion from keratinocytes. *Diabetes* **62**, 2530–2538 (2013).

163. Mendoza-Marí, Y., Garcia-Ojalvo, A., Fernández-Mayola, M., Herrera-Martínez, L. & Berlanga-Acosta, J. High glucose burden inhibits EGFR/PI3K/AKT1/mTOR signaling pathway in cutaneous fibroblasts. *Biotecnol. Apl.* **31**, 285–290 (2014).

164. Sen, C. K. Wound healing essentials: let there be oxygen. *Wound Repair Regen.* **17**, 1–18 (2009).

165. Botusan, I. R. *et al.* Stabilization of HIF-1alpha is critical to improve wound healing in diabetic mice. *Proc. Natl. Acad. Sci. U. S. A.* **105**, 19426–19431 (2008).

166. Christopher W Pugh & Peter J Ratcliffe. Regulation of angiogenesis by hypoxia: role of the HIF system. *Nat. Med.* **9**, 677–684 (2003).

167. Rivard, A. *et al.* Age-dependent impairment of angiogenesis. *Circulation* **99**, 111–20 (1999).

168. Bento, C. F. *et al.* The chaperone-dependent ubiquitin ligase CHIP targets HIF-1α for degradation in the presence of methylglyoxal. *PLoS One* **5**, 1–13 (2010).

169. Lan, C. E., Liu, I. H., Fang, a. H., Wen, C. H. & Wu, C. S. Hyperglycaemic conditions decrease cultured keratinocyte mobility: Implications for impaired wound healing in patients with diabetes. *Br. J. Dermatol.* **159**, 1103–1115 (2008).

170. Okano, J. *et al.* Hyperglycemia induces skin barrier dysfunctions with impairment of epidermal integrity in non-wounded skin of type 1 diabetic mice. *PLoS One* **11**, 1–22 (2016).

171. Doxey, D. L., Ng, M. C., Dill, R. E. & Iacopino, A. M. Platelet-derived growth factor levels in wounds of diabetic rats. *Life Sci.* **57**, 1111–1123 (1995).

172. Shukla, A., Dubey, M. P., Srivastava, R. & Srivastava, B. S. Differential expression of proteins during healing of cutaneous wounds in experimental normal and chronic

models. *Biochem. Biophys. Res. Commun.* **244**, 434–439 (1998).

173. Fadini, G. P. *et al.* Circulating endothelial progenitor cells are reduced in peripheral vascular complications of type 2 diabetes mellitus. *J. Am. Coll. Cardiol.* **45**, 1449–1457 (2005).

174. Radulovic, M., Baqader, N. O., Stoeber, K. & Godovac-Zimmermann, J. Spatial Cross-Talk between Oxidative Stress and DNA Replication in Human Fibroblasts. *J. Proteome Res.* (2016).

175. Eltzschig, H. K., Bratton, D. L. & Colgan, S. P. Targeting hypoxia signalling for the treatment of ischaemic and inflammatory diseases. *Nat. Rev. Drug Discov.* **13**, 852–869 (2014).

176. Sada, K. *et al.* Hyperglycemia induces cellular hypoxia through production of mitochondrial ROS followed by suppression of aquaporin-1. *PLoS One* **11**, 1–16 (2016).

177. Katavetin, P. *et al.* High glucose blunts vascular endothelial growth factor response to hypoxia via the oxidative stress-regulated hypoxia-inducible factor/hypoxia-responsible element pathway. *J. Am. Soc. Nephrol.* **17**, 1405–1413 (2006).

178. Barrientos, S., Stojadinovic, O., Golinko, M. S., Brem, H. & Tomic-Canic, M. Growth factors and cytokines in wound healing. *Wound Repair Regen.* **16**, 585–601 (2008).

179. Kaelin, W. G. & Ratcliffe, P. J. Oxygen Sensing by Metazoans: The Central Role of the HIF Hydroxylase Pathway. *Mol. Cell* **30**, 393–402 (2008).

180. Isaacs, J. S. *et al.* HIF overexpression correlates with biallelic loss of fumarate hydratase in renal cancer: Novel role of fumarate in regulation of HIF stability. *Cancer Cell* **8**, 143–153 (2005).

181. Blatnik, M., Frizzell, N., Thorpe, S. R. & Baynes, J. W. Formation of S-(2-Succinyl)Cysteine, a Novel Chemical Modification of Protein and Possible Biomarker of Mitochondrial Stress. **57**, 41–49 (2008).

182. Du, X. L. *et al.* Hyperglycemia-induced mitochondrial superoxide overproduction activates the hexosamine pathway and induces plasminogen activator inhibitor-1 expression by increasing Sp1 glycosylation. *Proc. Natl. Acad. Sci. U. S. A.* **97**, 12222–12226 (2000).

183. Huebschmann, A. G., Regensteiner, J. G., Vlassara, H. & Reusch, J. E. B. Diabetes and advanced glycoxidation end products. *Diabetes Care* **29**, 1420–1432 (2006).

184. Babizhayev, M. A. *et al.* The Role of Oxidative Stress in Diabetic Neuropathy: Generation of Free Radical Species in the Glycation Reaction and Gene Polymorphisms Encoding Antioxidant Enzymes to Genetic Susceptibility to Diabetic Neuropathy in Population of Type I Diabetic Patient. *Cell Biochem. Biophys.* **71**, 1425–1443 (2015).

185. Hehenberger, K. & Hansson, A. High glucose-induced growth factor resistance in human fibroblasts can be reversed by antioxidants and protein kinase C-inhibitors. *Cell Biochem. Funct.* **15**, 197–201 (1997).

186. Ishibashi, Y., Matsui, T., Takeuchi, M. & Yamagishi, S. Metformin inhibits advanced glycation end products (AGEs)-induced renal tubular cell injury by suppressing reactive oxygen species generation via reducing receptor for AGEs (RAGE) expression. *Horm. Metab. Res.* **44**, 891–895 (2012).

187. Bosch-Marce, M. *et al.* Effects of aging and hypoxia-inducible factor-1 activity on angiogenic cell mobilization and recovery of perfusion after limb ischemia. *Circ. Res.* **101**, 1310–1318 (2007).

188. Frenkel-Denkberg, G., Gershon, D. & Levy, A. P. The function of hypoxia-inducible factor 1 (HIF-1) is impaired in senescent mice. *FEBS Lett.* **462**, 341–344 (1999).

189. Varani, J. *et al.* Decreased collagen production in chronologically aged skin: Roles of age-dependent alteration in fibroblast function and defective mechanical stimulation. *Am. J. Pathol.* **168**, 1861–1868 (2006).

190. Fisher, G. J. *et al.* Collagen fragmentation promotes oxidative stress and elevates matrix metalloproteinase-1 in fibroblasts in aged human skin. *Am. J. Pathol.* **174**, 101–114 (2009).

191. Rivard, A. *et al.* Age-dependent defect in vascular endothelial growth factor expression is associated with reduced hypoxia-inducible factor 1 activity. *J. Biol. Chem.* **275**, 29643–7 (2000).

192. Rohrbach, S., Simm, A., Pregla, R., Franke, C. & Katschinski, D. M. Age-dependent increase of prolyl-4-hydroxylase domain (PHD) 3 expression in human and mouse heart. *Biogerontology* **6**, 165–171 (2005).

193. Sell, D. R. *et al.* Glucosepane is a major protein cross-link of the senescent human extracellular matrix: Relationship with diabetes. *J. Biol. Chem.* **280**, 12310–12315 (2005).

194. Abou-Seif, M. A. & Youssef, A. A. Evaluation of some biochemical changes in diabetic patients. *Clin. Chim. Acta* **346**, 161–170 (2004).

195. Maessen, D. E. M., Stehouwer, C. D. A. & Schalkwijk, C. G. The role of methylglyoxal and the glyoxalase system in diabetes and other age-related diseases. *Clin. Sci.* **128**, 839–61 (2015).

196. Uchiki, T. *et al.* Glycation-altered proteolysis as a pathobiologic mechanism that links dietary glycemic index, aging, and age-related disease (in nondiabetics). *Aging Cell* **11**, 1–13 (2012).

197. Genuth, S. *et al.* Skin Advanced Glycation Endproducts (AGEs) Glucosepane and Methylglyoxal Hydroimidazolone are Independently Associated with Long- term Microvascular Complication Progression of Type I diabetes. *Diabetes* 1–47 (2014). doi:10.2337/db14-0215

198. Ram, M. *et al.* Deferoxamine modulates cytokines and growth factors to accelerate cutaneous wound healing in diabetic rats. *Eur. J. Pharmacol.* **764**, 9–21 (2015).

199. Kelly, B. D. *et al.* Cell Type-Specific Regulation of Angiogenic Growth Factor Gene Expression and Induction of Angiogenesis in Nonischemic Tissue by a Constitutively Active Form of Hypoxia-Inducible Factor 1. *Circ. Res.* **93**, 1074–1081 (2003).

200. Duscher, D. *et al.* Transdermal deferoxamine prevents pressure-induced diabetic ulcers. *Proc. Natl. Acad. Sci.* **112**, 94–99 (2015).

201. Weir, L., Robertson, D., Leigh, I. M., Vass, J. K. & Panteleyev, A. A. Hypoxia-mediated control of HIF/ARNT machinery in epidermal keratinocytes. *Biochim. Biophys. Acta - Mol. Cell Res.* **1813**, 60–72 (2011).

202. Kim, D. *et al.* Activation of epidermal growth factor receptor/p38/hypoxia-inducible factor-1α is pivotal for angiogenesis and tumorigenesis of malignantly transformed cells induced by hexavalent chromium. *J. Biol. Chem.* **291**, 16271–16281 (2016).

203. Wang, G. L. & Semenza, G. L. Desferrioxamine induces erythropoietin gene expression and hypoxia-inducible factor 1 DNA-binding activity: Implications for models of hypoxia signal transduction. *Blood* **82**, 3610–3615 (1993).

204. Wang, G. L., Jiang, B. H., Rue, E. A. & Semenza, G. L. Hypoxia-inducible factor 1 is a basic-helix-loop-helix-PAS heterodimer regulated by cellular O 2 tension. *Proc. Natl. Acad. Sci. U. S. A.* **92**, 5510–5514 (1995).

205. Azevedo, M. M. *et al.* Synthesis and characterization of hypoxia-mimicking bioactive glasses for skeletal regeneration. *J. Mater. Chem.* **20**, 8854–8864 (2010).

206. Chen, H. *et al.* Quickly promoting angiogenesis by using a DFO-loaded photo-crosslinked gelatin hydrogel for diabetic skin regeneration. *J. Mater. Chem. B* **4**, 3770–3781 (2016).

207. Martin, J. R. *et al.* Local Delivery of PHD2 siRNA from ROS-Degradable Scaffolds to Promote Diabetic Wound Healing. *Adv. Healthc. Mater.* **5**, 2751–2757 (2016).

208. Hou, Z., Nie, C., Si, Z. & Ma, Y. Deferoxamine enhances neovascularization and accelerates wound healing in diabetic rats via the accumulation of hypoxia-inducible factor-1?? *Diabetes Res. Clin. Pract.* **101**, 62–71 (2013).

209. Mace, K. A., Yu, D. H., Paydar, K. Z., Boudreau, N. & Young, D. M. Sustained expression of Hif-1alpha in the diabetic environment promotes angiogenesis and cutaneous wound repair. *Wound Repair Regen.* **15**, 636–645 (2007).

210. Borkow, G. *et al.* Molecular mechanisms of enhanced wound healing by copper oxide-impregnated dressings. *Wound Repair Regen.* **18**, 266–75 (2010).

211. Werner, S., Breeden, M., Hübner, G., Greenhalgh, D. G. & Longaker, M. T. Induction of keratinocyte growth factor expression is reduced and delayed during wound healing in the genetically diabetic mouse. *J. Invest. Dermatol.* **103**, 469–473 (1994).

212. Xia, M. *et al.* Identification of chemical compounds that induce HIF-1α activity. *Toxicol. Sci.* **112**, 153–163 (2009).

213. Yuan, Y., Beitner-Johnson, D. & Millhorn, D. E. Hypoxia-inducible factor 2alpha binds to cobalt in vitro. *Biochem. Biophys. Res. Commun.* **288**, 849–854 (2001).

214. Yuan, Y., Hilliard, G., Ferguson, T. & Millhorn, D. E. Cobalt inhibits the interaction between hypoxia-inducible factor-α and von Hippel-Lindau protein by direct binding to hypoxia-inducible factor-α. *J. Biol. Chem.* **278**, 15911–15916 (2003).

215. Maxwell, P. & Salnikow, K. HIF-1: An oxygen and metal responsive transcription factor. *Cancer Biol. Ther.* **3**, 29–35 (2004).

216. Ciafrè, S. A., Niola, F., Giorda, E., Farace, M. G. & Caporossi, D. CoCl(2)-simulated hypoxia in skeletal muscle cell lines: Role of free radicals in gene up-regulation and induction of apoptosis. *Free Radic. Res.* **41**, 391–401 (2007).

217. Sanjuán-Pla, A. *et al.* A targeted antioxidant reveals the importance of mitochondrial reactive oxygen species in the hypoxic signaling of HIF-1α. *FEBS Lett.* **579**, 2669–2674 (2005).

218. Li, Q., Chen, H., Huang, X. & Costa, M. Effects of 12 metal ions on iron regulatory protein 1 (IRP-1) and hypoxia-inducible factor-1 alpha (HIF-1α) and HIF-regulated genes. *Toxicoloxy Aplied Pharmacol.* **71**, 233–236 (2006).

219. Hervouet, E. *et al.* Inhibition of cytochrome c oxidase subunit 4 precursor processing by the hypoxia mimic cobalt chloride. *Biochem. Biophys. Res. Commun.* **344**, 1086–1093 (2006).

220. Salnikow, K., Su, W., Blagosklonny, M. V. & Costa, M. Carcinogenic metals induce hypoxia-inducible factor-stimulated transcription by reactive oxygen species-independent mechanism. *Cancer Res.* **60**, 3375–3378 (2000).

221. Brunelle, J. K. *et al.* Oxygen sensing requires mitochondrial ROS but not oxidative phosphorylation. *Cell Metab.* **1**, 409–414 (2005).

222. Karovic, O. *et al.* Toxic effects of cobalt in primary cultures of mouse astrocytes Similarities with hypoxia and role of HIF-1a. *Biochem. Pharmacol.* **73**, 694–708 (2007).

223. Tanaka, T. *et al.* Cobalt promotes angiogenesis via hypoxia-inducible factor and protects tubulointerstitium in the remnant kidney model. *Lab. Investig.* **85**, 1292–1307 (2005).

224. Steinbrech, D. S. *et al.* VEGF expression in an osteoblast-like cell line is regulated by

a hypoxia response mechanism. *Am. J. Physiol. - Cell Physiol.* **278**, 853–860 (2000).

225. Martin, F. *et al.* Copper-dependent activation of hypoxia-inducible factor (HIF)-1: Implications for ceruloplasmin regulation. *Blood* **105**, 4613–4619 (2005).

226. Feng, W., Ye, F., Xue, W., Zhou, Z. & Kang, Y. J. Copper regulation of hypoxia-inducible factor-1 activity. *Mol. Pharmacol.* **75**, 174–182 (2009).

227. Zhao, S. *et al.* Wound dressings composed of copper-doped borate bioactive glass microfibers stimulate angiogenesis and heal full-thickness skin defects in a rodent model. **53**, (2015).

228. Sen, C. K. *et al.* Copper-induced vascular endothelial growth factor expression and wound healing. *Am. J. Physiol. Heart Circ. Physiol.* **282**, H1821–H1827 (2002).

229. Kaewpila, S., Venkataraman, S., Buettner, G. R. & Oberley, L. W. Manganese superoxide dismutase modulates hypoxia-inducible factor-1A induction via superoxide. *Cancer Res.* **68**, 2781–2788 (2008).

230. Shin, H. J. *et al.* Manganese-mediated up-regulation of HIF-1α protein in Hep2 human laryngeal epithelial cells via activation of the family of MAPKs. *Toxicol. Vitr.* **24**, 1208–1214 (2010).

231. Han, J. *et al.* Manganese (II) induces chemical hypoxia by inhibiting HIF-prolyl hydroxylase: Implication in manganese-induced pulmonary inflammation. *Toxicol. Appl. Pharmacol.* **235**, 261–267 (2009).

232. Kaczmarek, M. *et al.* The role of ascorbate in the modulation of HIF-1α protein and HIF-dependent transcription by chromium(VI) and nickel(II). *Free Radic. Biol. Med.* **42**, 1246–1257 (2007).

233. Gao, N. *et al.* p38 signaling-mediated hypoxia-inducible factor 1α and vascular endothelial growth factor induction by Cr(VI) in DU145 human prostate carcinoma cells. *J. Biol. Chem.* **277**, 45041–45048 (2002).

234. Kim, J. H., Gibb, H. J. & Howe, P. D. Cobalt and Inorganic Cobalt. *IPCS Concise Int. Chem. Assess. Doc.* **69**, 1–93 (2006).

235. Triantafyllou, A. *et al.* Cobalt induces hypoxia-inducible factor-1α (HIF-1α) in HeLa cells by an iron-independent, but ROS-, PI-3K- and MAPK-dependent mechanism. *Free Radic. Res.* **40**, 847–856 (2006).

236. Goldberg, M. A., Dunning, S. P. & Bunn, H. F. Regulation of the Erythropoietin Gene: Evidence that the oxygen sensor is a heme protein. *Br. J. Psychiatry* **111**, 1009–1010 (1965).

237. Neligan, P. C. Transcutaneous metal absorption following chemical burn injury. *Burns* **22**, 232–233 (1996).

238. Czarnek, K., Terpilowska, S. & Siwicki, A. K. Selected aspects of the action of cobalt ions in the human body. *Cent. Eur. J. Immunol.* **40**, 236–242 (2015).

239. Leggett, R. W. The biokinetics of inorganic cobalt in the human body. *Sci. Total Environ.* **389**, 259–269 (2008).

240. Lacy, S. A., Merritt, K., Brown, S. A. & Puryear, A. Distribution of nickel and cobalt following dermal and systemic administration with in vitro and in vivo studies. *Journal of Biomedical Materials Research* 279–283 (1996). Available at: http://onlinelibrary.wiley.com/doi/10.1002/(SICI)1097-4636(199610)32:2%3C279::AID-JBM18%3E3.0.CO;2-E/epdf. (Accessed: 13th November 2015)

241. Linna, A. *et al.* Exposure to cobalt in the production of cobalt and cobalt compounds and its effect on the heart. *Occup. Environ. Med.* **61**, 877–885 (2004).

242. Ole Simonsen, L. *et al.* Cobalt metabolism and toxicology-A brief update. *Sci. Total*

Environ. **432**, 210–215 (2012).

243. Saxena, S. *et al.* Hypoxia preconditioning by cobalt chloride enhances endurance performance and protects skeletal muscles from exercise-induced oxidative damage in rats. *Acta Physiol.* **200**, 249–263 (2010).

244. De Boeck, M., Kirsch-Volders, M. & Lison, D. Cobalt and antimony: Genotoxicity and carcinogenicity. *Mutat. Res. - Fundam. Mol. Mech. Mutagen.* **533**, 135–152 (2003).

245. Agency for Toxic Substances and Disease Registry. *Toxicological profile for Cobalt*. *U.S. DEPARTMENT OF HEALTH AND HUMAN SERVICES* (2004). doi:10.1111/j.1464-410X.1956.tb04795.x

246. Bresson, C. *et al.* An interdisciplinary approach to investigate the impact of cobalt in a human keratinocyte cell line. *Biochimie* **88**, 1619–29 (2006).

247. Ermolli, M. *et al.* Nickel, cobalt and chromium-induced cytotoxicity and intracellular accumulation in human hacat keratinocytes. *Toxicology* **159**, 23–31 (2001).

248. Paustenbach, D. J., Tvermoes, B. E., Unice, K. M., Finley, B. L. & Kerger, B. D. A review of the health hazards posed by cobalt. *Crit. Rev. Toxicol.* **43**, 316–362 (2013).

249. Azevedo, M. M. *et al.* Hypoxia inducible factor-stabilizing bioactive glasses for directing mesenchymal stem cell behavior. *Tissue Eng. - Part A* **21**, 382–389 (2015).

250. Hench, L. L. Chronology of Bioactive Glass Development and Clinical Applications. **2013**, 67–73 (2013).

251. Jones, J. R. Review of bioactive glass : From Hench to hybrids. *Acta Biomater.* **9**, 4457–4486 (2013).

252. Verné, E. *et al.* Sintering and plasma spray deposition of bioactive glass-Matrix composites for medical applications. *J. Eur. Ceram. Soc.* **18**, 363–372 (1998).

253. Li, W. 45S5 Bioactive Glass - Based Composite Scaffolds with Polymer Coatings for Bone Tissue Engineering Therapeutics. (2015).

254. Boccaccini, A. R. *et al.* Polymer / bioactive glass nanocomposites for biomedical applications : A review. *Compos. Sci. Technol.* **70**, 1764–1776 (2010).

255. Noh, K. T., Lee, H. Y., Shin, U. S. & Kim, H. W. Composite nanofiber of bioactive glass nanofiller incorporated poly(lactic acid) for bone regeneration. *Mater. Lett.* **64**, 802–805 (2010).

256. Ren, J. *et al.* Melt-electrospun polycaprolactone strontium-substituted bioactive glass scaffolds for bone regeneration. *J. Biomed. Mater. Res. - Part A* **102**, 3140–3153 (2014).

257. Quintero, F. *et al.* Laser spinning of bioactive glass nanofibers. *Adv. Funct. Mater.* **19**, 3084–3090 (2009).

258. Poologasundarampillai, G., Yu, B., Jones, J. R. & Kasuga, T. Electrospun silica/PLLA hybrid materials for skeletal regeneration. *Soft Matter* **7**, 10241–10251 (2011).

259. Koudehi, M. F. *et al.* Preparation and evaluation of novel nano-bioglass/gelatin conduit for peripheral nerve regeneration. *J. Mater. Sci. Mater. Med.* **25**, 363–373 (2014).

260. Kong, L. *et al.* Bioactive Injectable Hydrogels Containing Desferrioxamine and Bioglass for Diabetic Wound Healing. *ACS Appl. Mater. Interfaces* **10**, 30103–30114 (2018).

261. Liverani, L. *et al.* Simple fabrication technique for multilayered stratified composite scaffolds suitable for interface tissue engineering. *Mater. Sci. Eng. A* **557**, 54–58 (2012).

262. Li, J. *et al.* Preparation of copper-containing bioactive glass/eggshell membrane nanocomposites for improving angiogenesis, antibacterial activity and wound healing.

Acta Biomater. **36**, 254–266 (2016).

263. Chen, J. *et al.* Bioactive glasses-incorporated, core-shell-structured polypeptide/ polysaccharide nanofibrous hydrogels. *Carbohydr. Polym.* **92**, 612–620 (2013).

264. Xiangyun Jin, Dan Han, Jie Tao, Yinjun Huang, Zihui Zhou, Zheng Zhang, X. Q. and W. J. Dimethyloxallyl Glycine-Incorporated Borosilicate Bioactive Glass Scaffolds for Improving Angiogenesis and Osteogenesis in Critical-Sized Calvarial Defects. *Curr. Drug Deliv.* **16**, 565–576 (2019).

265. Gao, W. *et al.* A highly bioactive bone extracellular matrix-biomimetic nanofibrous system with rapid angiogenesis promotes diabetic wound healing. *J. Mater. Chem. B* **5**, 7285–7296 (2017).

266. Liang, D. *et al.* Tissue interaction with bioglass ceramic implanted in the rabbit cornea. *Yan ke xue bao (Eye Sci.* **17**, 198–201 (2001).

267. Asikainen, T. M. *et al.* Activation of hypoxia-inducible factors in hyperoxia through prolyl 4-hydroxylase blockade in cells and explants of primate lung. *Proc. Natl. Acad. Sci.* **102**, 10212–10217 (2005).

268. Baino, F. & Vitale-Brovarone, C. Bioceramics in ophthalmology. *Acta Biomater.* **10**, 3372–3397 (2014).

269. Kehoe, S., Abraham, R., Tonkopi, E. & Boyd, D. Novel radiopaque embolic agent for uterine fibroid embolization: determination of radiopacity and biological evaluation; cytocompatibility, intracutaneous reactivity and local effects after implantation. in *Journal of Vascular and Interventional Radiology* **23**, S33 (Elsevier Inc., 2012).

270. Zhang, X. F., O'Shea, H., Kehoe, S. & Boyd, D. Time-dependent evaluation of mechanical properties and in vitro cytocompatibility of experimental composite-based nerve guidance conduits. *J. Mech. Behav. Biomed. Mater.* **4**, 1266–1274 (2011).

271. Zhang, X. F. *et al.* Experimental composite guidance conduits for peripheral nerve repair: An evaluation of ion release. *Mater. Sci. Eng. C* **32**, 1654–1663 (2012).

272. Abou Neel, E. A., Ahmed, I., Pratten, J., Nazhat, S. N. & Knowles, J. C. Characterisation of antibacterial copper releasing degradable phosphate glass fibres. *Biomaterials* **26**, 2247–2254 (2005).

273. Blaker, J. J., Nazhat, S. N. & Boccaccini, A. R. Development and characterisation of silver-doped bioactive glass-coated sutures for tissue engineering and wound healing applications. *Biomaterials* **25**, 1319–1329 (2004).

274. Gholipourmalekabadi, M. *et al.* Silver- and fluoride-containing mesoporous bioactive glasses versus commonly used antibiotics: Activity against multidrug-resistant bacterial strains isolated from patients with burns. *Burns* **42**, 131–140 (2016).

275. Rivadeneira, J., Di Virgilio, A. L., Audisio, M. C., Boccaccini, A. R. & Gorustovich, A. A. Evaluation of antibacterial and cytotoxic effects of nano-sized bioactive glass/collagen composites releasing tetracycline hydrochloride. *J. Appl. Microbiol.* **116**, 1438–1446 (2014).

276. Hong, Y. *et al.* Fabrication and drug delivery of ultrathin mesoporous bioactive glass hollow fibers. *Adv. Funct. Mater.* **20**, 1503–1510 (2010).

277. Valappil, S. P. *et al.* Controlled delivery of antimicrobial gallium ions from phosphate-based glasses. *Acta Biomater.* **5**, 1198–1210 (2009).

278. Raja, F. N. S. *et al.* The Antimicrobial Efficacy of Hypoxia Mimicking Cobalt Oxide Doped Phosphate-Based Glasses against Clinically Relevant Gram Positive, Gram Negative Bacteria and a Fungal Strain. *ACS Biomater. Sci. Eng.* **5**, 283–293 (2019).

279. Barrioni, B. R. *et al.* Evaluation of in vitro and in vivo biocompatibility and structure of cobalt-releasing sol-gel bioactive glass. *Ceram. Int.* **44**, 20337–20347 (2018).

280. Moura, D. *et al.* Development of a bioactive glass-polymer composite for wound healing applications. *Mater. Sci. Eng. C* **76**, 224–232 (2017).

281. Chen, S. *et al.* In vitro stimulation of vascular endothelial growth factor by borate-based glass fibers under dynamic flow conditions. *Mater. Sci. Eng. C* **73**, 447–455 (2017).

282. Lin, Y., Brown, R. F., Jung, S. B. & Day, D. E. Angiogenic effects of borate glass microfibers in a rodent model. *J. Biomed. Mater. Res. - Part A* **102**, 4491–4499 (2014).

283. Lin, C., Mao, C., Zhang, J., Li, Y. & Chen, X. Healing effect of bioactive glass ointment on full-thickness skin wounds. *Biomed. Mater.* **7**, (2012).

284. Ostomel, T. A., Shi, Q., Tsung, C. K., Liang, H. & Stucky, G. D. Spherical bioactive glass with enhanced rates of hydroxyapatite deposition and hemostatic activity. *Small* **2**, 1261–1265 (2006).

285. Wang, C. *et al.* Highly Efficient Local Delivery of Endothelial Progenitor Cells Significantly Potentiates Angiogenesis and Full-thickness Wound Healing. *Acta Biomater.* **69**, 156–169 (2018).

286. Kim, W. Y. *et al.* Failure to prolyl hydroxylate hypoxia-inducible factor α phenocopies VHL inactivation in vivo. *EMBO J.* **25**, 4650–4662 (2006).

287. Terashi, H., Izumi, K., Deveci, M., Rhodes, L. M. & Marcelo, C. L. High glucose inhibits human epidermal keratinocyte proliferation for cellular studies on diabetes mellitus. *Int. Wound J.* **2**, 298–304 (2005).

288. Xuan, Y. H. *et al.* High-glucose inhibits human fibroblast cell migration in wound healing via repression of bFGF-regulating JNK phosphorylation. *PLoS One* **9**, (2014).

289. Esmaeelinejad, M., Bayat, M., Darbandi, H., Bayat, M. & Mosaffa, N. The effects of low-level laser irradiation on cellular viability and proliferation of human skin fibroblasts cultured in high glucose mediums. *Lasers Med. Sci.* **29**, 121–129 (2014).

290. Nakai, K., Kubota, Y. & Kosaka, H. Inhibition of nuclear factor kappa B activation and inducible nitric oxide synthase transcription by prolonged exposure to high glucose in the human keratinocyte cell line HaCaT. *Br. J. Dermatol.* **150**, 640–646 (2004).

291. Genuth, S. *et al.* Skin advanced glycation end products glucosepane and methylglyoxal hydroimidazolone are independently associated with long-Term microvascular complication progression of type 1 diabetes. *Diabetes* **64**, 266–278 (2015).

292. WHO. *Definition and Diagnosis of Diabetes Mellitus And Intermediate Hyperglycemia*. (2003).

293. Oyibo, S. O., Prasad, Y. D. M., Jackson, N. J., Jude, E. B. & Boulton, A. J. M. The relationship between blood glucose excursions and painful diabetic peripheral neuropathy: A pilot study. *Diabet. Med.* **19**, 870–873 (2002).

294. Wachtel, T. J., Tetu-Mouradjian, L. M., Goldman, D. L., Ellis, S. E. & O'Sullivan, P. S. Hyperosmolarity and acidosis in diabetes mellitus - A three-year experience in Rhode Island. *J. Gen. Intern. Med.* **6**, 495–502 (1991).

295. Thornalley, P. J. *et al.* Quantitative screening of advanced glycation endproducts in cellular and extracellular proteins by tandem mass spectrometry. *Biochem. J.* **375**, 581–592 (2003).

296. DeFronzo, R. A., Simonson, D. & Ferrannini, E. Hepatic and peripheral insulin resistance: A common feature of Type 2 (non-insulin-dependent) and Type 1 (insulin-dependent) diabetes mellitus. *Diabetologia* **23**, 313–319 (1982).

297. Dehne, N., Hintereder, G. & Brüne, B. High glucose concentrations attenuate hypoxia-inducible factor-1α expression and signaling in non-tumor cells. *Exp. Cell Res.* **316**, 1179–1189 (2010).

298. Bento, C. F. *et al.* Methylglyoxal-induced imbalance in the ratio of vascular endothelial

growth factor to angiopoietin 2 secreted by retinal pigment epithelial cells leads to endothelial dysfunction. *Exp. Physiol.* **95**, 955–970 (2010).

299. Lafosse, A., Dufeys, C., Beauloye, C., Horman, S. & Dufrane, D. Impact of hyperglycemia and low oxygen tension on adipose-derived stem cells compared with dermal fibroblasts and keratinocytes: Importance for wound healing in type 2 diabetes. *PLoS One* **11**, 1–18 (2016).

300. Fitsialos, G. *et al.* HIF1 transcription factor regulates laminin-332 expression and keratinocyte migration. *J. Cell Sci.* **121**, 2992–3001 (2008).

301. Spravchikov, N. *et al.* Glucose Effects on Skin Keratinocytes Implications for Diabetes Skin Complications. *Diabetes* **50**, 1627–1635 (2001).

302. Domínguez-Perles, R., Guedes, A., Queiroz, M., Silva, A. M. & Barros, A. I. R. N. A. Oxidative stress prevention and anti-apoptosis activity of grape (Vitis vinifera L.) stems in human keratinocytes. *Food Res. Int.* (2016). doi:10.1016/j.foodres.2016.06.030

303. Colombo, I. *et al.* HaCaT Cells as a Reliable In Vitro Differentiation Model to Dissect the Inflammatory/Repair Response of Human Keratinocytes. *Mediators Inflamm.* **2017**, 1–12 (2017).

304. Perlman, R. L. Mouse Models of Human Disease: An Evolutionary Perspective. *Evol. Med. Public Heal.* eow014 (2016). doi:10.1093/emph/eow014

305. Gudjonsson, J. E., Johnston, A., Dyson, M., Valdimarsson, H. & Elder, J. T. Mouse models of psoriasis. *J. Invest. Dermatol.* **127**, 1292–1308 (2007).

306. Gurtner, G. C., Wong, V. W., Sorkin, M., Glotzbach, J. P. & Longaker, M. T. Surgical approaches to create murine models of human wound healing. *J. Biomed. Biotechnol.* **2011**, (2011).

307. Mouse Genome Sequencing Consortium. Initial sequencing and comparative analysis of the mouse genome. *Nature* **420**, 520–562 (2002).

308. Schittek, B. *et al.* Dermcidin: A novel human antibiotic peptide secreted by sweat glands. *Nat. Immunol.* **2**, 1133–1137 (2001).

309. Galiano, R. D., Michaels V, J., Dobryansky, M., Levine, J. P. & Gurtner, G. C. Quantitative and reproducible murine model of excisional wound healing. *Wound Repair Regen.* **12**, 485–492 (2004).

310. Kligman, A. M. The Human Hair Cycle. *J. Invest. Dermatol.* **33**, 307–316 (1959).

311. H.B. Chase, Rauch, H. & Smith, V. W. Critical stages of hair development and pigmentation in the mouse. *Physiol Zool* **24**, 1–9 (1951).

312. Loots, M. A. M., Lamme, E. N., Mekkes, J. R., Bos, J. D. & Middelkoop, E. Cultured fibroblasts from chronic diabetic wounds on the lower extremity (non-insulin-dependent diabetes mellitus) show disturbed proliferation. *Arch. Dermatol. Res.* **291**, 93–99 (1999).

313. Lohmann, M. *et al.* Donor age of human platelet lysate affects proliferation and differentiation of mesenchymal stem cells. *PLoS One* **7**, 14–16 (2012).

314. Kaewkhaw, R., Scutt, A. M. & Haycock, J. W. Anatomical site influences the differentiation of adipose-derived stem cells for Schwann-cell phenotype and function. *Glia* **59**, 734–749 (2011).

315. Podlutsky, A., Hou, S. M., Nyberg, F., Pershagen, G. & Lambert, B. Influence of smoking and donor age on the spectrum of in vivo mutation at the HPRT-locus in T lymphocytes of healthy adults. *Mutat. Res. - Fundam. Mol. Mech. Mutagen.* **431**, 325–339 (1999).

316. Boukamp, P. *et al.* Normal Keratinization in a Spontaneously Immortalized. *J. Cell Biol.* **106**, 761–771 (1988).

317. Breitkreutz, D. *et al.* Epidermal differentiation and basement membrane formation by HaCaT cells in surface transplants. *Eur. J. Cell Biol.* **75**, 273–286 (1998).

318. Long, M. *et al.* An essential role of NRF2 in diabetic wound healing. *Diabetes* **65**, 780–793 (2016).

319. Yang, D. J. *et al.* Gallic Acid Promotes Wound Healing in Normal and Hyperglucidic Conditions. *Molecules* **21**, 1–15 (2016).

320. Moura, L. I., Cruz, M. T. & Carvalho, E. The effect of neurotensin in human keratinocytes - implication on impaired wound healing in diabetes. *Exp. Biol. Med.* **239**, 6–12 (2014).

321. Nakai, K. *et al.* Effects of high glucose on NO synthesis in human keratinocyte cell line (HaCaT). *J. Dermatol. Sci.* **31**, 211–218 (2003).

322. Runage, K., Bektas, M., Berkowitz, P. & Rubenstein, D. S. Targeting O-Glycosyltransferase (OGT) to promote healing of diabetic skin wounds. *J. Biol. Chem.* **289**, 5462–5466 (2014).

323. Cheng, T. L. *et al.* Thrombomodulin promotes diabetic wound healing by regulating toll-like receptor 4 expression. *J. Invest. Dermatol.* **135**, 1668–1675 (2015).

324. Ochoa-Gonzalez, F. *et al.* Correction: Metformin induces cell cycle arrest, reduced proliferation, wound healing impairment in vivo and is associated to clinical outcomes in diabetic foot ulcer patients. *PLoS One* **11**, 1–16 (2016).

325. Lan, C. C. E., Wu, C. S., Kuo, H. Y., Huang, S. M. & Chen, G. S. Hyperglycaemic conditions hamper keratinocyte locomotion via sequential inhibition of distinct pathways: new insights on poor wound closure in patients with diabetes. *Br. J. Dermatol.* **160**, 1206–1214 (2009).

326. Sen, C. K. *et al.* Oxidant-induced vascular endothelial growth factor expression in human keratinocytes and cutaneous wound healing. *J. Biol. Chem.* **277**, 33284–33290 (2002).

327. Park, J. Y. *et al.* Hypoxia leads to abnormal epidermal differentiation via HIF-independent pathways. *Biochem. Biophys. Res. Commun.* **469**, 251–256 (2016).

328. Bae, O.-N. *et al.* Chemical allergens stimulate human epidermal keratinocytes to produce lymphangiogenic vascular endothelial growth factor. *Toxicology and applied pharmacology* **283**, 147–55 (2015).

329. Cho, Y.-S. S. *et al.* HIF-1α controls keratinocyte proliferation by up-regulating p21(WAF1/Cip1). *Biochim. Biophys. Acta - Mol. Cell Res.* **1783**, 323–333 (2008).

330. Kwon, Y.-W. *et al.* Insulin-like growth factor-II regulates the expression of vascular endothelial growth factor by the human keratinocyte cell line HaCaT. *J. Invest. Dermatol.* **123**, 152–158 (2004).

331. Chaudhary, A., Bag, S., Barui, A., Banerjee, P. & Chatterjee, J. Honey dilution impact on in vitro wound healing: Normoxic and hypoxic condition. *Wound Repair Regen.* **23**, 412–422 (2015).

332. Habryka, A. *et al.* Cell type-dependent modulation of the gene encoding heat shock protein HSPA2 by hypoxia-inducible factor HIF-1: Down-regulation in keratinocytes and up-regulation in HeLa cells. *Biochim. Biophys. Acta - Gene Regul. Mech.* **1849**, 1155–1169 (2015).

333. Yang, C. *et al.* Hydrogen sulfide protects against chemical hypoxia-induced cytotoxicity and inflammation in HaCaT cells through inhibition of ROS/NF-kB/COX-2 pathway. *PLoS ONE* **6**, 1–9 (2011).

334. Ong, H. T. & Dilley, R. J. Novel non-angiogenic role for mesenchymal stem cell-derived vascular endothelial growth factor on keratinocytes during wound healing. *Cytokine*

Growth Factor Rev. **44**, 69–79 (2018).

335. Seo, M.-D., Kang, T.-J., Lee, C.-H., Lee, A.-Y. & Noh, M. HaCaT Keratinocytes and Primary Epidermal Keratinocytes have different transcriprional profiles of cornified envelope-associated genes to T Helper Cell Cytokines. *Biomol. Ther.* **20**, 171–176 (2012).

336. Wan, H. *et al.* Stem/Progenitor Cell-Like Properties of Desmoglein 3 dim Cells in Primary and Immortalized Keratinocyte Lines . *Stem Cells* **25**, 1286–1297 (2007).

337. Fernandes, I. R. *et al.* Fibroblast sources: Where can we get them? *Cytotechnology* **68**, 223–228 (2016).

338. Xiao, H., Gu, Z., Wang, G. & Zhao, T. The possible mechanisms underlying the impairment of hif-1α pathway signaling in hyperglycemia and the beneficial effects of certain therapies. *Int. J. Med. Sci.* **10**, 1412–1421 (2013).

339. Agarwal, V. *et al.* Evaluating the effects of nacre on human skin and scar cells in culture. *Toxicol. Res.* **3**, 223–227 (2014).

340. Quan, C. *et al.* Dermal fibroblast expression of stromal cell-derived factor-1 (SDF-1) promotes epidermal keratinocyte proliferation in normal and diseased skin. *Protein Cell* **6**, 890–903 (2015).

341. Ferrer, R. A. *et al.* Dermal Fibroblasts Promote Alternative Macrophage Activation Improving Impaired Wound Healing. *J. Invest. Dermatol.* **137**, 941–950 (2017).

342. Almeida, M. E. S. *et al.* Hyperglycemia reduces integrin subunits alpha v and alpha 5 on the surface of dermal fibroblasts contributing to deficient migration. *Mol. Cell. Biochem.* **421**, 19–28 (2016).

343. Phan, T. T., See, P., Lee, S. T. & Chan, S. Y. Protective effects of curcumin against oxidative damage on skin cells in vitro: its implication for wound healing. *J. Trauma* **51**, 927–931 (2001).

344. Falanga, V. *et al.* Hypoxia upregulates the synthesis of TGF-B1 by human dermal fibroblasts. *Soc. Investig. Dermatology* **97**, 634–637 (1991).

345. Baracca, A., Sgarbi, G., Padula, A. & Solaini, G. Glucose plays a main role in human fibroblasts adaptation to hypoxia. *Int. J. Biochem. Cell Biol.* **45**, 1356–1365 (2013).

346. Ansurudeen, I. *et al.* Carnosine enhances diabetic wound healing in the db/db mouse model of type 2 diabetes. *Amino Acids* **43**, 127–134 (2012).

347. Hehenberger, K. *et al.* Impaired proliferation and increased L-lactate production of dermal fibroblasts in the GK-rat, a spontaneous model of non-insulin dependent diabetes mellitus. *Wound Repair Regen.* **7**, 65–71 (1999).

348. Wright, C. S., Pollok, S., Flint, D. J., Brandner, J. M. & Martin, P. E. M. The connexin mimetic peptide Gap27 increases human dermal fibroblast migration in hyperglycemic and hyperinsulinemic conditions in vitro. *J. Cell. Physiol.* **227**, 77–87 (2012).

349. Zhai, J. & Wang, Y. MDI 301, a synthetic retinoid, depressed levels of matrix metalloproteinases and oxidative stress in diabetic dermal fibroblasts. *Oncotarget* **8**, 43889–43896 (2017).

350. Sibbitt, W. L. *et al.* Glucose inhibition of human fibroblasts proliferation and response to growth factors is prevented by inhibitors of aldose reductase. *Mech. Ageing Dev.* **47**, 265–279 (1989).

351. Deveci, M. *et al.* Glutathione enhances fibroblast collagen contraction and protects keratinocytes from apoptosis in hyperglycaemic culture. *Br. J. Dermatol.* **152**, 217–224 (2005).

352. The Emerging Risk Factors Collaboration. Diabetes Mellitus, Fasting Glucose, and Risk of Cause-Specific Death. *The New England Journal of Medicine* **2011**, 538–540

(2012).

353. Thomas, K., Kiwit, M. & Kerner, W. Glucose concentration in human subcutaneous adipose tissue: Comparison between forearm and abdomen. *Exp Clin Endocrinol Diabetes* **106**, 465–469 (1998).

354. Rheinwald, J. G. & Green, H. Growth of cultured mammalian cells on secondary glucose sources. *Cell* **2**, 287–293 (1974).

355. Yu, J., Choi, S., Um, J. & Park, K. S. Reduced Expression of YAP in Dermal Fibroblasts is Associated with Impaired Wound Healing in Type 2 Diabetic Mice. *Tissue Eng. Regen. Med.* **14**, 49–55 (2017).

356. Mendoza-Naranjo, A. *et al.* Overexpression of the gap junction protein Cx43 as found in diabetic foot ulcers can retard fibroblast migration. *Cell Biol. Int.* **36**, 661–667 (2012).

357. Smoak, I. W. Hyperglycemia-induced TGFβ and fibronectin expression in embryonic mouse heart. *Dev. Dyn.* **231**, 179–189 (2004).

358. Pan, F. *et al.* High glucose inhibits ClC-2 chloride channels and attenuates cell migration of rat keratinocytes. *Drug Des. Devel. Ther.* **9**, 4779–4791 (2015).

359. Lamers, M. L., Almeida, M. E. S., Vicente-Manzanares, M., Horwitz, A. F. & Santos, M. F. High glucose-mediated oxidative stress impairs cell migration. *PLoS One* **6**, 1–9 (2011).

360. Berlanga-Acosta, J. *et al.* Glucose toxic effects on granulation tissue productive cells: The diabetics' impaired healing. *Biomed Res. Int.* **2013**, (2013).

361. Yang, C. *et al.* Oxidative stress mediates chemical hypoxia-induced injury and inflammation by activating NF-kb-COX-2 pathway in HaCaT cells. *Mol. Cells* **31**, 531–538 (2011).

362. Catrina, S., Okamoto, K., Pereira, T., Brismar, K. & Poellinger, L. Hyperglycemia regulates hypoxia-inducible factor-1alpha protein stability and function. *Diabetes* **53**, 3226–3232 (2004).

363. Ahluwalia, a. & S. Tarnawski, a. Critical Role of Hypoxia Sensor - HIF-1α in VEGF Gene Activation. Implications for Angiogenesis and Tissue Injury Healing. *Curr. Med. Chem.* **19**, 90–97 (2012).

364. Bizzarro, V. *et al.* Annexin A1 N-Terminal Derived Peptide Ac2-26 Stimulates Fibroblast Migration in High Glucose Conditions. *PLoS One* **7**, 1–9 (2012).

365. Duscher, D. *et al.* Comparison of the Hydroxylase Inhibitor Dimethyloxalylglycine and the Iron Chelator Deferoxamine in Diabetic and Aged Wound Healing. *Plast. Reconstr. Surg.* **139**, 695e-706e (2017).

366. Lin, H. I. *et al.* Hyperbaric oxygen attenuates cell growth in skin fibroblasts cultured in a high-glucose medium. *Wound Repair Regen.* **16**, 513–519 (2008).

367. Madhyastha, R. *et al.* NFkappaB activation is essential for miR-21 induction by TGFβ1 in high glucose conditions. *Biochem. Biophys. Res. Commun.* **451**, 615–621 (2014).

368. Pang, L. *et al.* Transcriptomic study of high-glucose effects on human skin fibroblast cells. *Mol. Med. Rep.* **13**, 2627–2634 (2016).

369. Soares, M. A. *et al.* Restoration of Nrf2 signaling normalizes the regenerative niche. *Diabetes* **65**, 633–646 (2016).

370. Xue, S., Lei, J., Lin, D., Yang, C. & Yan, L. Changes in biological behaviors of rat dermal fibroblasts induced by high expression of MMP9. *World J. Emerg. Med.* **5**, 139 (2014).

371. Houreld, N. N. Irradiation at 660 nm modulates different genes central to wound healing in wounded and diabetic wounded cell models. *Mech. Low-Light Ther. IX* **8932**, 89320A

(2014).

372. Avitabile, S. *et al.* Interleukin-22 Promotes Wound Repair in Diabetes by Improving Keratinocyte Pro-Healing Functions. *J. Invest. Dermatol.* **135**, 2862–2870 (2015).

373. Lan, C. C. E. *et al.* High-glucose environment inhibits p38MAPK signaling and reduces human β-3 expression in keratinocytes. *Mol. Med.* **17**, 771–779 (2011).

374. Kulkarni, M. *et al.* Use of a fibrin-based system for enhancing angiogenesis and modulating inflammation in the treatment of hyperglycemic wounds. *Biomaterials* **35**, 2001–2010 (2014).

375. Lan, C. C. E., Huang, S. M., Wu, C. S., Wu, C. H. & Chen, G. S. High-glucose environment increased thrombospondin-1 expression in keratinocytes via DNA hypomethylation. *Transl. Res.* **169**, 91-101.e3 (2016).

376. Li, M. *et al.* Mesenchymal stem cell-conditioned medium improves the proliferation and migration of keratinocytes in a diabetes-like microenvironment. *Int. J. Low. Extrem. Wounds* **14**, 73–86 (2015).

377. Song, R. *et al.* Melatonin promotes diabetic wound healing in vitro by regulating keratinocyte activity. *Am. J. Transl. Res.* **8**, 4682–4693 (2016).

378. Zhang, C. *et al.* FOXO1 differentially regulates both normal and diabetic wound healing. *J. Cell Biol.* **209**, 289–303 (2015).

379. Kato, J. *et al.* Mesenchymal stem cells ameliorate impaired wound healing through enhancing keratinocyte functions in diabetic foot ulcerations on the plantar skin of rats. *J. Diabetes Complications* **28**, 588–595 (2014).

380. Kruse, C. R., Singh, M., Sørensen, J. A., Eriksson, E. & Nuutila, K. The effect of local hyperglycemia on skin cells in vitro and on wound healing in euglycemic rats. *J. Surg. Res.* **206**, 418–426 (2016).

381. Torimoto, K., Okada, Y., Mori, H. & Tanaka, Y. Relationship between fluctuations in glucose levels measured by continuous glucose monitoring and vascular endothelial dysfunction in type 2 diabetes mellitus. *Cardiovasc. Diabetol.* **12**, 1–7 (2013).

382. Yu, T., Robotham, J. L. & Yoon, Y. Increased production of reactive oxygen species in hyperglycemic conditions requires dynamic change of mitochondrial morphology. *Proc. Natl. Acad. Sci. U. S. A.* **103**, 2653–8 (2006).

383. Hooper, L. *et al.* Diagnostic accuracy of calculated serum osmolarity to predict dehydration in older people: Adding value to pathology laboratory reports. *BMJ Open* **5**, 1–11 (2015).

384. Kitabchi, A. E., Umpierrez, G. E., Miles, J. M. & Fisher, J. N. Hyperglycemic crises in adult patients with diabetes. *Diabetes Care* **32**, 1335–1343 (2009).

385. Thompson, C. J., Davis, S. N. & Baylis, P. H. Effect of blood glucose concentration on osmoregulation in diabetes mellitus. *Am. J. Physiol. Integr. Comp. Physiol.* **256**, R597–R604 (2017).

386. Keating, F. K., Sobel, B. E. & Schneider, D. J. Effects of increased concentrations of glucose on platelet reactivity in healthy subjects and in patients with and without diabetes mellitus. *Am. J. Cardiol.* **92**, 1362–1365 (2003).

387. Malek, A. M., Goss, G. G., Jiang, L., Izumo, S. & Alper, S. L. Mannitol at clinical concentrations activates multiple signaling pathways and induces apoptosis in endothelial cells. *Stroke* **29**, 2631–2640 (1998).

388. Beeri, M. S. *et al.* Serum concentration of an inflammatory glycotoxin, methylglyoxal, is associated with increased cognitive decline in elderly individuals. *Mech. Ageing Dev.* **132**, 583–587 (2011).

389. Rodrigues, L. *et al.* Advanced glycation end products and diabetic nephropathy: A

comparative study using diabetic and normal rats with methylglyoxal-induced glycation. *J. Physiol. Biochem.* **70**, 173–184 (2014).

390. Schalkwijk, C. G. Vascular AGE-ing by methylglyoxal: the past, the present and the future. *Diabetologia* **58**, 1715–1719 (2015).

391. P.J. Beisswenger, Howell, S. K., Nelson, R. G., Mauer, M. & Szwergold, B. S. α-Oxoaldehyde metabolism and diabetic complications.

392. Phillips, S. A. & Thornalley, P. J. The formation of methylglyoxal from triose phosphates: Investigation using a specific assay for methylglyoxal. *Eur. J. Biochem.* **212**, 101–105 (1993).

393. Brouwers, O. *et al.* Overexpression of glyoxalase-I reduces hyperglycemia induced levels of advanced glycation end products and oxidative stress in diabetic rats. *J. Biol. Chem.* **286**, 1374–1380 (2011).

394. Cantero, A.-V. *et al.* Methylglyoxal induces advanced glycation end product (AGEs) formation and dysfunction of PDGF receptor-β: implications for diabetic atherosclerosis. *FASEB J.* **21**, 3096–3106 (2007).

395. Martín-Gallán, P., Carrascosa, A., Gussinyé, M. & Domínguez, C. Biomarkers of diabetes-associated oxidative stress and antioxidant status in young diabetic patients with or without subclinical complications. *Free Radic. Biol. Med.* **34**, 1563–1574 (2003).

396. Matafome, P., Rodrigues, T., Sena, C. & Seiça, R. Methylglyoxal in Metabolic Disorders: Facts, Myths, and Promises. *Med. Res. Rev.* **37**, 368–403 (2017).

397. Sena, C. M. *et al.* Methylglyoxal promotes oxidative stress and endothelial dysfunction. *Pharmacol. Res.* **65**, 497–506 (2012).

398. Bourajjaj, M., Stehouwer, C. D. a, Van Hinsbergh, V. W. M. & Schalkwijk, C. G. Role of methylglyoxal adducts in the development of vascular complications in diabetes mellitus. *Biochem. Soc. Trans.* **31**, 1400–1402 (2003).

399. Heier, M. *et al.* The advanced glycation end product methylglyoxal-derived hydroimidazolone-1 and early signs of atherosclerosis in childhood diabetes. *Diabetes Vasc. Dis. Res.* **12**, 139–145 (2015).

400. Wang, W. Oxygen partial pressure in outer layers of skin: Simulation using three-dimensional multilayered models. *Microcirculation* **12**, 195–207 (2005).

401. Scheid, a. *et al.* Hypoxia-regulated gene expression in fetal wound regeneration and adult wound repair. *Pediatr. Surg. Int.* **16**, 232–236 (2000).

402. Gottrup, F. Oxygen in Wound Healing and Infection. *World J. Surg.* **28**, 312–315 (2004).

403. Breit, S., Bubel, M., Pohlemann, T. & Oberringer, M. Erythropoietin ameliorates the reduced migration of human fibroblasts during in vitro hypoxia. *J. Physiol. Biochem.* **67**, 1–13 (2011).

404. Aichele, K., Bubel, M., Deubel, G., Pohlemann, T. & Oberringer, M. Bromelain down-regulates myofibroblast differentiation in an in vitro wound healing assay. *Naunyn. Schmiedebergs. Arch. Pharmacol.* **386**, 853–863 (2013).

405. Lund, E. L. *et al.* Differential regulation of VEGF, HIF1α and angiopoietin-1, -2 and -4 by hypoxia and ionizing radiation in human glioblastoma. *Int. J. Cancer* **108**, 833–838 (2004).

406. Weng, R., Li, Q., Li, H., Yang, M. & Sheng, L. Mimic hypoxia improves angiogenesis in ischaemic random flaps. *J. Plast. Reconstr. Aesthetic Surg.* **63**, 2152–2159 (2010).

407. Pichiule, P., Chavez, J. C. & LaManna, J. C. Hypoxic Regulation of Angiopoietin-2 Expression in Endothelial Cells. *J. Biol. Chem.* **279**, 12171–12180 (2004).

408. Liu, L. *et al.* Age-dependent impairment of HIF-1α expression in diabetic mice: Correction with electroporation-facilitated gene therapy increases wound healing, angiogenesis, and circulating angiogenic cells. *J. Cell. Physiol.* **217**, 319–327 (2008).

409. Thangarajah, H. *et al.* HIF-1α dysfunction in diabetes. *Cell Cycle* **9**, 75–79 (2010).

410. Chi, J. T. *et al.* Gene expression programs in response to hypoxia: Cell type specificity and prognostic significance in human cancers. *PLoS Med.* **3**, 395–409 (2006).

411. Biswas, S. *et al.* Hypoxia inducible microRNA 210 attenuates keratinocyte proliferation and impairs closure in a murine model of ischemic wounds. *Proc. Natl. Acad. Sci. U. S. A.* **107**, 6976–6981 (2010).

412. Nishikawa, T. *et al.* Normalizing Mitochondrial Superoxide Production Blocks Three Pathways of Hyperglycaemic Damage. *Lett. to Nat.* **696**, 787–790 (2014).

413. Uemura, S. *et al.* Diabetes Mellitus Enhances Vascular Matrix Metalloproteinase Activity. *Oncogene Res.* **88**, 1291–1298 (2001).

414. Murphy, G. *Matrix Metalloproteinases*. *Encyclopedia of Cell Biology* **1**, (Elsevier Ltd., 2015).

415. Wang, H. & Kochevar, I. E. Involvement of UVB-induced reactive oxygen species in TGF-?? biosynthesis and activation in keratinocytes. *Free Radic. Biol. Med.* **38**, 890–897 (2005).

416. O'Toole, E. A., Koningsveld, R. Van, Chen, M. & Woodley, D. T. Hypoxia Induces Epidermal Keratinocyte Matrix Metalloproteinase-9 Secretion Via the Protein Kinase C Pathway. *J. Cell. Physiol.* **245**, 237–245 (2007).

417. Liu, Y. *et al.* Increased Matrix Metalloproteinase-9 Predicts Poor Wound Healing in Diabetic Foot Ulcers. *Diabetes Care* **32**, 117–119 (2009).

418. Lerman, O. Z. *et al.* Cellular dysfunction in the diabetic fibroblast: Impairment in migration, vascular endothelial growth factor production, and response to hypoxia. *Am. J. Pathol.* **162**, 303–312 (2003).

419. Brem, H. *et al.* The synergism of age and db/db genotype impairs wound healing. *Exp. Gerontol.* **42**, 523–531 (2007).

420. Avery, N. C. & Bailey, A. J. The effects of the Maillard reaction on the physical properties and cell interactions of collagen. *Pathol. Biol.* **54**, 387–395 (2006).

421. International Diabetes Federation. *IDF Diabetes Atlas*. *IDF Diabetes Atlas, 8th edition* (2017). doi:http://dx.doi. org/10.1016/S0140-6736(16)31679-8.

422. Nordquist, L. *et al.* Activation of Hypoxia-Inducible Factors Prevents Diabetic Nephropathy. *J. Am. Soc. Nephrol.* **26**, 328–338 (2015).

423. Rey, S. *et al.* Synergistic effect of HIF-1α gene therapy and HIF-1-activated bone marrow-derived angiogenic cells in a mouse model of limb ischemia. *Proc. Natl. Acad. Sci. U. S. A.* **106**, 20399–20404 (2009).

424. Ikeda, Y. *et al.* Deferoxamine promotes angiogenesis via the activation of vascular endothelial cell function. *Atherosclerosis* **215**, 339–347 (2011).

425. Elson, D. a, Ryan, H. E., Snow, J. W., Johnson, R. & Arbeit, J. M. Coordinate Up-Regulation of Hypoxia Inducible Factor (HIF) -1 α and HIF-1 Target Genes during Multi-Stage Epidermal Carcinogenesis and Wound Healing Coordinate Up-Regulation of Hypoxia Inducible Factor (HIF) -1 ␣ and HIF-1 Target Genes during Multi-St. *Cancer Res.* **60**, 6189–6195 (2000).

426. Bedogni, B. *et al.* The hypoxic microenvironment of the skin contributes to Akt-mediated melanocyte transformation. *Cancer Cell* **8**, 443–454 (2005).

427. Majumder, P. K. *et al.* mTOR inhibition reverses Akt-dependent prostate intraepithelial neoplasia through regulation of apoptotic and HIF-1-dependent pathways. *Nat. Med.* **10**, 594–601 (2004).

428. Asikainen, T. M. *et al.* Improved lung growth and function through hypoxia-inducible factor in primate chronic lung disease of prematurity. *FASEB J.* **20**, (2006).

429. Franke, K., Gassmann, M. & Wielockx, B. Erythrocytosis: the HIF pathway in control. *Blood* **122**, 1122–1128 (2013).

430. Schödel, J. *et al.* High-resolution genome-wide mapping of HIF-binding sites by ChIP-seq. *Blood* **117**, 207–217 (2011).

431. Elvidge, G. P. *et al.* Concordant regulation of gene expression by hypoxia and 2-oxoglutarate-dependent dioxygenase inhibition: The role of HIF-1α, HIF-2α, and other pathways. *J. Biol. Chem.* **281**, 15215–15226 (2006).

432. Befani, C. *et al.* Cobalt stimulates HIF-1-dependent but inhibits HIF-2-dependent gene expression in liver cancer cells. *Int. J. Biochem. Cell Biol.* **45**, 2359–2368 (2013).

433. Buttyan, R. *et al.* Acute intravesical infusion of a cobalt solution stimulates a hypoxia response, growth and angiogenesis in the rat bladder. *J. Urol.* **169**, 2402–2406 (2003).

434. Wu, S. *et al.* Enhancement of angiogenesis through stabilization of hypoxia-inducible factor-1 by silencing prolyl hydroxylase domain-2 gene. *Mol. Ther.* **16**, 1227–1234 (2008).

435. Liu, F. *et al.* Hypoxia modulates lipopolysaccharide induced TNF-α expression in murine macrophages. *Experimental Cell Research* 1327–1336 (2008). Available at: http://ac.els-cdn.com/S0014482708000244/1-s2.0-S0014482708000244-main.pdf?_tid=85b6f9e0-c69a-11e5-afa8-00000aab0f6c&acdnat=1454080447_2fe41a12b55a40db523e8e8ff2825b46. (Accessed: 20th January 2016)

436. Jiang, B. H., Zheng, J. Z., Leung, S. W., Roe, R. & Semenza, G. L. Transactivation and inhibitory domains of Hypoxia-inducible factor 1α: Modulation of transcriptional activity by oxygen tension. *J. Biol. Chem.* **272**, 19253–19260 (1997).

437. Pugh, C. W., O'Rourke, J. F., Nagao, M., Gleadle, J. M. & Ratcliffe, P. J. Activation of hypoxia-inducible factor-1; Definition of regulatory domains within the α subunit. *J. Biol. Chem.* **272**, 11205–11214 (1997).

438. Wang, C. *et al.* Local injection of deferoxamine improves neovascularization in ischemic diabetic random flap by increasing HIF-1α and VEGF expression. *PLoS One* **9**, 3–10 (2014).

439. Shen, X. *et al.* Prolyl hydroxylase inhibitors increase neoangiogenesis and callus formation following femur fracture in mice. *J. Orthop. Res.* **27**, 1298–1305 (2009).

440. Wahl, E. A., Schenck, T. L., Machens, H.-G. & Balmayor, E. R. VEGF released by deferoxamine preconditioned mesenchymal stem cells seeded on collagen-GAG substrates enhances neovascularization. *Sci. Rep.* **6**, 36879 (2016).

441. Najafi, R. & Sharifi, A. M. Deferoxamine preconditioning potentiates mesenchymal stem cell homing in vitro and in streptozotocin-diabetic rats . *Expert Opin. Biol. Ther.* **13**, 959–972 (2013).

442. Okumura, C. Y. M. *et al.* A New Pharmacological Agent (AKB-4924) Stabilizes Hypoxia Inducible Factor (HIF) and Increases Skin Innate Defenses Against Bacterial Infection. *J Mol Med* **90**, 1–7 (2012).

443. Zhdanov, A. V., Okkelman, I. A., Collins, F. W. J., Melgar, S. & Papkovsky, D. B. A novel effect of DMOG on cell metabolism: Direct inhibition of mitochondrial function precedes HIF target gene expression. *Biochim. Biophys. Acta - Bioenerg.* **1847**, 1254–1266 (2015).

444. Fukuda, R. *et al.* HIF-1 Regulates Cytochrome Oxidase Subunits to Optimize Efficiency of Respiration in Hypoxic Cells. *Cell* **129**, 111–122 (2007).

445. Yan, H., Zhang, D. X., Shi, X., Zhang, Q. & Huang, Y. S. Activation of the prolyl-hydroxylase oxygen-sensing signal cascade leads to AMPK activation in cardiomyocytes. *J. Cell. Mol. Med.* **16**, 2049–2059 (2012).

446. Weidemann, A. *et al.* HIF-1α activation results in actin cytoskeleton reorganization and modulation of Rac-1 signaling in endothelial cells. *Cell Commun. Signal.* **11**, 1 (2013).

447. Hill, P. *et al.* Inhibition of Hypoxia Inducible Factor Hydroxylases Protects Against Renal Ischemia-Reperfusion Injury. *J. Am. Soc. Nephrol.* **19**, 39–46 (2008).

448. Zhang, X. *et al.* Wound healing improvement with PHD-2 silenced fibroblasts in diabetic mice. *PLoS One* **8**, 1–11 (2013).

449. Janjić, K., Edelmayer, M., Moritz, A. & Agis, H. L-mimosine and hypoxia can increase angiogenin production in dental pulp-derived cells. *BMC Oral Health* **17**, 1–7 (2017).

450. Warnecke, C. *et al.* Activation of the hypoxia-inducible factor pathway and stimulation of angiogenesis by application of prolyl hydroxylase inhibitors. *FASEB J.* **17**, (2003).

451. Berchner-Pfannschmidt, U. *et al.* Chelation of cellular calcium modulates hypoxia-inducible gene expression through activation of Hypoxia-Inducible Factor-1α. *J. Biol. Chem.* **279**, 44976–44986 (2004).

452. Zhang, E., Gao, B., Yang, L., Wu, X. & Wang, Z. Notoginsenoside Ft1 promotes fibroblast proliferation via PI3K/Akt/mTOR signaling pathway and benefits wound healing in genetically diabetic mices. *J. Pharmacol. Exp. Ther.* **356**, 324–332 (2016).

453. Emerit, J., Beaumont, C. & Trivin, F. Iron metabolism, free radicals, and oxidative injury. *Biomed. Pharmacother.* **55**, 333–339 (2001).

454. Ortega, R. *et al.* Cobalt distribution in keratinocyte cells indicates nuclear and perinuclear accumulation and interaction with magnesium and zinc homeostasis. *Toxicol. Lett.* **188**, 26–32 (2009).

455. Semenza, G. L. & Wang, G. L. A nuclear factor induced by hypoxia via de novo protein synthesis binds to the human erythropoietin gene enhancer at a site required for transcriptional activation. *Mol. Cell. Biol.* **12**, 5447–5454 (1992).

456. Nguyen, L. K. *et al.* Correction to A dynamic model of the hypoxia-inducible factor 1a (HIF-1a) network [J. Cell Sci. 126, (2014) 1454-1463]. *J. Cell Sci.* **128**, 422 (2015).

457. McNamee, E. N., Korns Johnson, D., Homann, D. & Clambey, E. T. Hypoxia and hypoxia-inducible factors as regulators of T cell development, differentiation, and function. *Immunol. Res.* **55**, 58–70 (2013).

458. Ferrali, M., Signorini, C., Ciccoli, L. & Comporti, M. Iron release and membrane damage in erythrocytes exposed to oxidizing agents, phenylhydrazine, divicine and isouramil. *Biochem. J.* **285**, 295–301 (1992).

459. PALLER, M. S. & HEDLUND, B. E. Extracellular iron chalators protect kidney cells from hypoxia/reoxygenation. *Free Radic. Biol.* **17**, 597–603 (1994).

460. Yao, Q., Liu, Y., Tao, J., Baumgarten, K. M. & Sun, H. Hypoxia-Mimicking Nanofibrous Scaffolds Promote Endogenous Bone Regeneration. *ACS Appl. Mater. Interfaces* **8**, 32450–32459 (2016).

461. Kalucka, J. *et al.* Loss of Epithelial HIF Prolyl Hydroxylase-2 (PHD2) Accelerates Skin Wound Healing in Mice. *Mol. Cell. Biol.* **2**, 3426–3438 (2013).

462. Busch, W., Kühnel, D., Schirmer, K. & Scholz, S. Tungsten carbide cobalt nanoparticles exert hypoxia-like effects on the gene expression level in human keratinocytes. *BMC Genomics* **11**, (2010).

463. Vengellur, A., Phillips, J. M., Hogenesch, J. B. & LaPres, J. J. Gene expression profiling of hypoxia signaling in human hepatocellular carcinoma cells. *Physiol. Genomics* **22**, 308–318 (2005).

464. Semenza, G. L. Hypoxia-inducible factor 1: Oxygen homeostasis and disease pathophysiology. *Trends Mol. Med.* **7**, 345–350 (2001).

465. Martin, A. R., Ronco, C., Demange, L. & Benhida, R. Hypoxia inducible factor down-regulation, cancer and cancer stem cells (CSCs): ongoing success stories. *Med. Chem. Commun.* **8**, 21–52 (2017).

466. Rezvani, H. R. *et al.* HIF-1a in Epidermis: Oxygen Sensing, Cutaneous Angiogenesis, Cancer, and Non-Cancer Disorders. *J. Invest. Dermatol.* **131**, 1793–1805 (2011).

467. Gault, N. *et al.* Cobalt toxicity: Chemical and radiological combined effects on HaCaT keratinocyte cell line. *Toxicology in Vitro* **24**, 92–98 (2010).

468. Xia, Y., Choi, H.-K. K. & Lee, K. Recent advances in hypoxia-inducible factor (HIF)-1 inhibitors. *Eur. J. Med. Chem.* **49**, 24–40 (2012).

469. Mihaylova, M. M. & Shaw, R. J. The AMPK signalling pathway coordinates cell growth, autophagy and metabolism. *Nat. Cell Biol.* **13**, 1016–1023 (2011).

470. Datta, K. *et al.* Protein Kinase C ζ Transactivates Hypoxia-Inducible Factor α by Promoting Its Association with p300 in Renal Cancer. *Cancer Res.* **64**, 456–462 (2004).

471. Ouchi, N., Shibata, R. & Walsh, K. AMP-activated protein kinase signaling stimulates VEGF expression and angiogenesis in skeletal muscle. *Circ. Res.* **96**, 838–846 (2005).

472. Scott Budinger, G. R. *et al.* Hyperoxia-induced apoptosis does not require mitochondrial reactive oxygen species and is regulated by Bcl-2 proteins. *J. Biol. Chem.* **277**, 15654–15660 (2002).

473. Deng, X., Gao, F. & May, W. S. Bcl2 retards G1/S cell cycle transition by regulating intracellular ROS. *Blood* **102**, 3179–3185 (2003).

474. Aina, V., Malavasi, G., Fiorio Pla, A., Munaron, L. & Morterra, C. Zinc-containing bioactive glasses: Surface reactivity and behaviour towards endothelial cells. *Acta Biomater.* **5**, 1211–1222 (2009).

475. Chebassier, N., El Houssein, O., Viegas, I. & Dréno, B. In vitro induction of matrix metalloproteinase-2 and matrix metalloproteinase-9 expression in keratinocytes by boron and manganese. *Exp. Dermatol.* **13**, 484–490 (2004).

476. Bi, M. *et al.* ER stress-regulated translation increases tolerance to extreme hypoxia and promotes tumor growth. *EMBO J.* **24**, 3470–3481 (2005).

477. Rana, N. K., Singh, P. & Koch, B. CoCl 2 simulated hypoxia induce cell proliferation and alter the expression pattern of hypoxia associated genes involved in angiogenesis and apoptosis. *Biol. Res.* **52**, 12 (2019).

478. Ho, V. T. & Bunn, H. F. Effects of transition metals on the expression of the erythropoietin gene: Further evidence that the oxygen sensor is a heme protein. *Biochem. Biophys. Res. Commun.* **223**, 175–180 (1996).

479. An, S. *et al.* Administration of CoCl 2 improves functional recovery in a rat model of sciatic nerve transection injury. *Int. J. Med. Sci.* **15**, 1423–1432 (2018).

480. Dai, Z. J. *et al.* Up-regulation of hypoxia inducible factor-1α by cobalt chloride correlates with proliferation and apoptosis in PC-2 cells. *J. Exp. Clin. Cancer Res.* **31**, 28 (2012).

481. Jell, G., Hill, R., Azevedo, M. & Stevens, M. Hypoxia inducing factor (HIF) stabilising glasses. (2009).

482. Wu, C. *et al.* Hypoxia-mimicking mesoporous bioactive glass scaffolds with controllable cobalt ion release for bone tissue engineering. *Biomaterials* **33**, 2076–2085 (2012).

483. Hoppe, A. *et al.* Cobalt-releasing 1393 bioactive glass-derived scaffolds for bone tissue engineering applications. *ACS Appl. Mater. Interfaces* **6**, 2865–2877 (2014).

484. Quinlan, E. *et al.* Hypoxia-mimicking bioactive glass/collagen glycosaminoglycan composite scaffolds to enhance angiogenesis and bone repair. *Biomaterials* **52**, 358–366 (2015).

485. Papis, E. *et al.* Engineered cobalt oxide nanoparticles readily enter cells. *Toxicol. Lett.* **189**, 253–259 (2009).

486. De Boeck, M. *et al.* In vitro genotoxic effects of different combinations of cobalt and metallic carbide particles. *Mutagenesis* **18**, 177–186 (2003).

487. Jackson, M. J. Physiology of Zinc: General Aspects. 1–14 (1989). doi:10.1007/978-1-4471-3879-2_1

488. Nakatani, T., Tawaramoto, M., Opare Kennedy, D., Kojima, A. & Matsui-Yuasa, I. Apoptosis induced by chelation of intracellular zinc is associated with depletion of cellular reduced glutathione level in rat hepatocytes. *Chem. Biol. Interact.* **125**, 151–163 (2000).

489. Rostan, E. F., Debuys, H. V., Madey, D. L. & Pinnell, S. R. Evidence supporting zinc as an important antioxidant for skin. *Int. J. Dermatol.* **41**, 606–611 (2002).

490. Jourdan, E., Jeanne, R. M., Régine, S. & Pascale, G. Zinc-metallothionein genoprotective effect is independent of the glutathione depletion in HaCaT keratinocytes after solar light irradiation. *J. Cell. Biochem.* **92**, 631–640 (2004).

491. Frank, S., Kamper, H., Podda, M., Kaufmann, R. & Pfeilschifter, J. Identification of copper/zinc superoxide dismutase as a nitric oxide-regulated gene in human (HaCaT) keratinocytes: implications for keratinocyte proliferation. *Biochem. J.* **346**, 719 (2000).

492. Balasubramanian, P., Strobel, L. a., Kneser, U. & Boccaccini, A. R. Zinc-containing bioactive glasses for bone regeneration, dental and orthopedic applications. *Biomed. Glas.* **1**, 51–69 (2015).

493. Couñago, R. M. *et al.* Imperfect coordination chemistry facilitates metal ion release in the Psa permease. *Nat. Chem. Biol.* **10**, 35–41 (2014).

494. Skalnaya, M. G. *et al.* ICP-DRC-MS analysis of serum essential and toxic element levels in postmenopausal prediabetic women in relation to glycemic control markers. *J. Trace Elem. Med. Biol.* 0–1 (2017). doi:10.1016/j.jtemb.2017.09.008

495. Chausmer, a B. Zinc, insulin and diabetes. *J. Am. Coll. Nutr.* **17**, 109–15 (1998).

496. Mohanasundaram, D. *et al.* Ultrastructural analysis, zinc transporters, glucose transporters and hormones expression in new world primate (Callithrix jacchus) and human pancreatic islets. *Gen. Comp. Endocrinol.* **174**, 71–79 (2011).

497. Zhou, J. *et al.* In vivo and in vitro studies of borate based glass micro-fibers for dermal repairing. *Mater. Sci. Eng. C* **60**, 437–445 (2016).

498. Li, R., Clark, A. E. & Hench, L. L. An investigation of Bioactive Glass powders by Sol-Gel processing. *J. Appl. Biomater.* **2**, 231–239 (1991).

499. Wilson, J., Pigott, G. H., Schoen, F. J. & Hench, L. L. Toxicology and biocompatibility of bioglasses. *J. Biomed. Mater. Res.* **15**, 805–817 (1981).

500. Bischoff, J. L. Kinetics of Calcite Nucleation ' Magnesium. *J. Geophys. Res.* **73**, 3315–3322 (1968).

501. Hench, L. L. The story of Bioglass®. *J. Mater. Sci. Mater. Med.* **17**, 967–978 (2006).

502. Laurent, O., Mantisi, B. & Micoulaut, M. Structure and topology of soda-lime silicate glasses: Implications for window glass. *J. Phys. Chem. B* **118**, 12750–12762 (2014).

503. K. E. Wallace, R.G.Hill, Pembroke, J. T., Brown, C. J. & Hatton, P. V. Influence of sodium oxide content on bioactive glass properties. *J. Mater. Sci. Mater. Med.* **10**, 697–701 (1999).

504. Elgayar, I., Aliev, A. E., Boccaccini, A. R. & Hill, R. G. Structural analysis of bioactive glasses. *J. Non. Cryst. Solids* **351**, 173–183 (2005).

505. Sanders, D. M. & Hench, L. L. Mechanisms of Glass Corrosion. *J. Am. Ceram. Soc.* **56**, 373–377 (1973).

506. Azevedo, M. M. *et al.* Hypoxia Inducible Factor-Stabilizing Bioactive Glasses for Directing Mesenchymal Stem Cell Behavior. *Tissue Eng. Part A* **21**, 382–389 (2015).

507. Werner Vogel. *Structure and Properties of Colorless Glass*. *Glass Chemistry* **53**, (1994).

508. Kaur, G., Pickrell, G., Sriranganathan, N., Kumar, V. & Homa, D. Review and the state of the art: Sol–gel and melt quenched bioactive glasses for tissue engineering. *J. Biomed. Mater. Res. - Part B Appl. Biomater.* **104**, 1248–1275 (2016).

509. R&D Systems. Human VEGF Quantikine ELISA kit.

510. Quinlan, E. *et al.* Hypoxia-mimicking bioactive glass/collagen glycosaminoglycan composite scaffolds to enhance angiogenesis and bone repair. *Biomaterials* **52**, 358–366 (2015).

511. Watts, S. J., Hill, R. G., O'Donnell, M. D. & Law, R. V. Influence of magnesia on the structure and properties of bioactive glasses. *J. Non. Cryst. Solids* **356**, 517–524 (2009).

512. Rohanová, D. *et al.* Is non-buffered DMEM solution a suitable medium for in vitro bioactivity tests? *J. Mater. Chem. B* **2**, 5068–5076 (2014).

513. Thermofisher, G. DMEM Composition.

514. Thermofisher, G. RPMI Composition.

515. Parat, M. O. *et al.* Zinc and DNA fragmentation in keratinocyte apoptosis: Its inhibitory effect in UVB irradiated cells. *J. Photochem. Photobiol. B Biol.* **37**, 101–106 (1997).

516. Kontargiris, E., Vadalouka, A., Ragos, V. & Kalfakakou, V. Zinc inhibits apoptosis and maintains NEP downregulation, induced by ropivacaine, in HaCaT cells. *Biol. Trace Elem. Res.* **150**, 460–466 (2012).

517. Oki, A., Parveen, B., Hossain, S., Adeniji, S. & Donahue, H. Preparation and in vitro bioactivity of zinc containing sol-gel-derived bioglass materials. *J. Biomed. Mater. Res. - Part A* **69**, 216–221 (2004).

518. Anand, V., Singh, K. J. & Kaur, K. Evaluation of zinc and magnesium doped 45S5 mesoporous bioactive glass system for the growth of hydroxyl apatite layer. *J. Non. Cryst. Solids* **406**, 88–94 (2014).

519. Nardinocchi, L. *et al.* Zinc downregulates HIF-1α and inhibits its activity in tumor cells in vitro and in vivo. *PLoS One* **5**, (2010).

520. Kim, I. *et al.* Inhibitory effect of zinc on hypoxic HIF-1 activation in astrocytes. *Neuroreport* **19**, 1065–1068 (2008).

521. Chun, Y. S. *et al.* A new HIF-1 alpha variant induced by zinc ion suppresses HIF-1-mediated hypoxic responses. *J. Cell Sci.* **114**, 4051–4061 (2001).

522. Kitamura, M. Crystallization and transformation mechanism of calcium carbonate polymorphs and the effect of magnesium ion. *J. Colloid Interface Sci.* **236**, 318–327 (2001).

523. Maier, J. A. M., Bernardini, D., Rayssiguier, Y. & Mazur, A. High concentrations of

magnesium modulate vascular endothelial cell behaviour in vitro. *Biochim. Biophys. Acta - Mol. Basis Dis.* **1689**, 6–12 (2004).

524. Tennenbaum, T., Yuspa, S. H. & Kapitulnik, J. Magnesium and phosphate enrichment of culture medium stimulates the proliferation of epidermal cells from newborn and adult mice. *J. Cell. Physiol.* **143**, 431–438 (1990).

525. Lin, S. *et al.* A Magnesium-Enriched 3D Culture System that Mimics the Bone Development Microenvironment for Vascularized Bone Regeneration. *Adv. Sci.* **1900209**, (2019).

526. Fischer, R. J., Pang, D., Beatty, S. T. & Rosenberg, E. Silica-polyamine composite materials for heavy metal ion removal, recovery, and recycling. II. Metal ion separations from mine wastewater and soft metal ion extraction efficiency. *Sep. Sci. Technol.* **34**, 3125–3137 (1999).

527. Hämäläinen, H. *et al. Silicate-Free Peroxide Bleaching of mechanical plups: Efficiency of polymeric stabilizers*. *TAPPI, Kemira group*

528. Barnes, C. A. *et al.* Reproducible cornet assay of amorphous silica nanoparticles detects no genotoxicity. *Nano Lett.* **8**, 3069–3074 (2008).

529. Nabeshi, H. *et al.* Amorphous nanosilica induce endocytosis-dependent ROS generation and DNA damage in human keratinocytes. *Part. Fibre Toxicol.* **8**, 1 (2011).

530. Xie, Z. & Bikle, D. D. The recruitment of phosphatidylinositol 3-kinase to the E-cadherin-catenin complex at the plasma membrane is required for calcium-induced phospholipase C-γ1 activation and human keratinocyte differentiation. *J. Biol. Chem.* **282**, 8695–8703 (2007).

531. Postic, C., Shiota, M. & Magnuson, M. A. Cell-specific roles of glucokinase in glucose homeostasis. *Recent Prog. Horm. Res.* **56**, 195–217 (2001).

532. Siebel, A. L., Fernandez, A. Z. & El-Osta, A. Glycemic memory associated epigenetic changes. *Biochem. Pharmacol.* **80**, 1853–1859 (2010).

533. Siegers, C. P., Bumann, D. & Baretton, G. The effect of desferrioxamine on cell proliferation in human tumour cell lines. *Toxicol. Vitr.* **5**, 427–430 (1991).

534. Min, Z., Shichang, Z., Chen, X., Yufang, Z. & Changqing, Z. 3D-printed dimethyloxallyl glycine delivery scaffolds to improve angiogenesis and osteogenesis. *Biomater. Sci.* **3**, 1236–1244 (2015).

535. Norris, E. *et al.* Electrospinning 3D bioactive glasses for wound healing. *Biomed. Mater.* 0–9 (2019). doi:https://doi.org/10.1088/1748-605X/ab591d

536. FDA U.S. Department of Health and Human Services. *Benefit-Risk Factors to Consider When Determining Substantial Equivalence in Premarket Notifications (510(k)) with Different Technological Characteristics*. *FDA* **510**, 1–25 (2018).

537. FDA U.S. Department of Health and Human Services. FDA Regulation of Human Cells, Tissues, and Cellular and Tissue-Based Products (HCT/P's) Product List. *FDA* (2019). Available at: https://www.fda.gov/vaccines-blood-biologics/tissue-tissue-products/fda-regulation-human-cells-tissues-and-cellular-and-tissue-based-products-hctps-product-list.